The Fast Regulation of Photosynthesis in Diatoms: an inquiry into the physiological and physical origins of non-photochemical chlorophyll fluorescence quenching.

Allen Derks, BSc, MSc

Biological Sciences (Plant Sciences)

Submitted in partial fulfillment

of the requirements for the degree of

PhD

Faculty of Mathematics and Science, Brock University

St. Catharines, Ontario

The Fast Regulation of Photosynthesis in Diatoms: an inquiry into the physiological and physical origins of non-photochemical chlorophyll fluorescence quenching

Allen Derks

Diatoms are renowned for their robust ability to perform NPQ (Non-Photochemical Quenching of chlorophyll fluorescence) as a dissipative response to heightened light stress on photosystem II, plausibly explaining their dominance over other algal groups in turbulent light environs. Their NPQ mechanism has been principally attributed to a xanthophyll cycle involving the lumenal pH regulated reversible de-epoxidation of diadinoxanthin. The principal goal of this dissertation is to reveal the physiological and physical origins and consequences of the NPQ response in diatoms during short-term transitions to excessive irradiation. The investigation involves diatom species from different originating light environs to highlight the diversity of diatom NPQ and to facilitate the detection of core mechanisms common among the diatoms as a group. A chiefly spectroscopic approach was used to investigate NPQ in diatom cells. Prime methodologies include: the real time monitoring of PSII excitation and de-excitation pathways via PAM fluorometry and pigment interconversion via transient absorbance measurements, the collection of cryogenic absorbance spectra to measure pigment energy levels, and the collection of cryogenic fluorescence spectra and room temperature picosecond time resolved fluorescence decay spectra to study excitation energy transfer and dissipation. Chemical inhibitors that target the trans-thylakoid pH gradient, the enzyme responsible for diadinoxanthin de-epoxidation, and photosynthetic electron flow were additionally used to experimentally manipulate the NPQ response. Multifaceted analyses of the NPQ responses from two previously un-photosynthetically characterised species, *Nitzschia curvilineata* and *Navicula sp*., were used to identify an excitation pressure relief 'strategy' for each species. Three key areas of NPQ were examined: (i) the NPQ activation/deactivation processes, (ii) how NPQ affects the collection, dissipation, and usage of absorbed light energy, and (iii) the interdependence of NPQ and photosynthetic electron flow. It was found that *Nitzschia* cells regulate excitation pressure via performing a high amplitude, reversible antenna based quenching which is dependent on the de-epoxidation of diadinoxanthin. In *Navicula* cells excitation pressure could be effectively regulated solely within the PSII reaction centre, whilst antenna based, diadinoxanthin de-epoxidation dependent quenching was implicated to be used as a supplemental, long-lasting source of excitation energy dissipation. These strategies for excitation balance were discussed in the context of resource partitioning under these species' originating light climates. A more detailed investigation of the NPQ response in *Nitzschia* was used to develop a comprehensive model describing the mechanism for antenna centred non-photochemical quenching in this species. The experimental evidence was strongly supportive of a mechanism whereby: an acidic lumen triggers the diadinoxanthin de-epoxidation and protonation mediated aggregation of light harvesting complexes leading to the formation of quencher chlorophyll *a*-chlorophyll *a* dimers with short-lived excited states; quenching relaxes when a rise in lumen pH triggers the dispersal of light harvesting complex aggregates via deprotonation events and the input of diadinoxanthin. This model may also be applicable for describing antenna based NPQ in other diatom species.

Table of Contents

Abbreviations

CET, cyclic electron transport

Chl, chlorophyll

DCCD, N,N'-Dicyclohexylcarbodiimide

DCMU, 3-(3,4-dichlorophenyl)-1,1-dimethylurea

DD, diadinoxanthin

DT, diatoxanthin

DTT, dithiothreitol

FCP, fucoxanthin chlorophyll protein

Fm_{dark}, maximal fluorescence level attained in dark adapted cells with the application of a saturating light pulse

Fm', maximal fluorescence level attained in cells with the application of a saturating light pulse

Fo_{dark}, basal fluorescence level attained in dark adapted cells prior to application of a saturating light pulse

Fo', basal fluorescence level attained in cells after the application of a saturating light pulse during illumination (measured without illumination with the application of weak far-red light)

Ft, transient fluorescence level

FWHM, full width at half maximum

Fx, fucoxanthin

HL, 'high light', meaning illumination at an irradiance level that saturates the pre-existing photosynthetic capacity (i.e. 'excess light')

LHC, light harvesting complex

MDGD, monogalactosyldiacylglycerate

MV, methyl viologen

NADPH, Nicotinamide adenine dinucleotide phosphate

NPQ, non-photochemical quenching (of chlorophyll fluorescence)

$\mathcal{NPQ}$, The Stern-Volmer fluorescence quenching parameter

PAM, Pulse amplitude modulation

Pheo, pheophytin

PQ, plastoquinone

PSI, photosystem I

PSII, photosystem II

Q_A, quinone A

Q_B, quinone B

qE, non-photochemical excitation energy dissipation induced by energization of the thylakoid

qE_{nonXC}, qE not directly dependent on xanthophyll cycle pigments for induction and relaxation

qE_{XC}, qE directly dependent on xanthophyll cycle pigments for induction and relaxation

qP, coefficient of photochemical quenching

S.D., standard deviation of the mean

S.E., standard error of the mean

ΔpH, the trans-thylakoid proton gradient

σPSII, effective PSII absorbance cross section

ΦPSII, maximum quantum efficiency of PSII photochemistry

ϕPSII, effective quantum efficiency of PSII photochemistry

~, approximately

Index of Figures & Tables

Figures

Tables

pg.

1 Background Information

1.1 Diatoms are globally important

Diatoms (Phylum: Heterokontophyta, Class: Bacillariophyceae) are an extremely diverse and widespread group of planktonic and benthic algae; they are only second to higher plants in number of species (Mann 1999) and are one of the most rapidly evolving eukaryotic taxa on Earth (Oliver et al. 2007). Diatoms are split into two extant clades distinguishable by body plan: the bilaterally symmetric pennate species (Order: Pennales) and the ancestral radially symmetric centric species (Order: Centrales). Complete genome sequences are now available for a pennate (*Phaeodactylum tricornutum*) (Bowler et al. 2008) and centric diatom (*Thalassiosira pseudonana*) (Armbrust et al. 2004). Diatoms are found in all marine and freshwater ecosystems (Round et al. 1990) and form the foundation of many of the Earth's ecosystems, including the economically important fisheries found in coastal up-welling areas (Falkowski et al. 1998) and polar sea ice communities (Gleitz et al. 1998, Vardi et al. 2008). Diatoms are also important constituents of terrestrial algal communities ranging from the cryptogrammic crusts of arid lands to salt flats to polar soils (Broady 1996, Johansen 1993, Kirkwood and Henley 2006, Potter et al. 2006, Van de Vijver et al. 2002, van Kerckvoorde et al. 2000).

Global energy and nutrient cycles, and climate are intimately tied to diatom biology. More than 40% of aquatic primary production, corresponding to 25% of the Earth's yearly primary production, is provided by diatoms (Smetacek 1999). Diatoms affect the biogeochemical cycles of nitrogen and silica (a major component of diatom cell walls) (Sarthou

et al. 2005, Smetacek 1999). Diatoms act as effective carbon sinks in the ancient and modern oceans (Falkowski et al. 1998, Fry et al. 1996, Sarthou et al. 2005) with their fossilized remains being a major source of petroleum (Vardi et al. 2008). The contribution of diatoms to phytoplankton communities may only increase in the future as there is an increase in land dust deposal (a source of silica) into the oceans (Tréguer and Pondaven 2000) and acidification of the ocean may decrease competition from coccolithophores (algal group with a calcium carbonate exoskeleton) (Beaufort et al. 2011). Since many diatom species excrete lipids, they have been considered as a potential source of bio-fuel (Demirbas and Fatih Demirbas 2011).

1.2 The diatom approach to photosynthesis

1.2-1 Overview

Diatoms are derived from secondary symbiosis of a heterokont eukaryote host cell with a red algal type ancestor, which makes diatom metabolism (and their close relatives, the Phaeophyceae) quite distinct from the green algal lineage (Chloroplastida). Some of the particularities of their ancestry that affect photosynthesis (as reviewed by Wilhelm et al. 2006) include: transport across plastids with four outer membranes, no grana thylakoid arrangement, no Rubisco activase or thioredoxin regulation of the Calvin Cycle, cytochrome C_{553} replaces the intersystem electron carrier plastocyanin, the light-harvesting proteins (FCPs) contain a large proportion of carotenoid (principally fucoxanthin (Fx)) in addition to Chl *a* and replace Chl *b* with Chl *c*, the xanthophyll cycle involves a one-step de-epoxidation of diadinoxanthin (DD) to diatoxanthin (DT), and the energy storage products of photosynthesis are lipids and chrysolaminarin that are stored outside of the plastid. Centric diatoms generally have many

small chloroplasts, whereas pennates have one to several large chloroplasts. The thylakoids are grouped loosely in stacks of three and surrounded by an inner 'girdle stack' of three thylakoids inside the four membrane envelope (Lavaud 2007). Due to the absence of granal stacks and stroma lamellae, the photosystems and light harvesting complexes are believed to be distributed homogenously. However, specific thylakoid membrane domains might exist in diatoms as proposed by Lepetit et al. (2010), where the thylakoid membrane may be differentiated based on lipid composition. Regions composed of negatively charged lipids such as sulfoquinovosyldiacylgylcerol (SQDG) and phosphatidylglycerol could intersperse with the monogalactosyldiacylglycerol (MGDG) regions that are enriched in FCPs, DD and DT (Lepetit et al. 2010). Even though MGDG does not form bilayers, it is the most common polar lipid in thylakoid membranes (Gounaris and Barber 1983). MGDG is thought to give the lipid matrix fluidity to facilitate the diffusional processes of photosynthetic electron transport and optimise packing of the large membrane intrinsic proteins of the thylakoid (Gounaris and Barber 1983).

Photosynthetic efficiency in diatoms is enhanced by their abilities to shuttle inorganic carbon to the carbon fixation reactions. Diatoms contain form 1D Rubisco, the least O_2 sensitive form, and have been shown to actively engage in carbon concentrating mechanisms by importing bicarbonate ion and CO_2 (as reviewed by Giordano et al. 2005 and Wilhelm et al. 2006). Diatoms have been traditionally regarded as C3 photosynthesizers, but recent metabolic labeling and genome sequencing data suggest that some are capable of performing C4 photosynthesis (malate type), as has been observed in *Thalassiosira weissflogii* (Reinfelder et al. 2000, Roberts et al. 2007).

1.2-2 Photosynthetic pigments

The characteristic yellow-brown (gold) colour of diatoms is from their high carotenoid content and absence of Chl *b*. Chl *c* (present as Chl c_1, c_2, and/ or c_3) lacks the lipid tail, has higher symmetry, and different ionic properties than Chl *a* (Figure 1.1). Compared to Chl *a*, Chl *c* has a much weaker and blue shifted Q_y transition (around 636 nm *in vivo*), but has a more intense 25 nm red shifted Soret band (Figure 1.1). Diatoms are only able to synthesize carotenoids derived from the β-carotene pathway and not from α-carotene (Bertrand 2010). Fx is the major light harvesting carotenoid. Fx possesses an unusual carotenoid structure with low symmetry and a conjugated carbonyl group (Figure 1.1). This low symmetry makes the energy levels of Fx particularly sensitive to Coulombic interactions with its environment resulting in high sensitivity to solvent polarity (Frank et al. 2000) and protein environment. Distortions and red shifts by the protein environment *in vivo* result in mixing of the S_1 and S_2 states, enhancement of the S_1 transition dipole, and enhanced coupling of the optically 'forbidden' S_1 state to Chl *a* Q_y state (Macpherson and Hiller 2003). There is a large red shift in absorbance between the unbound (maximum at 460 nm) and protein bound (between 520 and 560 nm) forms of Fx (Lavaud 2007). DD and DT are additional important carotenoids. During transitions to 'high light', DD is rapidly de-epoxidised to DT, functioning in the photoprotective regulation of light absorption and dissipation. (The abbreviation 'HL' for 'high light' is used throughout this body of work and refers to illumination at irradiance greater than that to which the photosynthetic organism has been pre-acclimatized.) DD may have some limited light harvesting capabilities as well (Lavaud et al. 2003). High irradiance or intermittent light culture conditions can enhance DD and DT at the expense of Fx (and maybe Chl *c*) (Lavaud et al. 2003, Lavaud 2007). Labeling kinetics of carotenoid synthesis suggest that DD is a precursor of Fx

(Lohr and Wilhelm 2001). The evolutionary acquisition of Chl *c* and Fx in diatoms is believed to be an adaptive advantage to maximise the harvesting of blue-green light penetrating the water column (Macpherson and Hiller 2003).

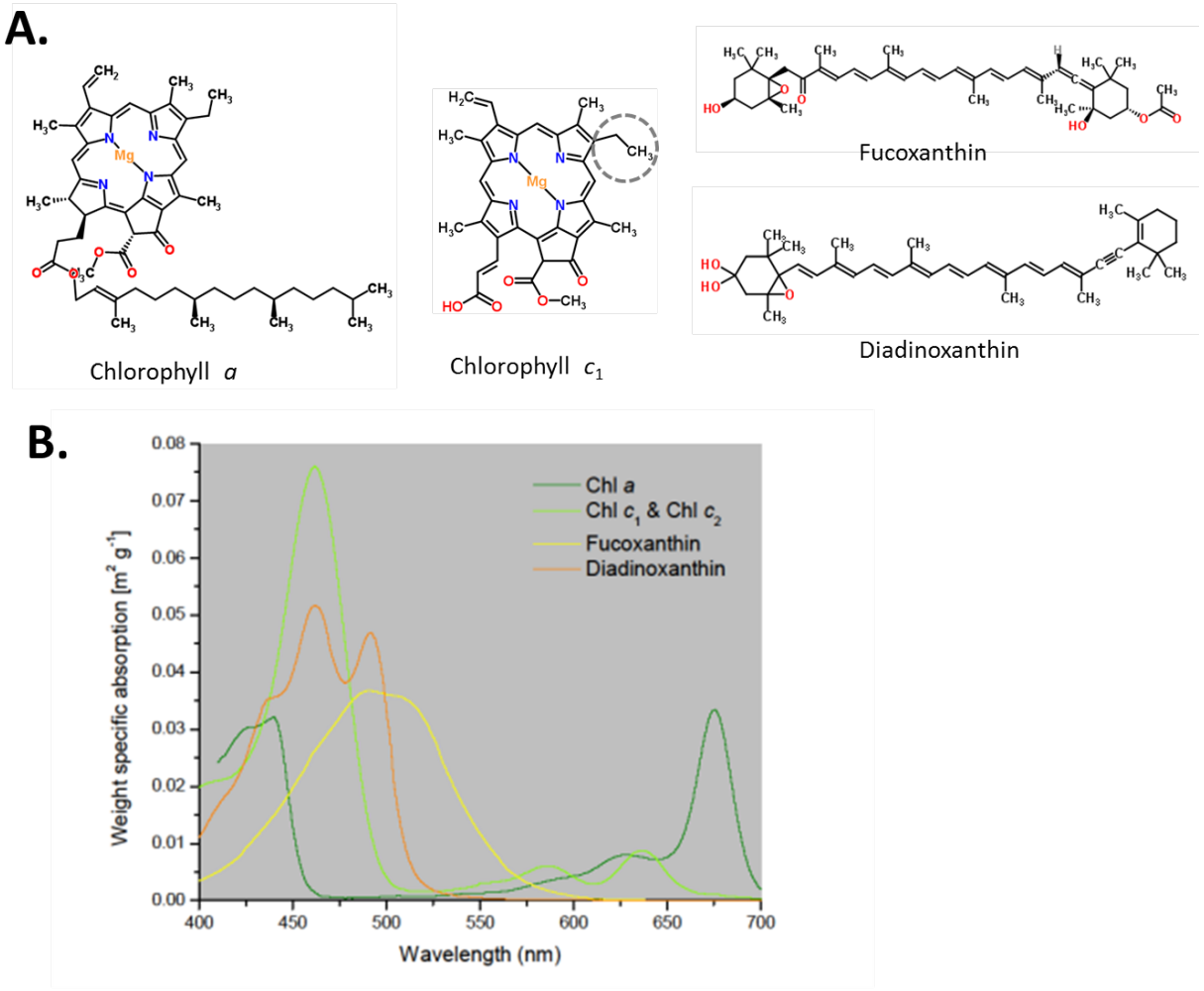

Figure 1.1 The light harvesting pigments in diatoms. A, Chemical structures. Chl c_2 substitutes the functional group -CH_2-CH_3 in Chl c_1 with -CH=CH_2 (circled). **B, Simulated absorbance spectra** of the pigments when protein bound *in vivo* according to Bricaud et al. (2004). The spectrum for Chl *c* is a combination of Chl c_1 and Chl c_2.

The DD pool is functionally and spatially heterogeneous. There are two distinct sub-pools, one capable of conversion to DT and one not. The low turnover DD pool generally comprises about half of the total DD (dependent on species) and is insensitive to culture light regimes (Lohr and Wilhelm 2001, Lavaud 2007, Lepetit et al. 2010). These DD molecules are

believed to be constitutive of the FCP and have a light harvesting function (Lavaud et al. 2003, Guglielmi et al. 2005). The high turnover DD pool is responsive to light regimes and contains DD molecules that (i) are involved in the rapid DD to DT de-epoxidation during transitions to HL and (ii) appear as 'free' pigments in the lipid matrix (Lepetit et al. 2010). Specific FCP monomers bind DD at the periphery of the light harvesting complexes, in so permitting access by DD de-epoxidase during the transition to HL (Lepetit et al. 2010). Free DD may provide a photoprotective role by preventing lipid peroxidation during times of oxidative stress and stabilizing the thylakoid (Lepetit et al. 2010, Schumann et al. 2007) and also would serve as a precursor reservoir for Fx synthesis (Lohr and Wilhelm 2001, Lavaud 2007).

1.2-3 Light harvesting complexes

The light harvesting antenna system of diatoms is composed of the multimeric integral membrane pigment-protein complexes termed FCPs (Fucoxanthin Chlorophyll Protein). FCP polypeptides show high sequence similarity between diatom species and with the FCPs from brown algae (Green 2003). *fcp* gene products are encoded in the nucleus and have to cross four membranes to reach the thylakoids, requiring two steps of processing during translocation into the plastid (Gruber et al. 2007). FCPs can be classified into three main groups: (i) the classical light harvesting complex proteins called LhcF, (ii) the red algal LHC I related proteins called LhcR, and (iii) LhcX that are related to the ancient LI818 light inducible member of the LHC superfamily (Green 2007, Bailleul et al. 2010). LhcX has been implicated with having photoprotective roles in diatoms (Bailleul et al. 2010). FCP apoproteins are of a lower molecular weight (between 17 and 22 kDa) as compared to higher plant LHCII (~27 kDa), with the hydrophilic loop regions connecting the helices being shortened in FCPs (Lavaud 2007).

FCPs seem to form LHCs as either trimers or higher oligomers, which may or may not contain more than one type of FCP (as reviewed by Lavaud 2007, Veith et al. 2009). FCP composition and organization have been most thoroughly described in *Phaeodactylum tricornutum* and *Cyclotella meneghiniana* with two major FCP fractions isolated in both species, LHCF F and LHCF D (Guglielmi et al. 2005) and FCPa and FCPb (Büchel 2003), respectively. LHCF F contains Chl *a*, Chl *c*, and Fx but no DD, whereas LHCF D contains Chl *a*, Fx, and DD but no Chl *c* (Guglielmi et al. 2005). FCP complexes in *P*. *tricornutum* are found as trimers or hexamers (Lepetit et al. 2007). FCPa forms trimers and can be quenched *in vitro* with DT (Gundermann and Büchel 2012), while FCPb forms higher order oligomers and is unaffected by the DD cycle (Büchel 2003).

FCPs are enriched in carotenoids. The Chl *a*: carotenoid stoichiometry is 1:1 in contrast to a 2:1 ratio observed in plant LHCII. There is no x-ray crystal structure for diatom FCPs, so protein structure and pigment placement is still somewhat uncertain. According to sequence homology, FCPs are composed of three membrane spanning helices. The 'standard' pigment stoichiometry for FCPs has been reported as 4 Chl *a* : 4 Fx : 1 Chl *c* (de Martino et al. 1997) but can vary significantly depending on the particular FCP and culturing light conditions with substitution of Fx with DD and DT and/ or enrichment with DD and DT (Guglielmi et al. 2005, Veith et al. 2009, Juhas and Büchel 2012, Gundermann et al. 2013). Wilhelm et al. (2006) built a model for pigment binding within FCP using sequence comparison and spectroscopy results: Helices 1 and 3 have the homology to higher plant LHC and in so are believed to similarly bind the Chl molecules; two Fx molecules are predicted to fulfill the same stabilizing structural role of lutein in higher plant LHCII (binding to the crossed helices 1 and 3). Premvardhan et al. (2010) presented a modernised structure for FCP pigment binding. Based on FCPs from

Cyclotella meneghiniana (FCPa trimers and FCPb oligomers) they determined via sequence homology with plant LHCII and resonance Raman spectroscopy measurements that the Wilhelm et al. (2006) model needs to be radically changed. Premvardhan et al. (2010) presented a model that nearly doubles the pigment content per FCP as previously thought, with 18 pigments per FCP monomer (8 Chl *a*, 8 Fx, 2 Chl *c*). This model of FCP complexes from *Cyclotella meneghiniana* including pigment positions is given in Figure 1.2.

The antenna pigments within FCPs show different degrees of energy transfer coupling to the Chl *a*s. Chl *c* to Chl *a* energy transfer has been found to be rapid (100 femtoseconds) and 100% efficient (Papagiannakis et al. 2005) supporting a close positioning of Chl *c* to Chl *a*. As such, Chl *c* does not fluoresce in FCPs (Di Valentin et al. 2012). Energy transfer from Fx to Chl *a* is dominated by S_1 to Q_y coupling (Macpherson and Hiller 2003). Fx may or may not be able to transfer energy to Chl *c* (Papagiannakis et al. 2005, Szabó et al. 2008, Di Valentin et al. 2012). The Fx populations appear to be heterogeneous in terms of the bathochromic shift induced by their protein environment. They are loosely identified by the colour of their maximal absorbance wavelength, such as Fx_{blue}, Fx_{green}, and Fx_{red} (Gildenhoff et al. 2010, Gundermann et al. 2013, Szabó et al. 2010). In FCP from *Cyclotella meneghiniana* there are at least 6 different Fxs buried in the protein, each with separate absorption maxima ranging from 453 to 510 nm (Premvardhan et al. 2010), although there is further evidence of red shifting up to ~550 nm (Juhas and Büchel 2012). Additional Fx molecules are likely to be loosely bound to the periphery of FCP trimers (Premvardhan et al. 2010). There is also heterogeneity reported on the energy transfer coupling between Fxs and Chl *a*, with some Fxs tightly coupled to Chl *a* while others are poorly coupled. Circular dichroism spectra of isolated FCPs from *Cyclotella*

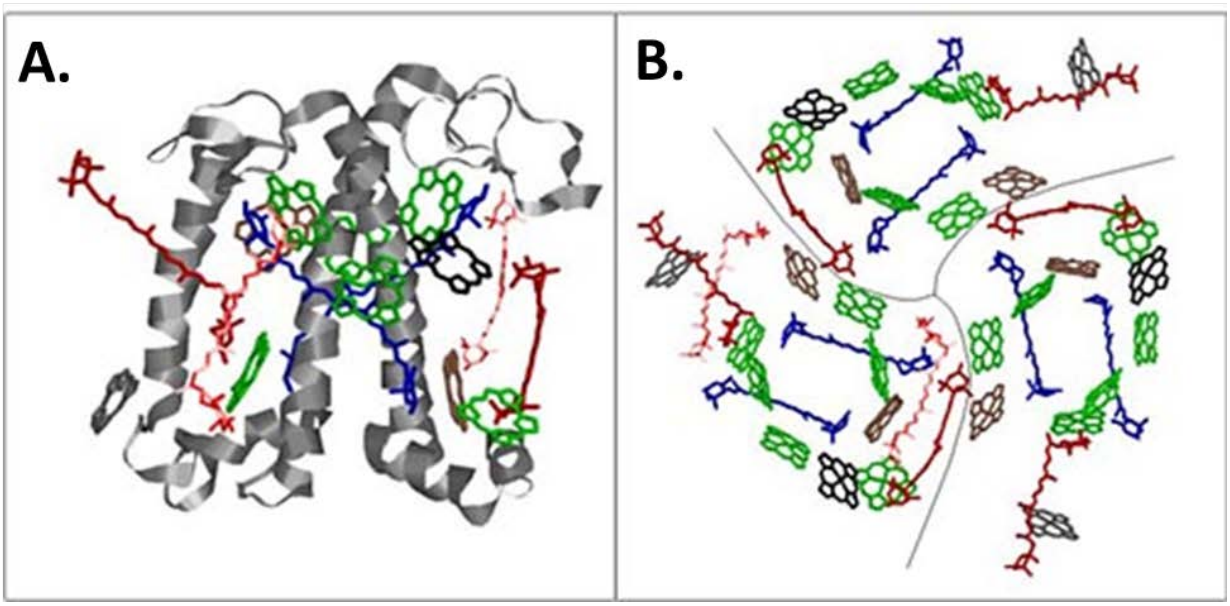

Figure 1.2 Model of FCP from *Cyclotella meneghiniana* including pigments shown as a monomer (side view, **A**) or trimer (stromal view, **B**). Chlorophyll *a* molecules are drawn in green, chlorophyll *c* in brown, high energy fucoxanthins are drawn in blue, low energy fucoxanthins are drawn in red, and black and grey chlorophyll *a* molecules refer to chlorophylls present in oligomeric FCP (FCPb) but absent in trimeric FCP (FCPa). Wavelength positions for maximum absorbance of the individual fucoxanthin molecules per monomer are at 453, 463, 492, 505, 510 nm, one fucoxanthin binding site can be mixed with diadinoxanthin binding giving a mixed absorbance maximum at 488 to 492 nm. Figure adopted from Premvardhan et al. (2010).

meneghiniana and *Phaeodactylum tricornutum* have a characteristic split signal at ~440 and ~467 nm indicating a Chl *a*-Fx excitonic dimer (Büchel 2003, Joshi-Deo et al. 2010). Gildenhoff et al. (2010) and Szabó et al. (2010) confirmed excitation energy transfer between two colours of Fx and Chl *a* in isolated trimeric FCPa complexes from *Cyclotella meneghiniana,* with red forms preferentially transferring excitation energy to PSII. Di Valentin et al. (2012) observed using optically detected magnetic resonance spectroscopy that at least one of the Fx in FCP from *Cyclotella meneghiniana* is poorly coupled to Chl *a*. The earlier work by Papagiannakis et al. (2005) also suggested that some Fxs are not coupled to Chl *a*. Fx has recently been shown to be able to directly quench Chl *a* triplet states as measured using optically detected magnetic resonance (ODMR) in isolated FCP from *Cyclotella meneghiniana*, somewhat homologous to

triplet–triplet energy transfer that occurs between Chl *a* and carotenoids in LHCII from higher plants, but only ¼ of Fx in FCP can quench triplet Chl *a* (Di Valentin et al. 2012).

Improved separation and biochemical methods give growing evidence towards PSII and PSI specific FCPs. The photosystems in diatoms have traditionally been thought to share a common antenna system due to no grana stacking. Such a view was supported by the biochemical analysis by Brakemann et al. (2006) in *Cyclotella cryptica*. Veith et al. (2009) points out that the study by Brakemann et al. (2006) did not use specific enough antibodies to distinguish between different FCPs when testing the FCP-photosystem fractions and is thus inconclusive. The occurrence of LHC1-like *fcp*s (LhcR) has been used as theoretical evidence for PSI specific FCP. Because FCPs possess high sequence similarities, have small differences in molecular weight, and are strongly hydrophobic, it has been a challenge to differentiate between polypeptides by immunological methods or sequencing (Veith et al. 2009). Veith et al. (2009) using *Cyclotella meneghiniana* was able to isolate PSII-FCP and PSI-FCP fractions identifying FCP complexes for PSII (trimeric FCPa complex of 18 kDa Fcp2 and Fcp6) and PSI (LHC1 related FCP4 and an undescribed 17 kDA FCP are tightly coupled to PSI; high oligomeric FCPb complexes composed of 19 kDa Fcp5 are loosely bound). In *Phaeodactylum tricornutum* there are also LHCI-like FCP monomers that are found physically and functionally tightly coupled with PSI (Veith and Büchel, 2007). Lavaud (2007) suggests that the observation of different subunit compositions for trimeric and higher oligomers of FCP LHCs between *Phaeodactylum tricornutum* and *Cyclotella meneghiniana* is indicative that diatom LHC organization may be species specific. The varying degree of coupling between FCP complexes and photosystems found during isolation procedures (as determined by polypeptide

composition and sensitisation of photosystem fluorescence with FCP pigment excitation) (Veith et al. 2009, Nagao et al. 2010, Juhas and Büchel 2012) suggests that, in a manner analogous to the light harvesting complexes in higher plants, the FCP complexes in diatoms are also functionally and physically separated into minor and major LHC populations.

1.3 Excitation Pressure

1.3-1 Excitation pressure defined

Environmental and physiological conditions favoring a higher rate of excitation energy (energy from pigment photon absorption events) reaching the PSII reaction center special Chl *a* pair (P680) than can be dissipated via photochemistry, leads to heightened 'excitation pressure' on PSII. Excitation pressure is formally defined as the relative measure of the reduction state of the first stable electron acceptor during PSII photochemistry (Q_A) (excitation pressure = $[Q_A^-]$ / $[Q_A]$ +$[Q_A^-]$) (Huner et al. 1998). Excitation pressure can be measured non-invasively using Chl *a* fluorometry and the photochemical quenching parameter (qP). qP represents the proportion of PSII reaction centers in an open state capable of performing photochemistry (Tyr_Z P680 Pheo Q_A Q_B). Excitation pressure can then be quantified as 1–qP, representing the proportion of PSII reaction centers in a closed state (Tyr_Z $P680^+$ Pheo Q_A^- Q_B) (Huner et al. 1998).

1.3-2 Photoinactivation & photoinhibition

When a closed PSII reaction centre is excited with light energy, damage may occur to the surrounding protein milieu, especially D1 (PsbA), through the process of photoinactivation. In an aerobic environment P680* can reduce molecular oxygen to form the superoxide anion radical ($^{\bullet}O_2^-$), and excited state triplet Chl *a* (^{3}Chl*a**) can excite O_2 to form singlet oxygen ($^1O_2$)

(Asada 1996). Additionally, $^{\bullet}O_2^-$ and/ or other reactive oxygen species such as the hydroxyl radical ($^{\bullet}OH$) and hydrogen peroxide have the potential to form during any of the electron transfer steps at both the donor and acceptor sides of the reaction centre (Pospíšil 2012). These reactive oxygen species cause oxidative damage to the amino acid residues and pigments of PSII and auto-oxidation of lipids within the surrounding matrix. The constitutive carotenoids of PSII limit photoinactivation by scavenging singlet oxygen and trapping triplet Chl (Martinez-Junza et al. 2008). When D1 photoinactivation exceeds D1 turnover, photoinhibition occurs and there is a net loss in PSII functionality (Murata et al. 2007).

1.3-3 PSII excitation vs. de-excitation

Excitation pressure is a measure of the balance between PSII excitation and de-excitation pathways. PSII excitation is dependent on the effective absorbance cross section (σPSII) and incident photon flux, whereas de-excitation is dependent on the redox state of the photosynthetic electron transport chain. There are multiple sources for electrons to enter and exit the photosynthetic electron transport chain within diatom chloroplasts. Sources include photochemistry and chlororespiration (Lavaud et al. 2002b, Armbrust et al. 2004); sinks include carbon and nitrite reduction (Lomas and Glibert 1999), photorespiration (Schnitzler Parker et al. 2004), and O_2 (the generation of reactive oxygen species which may be either 'controlled', as during the Mehler Reaction (water-water cycle) (Claquin et al. 2004), or uncontrolled). Since the 'fast' events of photon absorption, energy transfer within the pigment pool, and charge separation by PSII and PSI reaction centres occur at rates several orders of magnitude faster than the 'slow' processes of electron transport and metabolism, it is relatively easy for the two processes to become disjoined. Any factor disrupting this equilibrium leads to elevated

excitation pressure. Thus at the functional level, the photosynthetic apparatus does not discriminate between stressors affecting the 'fast' and 'slow' photosynthetic reactions.

1.3-4 Excitation pressure dissipation

The most ubiquitous mechanisms to combat heightened excitation pressure during short term stress transitions (seconds to several minutes timescale) are those mechanisms collectively described as contributing to NPQ (non-photochemical quenching of Chl fluorescence). NPQ can be readily quantified using PAM fluorometry by measuring the drop in maximal PSII Chl *a* fluorescence yield in the presence of background HL, as compared to the maximal PSII Chl *a* fluorescence measured prior to HL illumination. NPQ is quantified from PSII maximal fluorescence with the application of a 'multiturnover' saturating light pulse. The Stern-Volmer non-photochemical fluorescence quenching parameter is most commonly used for measuring NPQ: $\mathcal{NPQ} = (Fm_{dark} - Fm')/Fm'$, where Fm_{dark} denotes maximal fluorescence under dark adapted conditions and Fm' denotes maximal fluorescence under illumination conditions (Bilger and Björkman 1990). The saturating light pulse excites P680 at a rate faster than forward electron transport, which results in a lowering of the first order reaction rate of PSII de-excitation via photochemistry favoring de-excitation via the competitive pathway of radiative decay. Because the saturating light pulse effectively inhibits fluorescence quenching via photochemistry, any loss in the fluorescence signal during illumination from that preceding the illumination must be due to non-photochemical forms of energy dissipation.

NPQ is a very heterogeneous phenomenon both kinetically and mechanistically. NPQ has traditionally been described as having three components: qE (dependent on energization of the thylakoid and typically involving a 'xanthophyll cycle'), qT (the state transition, where

excitation balance of PSII to PSI is brought about via structural rearrangement of antenna complexes), and qI ('non-relaxable' quenching due to photoinhibition of PSII cores), all combining to lower the amount of absorbed light energy that reaches functional PSII reaction centres (Ruban et al. 2012). qE and qT are the fast inducing and rapidly reversible forms of NPQ, turning on and off over the seconds to several minutes time scales. qE and qT are not concurrently regulated by gene expression, but are controlled by reversible enzymatic activity. qE is triggered by the trans-thylakoid pH gradient (ΔpH), whereas qT is triggered by the redox state of the PQ pool (Ruban et al. 2012). Some variety of NPQ has been observed in O_2 evolving photosynthetic organisms ranging from cyanobacteria to eukaryotic algae to lower and higher plants (Horton and Ruban 2005, Goss and Jakob 2010, Niyogi and Truong 2013). NPQ also shows a high level of diversity both within and between photosynthetic taxonomic groups (Horton and Ruban 2005, Goss and Jakob 2010), suggesting a long history of strong evolutionary pressure to flexibly alleviate excitation pressure (Niyogi and Truong 2013).

The qE mechanism in higher plants has been investigated thoroughly (as reviewed by Horton and Ruban 2005, Horton et al. 2005, Ruban et al. 2007, Ruban et al. 2012, Jahns and Holzwarth 2012). There are four constituents to the qE 'scenario': 1) the trigger (protons), 2) site of action (antenna or reaction centre), 3) mechanics (antenna/ protein conformational changes), and 4) the quenchers (Chl *a* or carotenoids) (as reviewed by Ruban et al. 2012). The most dominant type of qE in higher plants targets the antenna complexes and is described hereafter. The transition to excess light acidifies the chloroplast lumen, activating violaxanthin de-epoxidase that then performs a two-step de-epoxidation of violaxanthin into antheraxanthin into zeaxanthin (Johnson et al. 2008). Dithiothreitol (DTT) is an inhibitor of the de-epoxidation

(Yamamoto and Kamite 1972) and is experimentally used to distinguish between xanthophyll cycle dependent NPQ and other forms of energy dissipation. Violaxanthin de-epoxidase is a lipocalin protein with a central barrel structure flanked by cysteine rich N-terminal and glutamate rich C-terminal ends; it is regulated by the protonation of the glutamic acid-rich domain and by the protonation of histidine residues located in the lipocalin region (Bugos and Yamamoto 1996, Hieber et al. 2002, Gisselsson et al. 2004). The N-terminal domain is rich in cysteine residues and is the predicted reducing site for DTT (Hieber et al. 2002). The X-ray structure of violaxanthin de-epoxidase crystals formed at pH 5 shows that dimerization of the water soluble monomers under acidic conditions initiates enzyme binding to the thylakoid lumenal surface and exposes the catalytic site (Arnoux et al. 2009).

Zeaxanthin is currently understood to be an allosteric regulator of the PSII light harvesting antenna, inducing conformational changes in the antenna system that favour pigment-pigment interactions conducive to non-radiative 'concentration dependent' quenching of pigment excited states (Horton and Ruban 2005, Horton et al. 2005). Three quenching domains and a zeaxanthin allosteric site have been identified within LHCII which are supportive of Chl *a*-Chl *a* interactions and Chl *a*-carotenoid interactions (as reviewed by Horton et al. 2005). Isolated LHCII trimers self-quench upon aggregation/ oligomerization and exhibit a characteristic relative loss in short wavelength emission (loss in 'F680') coupled to a relative increase in long emissions (gain in 'F700'), which has been interpreted as the formation of a poorly fluorescing Chl *a*–Chl *a* mixed exciton charge transfer state (see Miloslavina et al. 2008, Andreeva et al. 2009). The PsbS protein is required for qE in plants and is believed to be a pH sensor (via protonation of lumenal loop glutamate residues) that promotes quenching

interactions within the thylakoid (Li et al. 2004, Horton and Ruban 2005, Horton et al. 2005). qE relaxes when luminal pH rises to the level that PsbS deprotonates and violaxanthin de-epoxidase is deactivated, thereby permitting the constitutively active zeaxanthin epoxidase to cause a net conversion of zeaxanthin back to violaxanthin; PsbS deprotonation and zeaxanthin epoxidation induce the switching of the antenna system from light energy dissipation mode back to light harvesting mode (Horton and Ruban 2005). In this communication, qE directly dependent on the xanthophyll cycle is referred to as qE_{XC}.

qE_{XC} in plants can be induced without the concurrent conversion of violaxanthin into zeaxanthin, if there is a pre-existing accumulation of zeaxanthin. Once excess light is removed, NPQ relaxes rapidly (within 5 to 10 minutes) due to the dissipation of ΔpH and deprotonation of PsbS, and this relaxation does not necessarily require the conversion of zeaxanthin back to violaxanthin (Ruban et al. 2004). If the NPQ response is pumped with multiple illumination cycles, in a manner such that ΔpH is allowed to drop post illumination but with a limited epoxidation of zeaxanthin (as via a short transition away from the excess light), it is noticed that quenching is induced faster during subsequent illumination cycles (Ruban et al. 2004). These observations were taken as excellent *in situ* support for the allosteric role of zeaxanthin (Ruban et al. 2004). When zeaxanthin levels are elevated by a period of pre-illumination, subsequent HL treatment results in faster NPQ induction because the developing ΔpH can immediately activate quenching (via protonation of PsbS) without having to wait for the slower catalytic action of the violaxanthin de-epoxidase to transform the arrangement of the thylakoid into quenching mode.

Continual excitation pressure leads to structural changes to the photosynthetic machinery that are brought about by protein synthesis. Sustained high excitation pressure initiated by excess light, cold stress, or by artificially manipulating the redox state of the photosynthetic electron transport chain has been shown to induce pigmentation changes within the chloroplasts of higher plants, green algae, cyanobacteria, and diatoms (Escoubas et al. 1995, Lavaud 2007, Rosso et al. 2009, Wilson et al. 2003). It is hypothesised that the chloroplast redox state initiates a signal transduction pathway that is able to regulate photosynthetic gene expression, nuclear expression of stress related genes, plant morphology, and cyanobacteria cell differentiation (Huner et al. 1998). The reduction in the expression of light harvesting polypeptides and a concatenate increase in photoprotective proteins observed under prolonged periods of high excitation pressure are believed to be a response by photosynthetic organisms for limiting the probability of excitons (mobile 'particles' of absorbed photon energy that can diffuse through the pigment pool via energy transfer processes) reaching closed PSII reaction centres. Photostasis is achieved when the absorption of photons and the production of electrons by photochemistry are in balance with the dissipation of absorbed light energy through NPQ and electron use by metabolism/ growth (Rosso et al. 2009).

1.4 Fast Regulation of Excitation Energy by Diatoms

1.4-1 Success with fluctuating light

Both benthic and planktonic diatoms dominate over other algal groups in marine and fresh water turbulent environments such as coastal areas and estuaries (Lavaud 2007).

Phytoplankton, especially those without flagella, are slaves to the motions of the water column that they inhabit. Aquatic environments with turbulent waters (i.e. currents, water churned by wave/ tidal actions) have high rates of mixing through the water column. The underwater light climate that a phytoplankter experiences is dependent on its depth and the optical properties of the above water column, which can vary greatly depending on turbidity and phytoplankton composition. During times of mixing, plankton previously habituated to highly attenuated, nearly dark light environs can be transported to the surface and exposed to full sunlight (with ultraviolent components) in a time period of seconds to a few minutes (Raven and Geider 2003). These rapid changes in light intensity are stressful to the photosynthetic apparatus and can lead to photodamage. High mixing rates of the water column have been shown to decrease the primary productivity of phytoplankton by up to 25% (Falkowski and Raven 1997).

The growth rate and photosynthetic capacity of diatoms are less affected by light fluctuations than other groups of algae, whether measured in the laboratory (Mitrovic et al. 2003) or in the field (Petersen et al. 1998). Diatoms must contain an especially robust and/ or flexible photosynthetic apparatus that can cope with a fast (tens of seconds) fluctuating supply of incident light energy. Furthermore, the photoprotective mechanisms for handling transitions to excess light must be highly effective in diatoms, since diatoms show a higher resistance to photoinactivation when compared to other algal groups (Key et al. 2010).

1.4-2 Intro to diatom NPQ

NPQ in diatoms is dominated by qE. Diatoms have traditionally been considered not to perform qT (Ting and Owens 1993, Lavaud 2007), although the picosecond fluorescence decay kinetics study by Miloslavina et al. (2009) suggested that a minor amplitude state transition

may occur in *Phaeodactylum tricornutum* and *Cyclotella meneghiniana*. Diatom qE seems to use the same fundamental processes as plant qE. Acidification of the lumen activates DD de-epoxidase that performs the one step de-epoxidation of DD to DT. When ΔpH drops, DT epoxidase epoxidises DT to DD. NPQ induction requires both DD de-epoxidation and ΔpH (Lavaud 2007, Goss and Jakob 2010). There is no PsbS in diatoms (Niyogi and Truong 2013) to sense the pH changes in the lumen. Members of the light-harvesting complex stress-related protein family LI818 have been identified in diatoms (as LhcX) and their expression levels are responsive to irradiance and NPQ capacity (Bailleul et al. 2010), but LhcX expression upon transition to excess light was on a time scale too slow to be directly responsible for inducing NPQ. LI818 proteins in green algae, like PsbS in higher plants were shown to have lumenal exposed DCCD binding glutamate residues for service as pH sensors (Li et al. 2002b, Bonente et al. 2011). LhcX proteins in diatoms have been thought to fulfill the pH sensing role of PsbS within the diatom NPQ mechanism (Bailleul et al. 2010; see Figure 1.3). The LhcX member Fcp6 from *Cyclotella meneghiniana* binds DD/DT and can be found integrated within FCP complexes (Gundermann and Büchel 2012). In such, LhcX would provide the linkage between FCP, ΔpH, and DD/DT conversion during diatom qE.

Diatoms are able to perform qE at higher amplitudes than what is observed in most plants and other algae (Ruban et al. 2004, Lavaud 2007). Stern-Volmer NPQ values ($\mathcal{NPQ}$) of up to 10 or more have been reported in diatoms (Ruban et al. 2004), whereas qE in most other photosynthetic organisms can only reach values between 2 and 4 under saturating illumination (Goss and Jakob 2010, Ruban et al. 2012). Even though the $\mathcal{NPQ}$ values in diatoms can be up to five times that in higher plants, this does not correspond to an equivalent increase in thermal

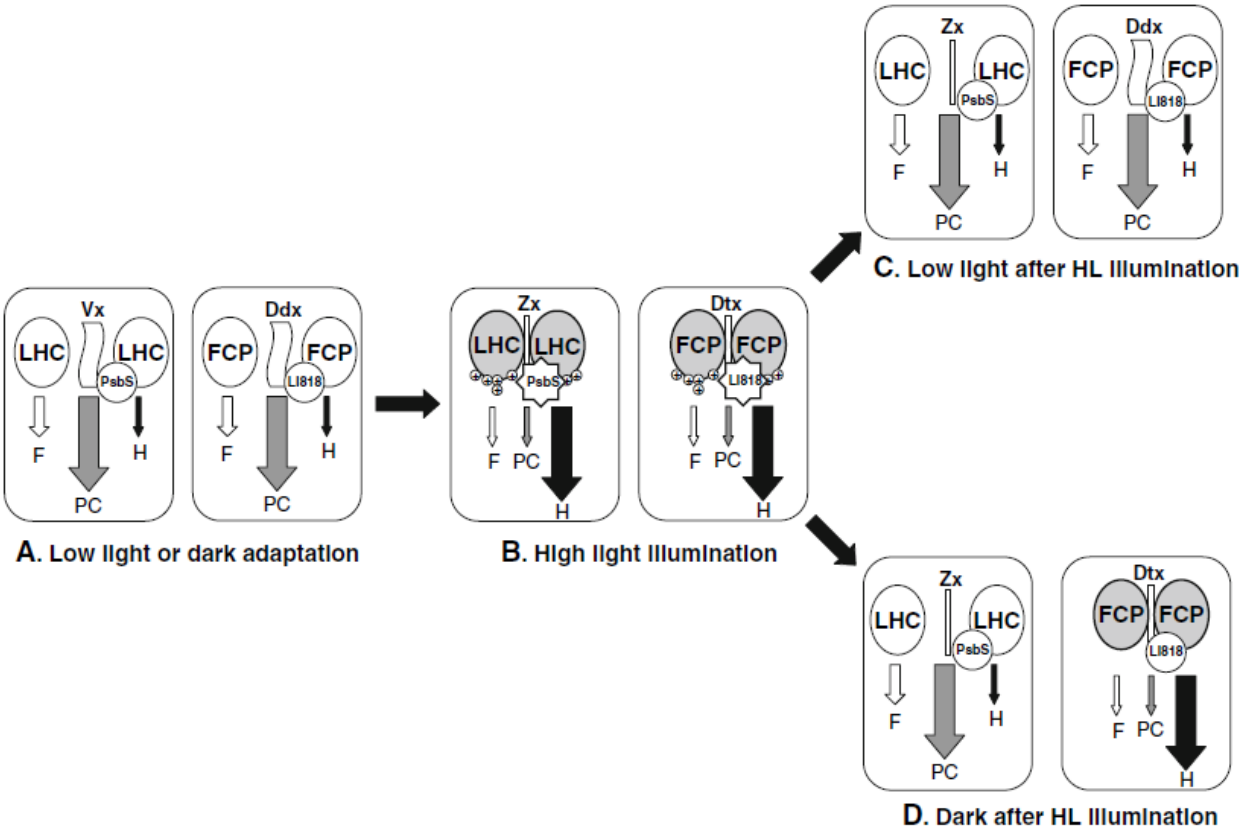

Figure 1.3 A Model for antenna regulation in higher plants and diatoms according to Goss and Jakob 2010 (Figure and caption adopted from Goss and Jakob 2010). Higher plants perform the violaxanthin (Vx) cycle, whereas diatoms perform the diadinoxanthin (Ddx) cycle. In low light (LL) or dark adapted plants and diatom cells (**A**) the antenna systems are in a non-aggregated state, the antenna proteins are not protonated and the xanthophyll cycle pigments are present in their epoxidized forms. The PsbS protein is an essential component of NPQ in vascular plants and is found unprotonated in LL or dark adapted plants. The LI818 (LhcX) protein most likely fulfills the role of PsbS in diatoms, and would be found uprotonated in LL or dark adapted cells. The non-aggregated antenna system is characterized by a low fluorescence and heat emission, and the largest part of the excitation energy is used to drive photochemistry. Upon a transition from LL or darkness to high light (HL) illumination (**B**) both the LHC and FCP become aggregated due to the protonation of antenna proteins and the de-epoxidation of Vx to Zx and Ddx to Dtx. Sensing of the low lumenal pH would occur via protonation of the PsbS and LI818 proteins. Both the aggregated LHC and FCP are characterized by a strong dissipation of the excitation energy as heat. When HL exposed plants and diatom cells are transferred into LL again (**C**), the antenna system is reverted back to a non-aggregated state, which is again characterized by a low fluorescence and heat emission and a high quantum efficiency of photosynthesis. The switch from the heat-dissipating state (B) back to the light harvesting state (C) is regulated differently in Vx and Ddx cycle containing organisms. In vascular plants, disaggregation of the LHC is triggered by the fast breakdown of the HL-driven proton gradient and deprotonation of PsbS. High Zx concentrations, which remain due to the slow Zx epoxidation, lose their ability to facilitate the dissipate of excitation energy as heat. In diatoms, FCP aggregation is reverted by the epoxidation of Dtx to Ddx upon relaxation of the proton gradient. If HL exposed diatoms are transferred from HL illumination into darkness (D), FCP can remain in an aggregated state, even in the complete absence of a proton gradient, due to the NADPH-limited epoxidation of Dtx. In vascular plants, however, the LHC quickly disaggregates upon a transition to darkness due to the loss of antenna protein protonation and switches back to efficient light-harvesting. F

fluorescence emission, PC photochemistry, H heat emission, LHC light-harvesting complex of vascular plants and green algae, FCP light-harvesting complex of diatoms and haptophytes, HL high light, LL low light, Vx violaxanthin, dx diadinoxanthin, Dtx diatoxanthin, Zx zeaxanthin. Aggregated light-harvesting complexes are depicted with a grey background, non-aggregated complexes with a white background.

dissipation of absorbed light energy. In comparison to a calculation of the quantum yield of NPQ (ϕNPQ, Hendrickson et al. 2004), an $\mathcal{NPQ}$ value of 4 corresponds to approximately 80% thermal dissipation of absorbed light energy, whereas an $\mathcal{NPQ}$ value of 10 is equal to about 90% dissipation (Goss and Jakob 2010). Upon cessation of excess light (as measured by turning HL *off* during laboratory experiments), NPQ in diatoms generally relaxes much slower than what is observed in higher plants; this phenomenon has been attributed to a strong dependence of NPQ relaxation on DT epoxidation in diatoms (Ruban et al. 2004, summarised by Lavaud 2007).

Much less is known about the particularities of the NPQ mechanism in diatoms, as compared to higher plants (Goss and Lepetit 2014). Research in diatom NPQ has been somewhat species limited, heavily concentrated on the pennate *Phaeodactylum tricornutum* (a morphologically 'atypical' planktonic species) and the centric *Cyclotella meneghiniana*, showing distinct differences between the species so far investigated (Lavaud et al. 2002b, Lavaud et al. 2004, Grouneva et al. 2009, Goss and Jakob 2010). A comparison summary of the NPQ mechanism between higher plants and diatoms according to Goss and Jakob (2010) is presented in Figure 1.3.

1.4-3 The DD cycle

The general consensus is that DD de-epoxidation to DT is a requirement for activation of qE (Horton and Ruban 2005, Lavaud 2007, Goss and Jakob 2010). As in the xanthophyll cycle of vascular plants, ΔpH activates the conversion of an epoxy-xanthophyll (DD) into an epoxy-free carotenoid (DT). A reason why NPQ may be so robust in diatoms is due to the requirements for

the de-epoxidation of DD and the reversal epoxidation of DT. De-epoxidation enzymes in both violaxanthin and DD systems are associated with the lumenal face of the thylakoid. Violaxanthin de-epoxidase of green algae and higher plants has a pH optimum around pH 5.2 with activation possible at pH values lower than pH 6.5 (Pfündel et al. 1994, Grouneva et al. 2006). For isolated DD de-epoxidase from *Phaeodactylum tricornutum*, the pH optimum is at pH 5.5 with activation still possible at a neutral pH of 7.2 (Jakob et al. 2001). Isolated DD de-epoxidase from *Cyclotella meneghiniana* was also active at neutral pH (Grouneva et al. 2006). Thus, diatom DD de-epoxidases have higher activity at lower ΔpHs than violaxanthin de-epoxidases. The de-epoxidase enzymes can also be limited by the availability of the co-substrate ascorbate in the lumen. DD de-epoxidase is able to maintain high activity at much lower concentrations of ascorbate than violaxanthin de-epoxidase (Grouneva et al. 2006). The thylakoid membrane lipid MGDG is required for the de-epoxidation of DD and violaxanthin (Goss et al. 2005, Goss et al. 2007). The lipid inverted hexagonal structures formed by MGDG in lipid bilayers are believed to be vital in making xanthophyll substrates available to the de-epoxidase active site (Latowski et al. 2004). DD is more soluble in MGDG than violaxanthin (Goss et al. 2005). Goss and Jakob (2010) suggest that this leads to higher diffusion rates of DD within the thylakoid matrix allowing DD molecules to disassociate from the LHCs, and migrate into the free lipid phase where they can be easily de-epoxidised. Another reason why de-epoxidation may be so robust in diatoms is that DD molecules are more easily accessed by DD de-epoxidase.

In contrast to higher plants, xanthophyll epoxidation does not compete with de-epoxidation in diatoms, which permits the rapid and efficient de-epoxidation of the DD pool

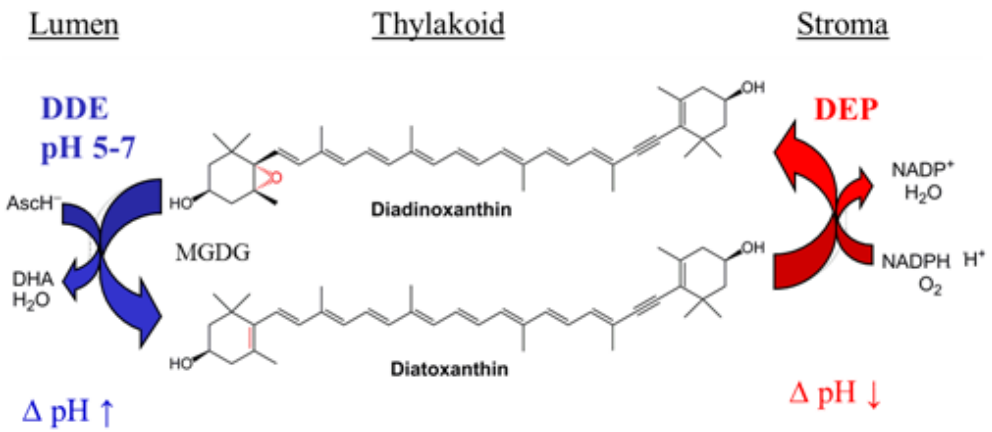

Figure 1.4 The diadinoxanthin (DD) cycle. DDE (DD de-epoxidase) is associated with the lumenal face of the thylakoid and acts on DD solubilised in the thylakoid lipid MGDG (monogalactosyldiacylglycerate). DDE is activated at pH 5-7 and requires the co-substrate ascorbate ($AscH^-$). DEP (diatoxanthin epoxidase) is associated with the stromal face of the thylakoid, is inhibited by a high ΔpH, and requires NADPH and O_2 as co-substrates. DHA, dehydroascorbic acid.

during HL. As with zeaxanthin epoxidase, DT epoxidase is located on the stromal side of the thylakoid and has the co-substrate requirements of NAD(P)H, FAD (Flavin adenine dinucleotide) and oxygen (Wilhelm et al. 2006). In plants, zeaxanthin epoxidase is much slower than violaxanthin de-epoxidase, has no specific activation pH, and is even active under HL (Goss et al. 2006). There is a net de-epoxidation of the xanthophyll pigment pool during high ΔpH because the de-epoxidase outcompetes the epoxidase. DT epoxidase is active at pH values around pH 7.5 and is inhibited during high ΔpH (Goss et al. 2006b); the exact mechanism behind the inhibition is not yet known. Furthermore, the rate constant of DT epoxidase is comparable to that of DD de-epoxidase (Goss et al. 2006b) allowing fast reversal of the DT pool once ΔpH diminishes. To summarize, diatoms are able to perform a fast and high amplitude DD cycle, as compared to the xanthophyll cycle in higher plants, due to the combination of there being only a one step de-epoxidation, the de-epoxidase enzyme showing higher activity at lower ΔpHs and lower ascorbate concentrations, the DD molecule being more soluble in the lipid matrix, and the epoxidation enzyme being inhibited with ΔpH.

1.4-4 The NPQ quenching mechanism in diatoms

As with higher plant NPQ, there is some controversy as to the exact photo-physical mechanism(s) behind the quenching of Chl *a* fluorescence during diatom NPQ. Two basic methods have been supported for the conversion of excited state energy into heat. The first is via the formation of Chl *a* aggregates due to conformational changes in the LHCs brought about by protonation and/ or DD de-epoxidation (Ruban et al. 2004, Horton and Ruban 2005, Miloslavina et al. 2009). LHCII aggregation in higher plants is believed to similarly contribute to NPQ (Horton et al. 2005). The second method of quenching is where the S_1 state of newly de-epoxidised DD (i.e. DT) molecules are able to accept excitation energy from Chl *a* Q_y and dissipate it as heat via internal conversion (Frank et al. 1996). The model proposed by Ruban et al. (2004) and modified by Miloslavina et al. (2009) best describes the events leading to the formation and maintenance of the qE observed in different diatom species: ΔpH leads to DT formation and protonation of antenna proteins leading to a conformational change of the antenna into a quenching arrangement; DT binds into hydrophobic protein regions of the quenched LHC, masking proton-binding domains from the lumen, thus stabilizing NPQ with respect to fluctuations in ΔpH and locking the LHC in a quenched state. The picosecond fluorescence decay kinetics by Miloslavina et al. (2009) from both *Phaeodactylum tricornutum* and *Cyclotella meneghiniana* cells strongly support that there are two independent types of quenching sites during steady state NPQ. The first quenching site is due to Chl *a*-Chl *a* interactions and is localised within aggregated FCPs that become functionally detached from the photosystem cores during NPQ. The second quenching site is localised in FCPs (likely

trimeric) that are closely associated with PSII, is proposed to be activated by DT, and could involve quenching of Chl *a* excited state directly by DT (Miloslavina et al. 2009).

In the diatoms thus far studied, the largest part of NPQ is composed of DD cycle dependent qE (qE_{XC}). However, additional quenching mechanisms may also be relevant in diatoms. A PSII reaction centre type of NPQ has been reported in *Phaeodactylum tricornutum* (Eisenstadt et al. 2008). Additionally, in *Cyclotella meneghiniana* NPQ appears to be more complex than that witnessed in *Phaeodactylum tricornutum*, being composed of at least three different components (Grouneva et al. 2008). There is also evidence for an NPQ component that is insensitive to the de-epoxidase inhibitor DTT in *Cyclotella meneghiniana* (Grouneva et al. 2008).

1.4-5 Chlororespiration & 'dark' NPQ

Chlororespiration denotes a respiratory pathway within chloroplasts in the dark that involves electron transport from NAD(P)H to oxygen via the PQ pool to build a trans thylakoid proton motive force for ATP synthesis (Bennoun 1982). Chlororespiration is best understood as a metabolic remnant of the prokaryotic ancestry of eukaryotic plastids (Goss and Jakob 2010); in cyanobacteria the photosynthetic and cellular respiratory enzymes share many of the same electron carriers. Chlororespiration is an important energy source within the chloroplast of higher plants during chloroplast maturation (Carol et al. 1999). Diatoms are known to have a remarkable capacity to withstand long periods of darkness and then, once returned to light, resume a high rate of growth (Murphy and Cowles 1997, Serôdio et al. 2005). Armbrust et al. (2004) and Wilhelm et al. (2006) have suggested that diatoms could use their high quantities of storage lipids when in the dark for gluconeogenesis and ATP generation. During

chlororespiration *Phaeodactylum tricornutum* is believed to utilize a type 1 NAD(P)H dehydrogenase (Ndh1) that directly pumps protons from the stroma to the lumen; PQ is oxidised via a PQ oxidase that releases water into the lumen (Goss and Jakob 2010 based on Grouneva et al. 2009). In *Cyclotella meneghinia*, a type 2 NAD(P)H dehydrogenase (Ndh2) is thought to be utilised; in this case Ndh2 does not directly pump protons, but instead proton pumping can occur via activity from the cytochrome b_6f complex (Goss and Jakob 2010 based on Grouneva et al. 2009). In diatoms the proton gradient produced by chlororespiration in the absence of light is sufficient to induce DD de-epoxidation and NPQ (Caron et al. 1987, Ting and Owens 1993, Jakob et al. 1999, Grouneva et al. 2009) giving rise to 'dark' NPQ. The weak acidification of the lumen from chlororespiratory electron flow can induce NPQ in diatoms because DD de-epoxidase is active at a neutral pH (Jakob et al. 2001, Grouneva et al. 2006).

1.4-6 PSII cyclic electron transfer

Even though diatoms are champions of performing NPQ via qE, they have an additional photoprotective mechanism for use during fast transitions to HL, PSII cyclic electron transfer (PSII CET). PSII CET has been described in cyanobacteria, green microalgae, and higher plants but only more recently in diatoms (Shinopoulos and Brudvig 2012, Lavaud et al. 2002b, Onno Feikema et al. 2006, Lavaud et al. 2007, Lavaud 2007). It avoids the over reduction of the PQ pool by passing electrons from Q_B back to $P680^+$ via a pathway(s) likely involving cytochrome b_{559}, as such competing with water oxidation and O_2 evolution (Lavaud et al. 2002b, Lavaud 2007). Thus the PSII CET reduces the probability of ROS generation by keeping forward electron transport within PSII active while lowering the local O_2 concentration. In the diatom species examined for PSII CET (as according to Lavaud 2007), PSII CET has been shown to be the first

line of defense against HL, turning on faster than qE (PSII CET switches on within a second, whereas qE takes several seconds to activate) (Onno Feikema et al. 2006) and developing at lower HL intensities than qE (Lavaud et al. 2002b, Lavaud et al. 2007). High amplitude PSII CET would allow diatom cells to maintain maximal capacity for photosynthesis by keeping qE_{XC} low, giving their photosynthetic apparatus a more dynamic ability to react to very rapid changes in irradiance than would be attainable with qE_{XC} alone (Lavaud 2007). The PSII CET in diatom species isolated from a highly fluctuating light environ is faster and has a higher amplitude than that in species originating from a habitat with a more stable light environ (Lavaud et al. 2007). The reapportioning of electrons within diatom chloroplasts via PSII CET, and other active alternate electron cycling pathways such as chlororespiration, PSI cyclic, Mehler Reaction, and nitrite reduction may contribute to why diatoms are able to maintain high conversion efficiencies of light energy into biomass under fluctuating light regimes (Wagner et al. 2006).

1.4-7 NPQ is regulated by the interaction of multiple feedback loops

As alluded to in the preceding discussions, the NPQ response is used to dynamically tune the energy transduction of absorbed light energy so as to equilibrate the excitation of the PSII reaction centre with electron transport and sink capacity. This balancing act is a complex interaction of biophysical and physiological processes. Over excitation of PSII is quickly manifested as a buildup of ΔpH and an over reduction in the redox status of the PSII electron acceptors. Multiple metabolic pathways within the diatom chloroplast are regulated by pH and/ or use the mobile electron carriers and reducing equivalents from the photosynthetic reactions (see Wilhelm et al. 2006). The major pathways that contribute to the redox and protonation state of the diatom chloroplast and how these interact with NPQ induction and

relaxation are summarised in Figure 1.5. During a fast transition to HL (i.e. seconds to a few minutes), diatoms must make do with their pre-existing capacity to perform NPQ because up-regulation of gene expression and *de novo* pigment synthesis is too slow. In *Phaeodactylum tricornutum*, the up-regulation of LHCX genes and the *de novo* synthesis of DD cycle pigments led to a pronounced rise in qE only after ~ 30 minutes of excess light exposure, with the effect being more substantial on an hour time scale (Lepetit et al. 2013).

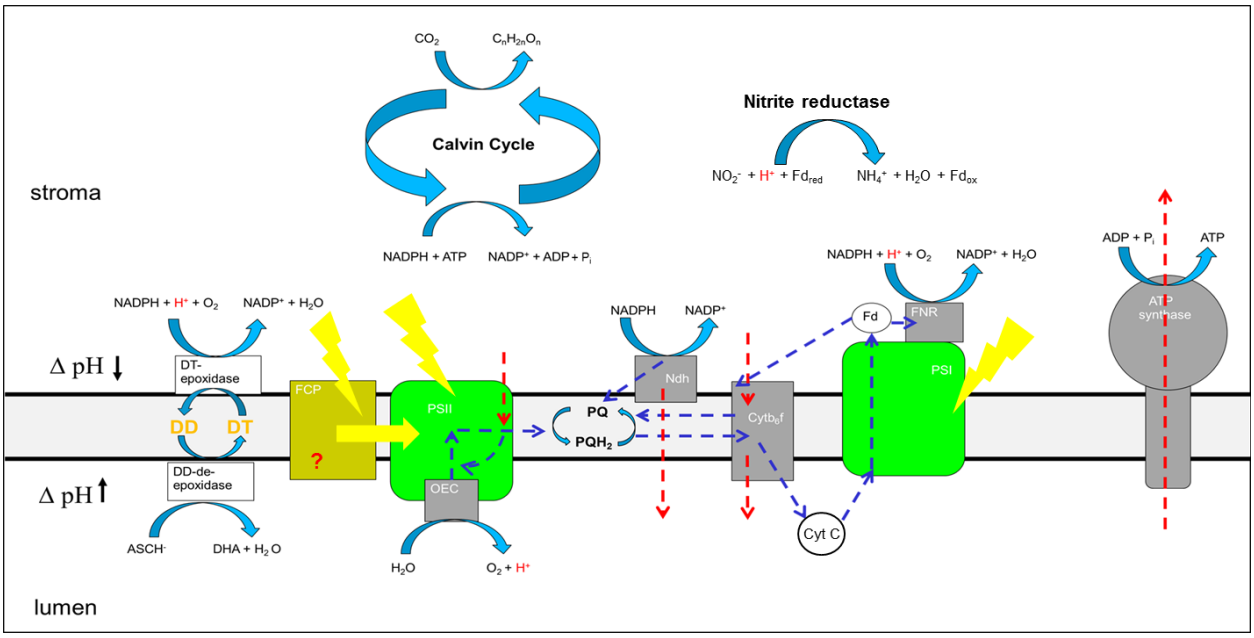

Figure 1.5 Summary of the major feedback loops within the diatom chloroplast for sensing redox state and ΔpH. **Red** dashed arrows indicate pathways for proton translocation; **blue** dashed arrows indicate pathways for electron transfer. The Calvin cycle and nitrite reductase are included to illustrate that both carbon dioxide and nitrite are important electron sinks in the chloroplasts of diatoms. Absorption of light energy for powering photochemistry is designated by the yellow lightning bolts and energy transfer from accessory light harvesting pigments to PSII is indicated by the yellow block arrow. PSI cyclic electron transport is specified by the blue dashed arrow connecting Fd to $Cytb_6f$. PSII cyclic electron transfer is indicated by the blue arc located within PSII. DD de-epoxidase is activated by a rise in ΔpH while DT epoxidase is inhibited by ΔpH. The red question mark on the FCP complex represents the possibility of proton sensing within light harvesting complexes. Chlororespiratory pathways utilizing Ndh (type 1 Ndh is shown here, even though there is also evidence for type 2 Ndh in diatoms; Grouneva et al. 2009) are seemingly active in diatoms during prolonged dark periods. $ASCH^-$, ascorbate; Cyt c, cytochrome c_{553} that fulfills the role of plastocyanin in chromophytes; DD, diadinoxanthin; DHA, dehydroascorbic acid; DT, diatoxanthin; FCP, fucoxanthin chlorophyll proteins that form the accessory light harvesting complexes for both PSII and PSI; Fd, ferredoxin (Fd_{red}, reduced Fd; Fd_{ox}, oxidised Fd);

FNR, ferredoxin $NADP^+$ reductase; Ndh, NAD(P)H dehydrogenase; OEC, oxygen evolving complex of PSII.

1.4-8 NPQ as an ecological marker for niche partitioning

The characteristics of NPQ (i.e. magnitude, induction and relaxation kinetics) from diatoms appear to be a functional marker for the light environment of their habitat. In a study by Lavaud et al. (2007), the photoprotective behaviour of five planktonic diatom species from marine habitats with different water mixing dynamics were compared. The diatoms from more stable light environs (e.g. open ocean and coastal waters) showed the lowest NPQ capacity; species from a highly dynamic underwater light climate (e.g. estuary) exhibited a three– to five-fold increase in NPQ magnitude; a species from a light environ with intermediate amplitude and frequency changes in light (e.g. a bay) exhibited an intermediate NPQ capacity. Comparable results were observed with diatom species that differ not only in habitat, but also in seasonal distribution (Meyer et al. 2000, Dimier et al. 2007, as discussed by Goss and Jakob 2010). A diatom species that blooms in low light conditions during late winter but is also present in higher light springtime in coastal areas showed an intermediate level of NPQ, which was strongly dependent on the light history of the algae (Dimier et al. 2007). Studies with *Phaeodactylum tricornutum* have shown that growing cultures of this species under an intermittent high light scheme enhances its NPQ capacity (Ruban et al. 2004). Thus inter- and intra-species variability in diatom NPQ is dependent not only on genetics but also on individual light histories. The kinetics, not just amplitude, of NPQ can also be a marker of phytoplankton photoadaptive state and ecological niche. Dimier et al. (2009b) looked at different DD and violaxanthin cycle containing phytoplankton species and determined that they could be separated into three groups based on their xanthophyll cycle characteristics and light environs.

High light adapted species (e.g. oceanic surface water habitats) had a large pool of xanthophyll cycle pigments, but showed slow xanthophyll conversion kinetics. Low light adapted species (deep water habitats) were characterised by a small pool of xanthophyll pigments in combination with slow pigment conversion kinetics. On the other hand, species in habitats with mixing of the water column had a fast xanthophyll cycle (Dimier et al. 2009b; as discussed by Goss and Jakob 2010).

Based on such results as discussed above, Goss and Jakob (2010) concluded that "the spatial and temporal distribution of diatom species is influenced by the dynamics of the water column, which in turn affects nutrient availability (Falkowski et al. 2004) and the underwater light climate (MacIntyre et al. 2000)". Thus, the NPQ capacity of individual diatom species can then be regarded as an adaptive response to their ecological conditions, which is likely also true for other planktonic, non-diatom, algal species (Dimier et al. 2009, Goss and Jakob 2010). The success of diatoms in a multitude of highly instable (and even stable) light environs must stem, at least in some part, from their ability to perform a NPQ that best fits the photophysiological needs created by each species' specific habitat.

1.5 Diatom Species of Interest

This body of research predominantly focuses on the NPQ photoprotective properties of two diatom species that have not previously been the subject of any photosynthetic investigations. The first species is a 'typical' pennate diatom. *Nitzschia curvilineata* was collected from the Long Island Sound shoreline in New Haven, Connecticut USA (41.2440N 72.8900W) by J. Lewin and R. Lewin in the early 1950s (NCMA 2013). It has been deposited in

the CCMP (predecessor of NCMA) algal culture collection since 1986 with the assigned strain number CCMP 555 (NCMA 2013). *N. curvilineata* cells range between 40 to 65 µm long and 10 to 15 µm wide. The *curvilineata* specific epitaph refers to the characteristic bulbous twist in the longitudinal terminal ends of the frustule (i.e. the cell wall composed of silica). Mucilage excretion from the raphe of *N. curvilineata* gives these benthic diatoms cell mobility. This species is an especially slimy diatom, producing large amounts of primarily carbohydrate extracellular polymeric substances (EPS) (Sutherland et al. 1998). EPS secretion in *N. curvilineata* has been shown to increase sediment stability (Sutherland et al. 1998). Cells generally grow as biofilm mats associated with the substrate but can float on top of the water surface when oxygen bubbles become entrapped in the mat (Sutherland et al. 1998). The shoreline habitat can be considered poikilophotic (i.e. of variable light conditions) due to continual wave action mixing the water column. One would hypothesize then that this diatom species would exhibit a robust NPQ response, capable of turning *on* and *off* in the time frame of movement through the water column.

The next species of interest is another pennate designated as *Navicula sp*. 110-1 by Kirkwood and Henley (2006). *Navicula sp*. was isolated by A. Kirkwood and W. Henley in July 2002 from soil surface samples during a survey of the algal communities found within the Great Salt Plains salt flat located in north-central Oklahoma, USA (Potter et al. 2006, Kirkwood and Henley 2006). This species is smaller than *N. curvilineata* being 6 - 10 µm long and 4 - 6 µm wide (NCMA 2013), yet still falling into the nano-plankton size class (based on cell width) (Sieburth et al. 1978). *Navicula sp*. was deposited into the CCMP algal culture in 2006 and assigned the strain number 2566 (NCMA 2013). To the author's knowledge, no NPQ studies

have yet been performed on a soil diatom. The characteristics of this unique environment merit further description. The soils of the Great Salt Plains salt flat are rarely completely dry at the soil surface because of the upward wicking of near-surface groundwater brine (Kirkwood and Henley 2006). Salt flats are unprotected by the moderating effects of permanent standing water experiencing large diurnal swings in temperature (Kirkwood and Henley 2006). Even though the algae isolated from these communities are viable under excessive hypersaline conditions (up to saturation levels of ≥ 300 ppt), isolates would generally only grow at salt levels of less than 150 ppt with optimal growth at or below 50 ppt (seawater = 35 ppt) (Potter et al. 2006, Kirkwood and Henley 2006). *Navicula sp*. grew optimally at 50 ppt with tolerance up to 150 ppt salinity (Kirkwood and Henley 2006). Similar to marine systems, algal biomass in these inland saline (athalassic) habitats is nutrient limited by the availability of nitrogen, specifically in the form of ammonium (Kirkwood and Henley 2006). It was concluded that the algae of the Great Salt Plains salt flats rarely achieve maximum growth rates *in situ*, and could only do so when intermittent rain events reduce salinity to optimal levels (Kirkwood and Henley 2006).

Even though the salt flat can be considered poikilotrophic due to high variability in soil temperature, salt concentration, and nutrient availability, it is a comparatively stable environment in terms of light. As there is no water column to move through, and no vegetation or large topographic features to cause transient shading, any fluctuations in the light environ would be due to atmospheric effects and slow diurnal movements of the sun. When salinity conditions are within the optimal range, growth would be limited by nutrient (nitrogen) availability and not by incident photon flux. Considering the above described environmental

pressures of the salt flat, the photosynthetic apparatus of *Navicula sp*. is expected to be organized so as to maximize the energetic efficiency of producing building blocks for growth (photoreduced nitrogen and carbon) during the periods when salinity conditions are optimal and nutrient supply is adequate. Conversely, during times of high salinity, or inadequate nutrient availability, the photosynthetic apparatus should reside in a locked photoprotective (quenched) state until favorable conditions return for the safe use of sunlight. One would predict that the salt flat environment would select for an NPQ response in *Navicula* that is relatively inexpensive to cellular energy reserves and is less dynamic over a broader range of irradiance intensities, as compared to *N. curvilineata*.

1.6 Objectives

The principal goal of this work was to reveal the physiological and biophysical origins and consequences of the NPQ response in diatoms during short-term (seconds to minutes) transitions to excessive irradiation. The investigation involved diatom species from different originating light environs to highlight the diversity of diatom NPQ and to facilitate the detection of core mechanisms common among the diatoms as a group. Multifaceted analyses of the NPQ responses from *Nitzschia curvilineata* and *Navicula sp*. will be used to identify an excitation pressure relief strategy for each species. These strategies will be compared to one another and to those alluded to by the literature. Three key areas of the NPQ phenomenon will be examined: (i) the NPQ activation and deactivation processes, (ii) how NPQ affects the collection, usage, and dissipation of absorbed light energy, and (iii) the interdependence of NPQ and photosynthetic electron flow.

A primarily spectroscopic approach will be used to investigate NPQ in diatom cells. Prime methodologies include: the real time monitoring of PSII excitation and de-excitation pathways via PAM fluorometry and pigment interconversion via transient absorbance measurements, the collection of cryogenic absorbance spectra to measure pigment energy levels, the collection of cryogenic fluorescence spectra to study excitation energy transfer, and picosecond time resolved fluorescence decay spectroscopy to investigate the relaxation of chlorophyll excited states. A multitude of chemical agents will be used to experimentally manipulate the contribution of ΔpH, DD de-epoxidation, and electron transport to the NPQ response. A hypothesis is presented that describes the dynamism in NPQ kinetics and amplitude observed within and between diatom species as being due to the differential activation/ deactivation and relative contribution of xanthophyll cycle dependent quenching located within the FCP antenna complexes (Q1 and Q2 quenching) and quenching within PSII reaction centres. The photo-electronic mechanism for antenna based quenching is principally attributed to the formation inter-FCP trimer Chl *a*-Chl *a* quencher dimers that have a short excited state lifetime. DD de-epoxidation and ΔpH facilitated aggregation of FCP complexes forms the FCP quenching aggregates. Q1 quenching targets outer PSII antenna FCP complexes, whereas Q2 targets inner PSII antenna FCP complexes. Because these three types of quenching sites are predicted to be contained within separate domains of the pigment-protein complexes, one anticipates the different types of quenching to have distinct spectral signatures even if occurring simultaneously. This study will identify spectral signatures for the different types of quenching. The NPQ response in *Nitzschia* will be studied in additional depth for elucidation of the molecular mechanisms behind FCP centred quenching.

2 Experimental Approach

2.1 Cell Culturing and Sample Preparation

2.1-1 Cell source

All diatom species were purchased from NCMA (Provasoli-Guillard National Center for Marine Algae and Microbiota, Bigelow Laboratory for Ocean Sciences, 60 Bigelow Drive, P.O. Box 380, East Boothbay, Maine 04544 U.S.A.). NCMA was formally known as CCMP. The CCMP 2566 (*Navicula* sp.) culture was taken from cryopreservation at the NCMA facility.

2.1-2 Growth media

An oligotrophic artificial sea water medium was developed based upon the ESAW (Harrison et al. 1980, Berges et al. 2001) and F/2 (Guillard and Ryther 1962, Guillard 1975) formulations. Micronutrient concentrations were slightly altered so as to sustain growth of *Nitzschia curvilineata* (CCMP 555) and *Navicula sp*. (CCMP2566). Silicate was added to the media in the form of Na_2SiO_3 x $9H_2O$ at a final concentration of 200 μM. The complete media recipe can be found in *Appendix 1*. Chemical components were obtained from Sigma-Aldrich or Caledon (Georgetown, Ont, Canada, L7G 4R9).

2.1-3 Culture conditions

Cultures were grown in 1 L polycarbonate square bottles (Corning, Corning, New York, USA 14831). The tops were vented with open top caps fitted with 0.2 micrometer polytetrafluoroethylene (PTFE) filter membranes (Sartorius Stedim Biotech GmbH, Goettingen,

Germany, 37070). Culture bottles were placed in an 18^{o}C water bath. Illumination was to the side provided by GE Daylight 6500K compact fluorescent lamps. Photon flux as measured with a calibrated quantum LI-189 lightmeter (Li-Cor, USA) reaching inside the culture bottles was 50 ± 10 μmol $m^{-2}s^{-1}$. Cultures were grown under an 18 hour day and 4 hour night cycle and gently shaken twice daily to facilitate diffusion of gases and mixing of solutes within the growth media. Cultures were constantly maintained in a quasi-exponential growth phase by diluting the cultures with fresh growth media at least bi-weekly. Cells were cultured under these continuous growth conditions in the lab for at least 2 months after receipt from the NCMA algal culture depository before being used for any physiological measurements. The cells would thus be considered acclimated to the controlled conditions *in lab*, not the natural environmental conditions from which the diatom ancestor cells were collected.

2.1-4 Cell collection and sample preparation

Experiments were performed at times corresponding to 'midday' of the photoperiod cycle. Cells to be used for physiological experiments were allowed to sink by temporarily removing the 1 L culture bottles from the growth light, then cells were collected from the bottom of the culture bottles and transferred to 250 mL bottles to a Chl *a* concentration of approximately 0.1 mg mL^{-1} for 30 minutes prior to experimentation. To negate any effects from suspending the cells during collection cycles, the 250 mL bottles were gently mixed in 15 minute intervals twice before actually collecting cells for experimentation. The 250 mL bottles were gently mixed prior to taking cell aliquots to insure equal cell densities between samplings.

Cell samplings were always treated to the following routine immediately prior to

experimentation: 1) Cell aliquots were dark adapted at 18^{o}C for 15 minutes in 15 ml centrifuge tubes. 2) Cells were concentrated by spinning at low RPM (speed 3 on IEC clinical centrifuge, Damon/IEC Division, Needham Hts, Mass, USA, 02194) for 30 seconds in the dark. 3) Supernatant was discarded. 4) Cells were suspended in fresh growth media supplemented with 10 mM $KHCO_3$ (or $NaHCO_3$ when indicated) for 5 minutes at 18^{o}C in the dark. Depending on the experiment, the growth media +10 mM $KHCO_3$ solution was further augmented with various chemical agents. Equivalent Chl *a* concentration of the suspension was approximately 0.1 mg mL^{-1}. All chemical treatment solutions were made fresh daily. 5) Cells were concentrated by spinning at low RPM for 30 seconds in the dark. 6) Supernatant was removed until desired Chl *a* concentration was reached for experimentation.

2.2 Pigment Analysis

The following procedures were performed under low light and/ or on ice whenever practical. Solvents were obtained from Sigma-Aldrich or Fischer Scientific (Fair Lawn, New Jersey, USA, 07410).

2.2-1 Pigment extraction

a. Methanol Extraction

   Cell pellets were suspended in ice cold methanol for 15 minutes. The extract was collected. Treatments with methanol were repeated until cell pellet was white.

b. DMSO Extraction

Cells were collected via centrifugation then rinsed in distilled water. The washed cell pellet was then suspended in dimethyl sulfoxide (DMSO) for 1 hr. The extract was collected. Treatments with DMSO were repeated until the cell pellet was white.

c. Multiple solvent Extraction

The following method is based on that of (Seely et al. 1972) using solvent ratios as described therein.

Cells were collected via centrifugation then rinsed in distilled water. The washed cell pellet was then suspended in DMSO for 15 minutes. The extract was collected then the pellet was suspended in acetone for 5 minutes. The extract was collected then the pellet was rehydrated with distilled water. Acetone treatment was repeated. The pellet was then suspended in 1:1 acetone: methanol for 5 minutes. The extract was collected.

2.2-2 Pigment separation

Pigments were separated via thin layer chromatography. Cell extracts in 100% methanol were vacuum-evapor-concentrated on ice then spotted onto 250 μm polyester backed silica gel TLC sheets (Whatman, GE Healthcare). 71.8 petrol ether: 18.6 ethyl acetate: 9.65 diethylamine volume: volume was used as the mobile phase. After separation individual pigment bands were excised from the TLC plate, dissolved in solvent, and separated from the silica by centrifugation.

2.2-3 Pigment quantification

Pigment concentrations were determined photometrically. Chl *a* estimates were calculated from methanol cell extracts with a Spectronic 20 (Bausch & Lomb) using the

extinction coefficient of Porra et al. (1989). Pigment composition of DMSO cell extracts were calculated from absorption spectra collected with a DW-2 scanning spectrophotometer (Aminco, USA) in split mode with an OLIS collection system (OLIS, Bogart, GA, 30622, USA) using a monochromator slit width of 1.0 nm and the extinction coefficients of Seely et al. (1972).

2.2-4 Qualitative cell pigment analysis

Cell samples were flash frozen in liquid N_2 under dark conditions or after exposure to 10 minutes of HL. The frozen samples were then ground in ice cold methanol and the steps outlined in 2.2-2 were followed. After separation, the TLC plate was scanned (CanoScan LiDE 700F; Canon) and the image was analyzed using CP ATLAS TLC and gel analysis software (http://lazarsoftware.com). Peak areas in channel 'blue' after baseline subtraction were calculated for chromatogram bands attributed to Chl *a*, Fx, DD, and DT. The carotenoid peak areas were then normalised by the Chl *a* peak area.

2.3 Protein Quantification

Procedures were performed in the laboratories of Douglas Campbell and Amanda Cockshutt, Mount Allison University, Sackville, NB E4L 1E2. All solutions were made up in Millipore filtered water. All chemicals were from Sigma unless stated otherwise. 1% w/v = 1g/100mL. 1% v/v = 1mL/100mL.

2.3-1 Whole cell protein extraction

Fifty μg Chl *a* worth of cells adapted to standard growth conditions were filter collected onto binder free glass fibre filters (Sigma), quick frozen in liquid N_2, and stored at -80^{o}C until use. The frozen cells were scraped from the membrane and suspended in 5 mL of 1% PSP (1.705% w/v Trisbase, 1.665% w/v TrisHCl, 2% w/v LDS, 1% w/v glycerol, 5 μM EDTA, 2% v/v Pefabloc 50X (Invitrogen)) in a 15 mL centrifuge tube, then frozen vertically in liquid N_2. The cells were lysed by sonicating the frozen samples until thawed, then refreezing in liquid N_2. This sonithaw process was repeated 3 times. After the final sonithaw the samples were kept on ice. The lysed cells were then spun for 5 minutes at 130 rpm. The supernatant from 5 separate cell extractions was then pooled together. The pooled supernatant was split into aliquots and kept frozen at $^{-}$80^{o}C until further use.

2.3-2 Protein concentration assay

Nine standard concentrations of BGG from 0-1.0 mg/mL were made up in 1% PSP. Protein concentrations were determined using the BioRad DC Protein Assay Kit. Absorbance values were read via a microplate reader (Molecular Devices VersaMax Tunable Microplate Reader). Both the standards and diatom samples were run in triplicates.

2.3-3 PAGE

Stock PsbA and PsaC protein standards (Agrisera) were serial diluted in 1X loading buffer + DTT (1% v/v 4X sample buffer (Invitrogen) + 0.05 M DTT (Invitrogen UltraPure)). Diatom protein extracts were diluted as needed in 1X loading buffer with a final concentration of 0.05 M DTT. Protein samples and standards were heated for 5 minutes at 70^{o}C.

For the detection of PsbA and PsaC, 0.2 µg and 2.0 µg of diatom protein extract were respectively loaded per well, into a 4-12% Bis-Tris Gel (Invitrogen NuPAGE). Ten microliters of the standards were loaded per well. Electrophoresis was performed using a vertical PAGE setup from Invitrogen with MES running buffer (5% v/v 20X MES SDS running buffer (Invitrogen NuPAGE)). 1.25mM DTT was added to MES running buffer to form the inner running buffer. Gels were run for 35 minutes at 200 V.

2.3-4 Western blotting

Protein from the gel was transferred onto a PVDF membrane (BioRad) by applying 30 V for 90 minutes using a transfer buffer of 5% v/v 20X transfer buffer (Invitrogen NuPAGE), 10% v/v methanol, 0.5mM DTT. The membranes were then treated with blocking media (2% w/v ECL Advance blocking agent (GE Healthcare) in TBS-T (0.8% w/v NaCl, 0.242% w/v TrizmaBase, 1% v/v Tween20, pH 7.6)) overnight at 4^{o} C.

Primary immunodetection was carried out with 1:25,000 anti-PsbA rabbit serum (a kind gift from Environmental Proteomics, product# AS05-084) and 1:2,000 anti-PsaC rabbit serum (a kind gift from Environmental Proteomics, product# AS04-042) in blocking media with shaking at room temperature for 1 hour. Afterwards the primary antibody solution was poured off and the membrane was quick rinsed twice in TBS-T followed by a 15 minutes rinse with shaking, and three 5 minutes rinses with shaking.

Secondary immunodetection was carried out with 1:40,000 anti-rabbit serum (a kind gift from Environmental Proteomics, abcam 6721) in blocking media with shaking for 1 hour.

Excess secondary antibody was washed away following the same rinse steps as used for the primary antibodies.

2.3-5 Visualization

The location of the secondary antibody was visualised by treating the membranes with GE ECL advanced Lumigen (GE Healthcare) according the manufacturer's directions for 5 minutes. The luminescence from the horseradish-peroxidase reaction was then captured with an imager (Kodak Image Station 4000mm Pro). Luminescence intensity from the individual immunoblots was quantified by subtracting local background intensity from net intensity using Kodak MI software.

2.4 Microscopy

2.4-1 Bright field transmission microscopy

Images of diatom cells were obtained using an inverted Olympus microscope (Olympus Corporation) fitted with a Nikon CCD microscope camera (Nikon Instruments Inc.) utilizing NIS elements imaging software (Nikon Instruments Inc.). Scale bars on the imaging software were calibrated to a stage micrometer.

2.4-2 Confocal fluorescence microscopy

Confocal fluorescence microscopy images of diatom cells were collected using a Fluoview system with an Olympus IX71 inverted microscope (Olympus Corporation). Excitation was provided by a 470 nm steady state diode laser (Laserglow Technologies, Toronto, ON M6C

1C4). To prevent scattered laser light from reaching the detection channels, a yellow glass filter was placed in the emission optic pathway prior to the channel selection dichroic mirror. Scale bars on the imaging software were calibrated to a stage micrometer.

2.5 PAM (Pulse Amplitude Modulated) Fluorometry

2.5-1 Experimental setup

Chlorophyll fluorescence quenching in response to HL treatments was tracked in real time using the method of pulse amplitude modulated (PAM) fluorometry. This method only measures the fluorescence directly induced by a modulated measuring light so that the application of additional light sources does not directly increase the measured fluorescence yield by increasing excitation. Changes in the modulated fluorescence signal thereby only stem from changes to the photosynthetic apparatus, either via affecting the amount of measuring light energy reaching the emitting Chl *a* molecules or by affecting their excited state relaxation pathways.

Fluorescence emission of wavelengths greater than 680 nm was selected for amplification with a 680 nm long pass Schott glass filter. The pulsed measuring light was provided by a 470 nm LED (Cree SiC Technology; Durham, NC 27703 USA). A PAM 101 chlorophyll fluorometer (Heinz Walz GmbH, Effeltrich, Germany, 91090) was used to modulate the measuring light and lock-in amplify the fluorescence signal. The PAM 101 was powered by an external battery. For quasi-dark measurements the measuring light was pulsed at 1.6 KHz giving an integrated photon flux reaching the sample of no more than 0.50 μmol m^{-2} s^{-1}. For

measurements under illumination conditions, the measuring light was pulsed at 100 KHz to increase kinetic resolution. Multiturnover saturating light pulses of 300 millisecond duration were used to momentarily close PSII reaction centres for collection of maximal fluorescence levels (Fm_{dark} & Fm'). Multiturnover saturating light pulses and actinic light (i.e. HL) were provided by a solid state triggered high power dual channel LED (neutral white, LED Engine) allowing independent control over intensity and duration for the saturating light pulses and actinic light. Photon flux reaching the sample from the saturating light pulse was 5,000 μmol m^{-2} s^{-1}. These white light sources were passed through a 675 nm high performance short pass filter (Edmund Optics). Photon flux from the 100 KHz measuring light was included when measuring actinic light photon flux. Far red light for collection of Fo' was provided by a solid state triggered 720 nm LED (LED Engine). The saturating light pulse/ actinic light, and far red light modules were designed and built *in lab* by the author.

The PAM 101 internal electronics were modified by the author to allow remote triggering of measuring light and pulse frequency selection. Fluorescence signal as voltage from the PAM 101 output was digitized with a 8 bit 240 samples/second analogue/digital converter (DataQ Instruments; www.dataq.com) for chart recordings of long time scale fluorescence transients (minutes) and a 12 bit 250,000 samples/second analogue/digital converter (PCI-DAS1000, Measurement Computing, Norton, Mass., USA, 02766) for collection of fast fluorescence transients and collection of fluorescence parameter readings. A software program was developed *in lab* by the author to control triggering over all of the light sources and to collect and process the fluorescence signal in real time.

Samples of 3 mg ml^{-1} Chl *a* were placed into 11 mm diameter X 2 mm height silicon walled sample chambers and covered with a #1 20 x 20 mm coverslip (Fischer Scientific). The sample chamber was then placed into a temperature controlled copper sample holder (i.e. stage). All experiments were performed at 18°C (growth temperature). A multifurcated fibre optic bundle was used to deliver the various light sources to the sample and collect the fluorescence signal from the sample. The common terminus of the fibre optic bundle was coupled to the sample from above. The fibres in the common terminus of the bundle were mixed to minimalize small scale positioning effects within the sample.

2.5-2 Definition of fluorescence quenching parameters

The coefficient of photochemical quenching: qP = (Fm'-Ft)/(Fm'-Fo'). The extent of Stern-Volmer non-photochemical fluorescence quenching (Bilger and Björkman 1990): $NPQ = (Fm_{dark} – Fm')/Fm'$. Quantum yields were calculated according to Hendrickson et al. (2004). Effective PSII quantum yield (also called quantum efficiency of photochemistry): ϕPSII = (Fm'-Ft)/Fm'. The quantum yield of energy dissipation associated with regulated thermal dissipation: ϕNPQ = (Ft/Fm') – (Ft/Fm). The quantum yield of energy dissipation associated with 'non-regulated' thermal dissipation and fluorescence: ϕNO = Ft/Fm.

2.6 NPQ Action Spectra

Action spectra were collected to determine the dependence of non-photochemical fluorescence quenching on spectral quality (i.e. wavelength) of HL. Fluorescence signal was induced and collected as described above in *Section 2.5-1*. Monochromatic light from 405 nm

to 705 nm was used as the HL source to drive NPQ. This light was provided by an array of high power LEDs of various colors. The light emitted from the array was spectrally selected by passing through 12.5 nm FWHM band pass filters before being integrated into the multifurcated fibre optic bundle used with the PAM experiments. The array was designed by the author and built *in lab* and *in house*. LED selection was mechanically controlled by a stepper motor. Luminous output from the array was mechanically controlled by a stepper motor and monitored by a calibrated quanta sensor (Licor). Photocurrent for monitoring the LED array's output was converted to voltage via a circuit board (Emesys.com) and read via an analogue digital converter (DI-145; DataQ Instruments). Control over the array was via a software program written by the author *in lab*.

2.7 OJIP Analysis

Fluorescence rise transients associated with the application of multiturnover saturating light pulses (i.e. OJIP transients) were obtained either during standalone experiments or during the collection of PAM traces. Chl fluorescence was induced and measured using PAM fluorometry as described in *Section 2.5-1*. Time resolution in this system after analogue-digital conversion and signal averaging was 100 microseconds. Time points along the fluorescence rise transients were labeled as: "O", fluorescence level immediately prior to saturating light pulse; "J", fluorescence level 3 milliseconds after start of saturating light pulse; "P", maximal achieved fluorescence level during application of saturating light pulse. OJIP parameters were taken from raw fluorescence transients via an algorithm composed by the author utilizing ORIGIN (OriginLab Corporation, Northampton, MA 01060, USA) functions.

2.8 Effective PSII Absorbance Cross Section Measurements

Effective PSII absorbance cross section (σPSII) measurements were collected following the approach of (Falkowski and Chen 2003). Diatom cells were dark adapted for 15 minutes, then resuspended in growth media +10mM $KHCO_3$ doped with 4 μM final concentration DCMU for 5 minutes prior to experimentation. Samples were held and light was delivered to the sample in the same method as described for the PAM measurements in *Section 2.5-1*. Measuring pulses (500 microsecond duration spaced 500 microseconds apart) were provided by a blue LED (Cree) with a 480 nm 12.5nm FWHM band pass filter in combination with a B440 Schott glass filter. The fluorescence detection photodiode (Si PIN type; Thor Labs, Inc, Newton, NJ 07860 USA) was protected with a 680 nm long pass Schott glass filter in combination with a 680 nm 12.5 nm FWHM bandpass filter. Photodiode current was amplified and converted to voltage using op-amp circuitry, then digitized (PCI-DAS1000, Measurement Computing, Norton, Mass., USA, 02766). Pulse triggering and data acquisition were performed using software developed *in lab* by the author. LED pulsing was via a fast response solid state analogue switch triggered by an internal pacer of the A/D board.

2.9 Dual Measurements of Chlorophyll Fluorescence and Cell Absorbance Changes

Simultaneous measurements of variable Chl fluorescence and changes in cell absorbance (measured as transmitted light) attributable to DD-DT interconversion were performed. During NPQ conditions, there is a drop in cell absorbance around 495 nm and a

concurrent increase in absorbance around 510 nm which has been attributed to the enzymatic catalysed de-epoxidation of DD molecules to DT molecules (Lavaud 2007).

Chlorophyll fluorescence was induced and measured as described in *Section 2.5*. Changes in transmittance were measured as the difference in transmitted light through the sample reaching two detector photodiodes. Transmitted light was collected into a bifurcated fibre optic bundle coupled to the underside of the stage. A scattering plate was positioned immediately below the sample prior to the fibre bundle. The detection photodiodes were protected with green Schott glass filters in combination with 10 nm dielectric bandpass filters (channel 1, 493 nm; channel 2, 510 nm). The photodiodes (Si PIN type; Thor Labs) were reversed biased. The detection circuitry measured individual output from the detection channels or the difference in photocurrent between the two channels amplified with an op-amp based precision instrumentation amplifier circuit. The last 100 milliseconds of the saturating light pulse were used as the measuring light. The signal was 'zeroed' prior to collecting data by adjusting the optical input power between the individual photodiodes with a few short bursts of measuring light. To correct for subtle changes in pigment concentration between samples, the difference signal was normalised to the single channel 1 signal. All detection side circuitry was designed and built by the author *in lab*. Much attention was given towards commonly electrically grounding all components of this experimental apparatus so as to minimize electrical noise and prevent signal drifting. The author further developed the software from *Section 2.5* to collect and analyse the transmittance signal in addition to the fluorescence signal.

2.10 Absorbance Spectra

Absorbance spectra were collected on a DW-2 UV Vis Spectrophotometer (Aminco, USA) integrated into an OLIS acquisition system (Bogart, GA, 30622, USA). The spectrophotometer was operated in splitmode where sample and reference are measured simultaneously while scanning wavelengths. Monochromator slit width was set to 1.0 nm. The scanning monochromator was calibrated to the absorbance peak of a 514.5 nm 1 nm FWHM laserline filter. The sample holder and optical coupling between measuring beam-to-sample-to-photomultiplier tube varied between measurement methods. Optical density values were kept below 0.3 when collecting data.

2.10-1 Transmission mode

a. Room Temperature Absorbance Spectra

Solvated samples were placed into 1cm quartz cuvettes positioned against a frosted quartz plate (for sample scattering correction) directly in front of the photomultiplier entrance window. The measuring beam was delivered to the sample in free space using the internal optics of the DW-2 spectrophotometer.

b. Low Temperature Absorbance Spectra

Solvated samples supplemented with glycerol were placed into chambers of a copper cold finger and sandwiched between two quartz windows (the window proximal to the detector was frosted). The cold finger was placed into a large radius Pyrex dewar (built *in house*) and submerged up to the quartz windows in liquid N_2. Compressed air was used to prevent

condensation build up on the outside face of the dewar and the surrounding optics. The measuring beam was delivered to the sample in free space using the internal optics of the DW-2 spectrophotometer.

2.10-2 Surface reflectance mode

a. Room Temperature Absorbance Spectra

Dark adapted cell samples were loaded onto 3/8" diameter circles of P8 filter paper (Fischer Scientific). The measuring beam was optically coupled into one leg of a bifurcated fibre optic bundle. The common end of the fibre optic bundle was used to both deliver the measuring light to the sample and collect the reflected signal light. The other leg of the fibre optic bundle was used to deliver the signal light to the photomultiplier detector. Another bifurcated fiber optic bundle was used in the same way for the reference signal. Filter paper plus the same buffer used with the sample was used as the reference 'blank'. The positioning of the fibre bundles was optimised to negate any positional effects from the individual fibres on light collection and emission from the bundles.

b. Low Temperature Absorbance Spectra

The same optical setup was used as described above in *Section 2.10-2a*. P8 filter paper was affixed to one end of ½" diameter steel rod cold fingers using a small amount of thermal grease. Samples were loaded onto the filter paper then flash frozen in liquid N_2. The author built a custom sample holder *in lab* to hold the cold fingers above the liquid N_2 reservoir and couple the fibre optic bundles. Actual temperature of the sample in this setup was 77 to 80^{o} K

as measured with a cryo-silicon diode (model 9600-1, Scientific Instruments Inc, West Palm Beach, Florida, USA, 33407). The samples were thermally stable for the duration of spectra collection.

2.11 Steady State Emission Spectra

2.11-1 Qualitative spectra

Excitation light was provided by a 470 nm LED (Cree) filtered through a 480 nm ±12.5 nm band pass filter. Samples of 0.18 mg mL^{-1} Chl *a* were loaded into 3/16 inch diameter, 1 mm deep wells of PVC sample 'sticks', flash frozen in liquid N_2 under the appropriate light condition, then positioned within the narrow stem of a custom Pyrex dewar filled with liquid N_2. Emission was collected 90^o to excitation by a fibre bundle protected with a 660 nm Schott long pass filter. The fibres of the distal-to-sample end of the bundle were arranged so as to form the entrance slit to the detection side monochromator (Triax 320; Jobin Yvon Inc, Edison, NJ 08820 USA). The detector was a liquid N_2 cooled CCD array (Symphony; Jobin Yvon). Control over the Triax and Symphony hardware and data acquisition for Symphony detector was via SynerJY software (Jobin Yvon). The system was calibrated to the spectral lines of a neon lamp and had a detection bandwidth (FWHM) resolution of 1.5 nm.

2.11-2 (Semi-) Quantitative spectra

Excitation light was provided by a high-power white LED (LED Engine, author built module) coupled to the excitation monochromator (Sciencetech Model 9055, Sciencetech Inc, London, ON, N6E 2V2) via a lens to match the f# of the monochromator. Output from the

excitation monochromator was passed through a 675 nm high performance short pass filter and/ or a yellow long pass Schott glass filter (for blue excitations only); the exit slit was formed by a slit arrangement of the fibres from one leg of a bifurcated fibre optic bundle. The common face of the fibre optic bundle was used to both deliver the excitation light to the sample and collect emission from the sample. The individual fibres were spatially mixed at the common end. The other leg of the bifurcated bundle was used to deliver the emitted light to the collection side optics. The collected emission was passed through a Schott glass 680 nm long pass filter (or a Schott glass 660 nm long pass filter) before being coupled into another fibre optic bundle which delivered the emission to the detection side monochromator (Triax 320; Jobin Yvon). The distal-to-sample end of this fibre optic bundle was arranged into a slit to form the entrance slit to the detection side monochromator. The detector was a liquid nitrogen cooled CCD array (Symphony; Jobin Yvon). Control over the Triax and Symphony hardware and data acquisition for Symphony detector was via SynerJY software (Jobin Yvon). Control over the excitation side monochromator was via author developed code which was in turn integrated into the SynerJY system via software developed by the author. The optical properties of this system gave an excitation bandwidth (FWHM) of 8.5 nm and a detection bandwidth (FWHM) resolution of 1.5 nm. The excitation and detection side optics were calibrated to the spectral lines of a neon lamp. Raw emission spectra were corrected by: 1) subtracting background spectra collected under the exact same experimental conditions, and 2) multiplying by an instrument response function that was created by fitting the collected emission spectra of a fluorescent dye (LDS-751 in ethanol) to published corrected spectra of the dye (Lakowicz 2006) to correct for detection side optics and differences in spectral sensitivity within the CCD array.

Dark adapted samples of 0.18 mg mL^{-1} Chl *a* were loaded into ¼" diameter x 2mm deep depressions in the end of ½" steel cold fingers (sample rods) and held in a temperature controlled stage. Samples were covered to prevent evaporation. Samples were exposed to the same experimental light regime as used during collection of PAM fluorescence traces (as described in *Section 2.5*).

a. Room Temperature Emission Spectra

After samples were treated to the appropriate light regime, the sample rods were coupled to the common face of the bifurcated bundle with a custom sample holder built by the author *in lab*. The sample rod was tightly sealed against the fibre bundle face to prevent evaporation during spectra collection.

b. Low Temperature Emission Spectra

After exposure to the required light treatment the sample loaded cold fingers were dropped into liquid N_2 and flash frozen under the corresponding light condition. The cold fingers were then suspended in a liquid N_2 reservoir and coupled to the bifurcated fibre optic bundle with a custom sample holder built by the author *in lab*. Actual temperature of the sample in this setup was 77 to 80^{o} K as measured with a cryo-silicon diode (model 9600-1, Scientific Instruments Inc). The samples were thermally stable for the duration of spectra collection.

c. Low Temperature Excitation Spectra

Emission spectra were collected at multiple excitation wavelengths from single samples. Raw emission spectra for each series of excitation wavelengths were processed using the following procedure: 1) Excitation wavelength specific background spectra collected under the same experimental conditions were subtracted. 2) Emission spectra were corrected with an instrument response function. 3) Emission spectra were corrected for excitation quanta (quanta as measured at the sample terminus of the fibre bundle with a calibrated Licor-189 quanta light meter, readings were corrected for differences in wavelength-specific sensitivity of the sensor). Mathematical operations were performed using a software program written by the author that called intrinsic Visual Basic functions and functions within the Origin Pro 8.0 (OriginLab Corporation, Northampton, MA 01060, USA) .net .dll library.

2.12 Time Resolved Picosecond Fluorescence Decay Traces

The theoretical modeled time slope of a fluorescence decay $F(t)$ is a sum of ith exponential decays: $F(t) = \sum a_i \, e^{-t/\tau_i}$ where τ is fluorescence lifetime and a is amplitude. The time slope of an experimentally measured fluorescence decay can be modeled by a sample decay function $I(t)$. If the fluorescence measured from a sample is induced by an infinitesimally short excitation light pulse then $I(t) = F(t)$ (Becker 2005, Lakowicz 2006b). In reality however, the excitation pulse is not instantaneous and the detection system has a limited response time described by an instrument response function $R(t)$, causing the initial part of the sample measurement to deviate from that described by $F(t)$ (Becker 2005, Lakowicz 2006b). To get information about the fast processes occurring within the sample that overlap within the time frame of the excitation pulse, the sample decay function needs to be de-convoluted. Thus the

sample decay function follows a convolution of the theoretical model function and the instrumental response function: $I(t) = F(t) * R(t)$ (Becker 2005, Lakowicz 2006b). Convolution of the instrument response function with the theoretical model requires an optimisation algorithm for finding the amplitude and lifetime values within $F(t)$. The approach is to minimize the chi-square value between the data and the model function ($I(t)$) during the fitting process. Interpretation of fluorescence decay at time regions in which there is no overlap with excitation (i.e. within the fluorescence tail) are less prone to convolution errors.

Fluorescence decay kinetics were collected using a time-correlated single photon counting system (system composed of ms125, DCC100, and SPC-830; Becker and Hickl GmbH, Berlin, 12277, Germany). Excitation was with a 407 nm pulsed diode laser. Sample chambers were 2cm x 2cm x 2mm deep and held in a temperature controlled stage. Laser induced fluorescence was collected from the cells via the optics of a scanning laser microscope (*Section 2.4-2*). A series of orange and red filters protected the detection system from the 200 µmol $m^{-2}s^{-1}$ blue-green actinic illumination used to drive NPQ. Fluorescence was collected from cells in an 'Fmax' state by closing PSII reaction centres using a slow (intense) laser scanning rate. During data collection for dark adapted cells, there was a 1 minute rest between laser scans to maintain cells in a dark adapted state. During HL data collection the laser was scanned at 15 second intervals until enough photon counts had been collected. The system had an instrument response with a time resolution of 168 picoseconds (FWHM of scattered laser pulse). Global fitting of the fluorescence decay transients to a sum of exponential decay functions reconvoluted with the instrument response function was performed using SPCimage

software Version 4.8 (Becker and Hickl GmbH). Mean lifetime of the decay transients was calculated as:

$$\tau_m = \frac{\sum_{i=1}^{N} a_i \tau_i}{\sum_{i=1}^{N} a_i}$$

2-13 Data Transformation

Fitting to numerical data was performed using ORIGIN 8.0 or Origin Pro 8.1 software. Graphs were generated using ORIGIN 8.0 or Origin Pro 8.1 software (OriginLab Corporation, Northampton, MA 01060, USA).

2-14 Software Development

When required the author developed software for use with Windows XP operating system using Visual Basic (VB) (Microsoft) programming language. When interfacing with analogue to digital (A/D) and in/out (I/O) hardware devices, DLL and function libraries and/ or command lines obtained from the manufacturer were called in the code. Mathematic operations were performed by calling intrinsic VB functions unless otherwise noted.

3 Results, Analysis, & Discussion

The inquiry into diatom NPQ has been subdivided into five chapters (*Sections 3.1* to *3.5*). The exploration of NPQ commences in *Section 3.1* with a general description of the diatom species studied and some preliminary observations of NPQ. In *Section 3.2*, the strategies for excitation pressure dissipation in *Nitzschia curvilineata* and *Navicula sp*. cells are presented with emphasis on light harvesting and energy transduction. *Section 3.3* describes the inter-relationship between NPQ and electron flow in *Nitzschia* and *Navicula* cells, with special consideration given towards the use of 'alternate' electron transfer pathways to reach photostasis. The intricacies of excitation energy redistribution and the photo-electronic mechanism for quenching during NPQ in *Nitzschia* cells are discussed in *Section 3.4*. In *Section 3.5* NPQ activation and deactivation in *Nitzschia* cells is shown to be due to a dynamic collaboration between ΔpH and DD epoxidation state.

3.1 Preliminary Observations on Diatom NPQ

3.1-1 Overview

Excessive illumination of diatom cells causes a net loss of fluorescence that cannot be attributed to photochemistry. This non-photochemical quenching of fluorescence is triggered by the acidification of the lumen and the enzymatic de-epoxidation of DD to DT. The purpose of this chapter is to offer an overview of the NPQ response in diatoms. The results from a series of basic experiments will be presented to illustrate: (i) NPQ is a non-photochemically induced loss in chlorophyll fluorescence, (ii) NPQ coincides with the conversion of DD to DT molecules, (iii) NPQ can be experimentally manipulated through the usage of chemical agents that target DD de-epoxidase and ΔpH, and (iv) NPQ is variable both within and between diatom species.

3.1-2 NPQ is a large loss in chlorophyll fluorescence during exposure to excess light

When diatom cells are exposed to high irradiation preceded by a period of darkness (or illumination ≤ that of which they were cultured) there is a readily observable loss in Chl *a* fluorescence. This drop in fluorescence is induced quickly (seconds) upon the transition to HL (the induction phase of NPQ), more or less stabilizes during HL illumination (steady state NPQ), and then recovers comparatively slowly once the HL is removed (recovery phase of NPQ). The quenching event can be observed *in vivo* at the cellular level by measuring Chl *a* autofluorescence from diatom cells using laser confocal microscopy (Figure 3.1-1). However, the results from Figure 3.1-1 do not effectively separate photochemical from non-photochemical quenching.

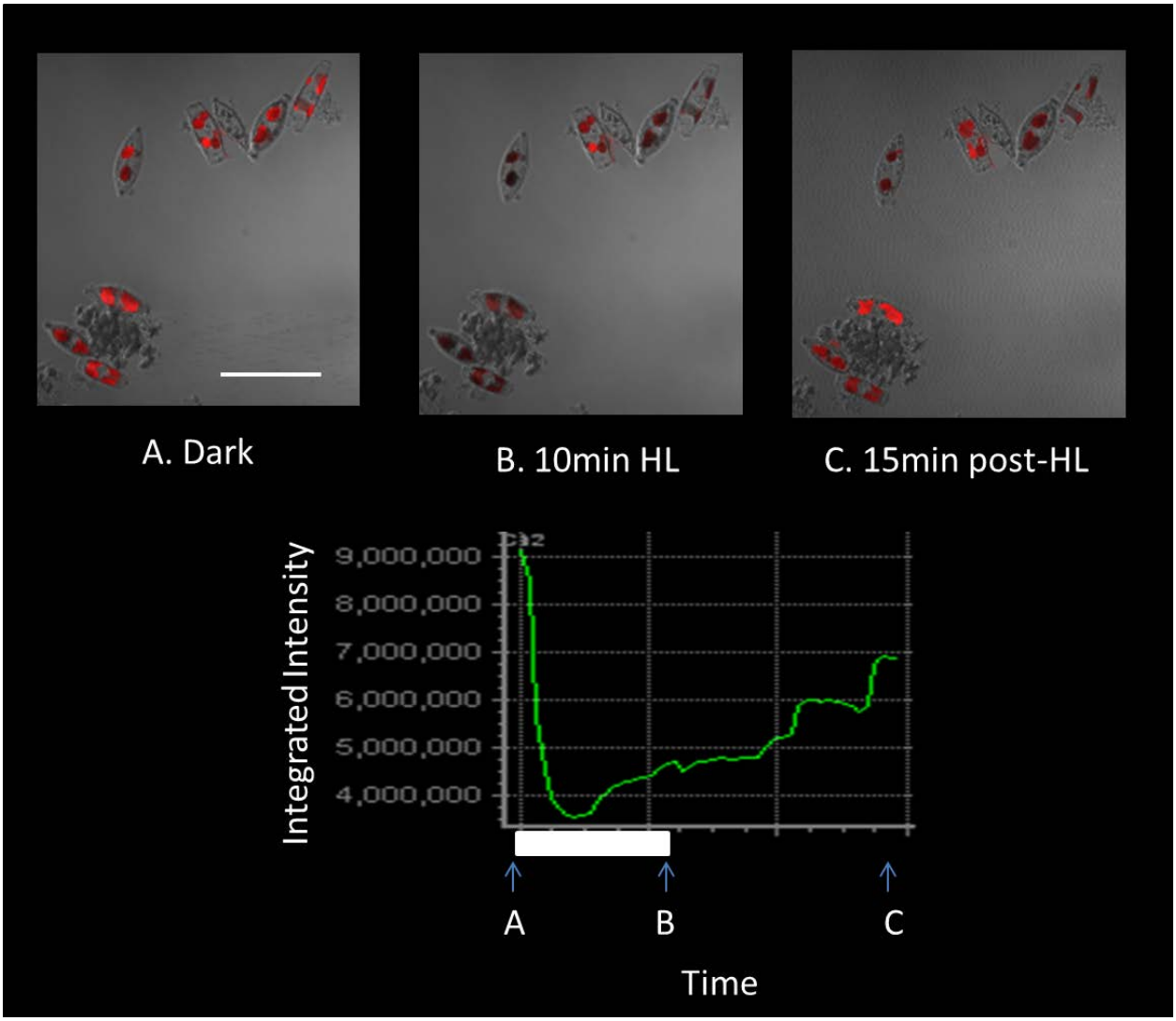

Figure 3.1-1 Fluorescence quenching at the cellular level. Top panels, Time course of confocal microscopy fluorescence images overlaid with differential interference contrast (DIC) images from *Nitzschia curvilineata* cells grown at 50 µmol $m^{-2}s^{-1}$ during a high light (HL) transition. **A**, in the dark prior to illumination; **B**, after 10 minutes (min) of 1000 µmol $m^{-2}s^{-1}$ HL illumination; **C**, in the dark for 15 minutes after HL is removed. Cells in the lower left hand corner are clumped around a mucilage (extracellular polymeric substance) globule, which is typical of this species**. Lower panel**, Fluorescence images were collected every 30 seconds during the HL transition and the integrated intensities were plotted against time. The white bar represents the 10 minute period of HL. A, B, C arrows correspond to the time points for the images in the top panels. Excitation was with a 470 nm steady state laser and fluorescence greater than 680 nm was selected. White scale bar in image panel 'A' represents 50 µm.

The preferred method for observing NPQ from a large population of cells is through the use of PAM fluorometry (Figure 3.1-2). The PAM method allows Chl *a* fluorescence yield to be measured autonomously from the HL illumination used to drive the NPQ response. Non-photochemical quenching is distinguished from photochemical quenching through the

application of brief, high intensity light pulses that temporarily saturate the PSII photochemical capacity (i.e. close PSII reaction centres), thereby eliminating any quenching of the fluorescence signal from photochemistry and giving rise to maximal PSII fluorescence (Fm). Applications of these saturating light pulses appear as sharp spikes in the PAM fluorescence trace (Figure 3.1-2). Any change in maximal PSII fluorescence during illumination (Fm') from the dark adapted state (Fm_{dark}) is due to non-photochemical events affecting the allocation of absorbed light energy within the thylakoid pigment pool. The extent of non-photochemical quenching is parameterised as $\mathcal{NPQ} = (Fm_{dark} - Fm') / Fm'$.

The capacity for photochemistry is also measured with the PAM saturating light pulse method. The maximum quantum efficiency for PSII photochemistry (ΦPSII) describes the ratio of open to closed PSII reaction centres. ΦPSII depends on the redox state of the PSII electron acceptors; an over reduced PQ pool will not allow forward electron transfer and charge separation in the reaction centre thereby increasing fluorescence yield. Maximum quantum efficiency must therefore be measured under conditions with a fully oxidised PQ pool. Dark adaptation is typically used to oxidise the PQ pool; however, the PQ pool in diatoms is often at least partially reduced in the dark due to chlororespiration. A brief application of far-red light (≥720 nm) can be used to preferentially excite PSI so as to fully oxidise the PQ pool prior to collection of basal fluorescence level. ΦPSII is measured as the amount of fluorescence inducible with a saturating light pulse over that of basal fluorescence (i.e. variable fluorescence, $Fm_{dark} - Fo_{dark}$) normalised by the maximal fluorescence level achieved with the saturating light pulse, so $\Phi PSII = (Fm_{dark}-Fo_{dark}) / Fm_{dark}$. A ΦPSII of 1 (assuming that only

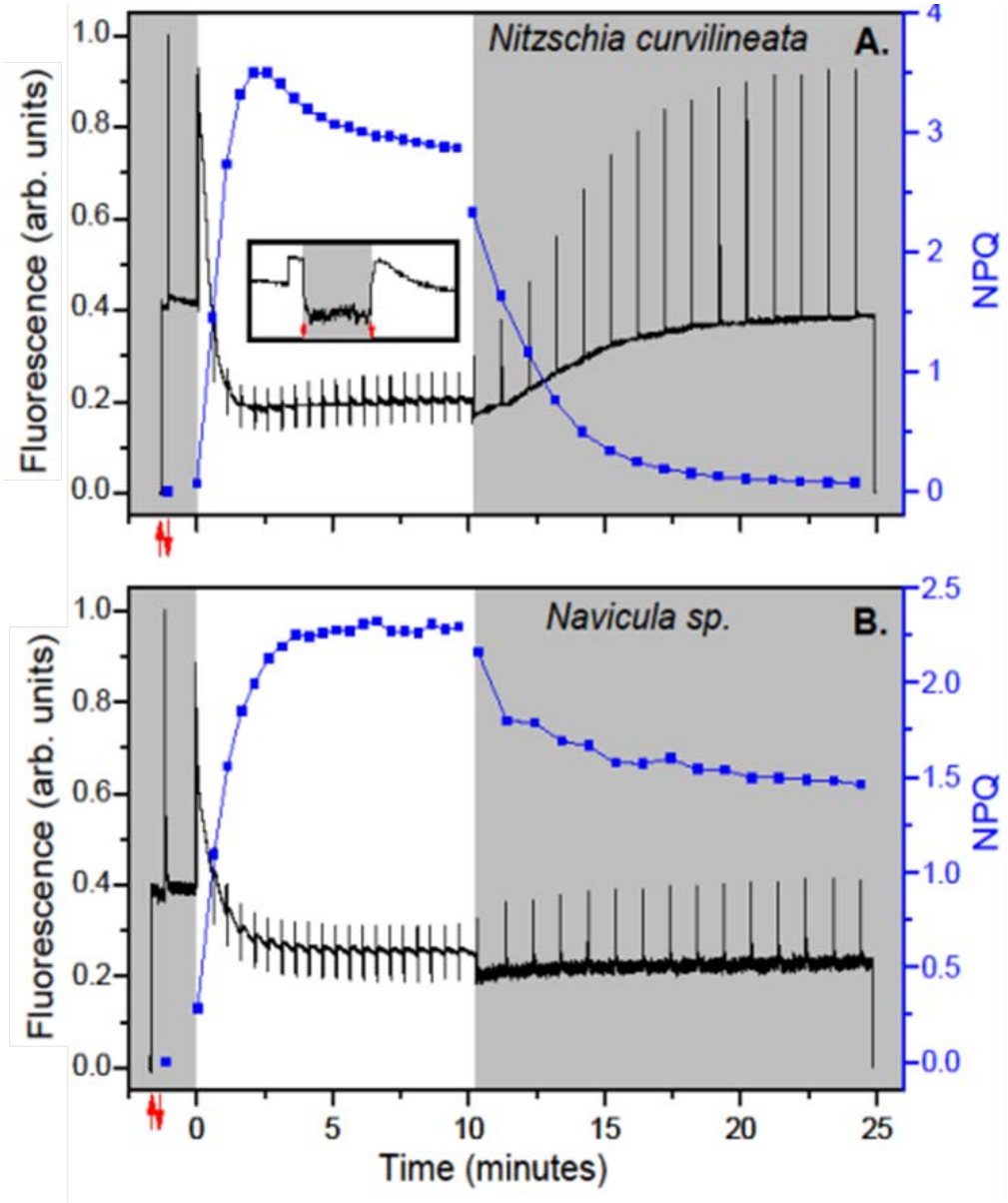

Figure 3.1-2 NPQ quantified using PAM fluorometry. Fluorescence yield (≥680 nm) is monitored with a weak measuring light (470 nm) as additional light sources are used to trigger photo-physiological events. Raw PAM fluorescence (black traces, left hand scaling) and the corresponding calculated $\mathcal{NPQ}$ values (blue squares, right hand scaling) are shown for **A**, *Nitzschia curvilineata* and **B**, *Navicula sp*. cells grown at 50 µmol $m^{-2}s^{-1}$ in response to a high light (HL) treatment of 500 µmol $m^{-2}s^{-1}$. Darkened plot areas indicate dark conditions and white plot areas indicate HL conditions. The sharp vertical spikes correspond to the application of 300 millisecond saturating light pulses to briefly close all PSII reaction centres for collection of maximal fluorescence (Fm_{dark} and Fm'; *dark* indicates dark conditions prior to illumination; ' indicates conditions other than dark). The red vertical arrows represent the application of far-red light to oxidise the PQ pool for collection of minimal fluorescence (Fo_{dark} and Fo'). The **insert** in panel A is a zoom in of the fluorescence trace showing the kinetics associated with the application of a saturating light pulse during HL illumination. (Note: $\mathcal{NPQ}$ was not calculated directly from the low resolution fluorescence traces shown here, but from separate simultaneous high resolution measurements.)

fluorescence from PSII is being measured, which is not completely realistic) means that all PSII reaction centres are capable of performing charge separation and no excitation energy reaching PSII is lost as fluorescence prior to the saturating light pulse; ΦPSII of 0 means that no PSII reaction centres are capable of performing charge separation and that all excitation energy reaching PSII is dissipated as fluorescence. ΦPSII of non-stressed dark adapted leaves is typically near 0.83 for most higher plant species (as reviewed by Maxwell and Johnson 2000). In the diatoms cultured here, ΦPSII values approaching 0.7 were rarely observed, with values typically in the 0.5 to 0.6 range. These ΦPSII values are comparable to those observed in *Phaeodactylum tricornutum* (as reviewed by Büchel and Wilhelm 1993). The proportion of PSII reaction centres that remain open during illumination can be indicated by the 'photochemical quenching' fluorescence parameter, qP. qP is calculated as the ratio of variable fluorescence during illumination (Fm'-Ft) to variable fluorescence with a fully oxidised PQ pool (Fm'-Fo'), so qP = (Fm'-Ft) / (Fm'-Fo'). If illumination does not cause any net reduction of Q_A then qP equals 1; if illumination is excessive of the adaptive state of the photosynthetic machinery then there is a net reduction of Q_A and qP values lessen.

3.1-3 NPQ involves a loss in DD and corresponding accumulation of DT

Fluorescence quenching during NPQ in diatoms is known to be associated with the de-epoxidation of DD to DT (see *Section 1.4-3*). This pigment interconversion is quantified in the literature using HPLC of solvated cell extracts (e.g. Ruban et al. 2004). In this study, thin layer chromatography was used in an effort to witness DD de-epoxidation. The results are suggestive of an increase in DT molecules at the expense of DD molecules during HL treatment (Figure 3.1-3); however, the changes were at the concentration resolution limit of this technique.

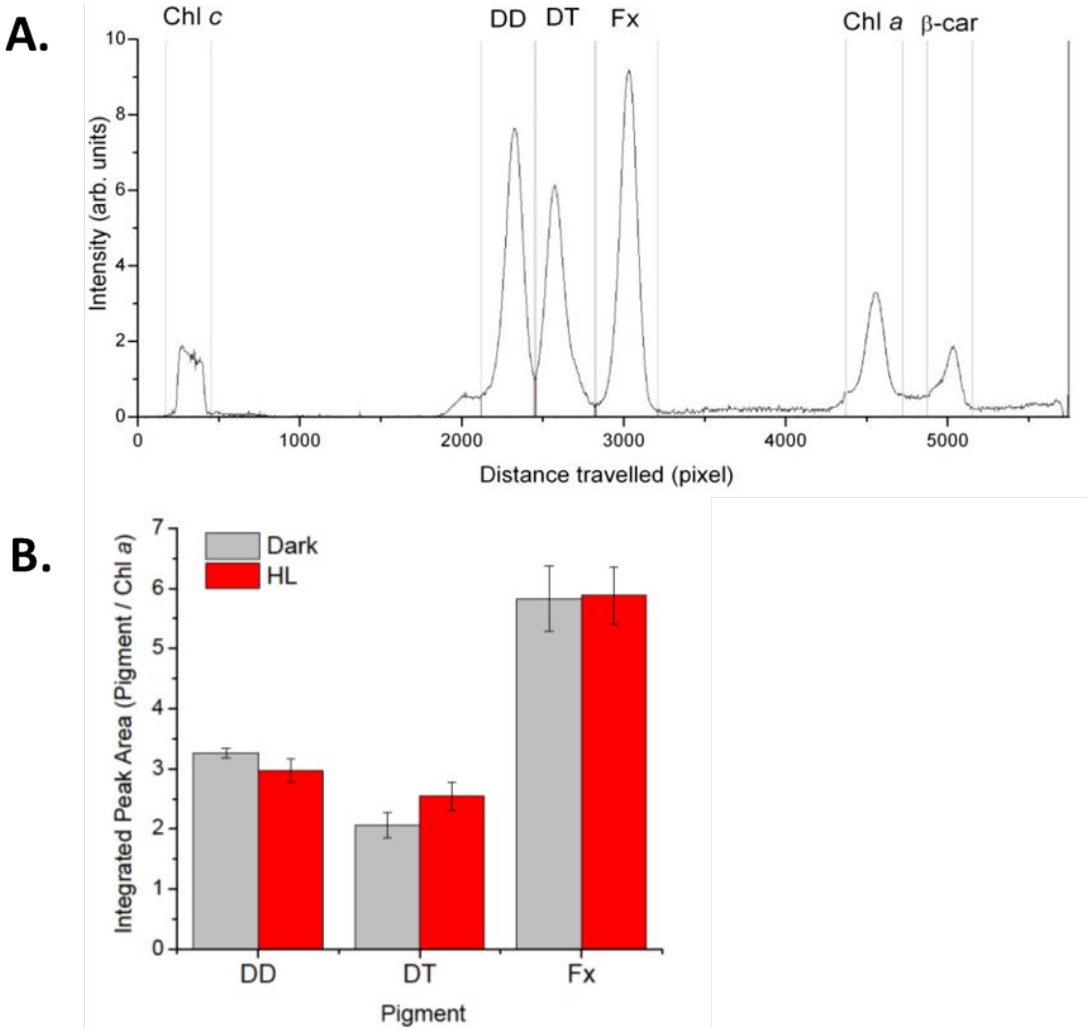

Figure 3.1-3 DD cycle epoxidation state. *Nitzschia curvilineata* cells were flash frozen in a dark adapted state (Dark) and after 10 minutes exposure to 2000 µmol $m^{-2}s^{-1}$ high light (HL). Cell extracts were separated via thin layer chromatography and the resulting chromatogram was digitized for analysis. For methodology details see *Section 2.2-4*. **A**, a representative chromatogram from dark adapted cells. **B**, carotenoid peak areas normalised to the chlorophyll *a* (Chl *a*) peak area. Error bars represent ± 1 standard deviation from the mean of 4 culture samplings. Chl *c*, chlorophyll *c* (including c_1 and c_2); DD, diadinoxanthin; DT, diatoxanthin; Fx, fucoxanthin; β-car, β-carotene.

3.1-4 The use of chemical agents to experimentally manipulate NPQ

NPQ in diatoms is known to have both ΔpH and DD de-epoxidation dependent components (see *Section 1.4*). ΔpH can be experimentally manipulated with the chemical agents NH_4Cl and DCCD, whereas DD de-epoxidation can be inhibited with DTT. Pre-treatment

with these inhibitors drastically alters the PAM fluorescence traces during transitions to and from HL (Figure 3.1-4).

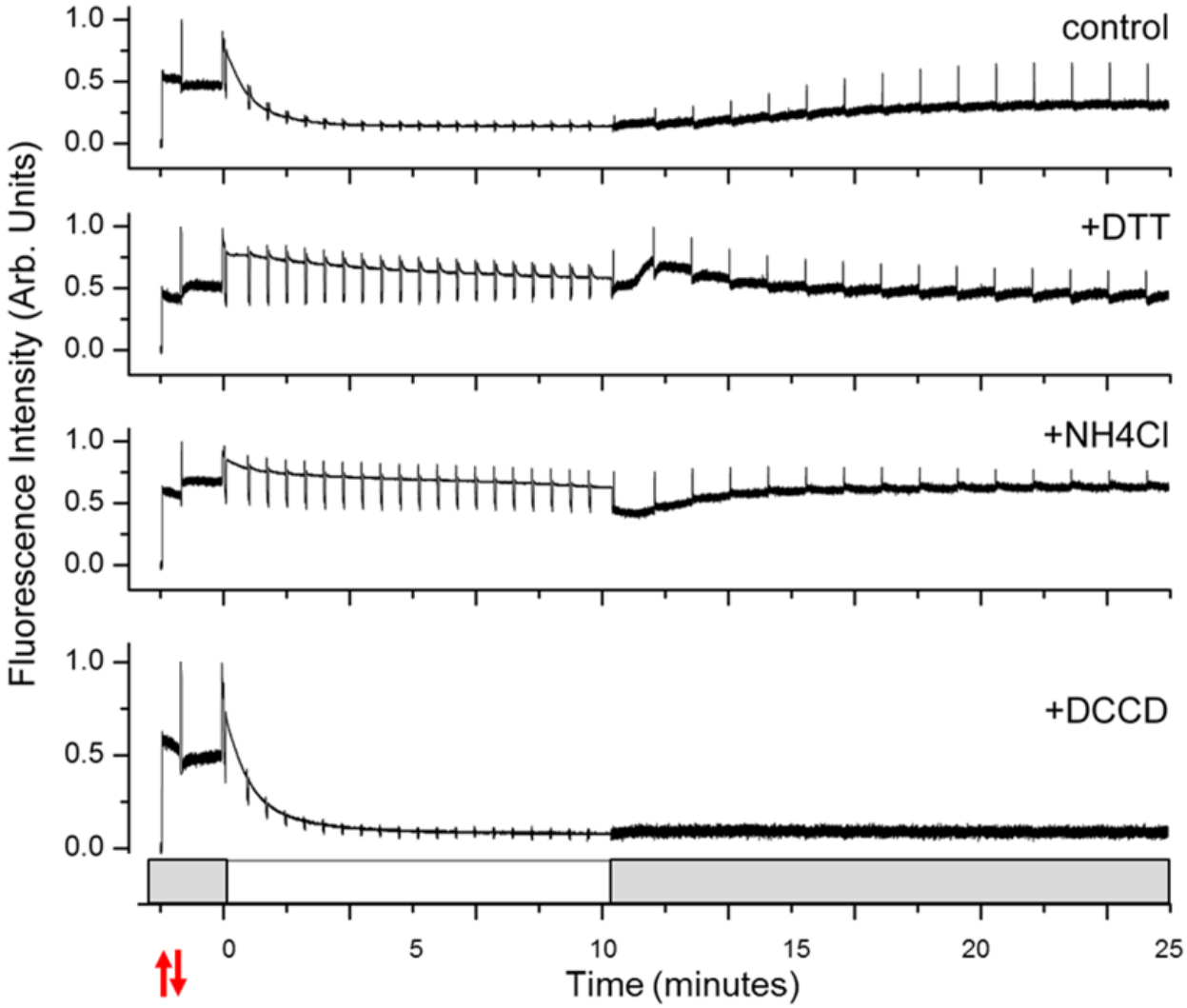

Figure 3.1-4 The effect of NPQ sensitising agents on PAM traces collected during high light transitions. Representative traces are shown for dark adapted *Nitzschia curvilineata* cells during a 10 minute illumination with 500 µmol $m^{-2}s^{-1}$ high light (HL). The dark shaded bars along the x axis indicate dark conditions and the white bar represents the period of HL. Dark adapted cells were pre-treated with 5.3 mM DTT to inhibit DD de-epoxidase, 2.8 mM of the proton scavenger NH_4Cl, or 320 µM of the ATP synthase inhibitor DCCD. Red arrows indicate a brief period of far red illumination for collection of minimal fluorescence prior to application of HL. PAM measurements as described in Figure 3.1-2. Cultures were grown at 50 µmol $m^{-2}s^{-1}$.

DTT is proposed to specifically inhibit the activation of de-epoxidases during HL.

Violaxanthin de-epoxidases in plants all have a highly conserved cysteine rich N-terminal

domain (Arnoux et al. 2009). This domain is not dispensable to enzymatic activity and has been thought to be responsible for inhibition of violaxanthin de-epoxidase by the reducing agent DTT (Hieber et al. 2002). Arvidsson et al. (1997) reported that DTT inhibition of violaxanthin de-epoxidase only occurs at low pH in plant chloroplasts, which the authors interpreted as the targeted disulfide bridge as being only accessible at low pH. This observation suggests that DTT is reducing cysteine residues that are exposed during the dimerization and activation steps that purportedly happen to violaxanthin de-epoxidase during acidification of the lumen (Arnoux et al. 2009). Outside of the N-terminal domain, there are two highly conserved cysteines in the central lipocalin domain (Cys118 and Cys249) that form a disulfide bridge in the monomer (based on structure of Arnoux et al. 2009). Cys118 is located within the L1-loop of the central lipocalin domain. This cysteine immediately adjoins to an aspartate, is two amino acid residues towards the C-terminus from a histidine, and three amino acid residues towards the N-terminus from another aspartate. These three residues have been implicated with performing the pH induced conformational and dimerization switch in the protein (Arnoux et al. 2009). Both Cys118 and Cys249 are located at the dimer interface (Arnoux et al. 2009; Figure 3.1-5). These observations lead one to hypothesize that the true target of DTT against violaxanthin de-epoxidase activity is via disruption in the formation of the active dimer form of the enzyme. It is further hypothesised that if dimerization is inhibited then violaxanthin de-epoxidase will not bind to the thylakoid, since dimerization has been implicated with inducing thylakoid attachment (Arnoux et al. 2009). Although these hypotheses are based on data from the higher plant system, they can be extended to DD de-epoxidases in diatoms. The protein sequence for DD de-epoxidase in the diatom *Thalassiosira pseudonana* contains these two cysteines (Figure

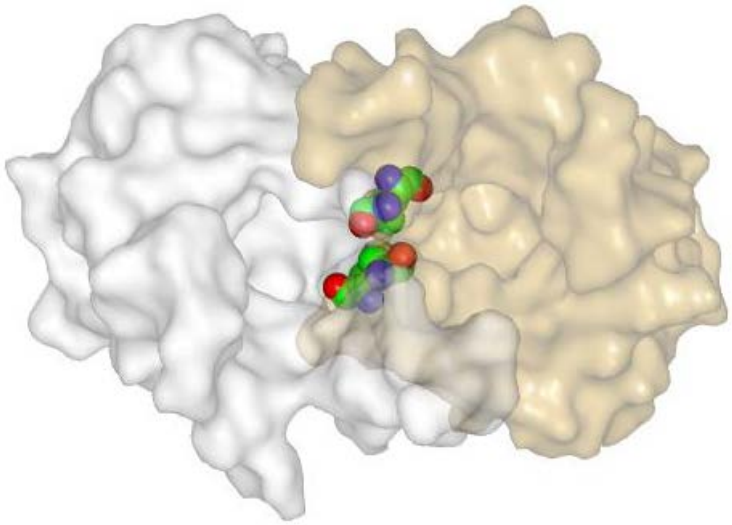

Figure 3.1-5 X-ray crystal structure of the central lipocalin domain of violaxanthin de-epoxidase from *Arabidopsis thaliana* at pH 5. The view is into the lipocalin cavity. The violaxanthin de-epoxidase monomer forms a dimer under acidic conditions. Protein surface of monomer A is shown in grey; surface of monomer B is shown in khaki. Each monomer contains 1 disulfide bridge (Cys118-Cys249). These disulfide bridges are located at the monomer-monomer interface upon dimerization. Structure deposited by Arnoux et al. 2009 (PDB 3CQR).

```
VDe   1   MAVATHCFTSPCHDRIRFFSSDDGIGRLGITRKRINGTFLLKILPPIQSADLRTTGGRSSRPLSAFRSGFSKGIFDIVPL  80
DDe   1   MKLFLSLVLAAAP--VSSFAPSN--------------------PVVSRTHSSVHSQQHNHVLEAHNDNMDDITFSLSAR  57

VDe  81   PSKNELKELTAPLLLKLVGVLACAFLI---------------VPSADAVDALKTCACLLKGCRIELAKCIANPACAANVA  145
DDe  58   NINNEIVERIGKVTTSALLALTLSFSAITSPISGPNGDVLSSIPSANAADGAKIGLCLVKKCRVPLAKCITNPNCLANVI  137

VDe 146   CLQTCNNRPDETECQIKCGDLFENSVVDEFNECAVSRKKCVPRKSDLGEFPAPDPSVLVQNFNISDFNGKWYITSGLNPT  225
DDe 138   CINSCNGKEDETGCQINCGNVFENDVVGEFNKCAVTDMTCVPQKKDDGSYPVPSKDVLVQSFDTKLWNGRWFITAGQNKL  217

VDe 226   FDAFDCQLHEFHTEGDNKLVGNISWRIKTLDSGFFTRSAVQKFVQDPNQPGVLYNHDNEYLHYQDDWYILSSKIENKPED  305
DDe 218   FDTFPCQVHFFTETAPGKFVGKLNWRIEEPDGEFFTRDAVQEFVQDPNNPAHLINHDNEYLHYQDDWYIVDYAADDNKEG  297

VDe 306   ---YIFVYYRGRNDAWDGYGGAVVYTRSSVLPNSIIPELEKAAKSIGRDFST-FIRTDNTC----------------  362
DDe 298   VPPFAFVYYRGENDAWIGYGGAVVYTRDSKLPESLLPRLREAAKKVNFDFDKDFDLTDNSCKALEKGEEVVLREKFAGKM  377

VDe 363   ------------------------GPEPALVERIEKTVEEG--------------ERIIVKEVEEIEEEVEKEVEKVGRT  404
DDe 378   AIQTEKQLQQQAVLARTAASNTVKGEVTAVEKSLQKIEEKALAFEKELMKDVVSVEKEIVKEVEEVEKEIVQEEQKI---  454

VDe 405   EMTLFQRLAEGFNELKQDEENFVRELSKEEMEFLDEIKMEASEVEKLFGKALPIRKVR  462
DDe 455   ----------------------------------------------FGG------IR  459
```

Figure 3.1-6 Amino acid sequence alignments of violaxanthin de-epoxidase (VDe) from *Arabidopsis thaliana* and diadinoxanthin de-epoxidase (DDe) from the diatom *Thalassiosira pseudonana* (CCMP1335). Conserved residues are in red font; conserved cysteine residues are highlighted in yellow; cysteines equivalent to Cys118 and Cys249 in Figure 3.1-5 are marked with an asterisk. (NCBI accession numbers NP_172331.1 & XP_002292080.1)

3.1-6). Dosage dependences of DTT on NPQ in *Nitzschia curvilineata* and *Navicula sp*. are given in Figure 3.1-7. Note how the cells of *Navicula* are more sensitive to DTT concentration, yet have a comparatively large amount of NPQ that cannot be inhibited with DTT.

Ammonium chloride is used as an uncoupler to prevent the development of ΔpH and to dissipate pre-existing ΔpH (Ruban et al. 2004). It dissociates in aqueous solution to ammonia gas; ammonia readily passes through membranes and functions as a proton scavenger. Pre-treatment with NH_4Cl effectively prevents qE induction in diatoms (Figures 3.1-4 & 3.1-8; Ruban et al. 2004). Nigericin is a more lipophylic uncoupler of thylakoid membranes and is used extensively in research of ΔpH dependent mechanisms in higher plant chloroplasts and other algal groups. However, nigericin concentrations of up to 20 µM had no effect on *Nitzschia curvilineata* cells (data not shown). Ruban et al. (2004) suggested that nigericin is not able to diffuse through the diatom cell wall (frustule) (at least in *Phaeodactylum tricornutum*), even though Ting and Owens (1993) successfully used 5 µM nigericin to abolish non-photochemical quenching in *P. tricornutum*. The specificity of ammonium as a NPQ sensitizer is illustrated in Figure 3.1-8.

High dosages of DCCD enhance $\mathcal{NPQ}$ amplitude during illumination by inhibiting ΔpH dissipation via ATP synthase activity. DCCD forms covalent adducts with the protonated carboxyl groups of amino acid residues within accessible hydrophobic environs. DCCD irreversibly binds with the Fo subunit c in CF1FO-ATP synthase blocking the CFo proton channel (Junge 1989). However, the effect of DCCD within chloroplasts is more complex, since it can form adducts with protonated carboxyl groups that are not specific to CF1FO-ATP synthase. At

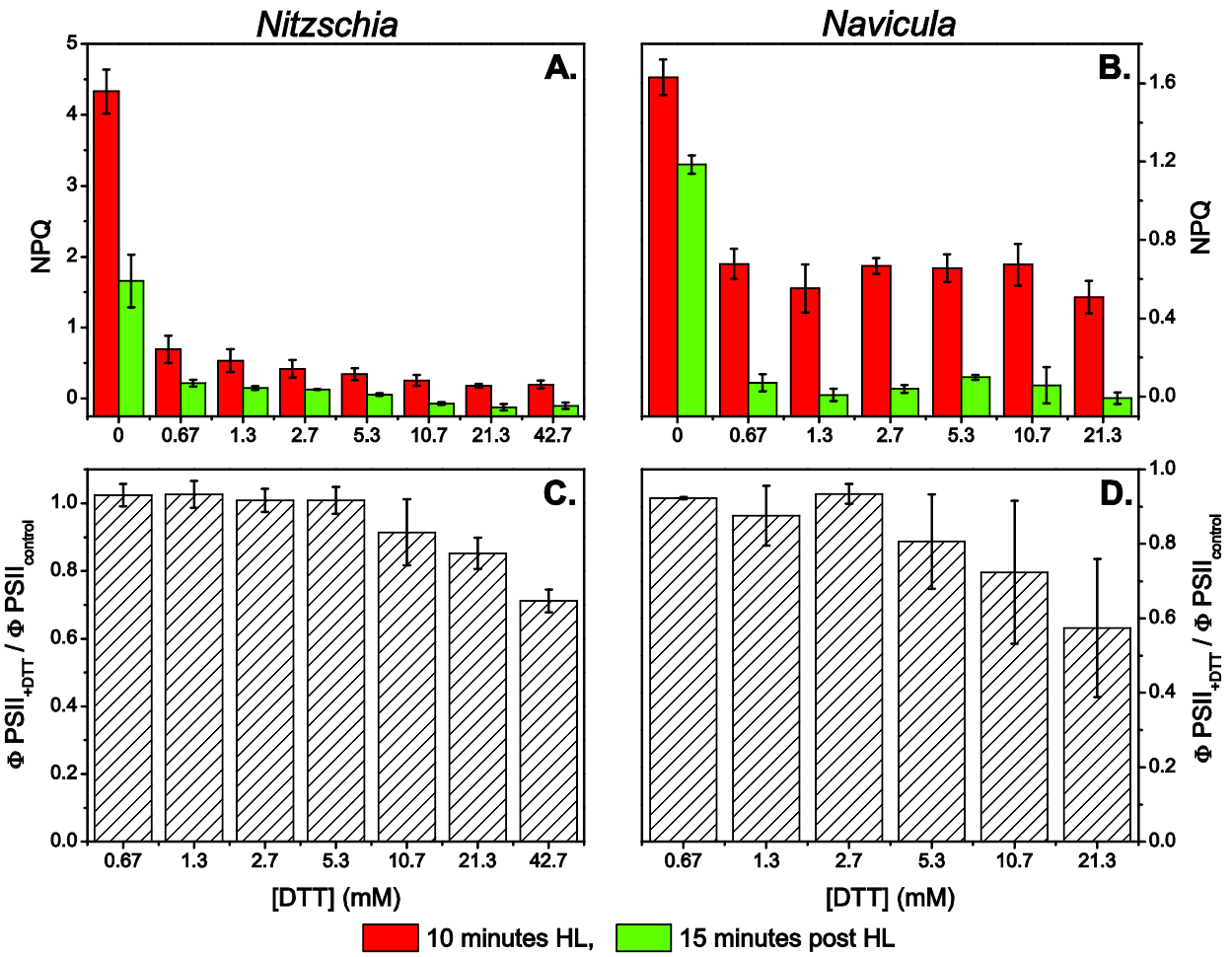

Figure 3.1-7 DTT dosage effects. Dark adapted cells of *Nitzschia curvilineata* (**A**, **C**) and *Navicula sp.* (**B**, **D**) were pre-treated for 5 minutes in the dark with DTT, then the cells were illuminated with 500 µmol $m^{-2}s^{-1}$ high light (HL). A, B, $\mathcal{NPQ}$ values at 10 minutes of HL (red bars) and at 15 minutes of dark following HL (green bars). C, D, the influence of DTT on ΦPSII. Error bars represent ± 1 standard deviation from the mean of 3 separate cultures grown at 50 µmol $m^{-2}s^{-1}$.

low dosages of DCCD (≤ 30 µM), the principle effect on spinach thylakoids is an uncoupling of ΔpH centred at PSII proton translocation (see Ruban et al. 1992). In higher plants DCCD inhibits qE by binding to PsbS residues (Ruban et al. 1992, Dominici et al. 2002). However, in the diatoms studied here, DCCD pre-treatment with high dosages enhanced $\mathcal{NPQ}$ in a manner consistent with ΔpH enhancement. Interestingly, lower DCCD dosages (40 µM) seemed to particularly inhibit PSII activity and also lower $\mathcal{NPQ}$ (Figure 3.1-9). This may be due to an uncoupler effect of DCCD at low concentrations, similar to what is observed in higher plants

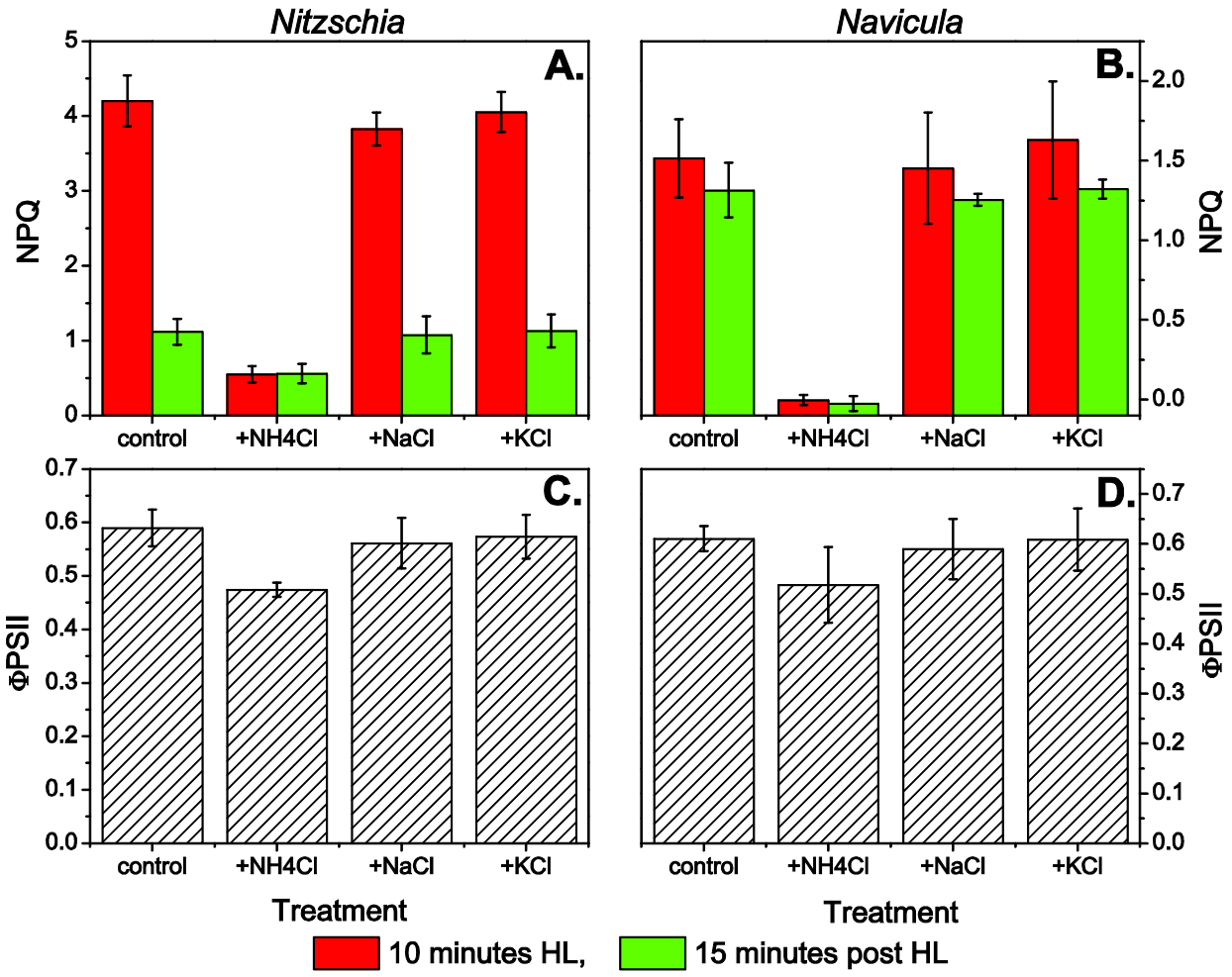

Figure 3.1-8 Ammonium effects. Dark adapted cells of *Nitzschia curvilineata* (**A**, **C**) and *Navicula sp*. (**B**, **D**) were pre-treated for 5 minutes in the dark with 2.8 mM of a chloride salt, then the cells were illuminated with 500 µmol $m^{-2}s^{-1}$ high light (HL) for 10 minutes. A, B, $\mathcal{NPQ}$ values at 10 minutes of HL (red bars) and at 15 minutes of dark following HL (green bars). C, D, the influence of the salt treatments on ΦPSII. Error bars represent ± 1 standard deviation from the mean of 3 separate cultures grown at 50 µmol $m^{-2}s^{-1}$.

(Ruban et al. 1992). As seen in Figures 3.1-4 and 9, DCCD enhances NPQ during HL and maintains this high $\mathcal{NPQ}$ even after the HL has been removed. The proton gradient will dissipate slowly after illumination even without the assistance of ATP synthase due to passive proton diffusion. There are two plausible explanations for why there is very little relaxation of NPQ in the dark after HL has ended with DCCD treatment. The first being that the lack of ATP production during the HL period hampers the transfer of photochemically derived electrons to

CO_2 (because there is no $NADP^+$ regeneration during the reduction phase of the Calvin Cycle), which unbalances the redox state of the chloroplasts leaving no available NADPH for DT epoxidase; the second being that a lack of ATP generation during HL promotes chlororespiratory generation of ΔpH post HL in a futile attempt to generate ATP and balance the supply of ATP and reducing equivalents.

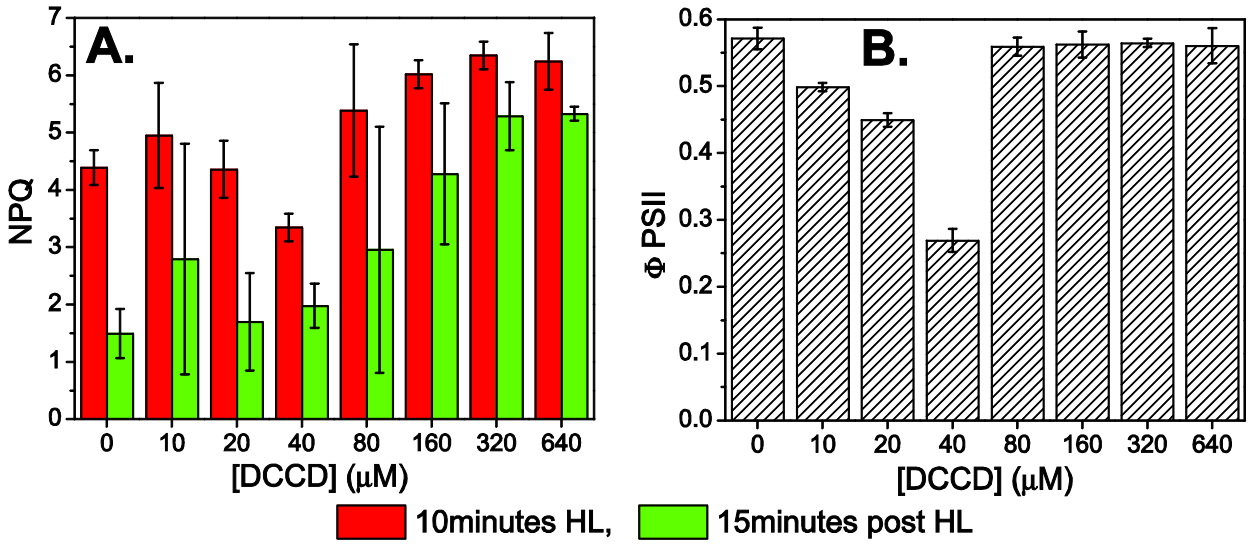

Figure 3.1-9 DCCD dosage effects. Dark adapted cells of *Nitzschia curvilineata* were pre-treated for 5 minutes in the dark with DCCD, then the cells were illuminated with 500 μmol $m^{-2}s^{-1}$ high light (HL) for 10 minutes. **A**, $\mathcal{NPQ}$ values at 10 minutes of HL (red bars) and at 15 minutes of dark following HL (green bars). **B**, the influence of DCCD on ΦPSII. Error bars represent ± 1 standard deviation from the mean of 3 separate cultures grown at 50 μmol $m^{-2}s^{-1}$.

Ideally the ΔpH effects of NH_4Cl and DCCD would be verified through direct measurements of pH within the chloroplast as thru the use of pH sensitive fluorescent dyes (e.g. 9-aminoacridine, see Takizawa et al. 2007) or by measuring absorbance changes induced by the electric field component (ΔΨ) of the transmembrane electrochemical proton potential difference ($\Delta\mu^+_H$) on specific carotenoids spanning the thylakoid. Even though electrochromic shifts (ECS) have been measured in *Phaeodactylum tricornutum* (Bailleul et al. 2010b), experimental attempts at identifying the ECS bands reported by Bailleul et al. (2010b) at 540

and 562 nm in *Nitzschia curvilineata* and *Navicula sp*. were unsuccessful. Nonetheless, the experimental effects of NH_4Cl and DCCD on NPQ strongly support a primary ΔpH role for these agents.

3.1-5 NPQ in diatoms shows a high level of intra- and inter-species variability

Both the amplitude and kinetics of NPQ induction and relaxation can show large variability within cell cultures depending on the time of photoperiod day, subtle changes in cell density, and time between dilutions with fresh growth media. Cultures of *Nitzschia curvilineata* and *Navicula sp.* never exhibited true logistic shaped growth curves with an exponential and log phase; instead they grew more at a linear rate before nutrients became depleted. Cultures of the same species with approximately the same Chl *a* concentration or ΦPSII did not always have the same NPQ characteristics. Especially variable is the recovery phase of NPQ; there can be full relaxation of NPQ once HL is removed (≥ 90 % relaxation of $\mathcal{NPQ}$ could be observed in *Nitzschia curvilineata*) to no recovery and even an enhancement of NPQ. The variability in NPQ was tracked during an extended growth period of *Nitzschia curvilineata* and *Navicula sp.* cultures (Figure 3.1-10). Pigment content, ΦPSII, and steady state photochemical quenching coefficients were also measured. The periodicity of cell samplings kept cell densities at a comparable level during the entire growth period. No strong correlations were observed between pigment composition and $\mathcal{NPQ}$ (statistics not shown).

NPQ also varies considerably between diatom species. $\mathcal{NPQ}$ transients are shown in Figure 3.1-11 for four species grown under the same culture conditions and measured under the same experimental conditions. These species differ in phylogeny, habitat, and cell size (see

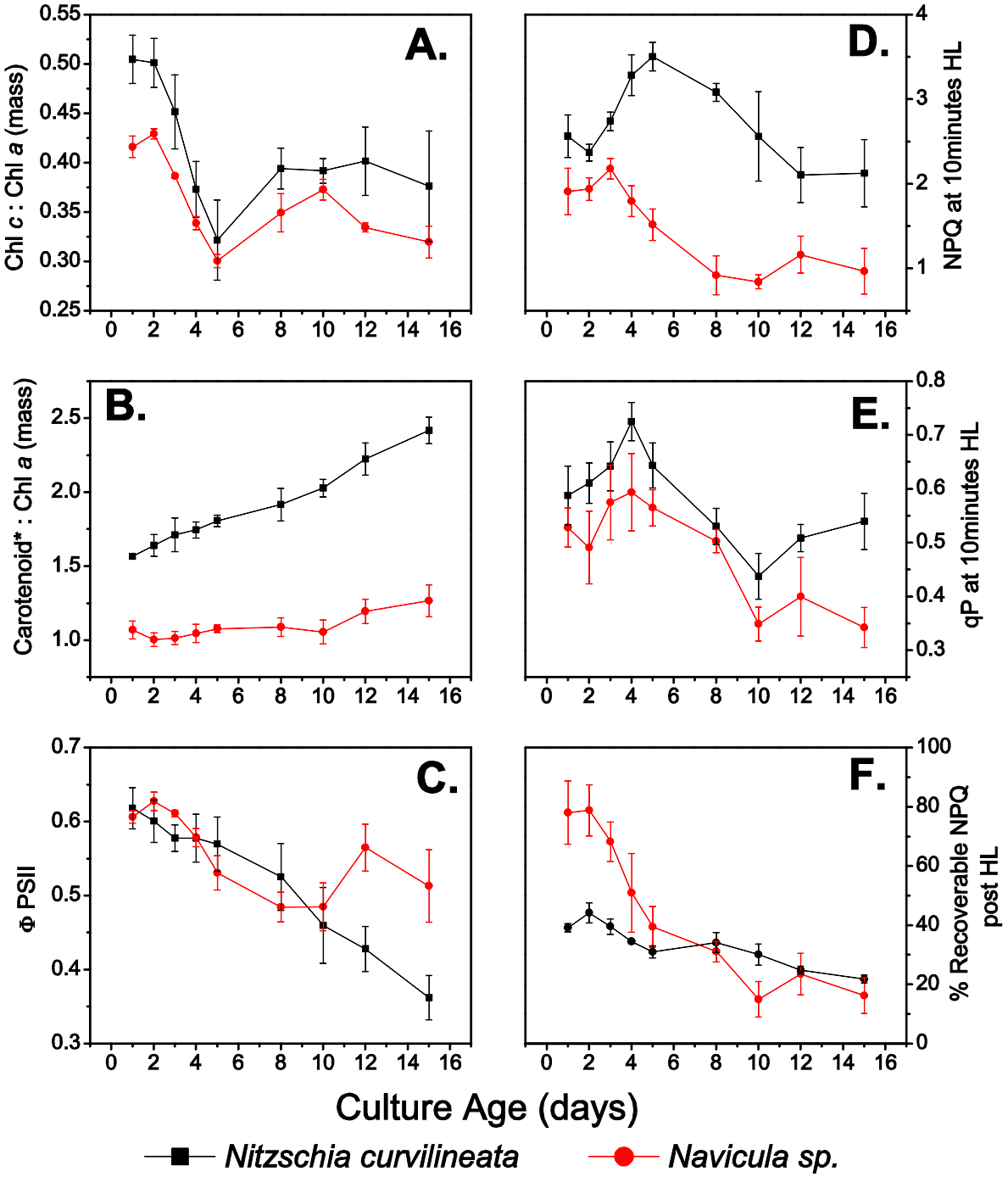

Figure 3.1-10 Photophysiological monitoring of diatom cultures over an extended growth period. Day zero corresponds to inoculation of fresh culture media. Solvent extracts of dark adapted cells were used to photometrically monitor pigment composition in terms of **A**, Chl *c* (including chlorophyll c_1 and c_2) and **B**, carotenoids. Chlorophyll *a* fluorescence was used to measure maximal PSII quantum efficiency (ΦPSII; **C**) for dark adapted cells, $\mathcal{NPQ}$ (**D**) and photochemical quenching (qP; **E**) after 10 minutes irradiance with 500 µmol $m^{-2}s^{-1}$ high light (HL), and the amount of $\mathcal{NPQ}$ that can recovery during 15 minutes of dark after 10 minutes of HL (expressed as percent of $\mathcal{NPQ}$ at 10 minutes HL; **F**). Error bars represent ± 1 standard deviation from the mean of 3 separate cultures grown at 50 µmol $m^{-2}s^{-1}$. *, all carotenoids including diadinoxanthin, diatoxanthin, fucoxanthin, β –carotene.

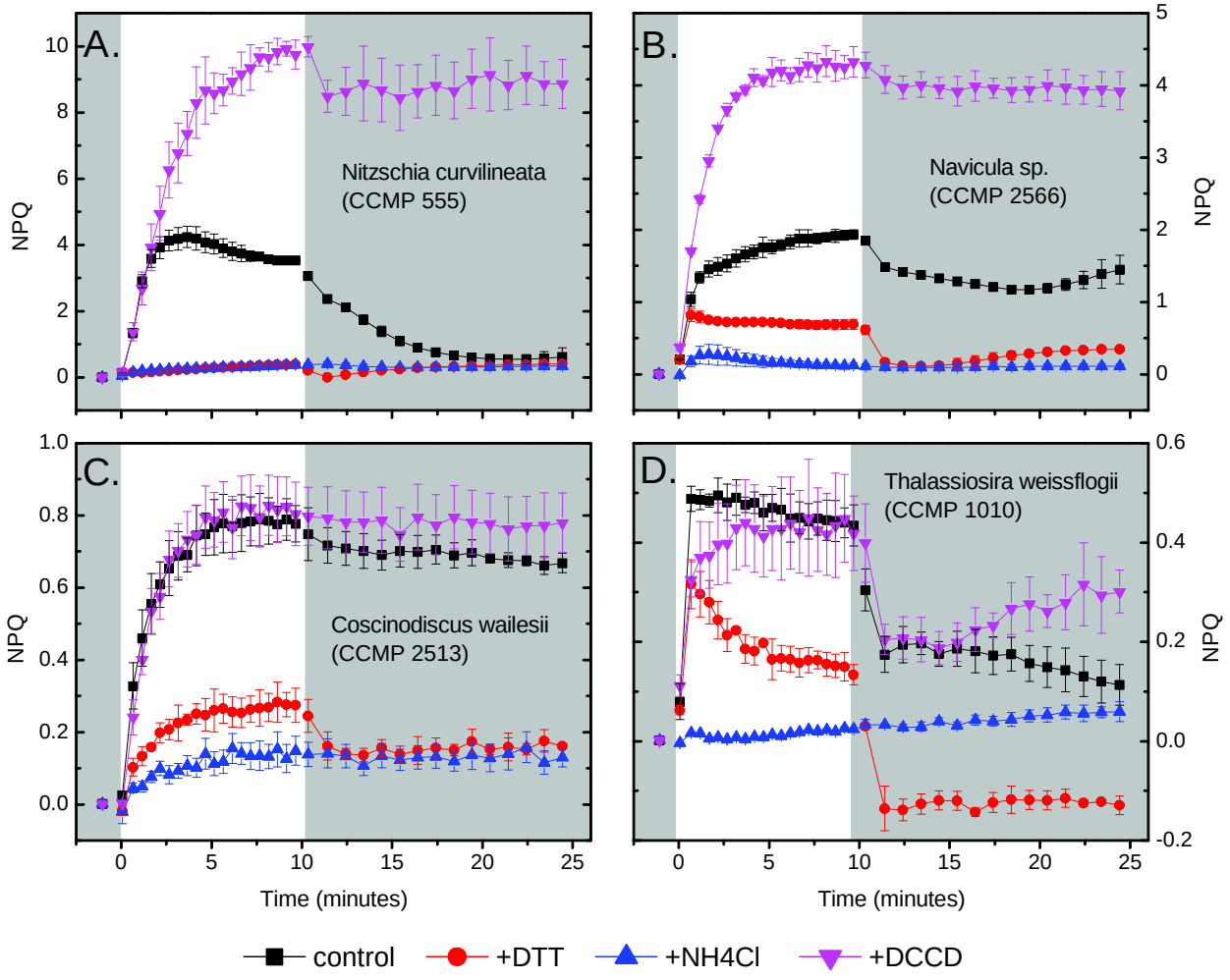

Figure 3.1-11 Diatom species diversity in non-photochemical excitation energy dissipation. **A, B, C, D,** $\mathcal{NPQ}$ transients were obtained with pre-treatments of the de-epoxidase inhibitor DTT (2.65 mM for *Navicula*, 5.3 mM for *Nitzschia*, *Coscinodiscus*, *Thalassiosira*), the uncoupler NH_4Cl (2.8 mM), or the ATP synthase inhibitor DCCD (320 µM) in order to determine the relative contribution of ΔpH and DD-de-epoxidase activity to the non-photochemical energy dissipation observed within four diatom species. The regions of the plot area with a dark background correspond to dark conditions and the white portion of the background corresponds to the time that 500 µmol $m^{-2}s^{-1}$ high light was applied. Error bars represent ± 1 standard deviation from the mean of 3 separate cultures grown at 50 µmol $m^{-2}s^{-1}$.

Figure 3.1-12 and Table 3.1-1). The two benthic pennate species (*Nitzschia curvilineata* and *Navicula sp.*) can attain NPQ of much greater amplitude than the open water centric species (*Thalassiosira weissflogii* and *Coscinodiscus wailesii*). NPQ induction kinetics differ between species, with *T. weissflogii* attaining maximal $\mathcal{NPQ}$ after only 30 seconds of HL. There is also considerable variation in NPQ recovery post HL, with $\mathcal{NPQ}$ relaxing more in *N. curvilineata* and

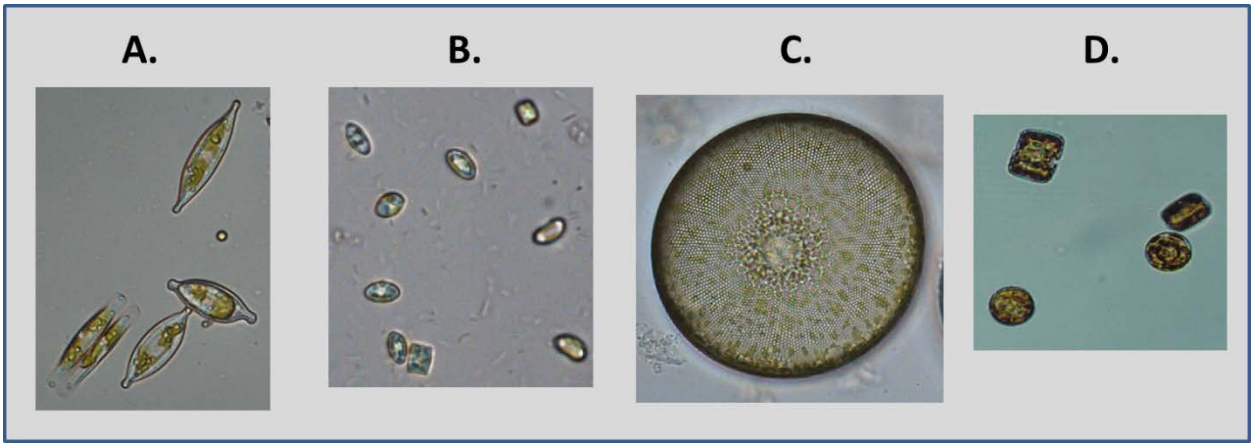

Figure 3.1-12 Bright field images of A, *Nitzschia curvilineata*; **B**, *Navicula sp.*; **C**, *Coscinodiscus wailesii*; **D**, *Thalassiosira weissflogii* cells. For cell sizes see Table 3.1-1.

Table 3.1-1 Specifications for the diatom species in Figures 3.1-11 & 3.1-12. Information obtained from the NCMA database (NCMA 2013). Cell size ranges were verified using cultures grown *in lab*.

Species (Figure 3.1-10 & 11 panels)	**Strain**	**Class**	**Collection Site**	**Cell length (µm)**	**Cell width (µm)**
Coscinodiscus wailesii (C)	Gran et Angst (CCMP 2513)	Coscinodiscophyceae (centrics)	South Atlantic Bight, off of Georgia Coast, USA	100 - 250	100 - 250
Navicula sp. (B)	110-1 (Kirkwood & Henley 2006) (CCMP 2566)	Bacillariophyceae (pennates)	Soil of the Great Salt Plains, Oklahoma, USA	6 - 10	4 - 6
Nitzschia curvilineata (A)	(Hustedt) Lewin et Lewin (CCMP 555)	Bacillariophyceae (pennates)	Shoreline of Long Island Sound, New Haven, Connecticut, USA	40 - 65	10 - 15
Thalassiosira weissflogii (D)	(Hustedt) Hasle et Heimdal (CCMP 1010)	Coscinodiscophyceae (centrics)	Gulf Stream, between Bermuda and New York	13 - 18	10 - 12

T. weissflogii and less in *Navicula sp*. and *C. wailesii* (Figure 3.1-11). The relative contribution of the trans-thylakoid proton gradient to NPQ was determined by pre-treatment with NH_4Cl to remove ΔpH or DCCD to maximise ΔpH. NH_4Cl effectively inhibited NPQ in all four species, proving that NPQ in these diatoms *is* indeed qE. In the two open water species (*T. weissflogii* and *C. wailesii*) the ΔpH contribution appears to maximise at the HL (100 x culture light conditions) used for collection of the *NPQ* transients. Interestingly, DD de-epoxidation may not be completely obligatory for NPQ in the species with the smallest cell sizes (*Navicula sp*. and *T. weissflogii*), as NPQ was observed even with DTT pre-treatment. This DTT insensitive NPQ has fast induction kinetics (Figure 3.1-11B & D).

3.1-6 How to describe 'typical' NPQ?

In a natural environment diatoms are likely to exhibit differing degrees of NPQ induction and relaxation, depending on nutrient availability and light field. An analogous variability in NPQ was observed even when culturing cells within the stable conditions of a laboratory (but not chemostat conditions). Unfortunately, the dynamism of diatom NPQ can make it rather challenging to directly compare the results of one set of HL transition experiments to another. How do you scientifically approach the investigation of a phenomenon in which the control is never the same? To remediate this conundrum, special attention was given towards the design of HL transition experiments. Large scale 'batch' experiments were used in which multiple experiments (treatments) were performed on cells collected from the same culture on the same day. These experiments were repeated with multiple cultures (usually 3 separate cultures) to insure that only trends transcending subtle physiological variants are being reported. HL transition experiments on *Nitzschia curvilineata* and *Navicula sp.* were generally

performed on cultures showing 'typical' NPQ. Typical NPQ can be described as when with moderate HL (500 µmol $m^{-2}s^{-1}$) $\mathcal{NPQ}$ induction kinetics stabilize after 10 minutes of illumination and $\mathcal{NPQ}$ relaxes noticeably once HL ends. These traits were common with cultures exhibiting ΦPSII of 0.55 to 0.60, corresponding to values achieved with actively growing nutrient replete cultures (see Figure 3.1-10).

3.1-7 Conclusions

NPQ in diatoms is characterised by a fast induction of quenching during HL illumination and a slow recovery of fluorescence once HL ends. During NPQ there is conversion of DD molecules to DT molecules. The amplitude of $\mathcal{NPQ}$ induced during HL and the amount recoverable post HL varies with culture age. Chemical agents can be used to experimentally manipulate ΔpH (with NH_4Cl and DCCD treatments) and inhibit the enzymatic catalysis of DD de-epoxidation (with DTT treatment) to determine the relative contribution of each towards NPQ. The two diatom species from open water habitats have a limited capacity for $\mathcal{NPQ}$ as compared to the shoreline and soil species. The two smallest species have a fast NPQ component that is insensitive to DTT, suggesting that there are also quenching mechanisms in diatoms that are independent of DD de-epoxidation. This is an important observation, as DTT insensitive NPQ has only been described once in the literature for diatoms (in the centric *Cyclotella meneghiniana*, Grouneva et al. 2008). With the limited number of species surveyed here, the assignment of NPQ trends that span individual species variation has to be cautious. Lastly, the intrinsic variability found within and between diatom species when investigating NPQ suggests that there is a highly dynamic mechanism behind diatom NPQ that is easily tunable to fit the diverse needs of individual species.

3.2 Divergent Strategies for the Fast Dissipation of Excitation Pressure in two Pennate Diatoms

3.2-1 Overview

Diatoms are renowned for their robust ability to perform NPQ (non-photochemical quenching of chlorophyll fluorescence) as a dissipative response to heightened excitation pressure (light stress) on PSII, plausibly explaining their dominance over other algal groups in turbulent light environs. Their NPQ mechanism has been principally attributed to a xanthophyll cycle involving the reversible de-epoxidation of DD activated by acidification of the lumen. *Nitzschia curvilineata* (CCMP 555) and *Navicula sp.* (CCMP 2566) are two previously photosynthetically uncharacterised benthic pennate diatom species that were originally collected from a marine shoreline community and the soil of an inland salt flat, respectively. It is predicted that these two species will have different susceptibilities to excitation pressure and different NPQ responses to dissipate that excitation pressure, all in accordance to the unique environmental properties of their source habitats. The objective of this chapter is to highlight the difference in the ways that these two pennate species dissipate excess excitation energy during NPQ. Variable chlorophyll fluorescence, in combination with chemical agents that manipulate differing aspects of the NPQ response, was used to monitor photochemical and non-photochemical excitation energy dissipation during cell transitions to excess light. Low temperature absorbance and fluorescence measurements were used to investigate pigment energy levels and excitation energy distribution. Action spectra depicting the dependence of NPQ on HL quality were collected to give *in situ* information on the spectral sensitivity of PSII excitation and the ability of the NPQ mechanism to relieve the generated excitation pressure. It

was found that *Nitzschia* has a larger antenna system that generates more excitation pressure at low to moderate light levels. During NPQ, the antenna system of *Nitzschia* enters a deeply quenched, yet highly reversible state that is dependent on DD de-epoxidation. *Navicula* cells perform a less robust NPQ that may contain a mechanistically distinctive component from what was observed in *Nitzschia*: NPQ can show a high degree of independence from DD de-epoxidation. These different strategies for excitation balance are discussed in the context of resource allocation within the species' native environments.

3.2-2 NPQ responsiveness to excitation pressure

Dissipative responsiveness of the photosynthetic apparatus was first investigated by titrating $\mathcal{NPQ}$ against excitation pressure using HL of varying intensities. As seen in Figure 3.2-1, excitation pressure follows a saturating growth curve with the intensity of applied HL in both diatom species. The *Navicula* species appears to be more resistant to HL generation of excitation pressure at low to moderate HL levels, especially immediately after the onset of HL irradiation (Figure 3.2-1). After 10 minutes of HL exposure excitation pressure dissipates to a sustainable level as the cells reach steady state conditions where photochemical quenching (qP) and PSII effective quantum yield (ϕPSII) remain relatively constant over time. The HL irradiation vs. excitation pressure curves in Figure 3.2-1 were fit to a Michaelis–Menten type model ($excitation\ pressure = max\ excitation\ pressure\ \frac{irradiance^n}{Km^n + irradiance^n}$). A Hill equation was needed to adequately explain the weak sigmoidal shape in the *Navicula* data (n = 1.59 ±0.08 (S.E.)). The Km value from such fits (HL irradiance level at half excitation pressure saturation) is a convenient way to compare the excitation pressure sensitivity of cells to irradiation intensity; this Km is indicative (inversely) of the effective absorbance cross section for excitation pressure

generation (a larger Km would indicate a smaller effective absorbance cross section). At 30 seconds HL *Navicula* has a larger Km than *Nitzschia* (*Nitzschia*, 209.2 ±23.8(S.E.) µmol $m^{-2}s^{-1}$; *Navicula*, 349.2 ±16.2(S.E.) µmol $m^{-2}s^{-1}$), whereas at 10 minutes HL the Km values are more similar (*Nitzschia*, 868.1 ±177.3(S.E.) µmol $m^{-2}s^{-1}$; *Navicula*, 662.2 ±43.4(S.E.) µmol $m^{-2}s^{-1}$) (fit parameters given in *Supplemental Table 3.2-1*).

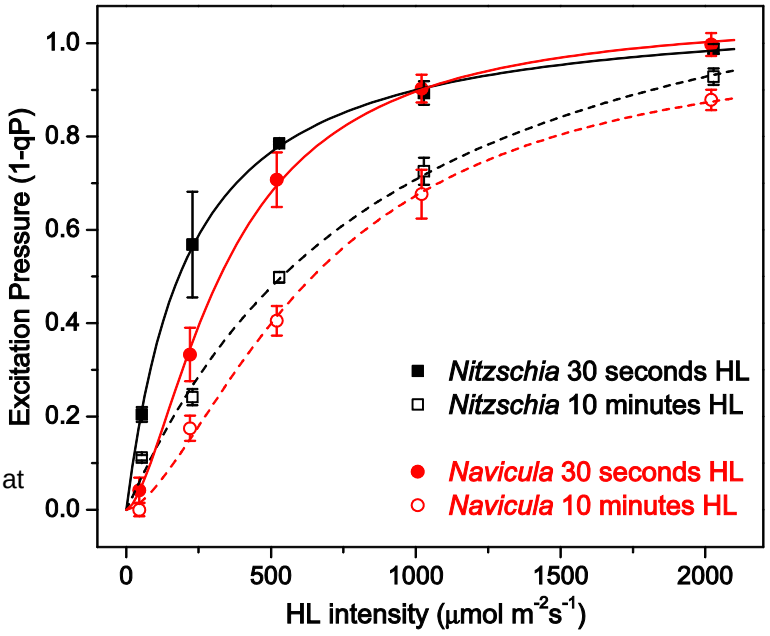

Figure 3.2-1 The conversion of high light to excitation pressure. Excitation pressure at 30 seconds after the onset of high light (HL) irradiation and at 10 minutes of HL. Solid and dashed lines represent Hill fits of the data at 30 seconds and at 10 minutes, respectively. Fit parameters given in *Supplemental Table 3.2-1*. Error bars represent ± 1 standard deviation from the mean of 3 separate cultures grown 50 µmol $m^{-2}s^{-1}$.

at

The kinetics and amplitudes of $\mathcal{NPQ}$ induction during HL and $\mathcal{NPQ}$ relaxation after HL differ between *Nitzschia* and *Navicula* (Figure 3.2-2). In general, *Nitzschia* cells perform higher amplitude $\mathcal{NPQ}$ during HL and show more relaxation of $\mathcal{NPQ}$ both during and after HL. *Navicula* cultures always had a maximum $\mathcal{NPQ}$ capacity approaching 4, whereas *Nitzschia* cultures, especially those with high cell densities, could have $\mathcal{NPQ}$ values near 10 (data not shown). Pre-treatment of *Navicula* cells with a saturating amount of the DD de-epoxidase inhibitor DTT only partially inhibits the magnitude of obtainable $\mathcal{NPQ}$, as opposed to what was observed in *Nitzschia* (Figure 3.2-2). Using $\mathcal{NPQ}$ dosage responses to DTT final concentrations of 0 to 21

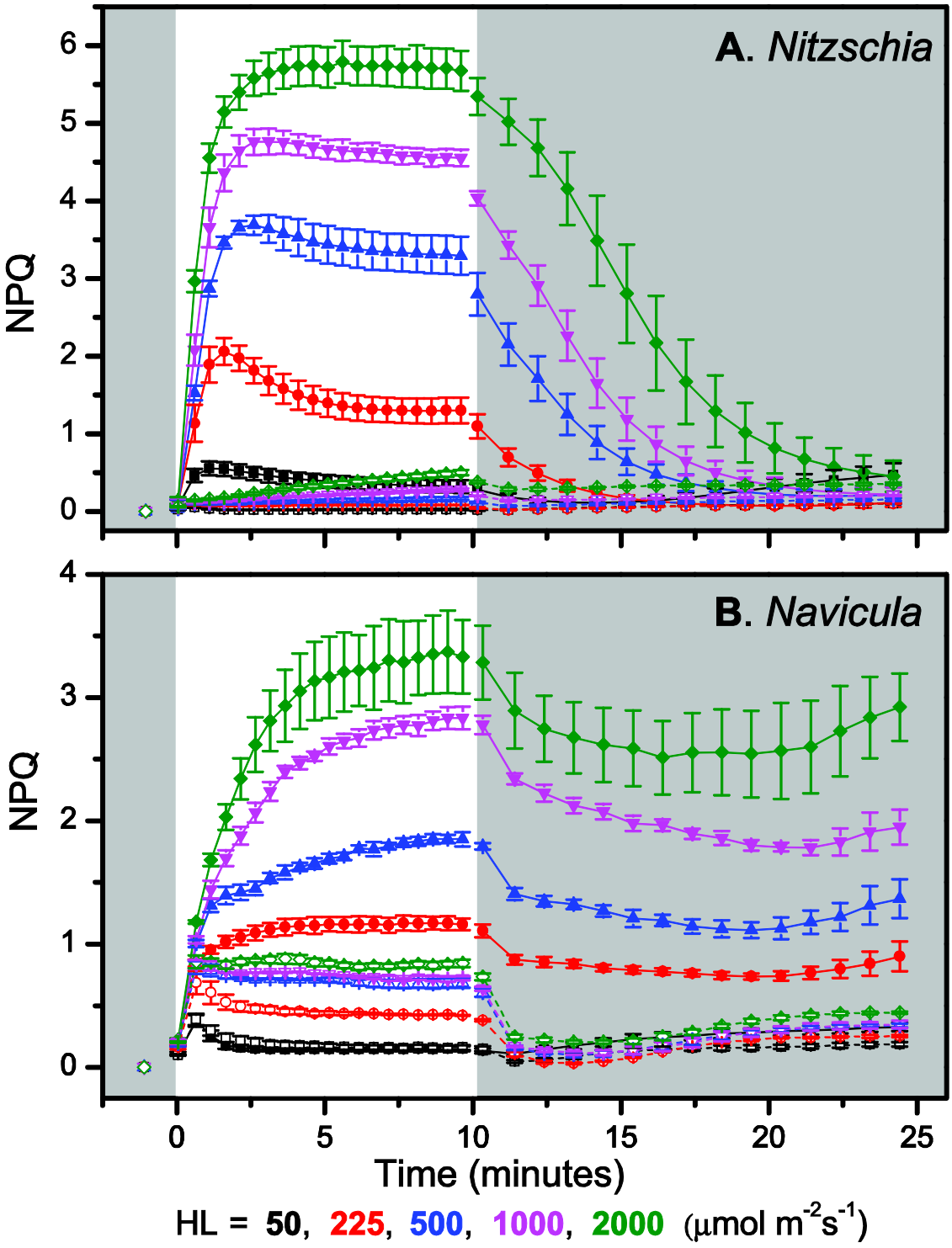

Figure 3.2-2 NPQ transients during the transition from dark-to-high light-to-dark in **A**, *Nitzschia* and **B**, *Navicula* cells. The magnitude of high light (HL) varied from 50 (growth light) to 2000 (full sunlight) µmol $m^{-2}s^{-1}$. *NPQ* transients were collected without (**filled symbol shapes** with solid lines) and with (**open symbol shapes** with dashed lines) a pre-treatment of the DD de-epoxidase inhibitor DTT (2.65 mM for *Navicula*, 5.3 mM for *Nitzschia*). The regions of the plot area with a dark background correspond to dark conditions and the white portion of the background corresponds to the time frame that HL was applied. Error bars represent ± 1 standard deviation from the mean of 3 separate cultures.

mM (*Figure 3.1-7*), DTT dosages above 5 mM did not further inhibit *NPQ* in *Nitzschia* but did negatively affect PSII maximum quantum yield of photochemistry. Only half as much DTT was required in *Navicula* to achieve comparable results (*Figure 3.1-7*), suggesting that *Navicula* cells have ~1/2 as much DD de-epoxidase per Chl *a*.

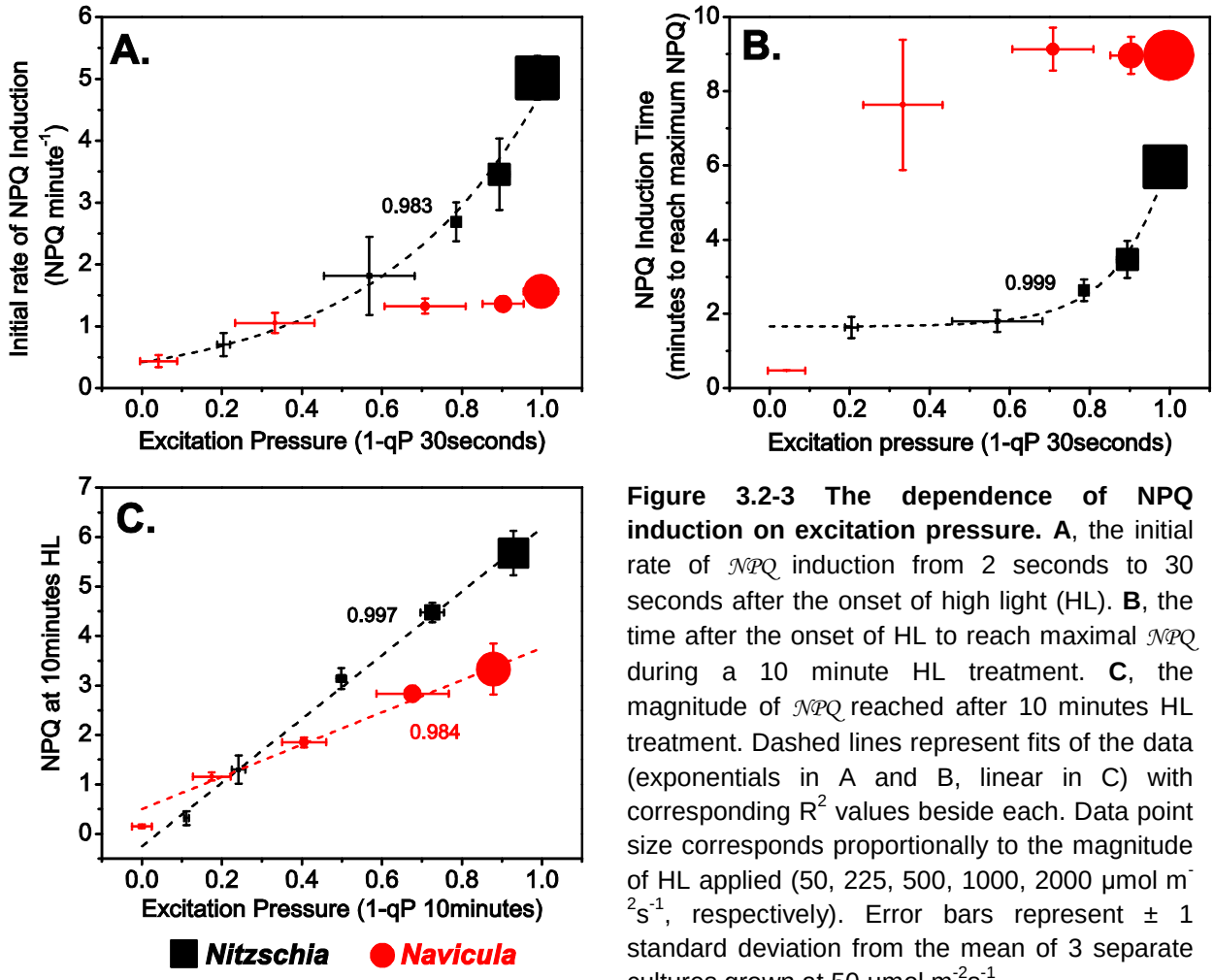

Figure 3.2-3 The dependence of NPQ induction on excitation pressure. A, the initial rate of *NPQ* induction from 2 seconds to 30 seconds after the onset of high light (HL). **B**, the time after the onset of HL to reach maximal *NPQ* during a 10 minute HL treatment. **C**, the magnitude of *NPQ* reached after 10 minutes HL treatment. Dashed lines represent fits of the data (exponentials in A and B, linear in C) with corresponding R^2 values beside each. Data point size corresponds proportionally to the magnitude of HL applied (50, 225, 500, 1000, 2000 µmol $m^{-2}s^{-1}$, respectively). Error bars represent ± 1 standard deviation from the mean of 3 separate cultures grown at 50 µmol $m^{-2}s^{-1}$.

NPQ induction is intimately linked to the level of excitation pressure felt by the photosynthetic systems in both diatom species; however, the relationship varies between species. The initial rate of *NPQ* induction increases exponentially with excitation pressure in *Nitzschia*, whereas the rate remains relatively constant (and slower) in *Navicula* once a

sufficient level of excitation pressure has been reached (Figure 3.2-3A). $\mathcal{NPQ}$ induction time increases exponentially in response to excitation pressure in *Nitzschia*, but approaches saturation with lower excitation pressures in *Navicula* (Figure 3.2-3B). *Navicula* takes longer to reach a maximal $\mathcal{NPQ}$ during HL at all but the lowest excitation pressure (Figure 3.2-3B). During steady state conditions (10 minutes of HL) $\mathcal{NPQ}$ amplitude increases linearly with excitation pressure in both species, albeit $\mathcal{NPQ}$ develops less in response to excitation pressure in *Navicula* (Figure 3.2-3C). To recap, *Nitzschia* generally has a more dynamic NPQ response over a wider range of excitation pressures (Figure 3.2-3), but this does not translate to enhanced dissipation of excitation pressure during HL (Figure 3.2-1).

3.2-3 Photoinactivation

Both *Navicula* and *Nitzschia* cells seem to have a high intrinsic resistance to photoinactivation. Lincomycin (a specific inhibitor for 70S ribosomes and therefore D1 turnover) treatments of up to 6.4 mg/mL had no effect on $\mathcal{NPQ}$ or PSII effective quantum yield during a 10 minute HL treatment of 500 μmol $m^{-2}s^{-1}$ (data not shown). Furthermore, HL treatments of 1500 μmol $m^{2}s^{-1}$ in the dual presence of DTT and 0.4 mg/mL lincomycin did not increase non-recoverable $\mathcal{NPQ}$ (as determined during a 15 minute dark period following HL) that would be attributable to photoinactivation (data not shown).

3.2-4 DTT insensitive NPQ

Pre-treatment with saturating concentrations of DTT inhibited 90% of the $\mathcal{NPQ}$ witnessed in *Nitzschia*. Conversely, *Navicula* was still able to reach substantial levels of $\mathcal{NPQ}$ when pre-treated with DTT; in fact, at the lowest HL irradiance DTT did not reduce $\mathcal{NPQ}$ at all (Figure 3.2-4A). DTT pre-treatment enhanced excitation pressure generation in *Nitzschia* cells

during NPQ induction and steady state NPQ (Figure 3.2-4B); whereas DTT had little effect on excitation pressure in *Navicula* cells (Figure 3.2-4C). In *Nitzschia* cells, DTT pre-treatment approximately halved the HL irradiance level at half excitation pressure saturation (i.e. the Km in Section 3.2-2) during steady state conditions (control at 10 minutes HL, 868.1 ±177.3(S.E.)

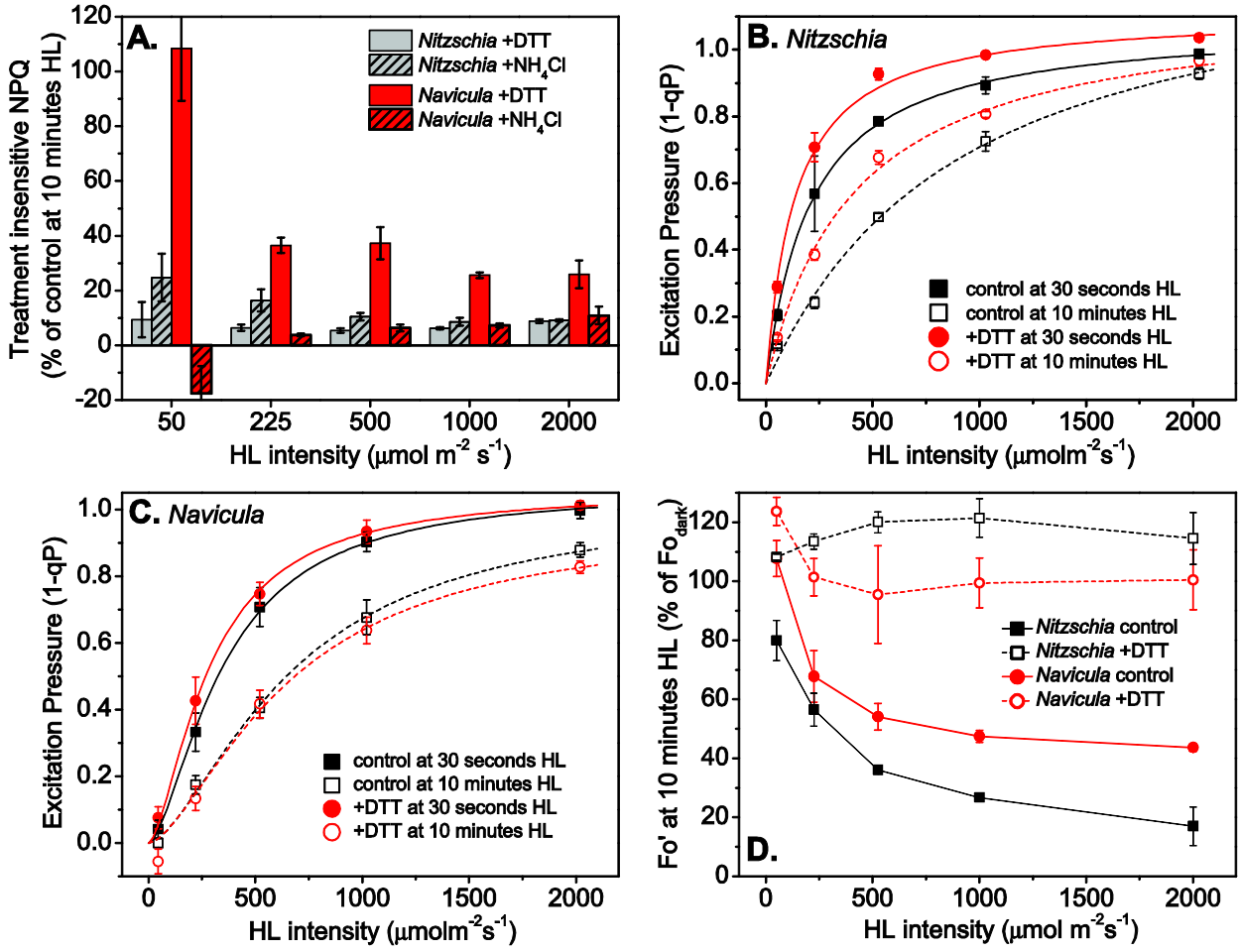

Figure 3.2-4 NPQ and excitation pressure sensitivity to DTT pre-treatment. A, DTT insensitive NPQ during steady state high light (HL) conditions. $\mathcal{NPQ}$ not inhibited by a pre-treatment with the DD de-epoxidase inhibitor DTT (2.65 mM for *Navicula*, 5.3 mM for *Nitzschia*) expressed as percentage of control (complete inhibition of $\mathcal{NPQ}$ by DTT would give a value of 0). Pre-treatment with the ΔpH uncoupler NH_4Cl (2.8 mM) is included as a negative control for qE. The negative value for *Navicula* +NH_4Cl indicates that the NH_4Cl treatment slightly enhanced fluorescence over the control at 50 µmol $m^{-2}s^{-1}$ HL. **B** & **C**, The conversion of HL to excitation pressure in cells pretreated with DTT. Solid and dashed lines represent Hill fits of the data at 30 seconds and at 10 minutes, respectively, for control (black) and +DTT (red) samples. Fit parameters given in *Supplemental Table 3.2-1*. **D**, Quenching of fluorescence with open PSII reaction centres; expressed as minimal fluorescence measured in the presence of far red light at 10 minutes of HL (Fo') as percentage of minimal fluorescence measured in the presence of far red light prior to HL (Fo_{dark}). Error bars represent ±1 standard deviation from the mean of 3 separate cultures grown at 50 µmol $m^{-2}s^{-1}$.

µmol $m^{-2}s^{-1}$; +DTT at 10 minutes HL, 408.5 ±70.6(S.E.) µmol $m^{-2}s^{-1}$); whereas in *Navicula* cells there was no change (control at 10 minutes HL, 662.2 ±43.4(S.E.) µmol $m^{-2}s^{-1}$; +DTT at 10 minutes HL, 655.3 ±102.7(S.E.) µmol $m^{-2}s^{-1}$) (see *Supplemental Table 3.2-1* for fitting details). All NPQ was stopped with a pre-treatment of the ΔpH uncoupler NH_4Cl (Figure 3.2-4A), indicating that the DTT insensitive NPQ witnessed in *Navicula* is a type of qE that is independent of DD de-epoxidation. qE can thus be divided into two subtypes: qE_{XC} for xanthophyll cycle dependent qE and qE_{nonXC} for xanthophyll cycle independent qE. Antenna based qE causes fluorescence quenching when PSII reaction centres are closed (Fm quenching) and also when PSII reaction centres are open (Fo quenching) (Ruban et al. 2012). According to Figure 3.2-4D, the qE_{nonXC} in *Navicula* is not antenna based, since Fo quenching is absent. However, quenching of fluorescence within the antenna can also occur via the accumulation of excited state triplet Chl *a* (^{3}Chl *a**) during illumination (Di Valentin et al. 2009, Di Valentin et al. 2012, Ballottari et al. 2013). The formation of triplet Chl *a* within the antenna is in function a type of NPQ, and since this quenching is not directly dependent on the xanthophyll cycle it can be classified as qE_{nonXC}. Excited state quenching within the PSI reaction centre via the $P700^+$ radical (Schlodder et al. 2005) could also contribute to qE_{nonXC}. Nevertheless, the 'robust', ΔpH dependent qE_{nonXC} in *Navicula* has been assigned to PSII reaction centre based quenching, presumably via recombination reactions of $P680^+$ (Ruban et al. 2012).

3.2-5 Basal light harvesting

For ease of discussion, the FCP complexes in *Nitzschia* and *Navicula* have been labeled according to the model in Figure 3.2-5; this is a purely functional description since the protein compositions of FCPs in these species are unknown. Analogous to what is observed in higher

plants and what has been found during the biochemical characterisation of diatom FCPs (see *Section 1.2-3*), the model in Figure 3.2-5 divides FCP complexes into outer (major) antenna and

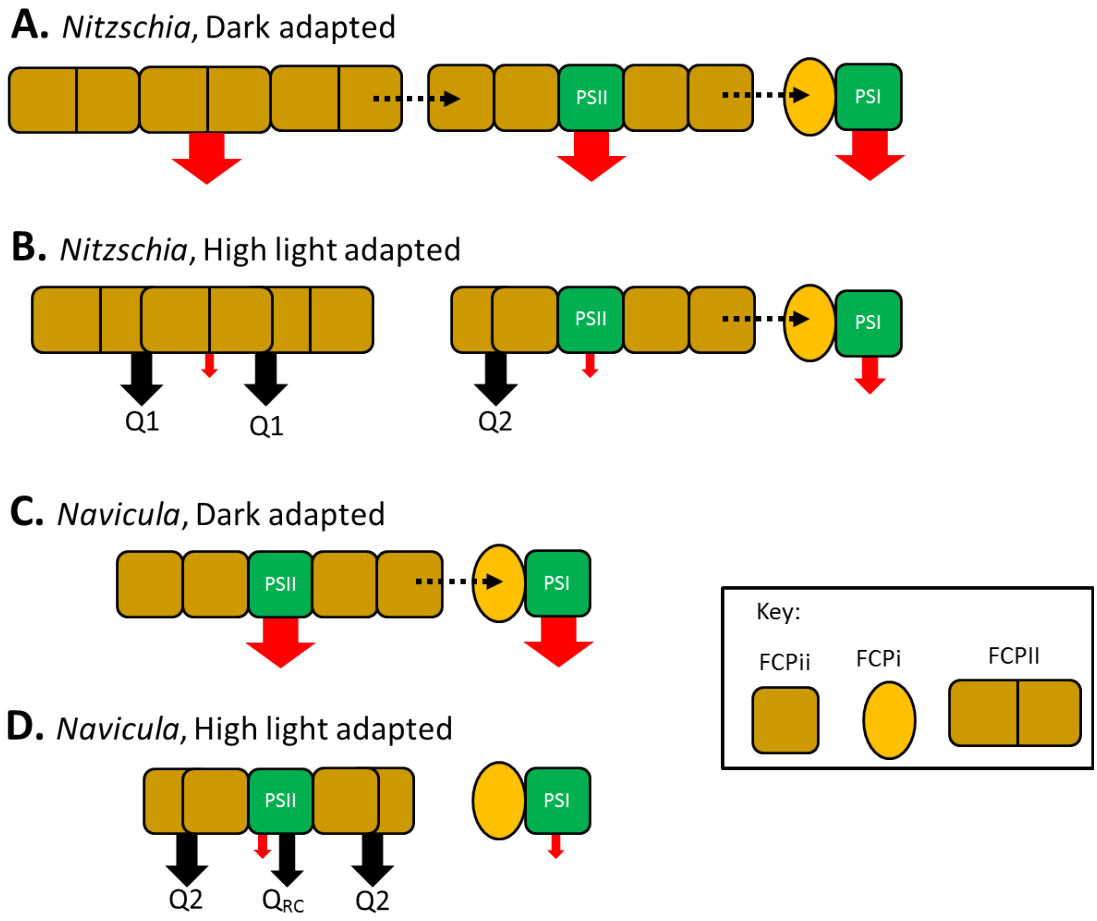

Figure 3.2-5 Functional model of hypothesized FCP antenna compartments and quenching sites. FCPII corresponds to outer (major) antenna complexes. FCPii refers to inner (minor) antenna complexes that tightly couple to PSII. FCPi refers to inner antenna complexes that tightly couple to PSI. FCPii are likely present as trimers, FCPi could be monomeric or trimeric, and FCPII are likely present as higher order oligomers (groups of hexamers). The protein composition of each type of FCP complex is unknown in these species. Dashed arrows represent excitation energy transfer between pigment pools. Red arrows, fluorescence at 77K; black arrows, non-photochemical quenching of excitation energy. Size of arrows is indicative of the relative amount of excitation energy dissipation. **A**, FCP organisation in dark adapted *Nitzschia* cells. FCPII complexes are loosely coupled to PSII, emitting at 687 nm at 77K. **B**, diadinoxanthin (DD) de-epoxidation and ΔpH during high light conditions in *Nitzschia* triggers the aggregation of adjacent FCP complexes (indicated by overlapping shapes) and the activation of quenching sites. FCPII aggregation results in a decoupling of FCPII from the PSII. Q1 and Q2 represent non-photochemical quenching sites within FCPII and FCPii quenching aggregates, respectively. **C**, FCP organisation in dark adapted *Navicula* cells. *Navicula* has a smaller FCP antenna size, lacking FCPII. **D**, DD de-epoxidation and ΔpH during high light conditions in *Navicula* triggers the formation of FCPii quenching aggregates and the activation of Q2 quenching sites. Q_{RC} represents reaction centre based quenching within PSII cores.

inner (minor) antenna. The outer FCP antenna complexes (ostensibly designated as FCPII) are composed of higher than trimer FCP oligomers. FCPII are responsible for the bulk of light harvesting, able to transfer excitation energy to PSII and PSI. The inner FCP antennae, ostensibly designated FCPii and FCPi, closely couple to the photosystems serving to selectively excite PSII and PSI, respectively. The inner antennae most likely represent a heterogeneous population with differing subtypes of both FCPii and FCPi depending on protein/pigment composition. FCPii are likely trimers and FCPi are likely trimers or possibly monomers (Lepetit et al. 2007, Veith and Büchel 2007). The LHC1-like proteins (LhcR) found in diatoms would be constituents of FCPi.

The two diatom species have distinct antenna systems. *Nitzschia* cells are richer in antenna pigments having more carotenoid and Chl *c* per Chl *a* (Table 3.2-1). Low temperature absorbance spectra from dark adapted cells (Figure 3.2-6) were collected to compare pigment energy level composition. It is important to note that some of the absorbance differences between the two species may not be entirely from differences in pigment composition, but due to spectral distortions from light scattering and sieve effects between the diatom cells and or ice crystals within the frozen sample. Diatom cells are highly scattering due to their frustules (silica cell walls). The frustules can highly and selectively scatter and or absorb specific bands of visible light (Fuhrmann et al. 2004, Yamanaka et al. 2008); the species specificities of frustule light scattering are unknown in *Nitzschia curvilineata* and *Navicula sp*. cells. The absorbance spectra have been normalised to the Q_x Chl *a* absorption peak at 623 nm because this peak is least susceptible to pigment packaging effects (Stuart et al. 1998, Stuart et al. 2000). Enhanced 77K cellular absorbance in *Nitzschia* (relative to bulk Chl *a*) (Figure 3.2-6A) was assigned to Chl *c*

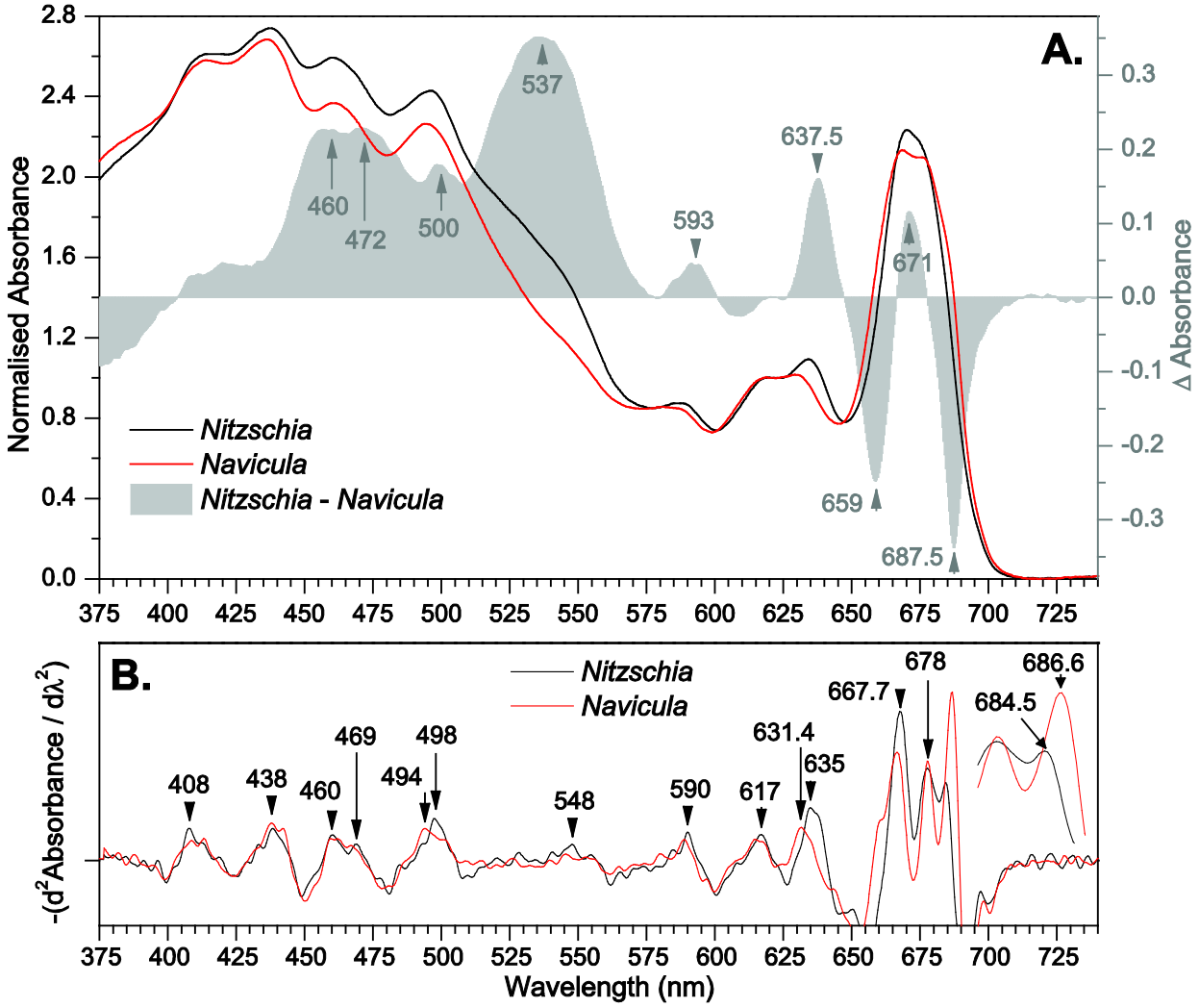

Figure 3.2-6 Specie dissimilarities in low temperature cell absorbance. A, 77K absorbance spectra of dark adapted *Nitzschia* and *Navicula* cells normalised to chlorophyll Q_x peak at 623 nm, also shown is the difference in the normalised spectra between the two species. **B**, inverted second derivative, 5 nm integration interval. Important peak positions are labeled with arrows. The insert is a zoom in from 675 to 690 nm. Spectra are the average of 3 samplings from 4 separate cultures (n=12).

(~460, 593, and, ~638 nm) and carotenoids (~472, 500, and 537 nm) using 77K absorbance spectra of isolated pigments in DMSO (Figure 3.2-7), absorption maximum assigned by the FCP model by Premvardhan et al. (2010), and the remarks of Lavaud (2007). The broad peak of enhanced absorption centred at ~537 nm represents a mixed population of Fx molecules with different degrees of bathochromic red shifting. There are also distinct differences in Chl *a* Q_y

absorbance between the species; *Nitzschia* has more absorption at 671 nm, whereas *Navicula* has more absorption at 659 and ~688 nm. Enhanced absorption at 671 nm in *Nitzschia* is being attributed to an increase (per total Chl *a*) of FCPs in *Nitzschia*, since isolated FCP complexes absorb maximally near ~670 nm (Büchel 2003, Veith et al. 2009, Premvardhan et al. 2010). Enhanced absorption at ~688 nm in *Navicula* is being attributed to an increase (per total Chl *a*) in PSI complexes (according to the absorbance spectra of isolated PSI complexes in Veith et al. 2009). Second derivative analysis of the 77K absorbance spectra revealed no obvious appearance of novel absorbance bands between species, although a few notable shifts were observed (Figure 3.2-6B). There is a blue shift of the 635 nm Chl *c* Q_y band in *Nitzschia* to 631.4 nm in *Navicula*. Of particular note is the red shifting of the 684.5 nm band in *Nitzschia* to 686.6 nm in *Navicula* (Figure 3.2-6B insert), which is likely responsible for the enhanced deep red absorption in *Navicula*.

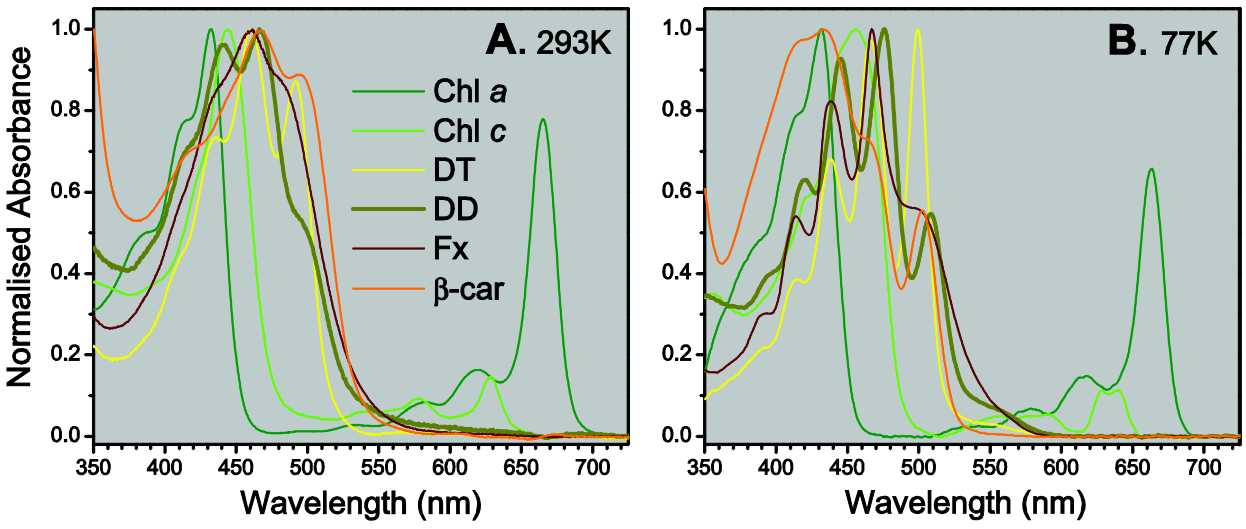

Figure 3.2-7 Absorbance spectra of isolated pigments. A, at room temperature in 100% DMSO. **B**, at 77K in 1:4 DMSO: glycerol. Chl *a*, chlorophyll a; Chl *c*, chlorophyll *c* (including c_1 and c_2); DD, diadinoxanthin; DT, diatoxanthin; Fx, fucoxanthin; β-car, β -carotene. Pigments were isolated from methanol extracts of dark adapted *Nitzschia* cells using TLC. See *Section 2.13* for methodology details.

The apparent enhancement of light harvesting by FCPs in *Nitzschia* was verified by measuring effective PSII absorbance cross sections (σPSII) with excitation of Chl *c* and carotenoids (480 ±12.5 nm FWHM excitation). *Nitzschia* cells gave a σPSII 1.6x that of *Navicula* cells, resulting in an equivalent enhancement of maximal PSII fluorescence per Chl *a* with FCP excitation (Table 3.2-1). *Nitzschia* cells also have 1.6x the amount of carotenoids per Chl *a* as *Navicula* cells (Table 3.2-1). These results are congruent with *Nitzschia* cells having a larger (~1.6x that of *Navicula*) FCP antenna size per total Chl *a* for PSII.

Table 3.2-1 Light Harvesting Summary for dark adapted cells**.** Pigment concentrations were determined photometrically from solvent extracts. σPSII were calculated by applying a rapid succession of 480 nm low energy flashes (I) to cells poisoned with DCMU (4mM final concentration) to pump the fluorescence signal (Y) to a maximum (Y_{max}); the resulting curves were fit to a cumulative one-hit Poisson distribution ($Y \bullet Y_{max}^{-1} = 1\text{-}e^{\sigma I}$) (Falkowski and Chen 2003). Fm_{dark}, maximal fluorescence level from dark adapted cells with application of saturating light pulse with a probing excitation of 470 nm. Respective standard deviations are given beside the means of 3 separate cultures.

Species	**[Chl *c*]*/ [Chl *a*]**	**[Car]†/ [Chl *a*]**	**σPSII ($A^2 \bullet quanta^{-1}$)**	**Fm_{dark} / [Chl *a*] (arb. units)**
Nitzschia curvilineata	0.503 ±0.054	1.64 ±0.09	859.6 ±73.5	3400 ±304
Navicula sp.	0.411 ±0.020	1.03 ±0.05	550.9 ±19.5	2107 ±368

*, Chl *c* includes both chlorophylls c_1 and c_2. †, all carotenoids including fucoxanthin, diadinoxanthin, diatoxanthin, and β-carotene.

Whole cell 77K emission spectra were used to investigate energy transfer among the thylakoid pigments. Förster resonance energy transfer (FRET) is the most commonly described mechanism for excitation energy migration between pigments in photosynthetic antenna systems (there are exceptions when pigments are tightly coupled). Förster resonance energy transfer is dependent on donor pigment-to-acceptor pigment dipole orientations and by an

inverse 6th power law for donor-to-acceptor separation distance (Förster 1948). The pigment-protein complexes (FCPs, PSII, and PSI) separate the chromophore matrix of the thylakoid into individual pigment compartments. Excitons settle upon the lowest energy chromophore within each pigment compartment accessible by energy transfer. Emission from a pigment compartment is from these exciton traps. Due to inter-complex coupling inefficiencies, energy transfer between compartments is generally slower than exciton equilibrium within a single compartment. Pigment compartments uncoupled from other compartments fluoresce from their own low energy emitter. Strongly coupled pigment compartments will fluoresce from the lowest energy emitter within the shared pigment pool. At 77K isolated PSII from plants, algae, and cyanobacteria has two main emission peaks. Fluorescence at ~685 nm arises from several ~683 nm absorbing Chl *a*s located in the CP43 and/or CP47 subunits of PSII, and fluorescence at 695 nm arises from one 690 nm absorbing chlorophyll in CP47 (Andrizhiyevskaya et al. 2005). The red Chl *a*s of energy levels below P700 found in all PSI complexes produce species dependent emitters for PSI that fluoresce maximally in the ~715 nm region. Isolated PSI cores from diatoms have an emission peak at ~710 to 717 nm at 77 K (Veith et al. 2009, Juhas & Büchel 2012, and references therein). In addition to the dominant Chl *a* fluorescence originating from the S_1 (0,0) state, Chl *a* also fluoresces from the vibration sub-level S_1 (0,1) state resulting in a weak satellite fluorescence band that is red shifted some 1000 to 1200 cm^{-1} from the main band.

77K emission spectra collected with 470 nm excitation preferentially exciting the pigments within FCP complexes are given in Figure 3.2-8A. In addition to the 695 nm PSII assignable peak, there is an emission peak at ~687 nm in *Nitzschia*. Since FCP trimers and

oligomers in the pennate diatom *Phaeodactylum tricornutum* emit at ~683 nm (Lepetit et al. 2007), the ~687 nm peak in *Nitzschia* could have contributions from both the PSII 685 nm peak and an FCP peak. Inconsistent with both the ~687 and ~695 nm peaks originating solely from PSII, the ratio of ~687 to ~695 nm emission varied between *Nitzschia* cultures (data not shown). The ~687 nm peak must therefore have substantial contribution from FCP emission. The 687 nm emitter would arise from FCPII complexes that are weakly coupled and/ or uncoupled to the photosystems (see Figure 3.2-5A). The complete absence of a detectable ~685 nm emission peak in *Navicula* cells suggest that energy transfer within PSII in the intact thylakoid is unidirectional to the PSII ~695 nm emitter and that the exciton trapping efficiency of the ~685 nm PSII emitters is very poor. One can presume that 'all' 77K emission at ~685 nm in intact diatom thylakoids is from antenna complexes and not from PSII cores. Intact cells and O_2 evolving thylakoids in *P. tricornutum* emit maximally at ~685 nm (Martinson et al. 1998). The derivative resolved peak at ~702 nm in the *Nitzschia* emission spectrum (Figure 3.2-8B) is being assigned to PSI associated FCP complexes (FCPi), congruent to the 697 nm emitter found in PSI-FCP complexes from low light iron stressed *Cyclotella meneghiniana* cells (Juhas and Büchel 2012), since no similar FCP emission peak could be found in the literature for *P. tricornutum*. PSI attributed emission at ~712 nm was readily observable in the *Navicula* emission spectra, derivative analysis was needed to resolve a PSI assignable peak at ~712 nm in *Nitzschia* (Figure 3.2-8B). The derivative peak at ~724 nm would be from the lowest energy Chl *a* of PSI. The complex broad emission peak/ shoulder around 750 nm in both species is from a mixture of Chl *a* vibrational sub-bands from all the emitters (seen as the derivative peaks at and above ~735 nm).

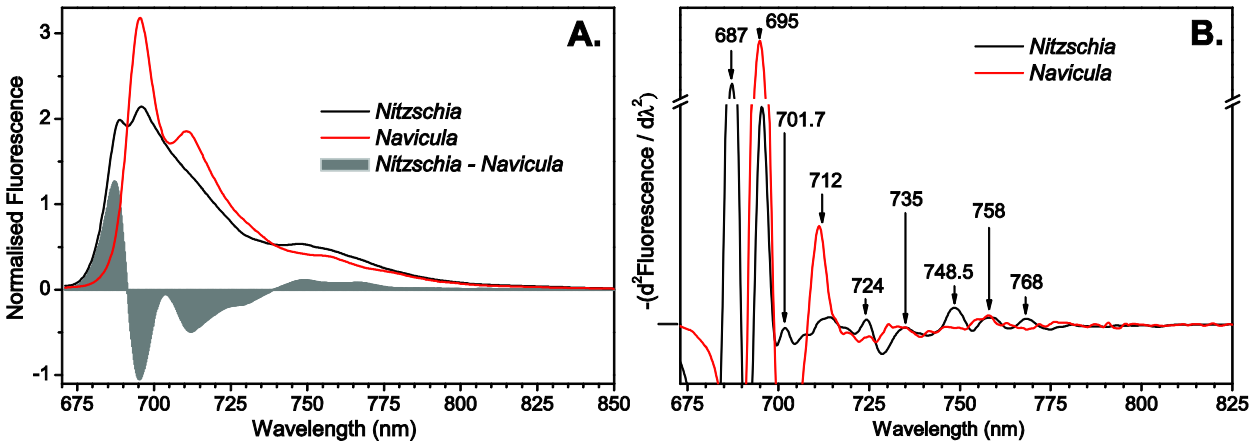

Figure 3.2-8 Specie dissimilarities in low temperature cell emission. **A,** 77K emission spectra (470 nm excitation) collected from dark adapted cells normalised to integrated emission (from 670 to 850 nm), included is the difference in the normalised spectra between the two species. **B**, inverted second derivative, 5.0 nm integration interval. Peaks of note are labeled with arrows. Spectra are averaged from 3 separate cultures.

Cell emission at 77K in *Nitzschia* is dominated by FCP emission, whereas emission in *Navicula* arises predominantly from the photosystems. The difference in emission between the two species can be largely explained by a lack of emission from the FCPII at 687 nm and an increase in emission from PSII (at 695 nm) and PSI (at 712 and 724 nm) in *Navicula* cells (Figure 3.2-8A). The satellite emission band centred at 748.5 nm is being assigned to the 687 nm FCPII emitter because it was not detectable in *Navicula* cells (Figure 3.2-8A & B). Emission from the ~702 nm emitter in *Navicula* is masked by the strong 695 nm emission peak; a ~702 nm peak is not resolvable in the derivative presented in Figure 3.2-8B, but was resolvable using a 2 nm derivative interval (data not shown). The non-symmetric shape of the 687 nm difference peak in Figure 3.2-8A suggests that *Nitzschia* cells have an additional, weak emitter near 680 nm (ostensibly assigned to FCPII). Quantitative western blots of dark adapted cells revealed a 2.82 (± 0.33 S.D.) PSII:PSI (PsbA:PsaC) stoichiometry in *Nitzschia* cells. Photosystem stoichiometry was not measured directly by protein content in *Navicula*.

To summarise, the light harvesting system in *Nitzschia* cells is enriched in FCP complexes as compared to the light harvesting system in *Navicula*.

A large amount of the absorbed photons in both species are not utilized for photosynthesis. The low temperature excitation spectra (Figure 3.2-9) revealed that cell fluorescence sensitization differs substantially from what would be predicted from cell absorbance. An estimate for the absorbed photons that do not contribute to cell emission was calculated by subtracting the excitation spectrum from the absorbance spectrum (Figure 3.2-9). Excitations at ~468 and 497 nm seem to be strongly lost relative to direct Chl *a* excitation at 670 nm (Figure 3.2-9); absorbance in this region is dominated by carotenoids (Figure 3.2-7B). The loss of excitations at ~497 nm could be due to a pool of DD/ DT pigments not functionally coupled to the antenna complexes. Lepetit et al. (2010) has shown that in *Cyclotella meneghiniana* and *Phaeodactylum tricornutum*, DD cycle pigments exist as two spatially and functionally distinctive sub-populations. One population is bound to antenna apoprotein and appears to directly function in DD cycle induced qE. The other population is not bound to antenna apoprotein, but is located in a lipid shield of MDGD surrounding the FCPs. The lipid dissolved pigment pool seems to be preferentially increased when cells are grown under high light culturing conditions (Lepetit et al. 2010). Possible roles for the lipid DD pool could be a metabolic precursor for Fx synthesis, a lipid antioxidant, or as a sunscreen. A population of red Fxs that weakly transfer excitation energy to Chl *a* may be responsible for the loss of excitations from ~550 to 600 nm (Figure 3.2-9). Blue Fxs that weakly transfer excitation energy to Chl *a* could also contribute to the loss of excitations in the ~450 to 525 nm region. To recap,

excitations that are principally absorbed by carotenoids are relatively weak sensitizers (as compared to direct Chl *a* excitation at 670 nm) for cell emission in both species.

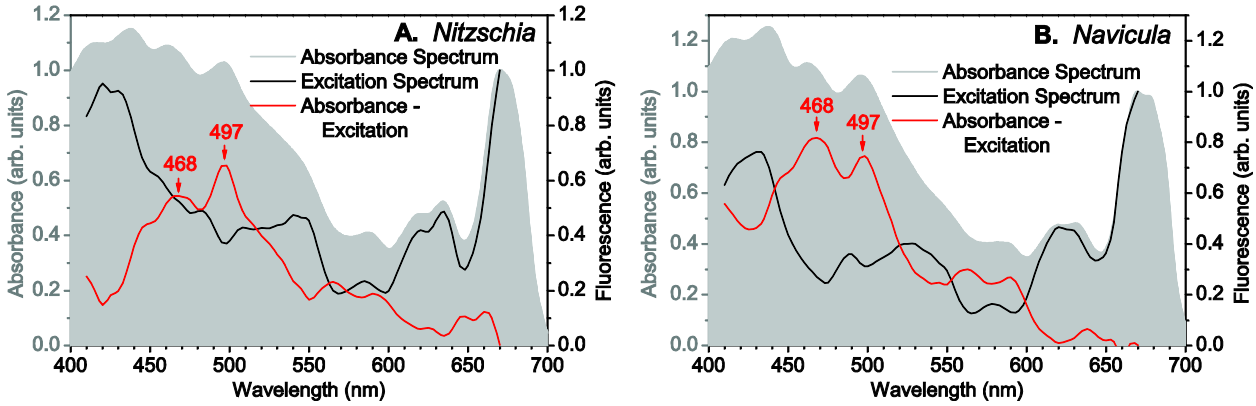

Figure 3.2-9 Excitation spectra for low temperature cell emission in dark adapted *Nitzschia* (**A**) and *Navicula* (**B**) cells. Emission at 77K was monitored at 695 nm (black line) with excitations of equivalent quanta from 410 to 670 nm. Representative 77K absorbance spectra of dark adapted cells are shown as the grey background plot. Absorbance and excitation spectra are normalised to the Chl *a* Q_y absorption peak at 670 nm. Spectra are averaged from 3 separate cultures.

3.2-6 Light harvesting during NPQ

The NPQ response during HL treatment coincides with distinct changes in cell absorbance and emission. Cells were illuminated with 2000 µmol $m^{-2}s^{-1}$ to elicit the strongest NPQ response and thus aid in the search for steady state absorbance and fluorescence signatures of NPQ. 77K absorbance spectra collected during the high light transition (Figure 3.2-10A & B) were normalised to the Q_x Chl *a* absorbance peak at 623 nm because this peak is least susceptible to Chl *a* aggregation effects (Sauer et al 1966, Ruban et al. 1997) and pigment packaging effects (Stuart et al. 1998, Stuart et al. 2000). Even though the experimental setup was in such a way as to limit signal loss due to scattering from the frozen samples (see *Section 2.10-2*), absolute changes in magnitude at short wavelengths have to be interpreted with caution due to the effects of Rayleigh scattering. However, scattering loss within the red spectral region would be much less (scattering at 400 nm is 9.4x that at 700 nm), so the

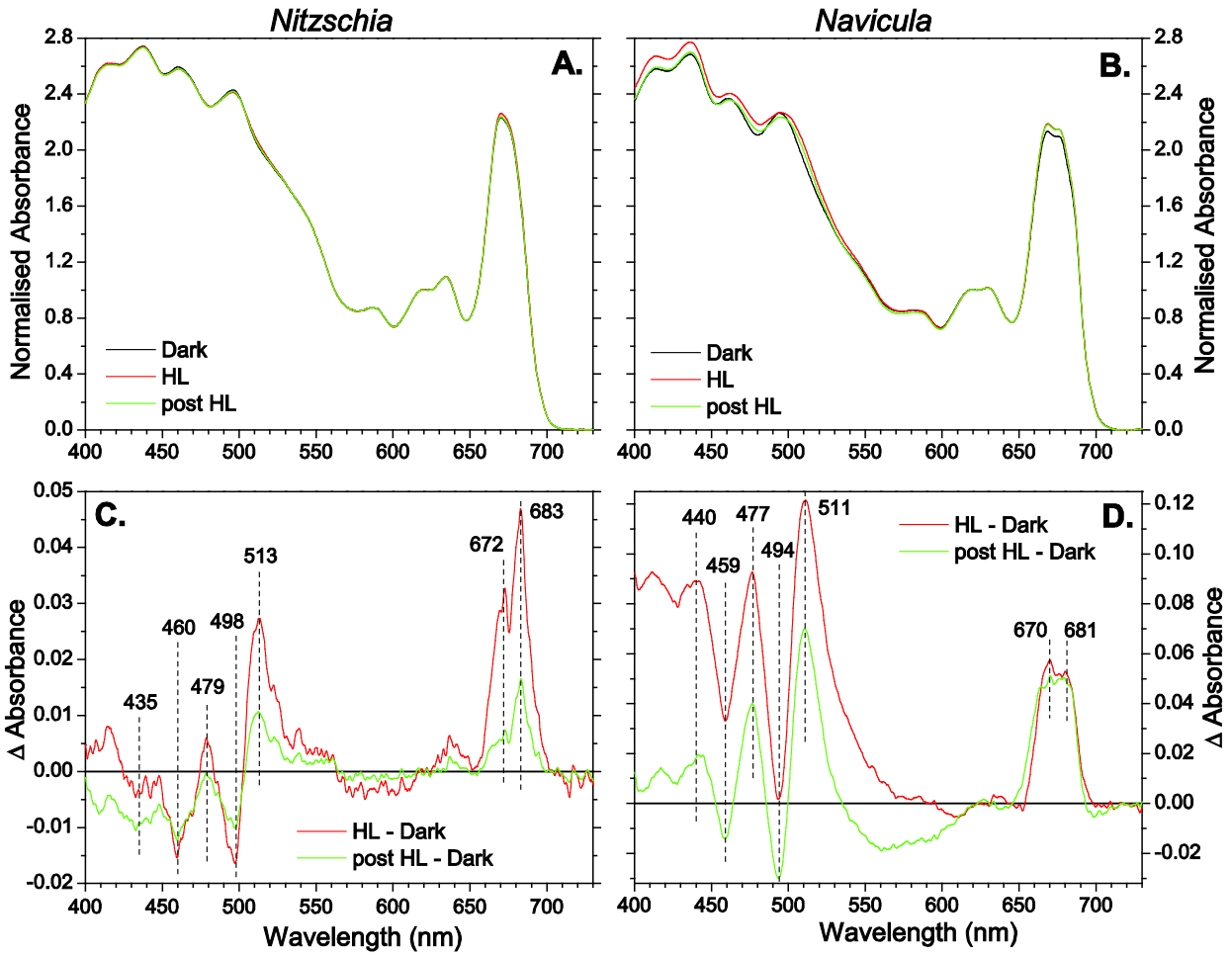

Figure 3.2-10 HL induced changes in cell absorbance. A & **B**, 77K absorbance spectra from dark adapted *Nitzschia* (A) and *Navicula* (B) cells prior to (Dark), at 10 minutes of 2000 µmol $m^{-2}s^{-1}$ high light (HL), and in dark 15 minutes post HL. Spectra have been normalised to chlorophyll *a* Q_x absorbance at 623 nm. **C** & **D**, Difference spectra for the spectra in panels A & B, peak positions of interest are identified with vertical dashed lines. *Nitzschia* spectra are the average of 3 samplings from 5 separate cultures (n=15) and *Navicula* spectra are the average of 3 samplings from 4 separate cultures (n=12) grown at 50 µmol $m^{-2}s^{-1}$.

amplitude of absorbance changes in this region are of high confidence. The HL absorbance difference spectra are shown in Figure 3.2-10C & D. A spectroscopic signature for NPQ in intact cells of *Phaeodactylum tricornutum* is a light induced increase in absorption at ~512 nm and a loss in absorption at ~495 nm, which can be directly attributed to the de-epoxidation of DD to DT (Ruban et al. 2004). In both *Nitzschia* and *Navicula* cells, HL induced a distinctive increase in absorption at ~512 nm compared to ~495 nm (Figure 3.2-10C & D). Yet the absorbance

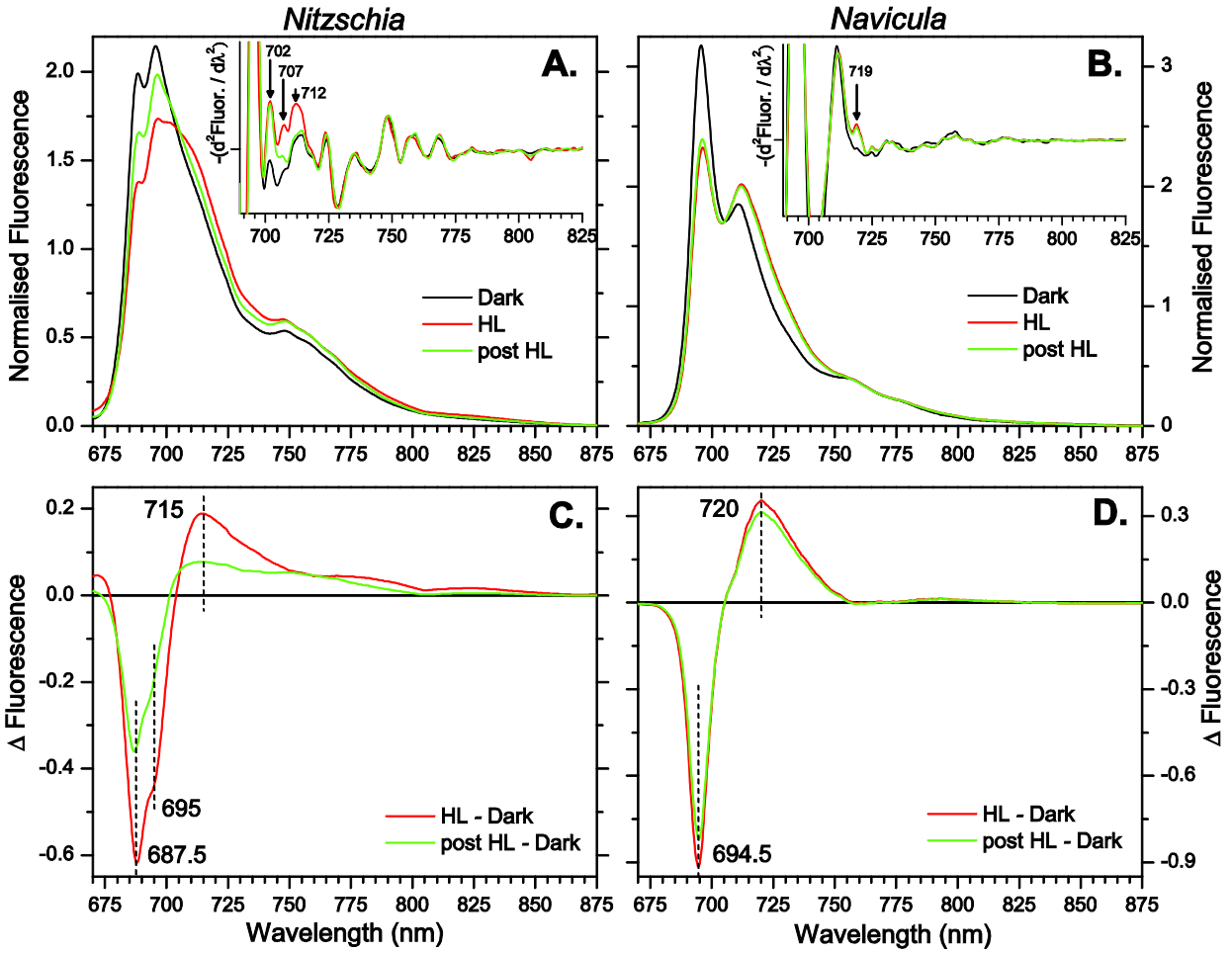

Figure 3.2-11 The redistribution of cell emission during high light transitions. 77K emission spectra (470 nm excitation) from dark adapted *Nitzschia* (**A**) and *Navicula* (**B**) cells prior to (Dark), at 10 minutes of 2000 µmol $m^{-2}s^{-1}$ high light (HL), and in dark 15 minutes post HL. Spectra are normalised to integrated emission (from 670 to 850 nm). Inserts show inverted second derivatives of the spectra with 5 nm resolution. **C** & **D**, the differences of the normalised spectra in A & B, peak positions identified by vertical dashed lines. Spectra are the mean from 3 separate cultures grown at 50 µmol $m^{-2}s^{-1}$.

changes that occur during HL cannot simply be explained by a loss of absorption by DD and an increase in absorption by DT, especially within the Chl *a* Q_y regions. In both species HL treatment causes a large scale loss in Chl *a* emission from all wavelengths with excitation of FCP pigments (at 470 nm). Normalised 77K emission spectra for cells quick frozen during different phases of the high light transition are shown in Figure 3.2-11. The changes in emission spectra shape in response to HL in Figure 3.2-11 reveal 'relative' redistributions of excitation energy

between the terminal emitters. In *Nitzschia* there is a relative loss in emission corresponding to FCPII (at ~687 nm) and PSII (at ~695 nm) with a relative enhancement in emission peaking at ~715 nm extending deep into the far-red. In *Navicula* there is a relative loss in emission corresponding to PSII at ~695 nm with a relative enhancement in emission peaking at ~720 nm with no far-red component.

Excess light induced excitation energy redistribution in Nitzschia curvilineata

In higher plant thylakoids qE is associated in the red spectral region with an increase in absorbance at 685 nm and a broad increase in absorbance in the green peaking at 520 nm, and in the blue spectral region a loss in absorbance at ~437 nm (Ruban et al. 1992). Isolated LHCII show similar changes in absorbance upon aggregation, with loss in absorbance also at 437 nm and increase in absorbance at 505 and 685 nm, but there is also a loss in absorbance at 672 nm (Ruban et al. 1992, Ruban et al. 1997). The Chl *a* attributed changes in LHCII aggregation at 437 nm, and especially at 671 and 685 nm, are signatures of Chl *a* dimerization/ aggregation in solution *in vitro* (Sauer et al. 1966, Shipman et al. 1976). Such observations led to the understanding that the qE mechanism in higher plants induces changes in LHCII macro-organisation that create Chl *a* higher aggregates (Horton and Ruban 2005). The enhancement of absorbance at ~520 nm during higher plant qE (exact peak wavelength is dependent on species and preparation method, but is usually between 520 and 535 nm) has been attributed to a red shifting of carotenoids during LHCII aggregation (Ruban et al. 1997) with a theoretical contribution from a change in thylakoid thickness induced by energization of the thylakoid during illumination (Duffy et al. 2010). Ruban et al. (2004) observed an increase in room temperature cell absorbance of *Phaeodactylum tricornutum* at 690 nm during HL, which could

correspondingly indicate Chl *a* (and FCP) aggregation during NPQ in diatoms. Unfortunately the study by Ruban et al. (2004) did not show any absorbance change data below 450 nm, so it is unknown if they saw a drop in 437 nm absorbance during HL (as in plants) in *P*. *tricornutum*. Consistent with a model that qE in *Nitzschia* also involves an aggregation of FCP Chl *a*, there is a sharp increase in Chl *a* Q_y absorbance during HL (Figure 3.2-10C). The HL induced increase in absorbance at 513 and 479 nm and loss in absorbance at 498 nm (Figure 3.2-10C) are very consistent with the accumulation of DT within *P*. *tricornutum* thylakoids (Ruban et al. 2004). Thus the absorbance changes induced during HL in *Nitzschia* cells can be largely explained as a sum of the absorbance changes associated with (i) the concurrent loss of DD absorbance and increase in DT absorbance from DD de-epoxidation and (ii) FCP Chl *a* aggregation.

Emission at energies equivalent to FCPII emission (at ~687 nm) and PSII emission (at ~695 nm) are most quenched during HL, with a relative enhancement in emission peaking at ~715 nm with a shoulder at ~750 nm extending all the way to ~800 nm (Figure 3.2-11C). This quenching pattern can be explained by placing a quencher (Q1) within the outer FCP complexes (FCPII) and a secondary quencher (Q2) within the inner FCP complexes (FCPii) (see Figure 3.2-5B). Q1 quenches FCPII emission at 687 nm; Q2 quenches emission at 695 nm from inner FCP-PSII complexes. The broad relative increase in lower energy emission is a marker for aggregation quenching in LHCII (Ruban and Horton 1992, Miloslavina et al. 2008, Andreeva et al. 2009) and for aggregation and pH induced quenching in FCP complexes (Miloslavina et al. 2009, Gundermann and Büchel 2012). Aggregation of LHCII is believed to bring inter-trimer Chl *a* molecules into close proximity so as to form Chl *a* –Chl *a* dimers. This causes a loss in emission from monomeric Chl *a* at 680 nm (F680) and an increase in emission from the weak

emitting Chl *a* dimer at 700 nm (F700) (Andreeva et al. 2009). The Chl *a*-Chl *a* mixed exciton charge transfer state of the dimer has a very strong electron–phonon coupling, leading to a large Stokes shift, very strong spectral broadening, and strong vibrational tails (Miloslavina et al. 2008). The relative rise in emission at ~715 nm could stem from less quenching of PSI due to the absence of a quencher within FCPi and/ or an increase in energy transfer from PSII to PSI during HL illumination (see Figure 3.2-5B). Emission near ~715 nm could also contain emission from 'F700's within the quenched FCP complexes.

Chl *a* aggregation within FCPII and FCPii would be responsible for the enhancement of Chl *a* Q_y absorbance in the HL exposed *Nitzschia* cells. Chl *a* aggregation within FCPII is hypothesized to be due to inter-trimer interactions between FCPII complexes, in a manner analogous to LHCII aggregation. Chl *a* aggregation within FCPii is hypothesized to be due to inter-trimer interactions induced by more subtle conformational changes within FCPii trimers. There are two distinct positive Chl *a* Q_y absorbance peaks that develop during HL at ~672 and ~683 nm (Figure 3.2-10C). This enhanced absorbance might represent the direct formation of Chl *a*-Chl *a* quencher dimers or could merely be an ancillary consequence of HL induced changes within the pigment-protein environment.

During excess light conditions, in addition to the dominant transfer of excitation energy to Q1 and Q2, there seems to be a disruption of energy transfer within/ between FCP complexes which uncouples some Chl *a*. Uncoupling of Chl *a* is observed as a weak relative enhancement of emission at ~673 nm (Figure 3.2-11C).

The dual usage of Q1 and Q2 provides *Nitzschia* cells with two layers of antenna based quenching for PSII. Q2 quenching specifically targets the inner FCP antenna of PSII, serving as

an additional quencher to the more ubiquitous Q1 quenching. Q1 is consistent with the quencher that Miloslavina et al. (2009) placed within FCP complexes that become functionally decoupled from PSII during HL and Q2 is consistent with the quencher that Miloslavina et al. (2009) placed within FCP complexes that remain coupled with PSII. Antenna based quenching would be activated by the conversion of DD to DT, as witnessed by the absorbance changes at ~513 and 498 nm (Figure 3.2-10C).

State transitions (qT) are a well-recognised component of the 'slower' NPQ response in cyanobacteria and higher plants. State transitions involve a redistribution of excitation energy brought about by a mobile antenna system or by 'spillover' of excitons from saturated PSII cores to PSI (Wollman 2001, McConnell et al. 2002). In higher plants, state transitions involve a kinase activated and electrostatic mediated migration of LHCII complexes from PSII to PSI rich regions in the thylakoids (Wollman 2001). State transitions do not occur in *Phaeodactylum tricornutum* (Ting and Owens 1993), are commonly not believed to be present in diatoms (Lavaud 2007), and only alluded to by Miloslavina et al. (2009). Since direct measurement of PSI absorbance cross sections were not compared between dark and HL adapted cells, it cannot be fully distinguished whether the relative enhancement in emission at ~715 nm during HL in is due to an increase in PSI absorbance cross section caused by re-association of FCP complexes with PSI or by a spillover of excitation energy from PSII to PSI, or if it is due to a preferential quenching of PSII coupled FCP complexes, or if it is from emission of Chl *a*-Chl *a* quencher dimers. Since there is no granum stacking in diatoms, PSII and PSI are not spatially separated into separate domains within the thylakoid. Instead the photosystems can be predicted to be physically separated via the FCP complexes that surround them and by local variations in lipid

composition. During the near saturating illumination used in Figure 3.2-11, FCPII is predicted to form large quenching aggregates of multiple FCP oligomers. FCP coalescence could promote PSII-to-PSI energy transfer by removing the FCP complex imposed steric hindrance that maintains spatial separation of PSII and PSI complexes. To summarize, it is plausible that there is an enhancement in PSII-to-PSI energy transfer during HL, though its significance is currently unknown.

The relaxation of NPQ in the dark proceeding HL involves a reversal of the absorbance and energy transfer alterations that occurred during HL. Much of the NPQ formed during HL is able to relax within 15 minutes of transition to dark (Figure 3.2-2A). A residual $\mathcal{NPQ}$ value of 0.5 at 15 minutes post HL corresponds to a 50% recovery of pre-HL fluorescence and a residual $\mathcal{NPQ}$ value of 1.0 corresponds to a 33% recovery. Consistent with the quenching being regulated by DD de-epoxidation, much of the enhanced absorbance at 513 nm as compared to 498 nm relaxes post HL (Figure 3.2-10C). Much of the Chl *a* Q_y absorption enhancement is also lost post HL. The reversal of these absorbance changes post HL coincide with a comparable scaled reversal of the changes to cell emission shape (Figure 3.2-11C). Thus the relaxation of $\mathcal{NPQ}$ amplitude under physiological conditions post HL originates from a reversal of the HL induced changes in excitation energy distribution detected at 77K, and a reversal of the HL enhanced Chl *a* Q_y and DT absorption.

Excess light induced excitation energy redistribution in Navicula sp.

Similar to what was observed in *Nitzschia*, HL induces a strong increase in absorbance at 511 nm attributed to DT formation and an increase in Chl *a* Q_y absorption that can be attributed to Chl *a* aggregation (Figure 3.2-10D). Contrary to what was seen in *Nitzschia*, HL induces a

strong increase in band absorption in the blue region at ~412, 440, and 477 nm. This is being attributed to an enhancement in DT absorption during HL, since DT has secondary absorbance bands at these positions (Figure 3.2-7), although precise assignment is difficult because all carotenoids absorb in this region. *De novo* synthesis of DT during the 10 minutes of HL could account for the strong increase in absorption at all DT absorbance bands, and not just the de-epoxidation specific ~512 nm band.

As in *Nitzschia*, FCP centred quenching in *Navicula* would result from the formation of Chl *a*-Chl *a* associations brought about by HL induced formation of FCP quenching aggregates (see Figure 3.2-5D). The details of Chl *a* aggregation quenching are somewhat different in *Navicula*. HL induced a more equivalent increase in absorbance between the two Chl *a* Q_y bands (at ~670 and 681 nm) (Figure 3.2-10D) and there was no relative enhancement of the greater than ~750 nm emission that was observed in *Nitzschia* (Figure 3.2-11D). The absence of enhanced low energy vibrational sub-band emission could suggest that the Chl *a*-Chl *a* dimers formed during NPQ in *Navicula* are within more restricted protein environments. Wide bandwidth emission at ~720 nm increased in relative amplitude during HL (Figure 3.2-11 D), which may represent the 'F700' for Chl *a*-Chl *a* quenching in *Navicula*. Placement of Chl *a*-Chl *a* quenching within Q2 (inner FCP) is rather trivial since there is no evidence for outer FCPs in *Navicula*; quenching targets PSII emission at 695 nm.

NPQ amplitude in *Navicula* relaxes in the dark following HL in a very limited amount. After an initial drop in $\mathcal{NPQ}$ at 1 minute post HL, sustained relaxation is very slow (Figure 3.2-2A). The HL induced changes in Chl *a* Q_y absorbance attributed to Chl *a*-Chl *a* aggregation show very limited relaxation within 15 minutes post HL, whilst the DT attributed absorbance changes

in the blue and green regions relax modestly (Figure 3.2-10D). The HL induced redistribution of excitation energy also relaxes in a very limited manner (Figure 3.2-11D). Relaxation of antenna centred quenching post HL seems to necessitate strong deprotonation or large scale DT epoxidation, since a partial reversal of DT absorption does not induce an equivalent reversal of Chl *a* Q_y absorption or a relaxation of emission redistribution. The residual $\mathcal{NPQ}$ post HL could be artificially relaxed with the uncoupler NH_4Cl for sub-saturating NPQ levels (*Figure 3.3-8*). Perhaps the pH for deactivating FCP-based Chl *a* -Chl *a* quenching in *Navicula* is very low or DT has an especially strong role in regulating the quenching site. These differences in Chl *a*-Chl *a* quenching deactivation could certainly be explained by inter-species differences in FCP protein composition.

To keep things in perspective, the NPQ response during HL causes a loss in emission at an order of magnitude greater than the corresponding changes in cell absorbance. The enhancement in the amount of NPQ that *Nitzschia* can perform during HL seems to be directly due to there being a larger FCP antenna size in *Nitzschia* (maximal $\mathcal{NPQ}$ in *Nitzschia* is ~ 1.6x that in *Navicula*, equivalent to the increase in σPSII).

3.2-7 Excitation pathway dependence on the effectiveness of NPQ

The emission spectra in Figure 3.2-11 revealed changes in energy transfer from antenna pigments to the low energy emitters of FCP complexes (*Nitzschia* only) and PSII during NPQ. These spectra were collected at 77K, which has several practical purposes: to improve spectral band resolution, inhibit quenching of fluorescence due to reaction centre photochemistry (diffusion of mobile electron carriers is inhibited at low temperature), and to maintain the sample in a fixed, stable state. However, pigment-to-pigment energy transfer pathways are

different at cryogenic temperatures (Andrizhiyevskaya et al. 2005). Fewer electronic couplings become possible as molecular vibration is restrained and pigment dipole fluctuations become restricted - the lower the temperature, the more pigments become uncoupled (Andrizhiyevskaya et al. 2005). Also at low temperature, 'back energy transfer' to pigments of higher energy levels becomes less possible due to the lack of enthalpy input into the system (e.g. excitation of P700 with >720 nm light). To gain a better understanding of the energy transfer dynamics associated with NPQ, as they actual occur under physiological relevant conditions, action spectra of excitation pressure and $\mathcal{NPQ}$ were collected using a series of monochromatic (12.5 nm FWHM) HL illuminations spanning the photosynthetically active spectral region (~400 to 700 nm). These action spectra give *in situ* information on both the excitation of photosystems and the ability of the NPQ mechanism to relieve the excitation pressure that is generated by the HL. In these experiments NPQ was pumped with different colours of HL but always probed with a 470 nm measuring light, so that the measured fluorescence from PSII always originated from the indirect excitation of PSII by energy transfer from FCP complexes. The raw action spectra for *Nitzschia* cells and *Navicula* cells are shown as contour plots in Figures 3.2-12 & 13, respectively, with the results summarised in Figure 3.2-14.

Excitation of PSII was measured as excitation pressure (1-qP); 1-qP at 30 seconds after HL is turned on is a good indicator for basal excitation of PSII prior to large scale modifications by the NPQ response. As expected, the action spectra for excitation pressure (Figure 3.2-14A & B) mimics that of the excitation spectra for cell emission at 695 nm (dominated by PSII fluorescence) collected at 77K (Figure 3.2-9). Yet there are a few conspicuous dissimilarities. The relative importance of Fx_{red} excitation (peak at ~530 nm) is enhanced and the relative

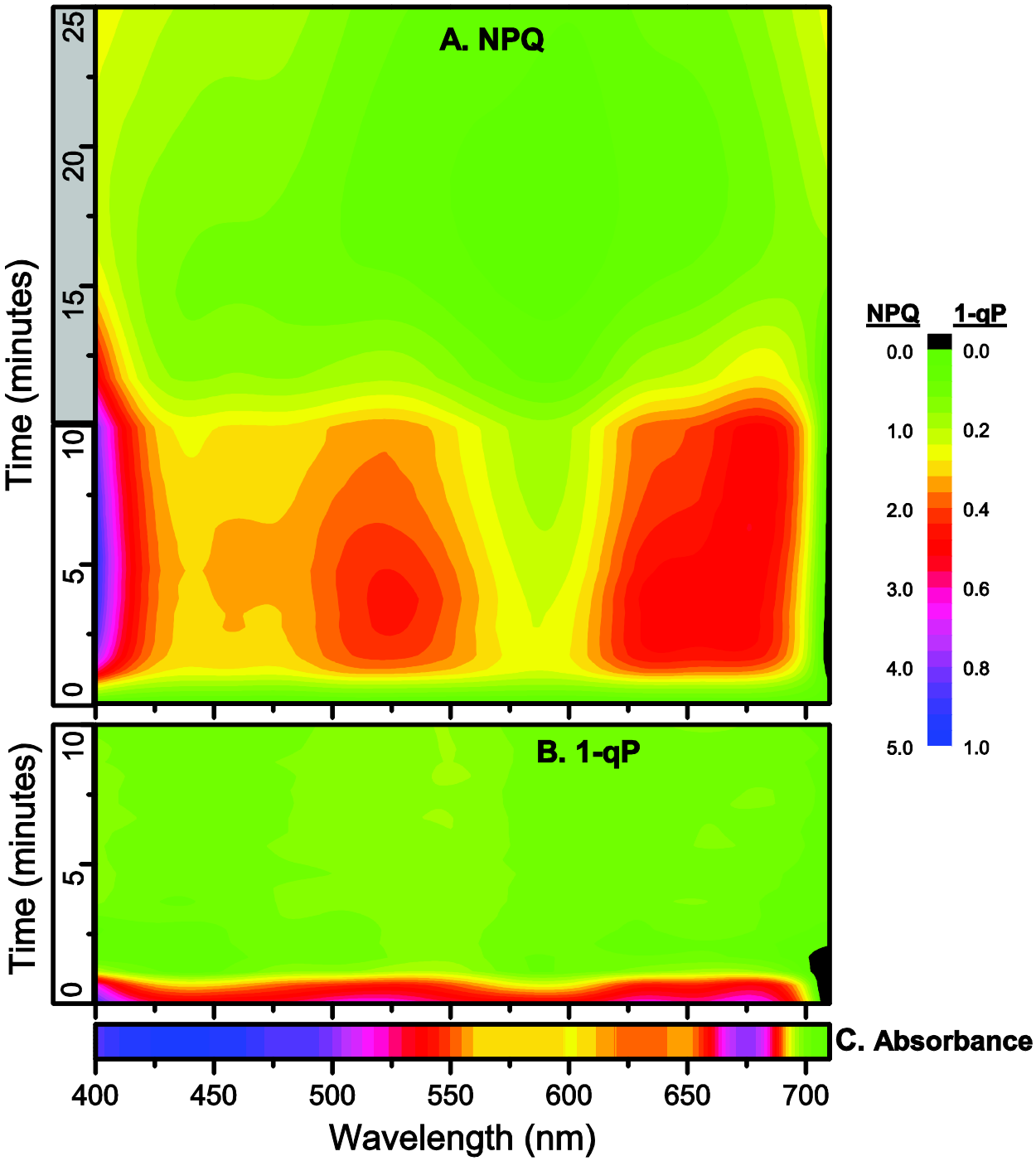

Figure 3.2-12 NPQ and excitation pressure (1-qP) action spectra contour plots for *Nitzschia* cells. $\mathcal{NPQ}$ (**A**) and 1-qP (**B**) were collected during dark-to-high light-to-dark transitions with 220 µmol $m^{-2}s^{-1}$ monochromatic high light (HL) illumination ranging from 405 to 705 nm (±12.5 nm FWHM). Time zero corresponds to the onset of HL. White boxes along the y-axis indicate the period of HL; dark boxes indicate the period of darkness following HL. See *Section 2.6* for details on methodology. **C**, the room temperature absorbance spectrum of dark adapted cells is included for comparison. Plots are the mean from 3 cultures grown at of 50 µmol $m^{-2}s^{-1}$.

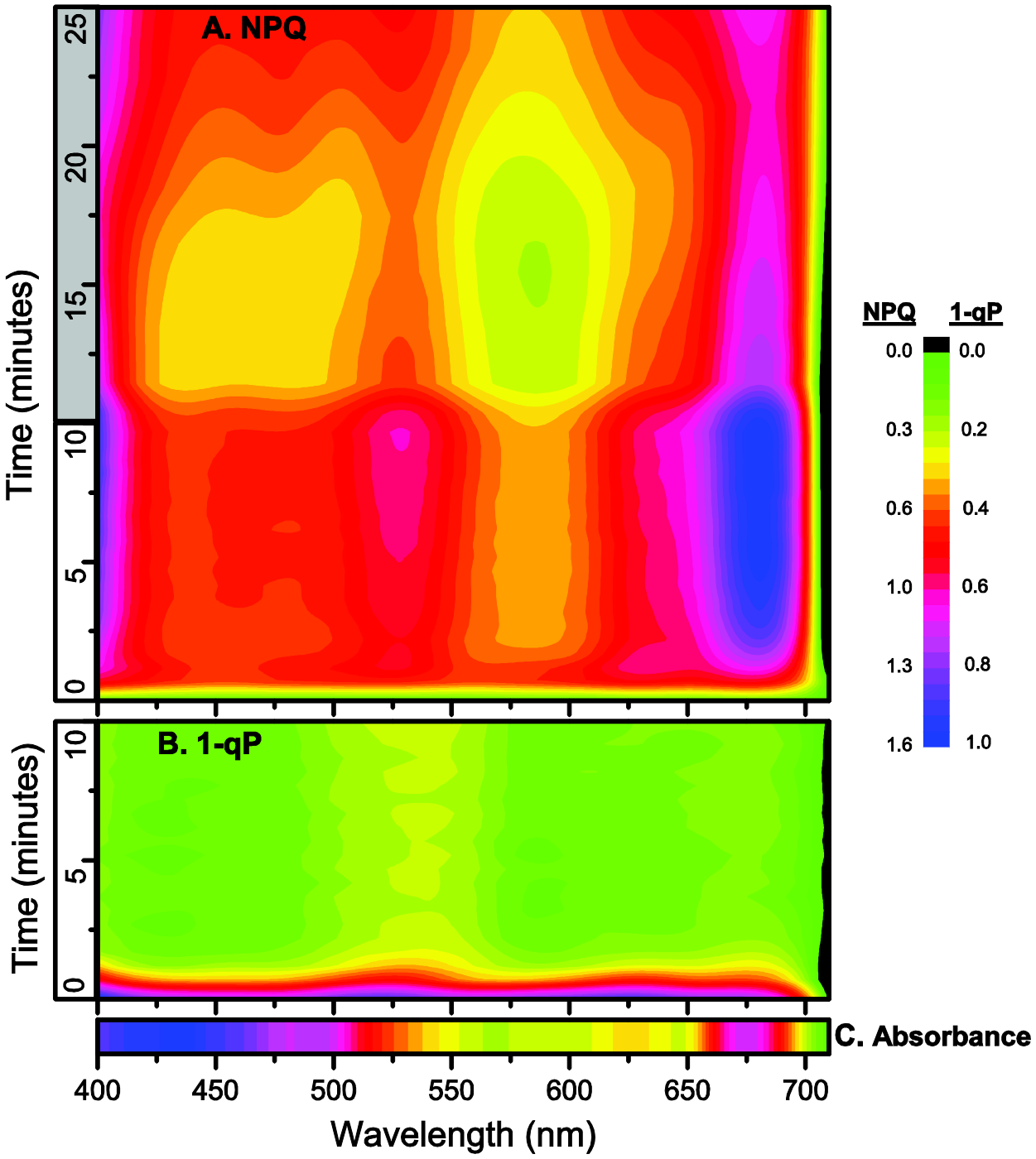

Figure 3.2-13 NPQ and excitation pressure (1-qP) action spectra contour plots for *Navicula* cells. $\mathcal{NPQ}$ (**A**) and 1-qP (**B**) were collected during dark-to-high light-to-dark transitions with 220 µmol $m^{-2}s^{-1}$ monochromatic high light (HL) illumination ranging from 405 to 705 nm (±12.5 nm FWHM). Time zero corresponds to the onset of HL. White boxes along the y-axis indicate the period of HL; dark boxes indicate the period of darkness following HL. See *Section 2.6* for details on methodology. **C**, the room temperature absorbance spectrum of dark adapted cells is included for comparison. Plots are the mean from 3 cultures grown at of 50 µmol $m^{-2}s^{-1}$.

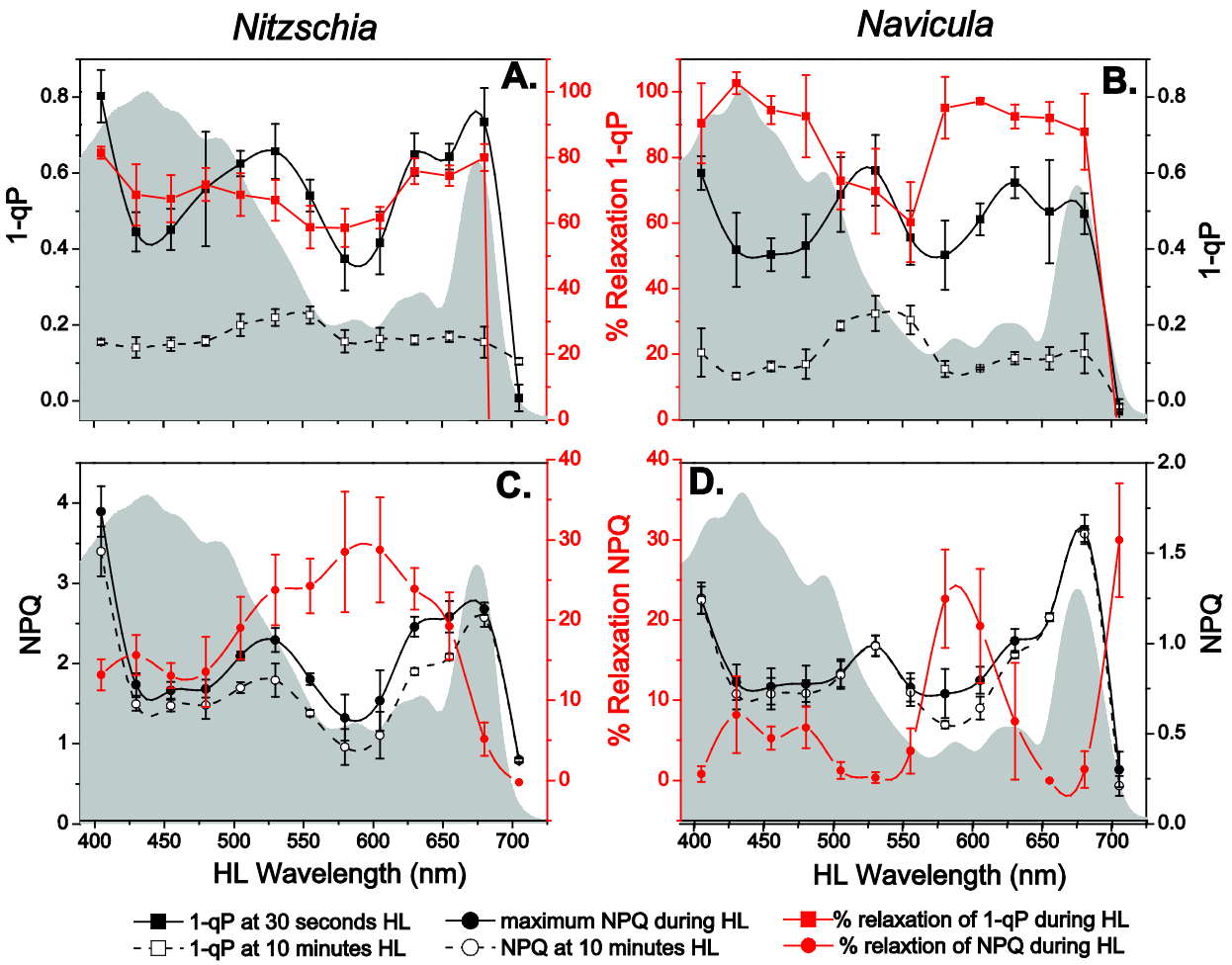

Figure 3.2-14 Summary of the influence of illumination wavelength on excitation pressure (1-qP) and NPQ. **A** & **B,** 1-qP at 30 seconds (black solid filled squares) and 10 minutes (black open squares) of 220 µmol $m^{-2}s^{-1}$ monochromatic high light (HL) illumination in *Nitzschia* and *Navicula* cells, respectively. The relaxation of 1-qP during HL (red squares) is presented as percentage relaxation (100•(1-$qP_{30seconds}$ – 1-$qP_{10minutes}$) /1-$qP_{30seconds}$). **C** & **D,** maximal $\mathcal{NPQ}$ during HL (black solid filled circles) and $\mathcal{NPQ}$ at 10 minutes of HL (black open circles) illumination in *Nitzschia* and *Navicula* cells, respectively. The relaxation of $\mathcal{NPQ}$ during HL (red circles) is presented as percentage relaxation (100•($\mathcal{NPQ}_{maximum}$ – $\mathcal{NPQ}_{10minutes}$) / $\mathcal{NPQ}_{maximum}$). See Figures 3.2-12 & 13 for additional information. Error bars represent ±1 standard deviation from the mean of 3 cultures grown at of 50 µmol $m^{-2}s^{-1}$.

importance of Chl *a* Q_y excitation (655 to 680 nm) is reduced at physiological temperature in both species. The physiological temperature enhanced sensitivity of PSII excitation with Fx_{red} absorbed light suggests that energy transfer from Fx to PSII has become more efficient at the higher temperature. Hence, Fx-to-PSII energy transfer involves energy transfer step(s) that require thermal energy input or, are easily disrupted by subtle structural changes in the protein

milieu induced by freezing of the thylakoid. The uncoupled red Fxs can be ostensibly localised to the FCP periphery, since peripheral Fx have been previously found to be uncoupled (reviewed by Wilhelm et al. 2006 and Lavaud 2007, Premvardhan et al. 2010). The apparent loss in PSII excitation at physiological temperature with direct excitation of Chl *a* Q_y bands is likely due to enhanced trapping of these excitons by PSI in the fluid thylakoid.

HL irradiance wavelength has amplitude and kinetic effects on NPQ induction and relaxation. Illumination wavelengths that are effectively quenched by the NPQ response will lower excitation pressure and give negative feedback (a drop in ΔpH) to the NPQ quenching response. Excitation pressure during steady state HL conditions (10 minutes of HL) drops substantially below the initial values in both species. Quantification of excitation pressure relaxation during HL (Figure 3.2-14A & B) shows that all wavelengths of HL except for 705 nm can be effectively regulated. Far red light at 705 nm is probably poorly regulated because this excitation is less effective at generating a NPQ triggering ΔpH and/ or the NPQ quenching sites are at energy levels above and inaccessible to the 705 nm absorbing pigments. $\mathcal{NPQ}$ amplitude did not reach saturation with the moderate HL intensity (220 µmol $m^{-2}s^{-1}$) used in the collection of the action spectra. DT-epoxidation is unlikely to develop during the illumination period used here because the presence of a ΔpH inhibits DT epoxidase (see the discussion by Goss and Jakob 2010), so any NPQ relaxation during illumination would stem from a direct ΔpH 'tuning' of quenching. In both species, the weak $\mathcal{NPQ}$ induced with ~580 to 605 nm excitations relaxes substantially during illumination (Figure 3.2-14C & D). In *Nitzschia*, $\mathcal{NPQ}$ is able to relax (greater than 10%) with all HL wavelengths absorbed by FCP pigments (Figure 3.2-14C), indicating that the NPQ induced by excitation of FCP pigments is dynamic in *Nitzschia*. The relaxation of

quenching during illumination is hypothesized to arise when ΔpH drops during photostasis permitting a partial deactivation of the antenna centred quenching sites. HL excitations that are competitively absorbed directly by the PSII (~680 nm) induce a sustained $\mathcal{NPQ}$ in *Nitzschia* (Figure 3.2-14C) because these excitations are less effectively regulated by FCP based quenching. The $\mathcal{NPQ}$ induced in *Navicula* with all excitations absorbed by the FCP accessory pigments exhibits very little relaxation during illumination (Figure 3.2-14D), which can be explained by the locked-in quenching that develops in this species.

Illumination wavelength affects NPQ in ways that are independent of excitation pressure. Recall that $\mathcal{NPQ}$ amplitude is linearly dependent on excitation pressure (Figure 3.2-3C); however, this dependency does not hold true if 1-qP values are titrated by using different wavelengths of illumination. A linear correlation analysis was performed for $\mathcal{NPQ}$ dependency on excitation pressure generated by a full photosynthetically active range of monochromatic illuminations (Figure 3.2-15). This analysis revealed that the linearity between excitation pressure and $\mathcal{NPQ}$ remains in *Nitzschia* cells during NPQ induction (as shown by a high linear correlation between 1-qP at 30 seconds and maximum $\mathcal{NPQ}$, r= 0.977). However, during steady state NPQ (at 10 minutes HL) HL wavelength disrupts the linear relationship between excitation pressure and $\mathcal{NPQ}$ (as shown by a weak linear correlation between 1-qP and $\mathcal{NPQ}$ at 10 minutes; r= 0.593). To recapitulate, NPQ during steady state conditions in *Nitzschia* is less dependent on the amount of excitation pressure, but more by the wavelength of illumination used to elicit the excitation pressure. So it seems that the steady state NPQ maintained by low excitation pressures is largely a residual of the NPQ that developed during the initial transition to HL. Interestingly, HL illumination at 405 nm causes 'unusually' high $\mathcal{NPQ}$ for the amount of

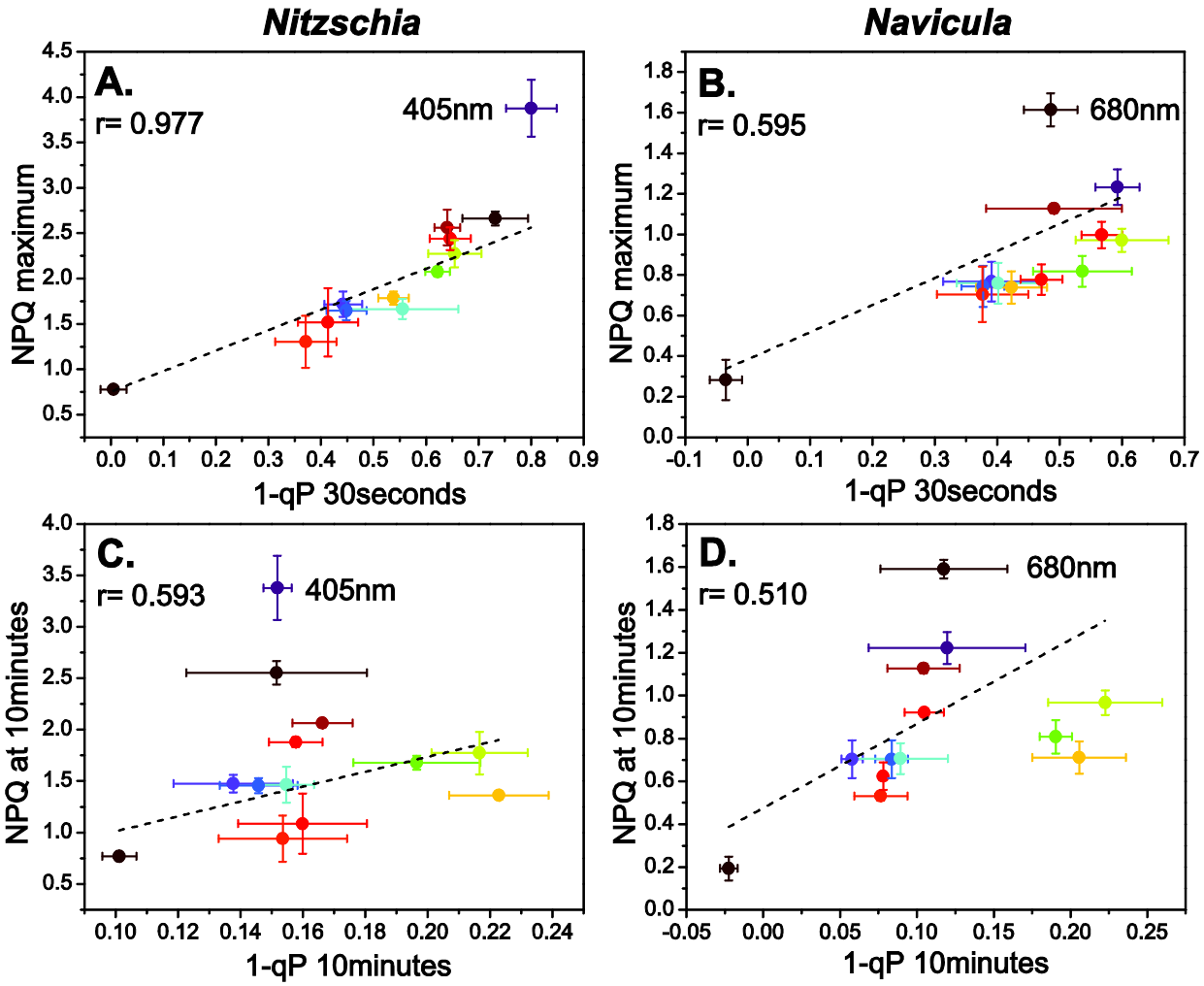

Figure 3.2-15 The dependence of NPQ on excitation pressure when generated with a full photosynthetically active range of monochromatic high light illuminations. High light (HL) illumination of 220 µmol $m^{-2}s^{-1}$ was used to induce excitation pressure (1-qP) and elicit NPQ in *Nitzschia* (**A** & **C**) and *Navicula* (**B** & **D**) cells. Linear regressions for the dependency of $\mathcal{NPQ}$ amplitude on excitation pressure (mean of 3 separate cultures grown at 50 µmol $m^{-2}s^{-1}$, error bars represent ±1 standard deviation) are shown as dotted lines; corresponding Pearson's r value is given in each panel. Data point color corresponds spectrally to wavelength (nm) of HL; 'outlier' HL wavelengths are labeled. **A** & **B**, Regression for NPQ induction (1-qP at 30 seconds to maximum $\mathcal{NPQ}$ obtained during HL). **C** & **D**, Regression for steady state NPQ (1-qP at 10 minutes to $\mathcal{NPQ}$ at 10 minutes). See Figures 3.2-12 & 13 for further experimental details.

induced excitation pressure, as compared to other illumination wavelengths (seen as an 'outlier' in Figure 3.2-15A & C). This suggests that near UV illumination induces an NPQ that is mechanistically different than NPQ triggered by lower energy wavelengths. UV induced photodamage (photoinhibition) of PSII could be the source of the enhanced $\mathcal{NPQ}$. Still most of

the NPQ induced with 405 nm HL was via reversible qE, because NPQ was still quite relaxable both during and after illumination.

In *Navicula* cells, the linear relationship between excitation pressure and $\mathcal{NPQ}$ is never preserved across illumination wavelength (shown by a poor linear correlation between 1-qP and $\mathcal{NPQ}$ during induction and steady state phases, r= 0.595 and 0.510, respectively). Direct excitation of PSII reaction centre with 680 nm HL induces the highest amplitude $\mathcal{NPQ}$. 680 nm HL also induces an 'unusually' high $\mathcal{NPQ}$ based on excitation pressure (seen as an 'outlier' in Figure 3.2-15B & D). Direct non-photochemical quenching within the PSII reaction centre (qE_{nonXC}) could be responsible for this disjoint between NPQ and excitation pressure.

3.2-8 Quantum yields of excitation energy conversion

Three quantum yields of energy conversion can be used to describe the fate of photon energy on its journey from being absorbed by antenna pigments to being trapped by a PSII reaction centre (Hendrickson et al. 2004). The quantum efficiencies of photochemistry (equivalent to PSII effective quantum yield, ϕPSII), regulated non-photochemical dissipation (ϕNPQ), and constitutive thermal dissipation and fluorescence (ϕNO) sum the yields of PSII energy flux to unity (Kramer et al. 2004, Hendrickson et al. 2004). These parameters are valid for both 'lake' and 'puddle' paradigms of PSII connectivity (Hendrickson et al. 2004, Klughammer and Schreiber 2008). Energy conversion not contributing to photochemical forward electron transport has been subdivided: ϕNPQ is the quantum yield of excitation energy dissipation associated with regulated thermal dissipation (ostensibly by qE), and ϕNO is the quantum yield of excitation energy dissipation associated with 'non-regulated' thermal dissipation and fluorescence from PSII cores.

Figures 3.2-16 and 17 show transients for the quantum yields of energy conversion in *Nitzschia* and *Navicula* cells (with and without DTT pre-treatment) during HL transitions. The quantum yields reached during steady state conditions are summarized in Figure 3.2-19A and B. ϕPSII recovers less after HL in N*avicula*, which would be a consequence of the sustained ϕNPQ post HL (Figures 3.2-17A vs. 16A). With DTT, ϕPSII is able to remain relatively high in both species during HL, but electron transport is reduced more post HL in *Nitzschia* (Figures 3.2-16B vs. 17B). *Nitzschia* cells pre-treated with DTT have a greatly reduced ϕNPQ with a slow induction at high irradiance HL (Figure 3.2-16C vs. D). In contrast, *Navicula* DTT pre-treated cells maintain a fast acting ϕNPQ, which is able to initially dissipate as much photon energy as control cells at low to moderate HL irradiances and relaxes quickly once HL is removed (Figure 3.2-17C vs. D). For high irradiances, ϕNO accounts for some 80 percent (or more) of energy conversion in both species immediately following transfer to HL, then quickly relaxes within 30 seconds (Figures 3.2-16E & 17E). Steady state ϕNO amplitudes are negatively related to HL intensity and ϕNPQ (Figure 3.2-19A & B), suggesting that non-regulated means of excitation energy dissipation may be important at lower excitation pressures that do not elicit strong NPQ responses. When cells of both species are pre-treated with DTT, dissipation of excitons via ϕNO remains heightened during the entire HL period; yet *Nitzschia* cells depend more heavily on ϕNO for energy dissipation (*Nitzschia* has less relaxation of ϕNO and slower relaxation kinetics, Figures 3.2-16F & 17F). Interestingly, steady state ϕNO seems to be independent of HL intensity for *Navicula* cells with DTT (Figure 3.2-19B). To recapitulate, *Navicula* cells retain a fast acting regulated mechanism for excess excitation energy dissipation even when qE_{XC} has

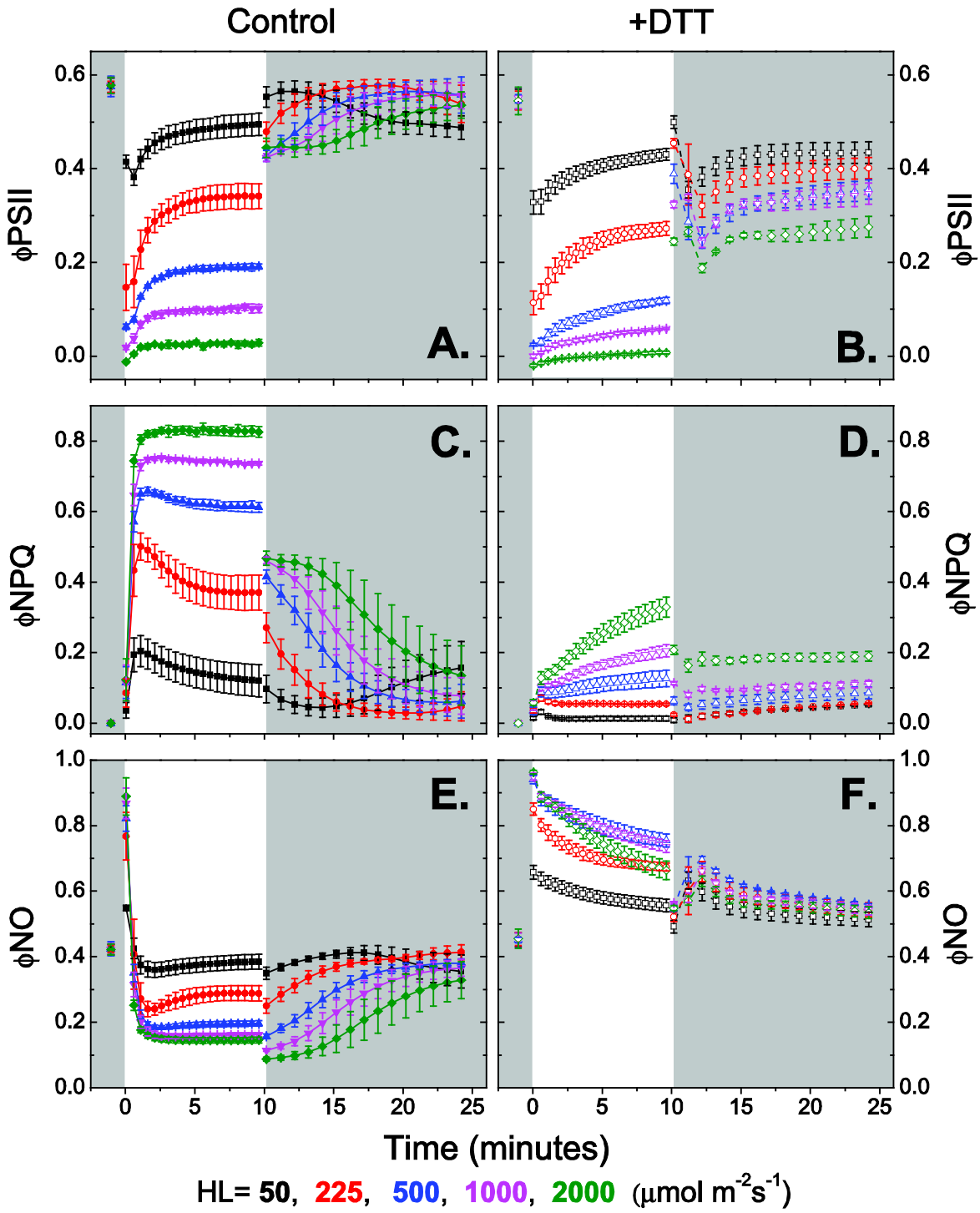

Figure 3.2-16 Quantum yields of excitation energy conversion during high light transitions in *Nitzschia* cells. **A**, **C**, & **E**, control cells. **B**, **C**, & **F**, cells pre-treated with 5.3 mM of the DD de-epoxidase inhibitor DTT. The regions of the plot area with a dark background correspond to dark conditions and the white portion of the background corresponds to the time that high light (HL) was applied. **A** & **B**, quantum yield of PSII photochemical energy conversion (ϕPSII). **C** & **D**, quantum yield of regulated non-photochemical energy dissipation (ϕNPQ). **E** & **F**, quantum yield of non-regulated non-photochemical energy dissipation (ϕNO). See text for further explanation of quantum yields. Error bars represent ± 1 standard deviation from the mean of 3 separate cultures grown at 50 µmol $m^{-2}s^{-1}$.

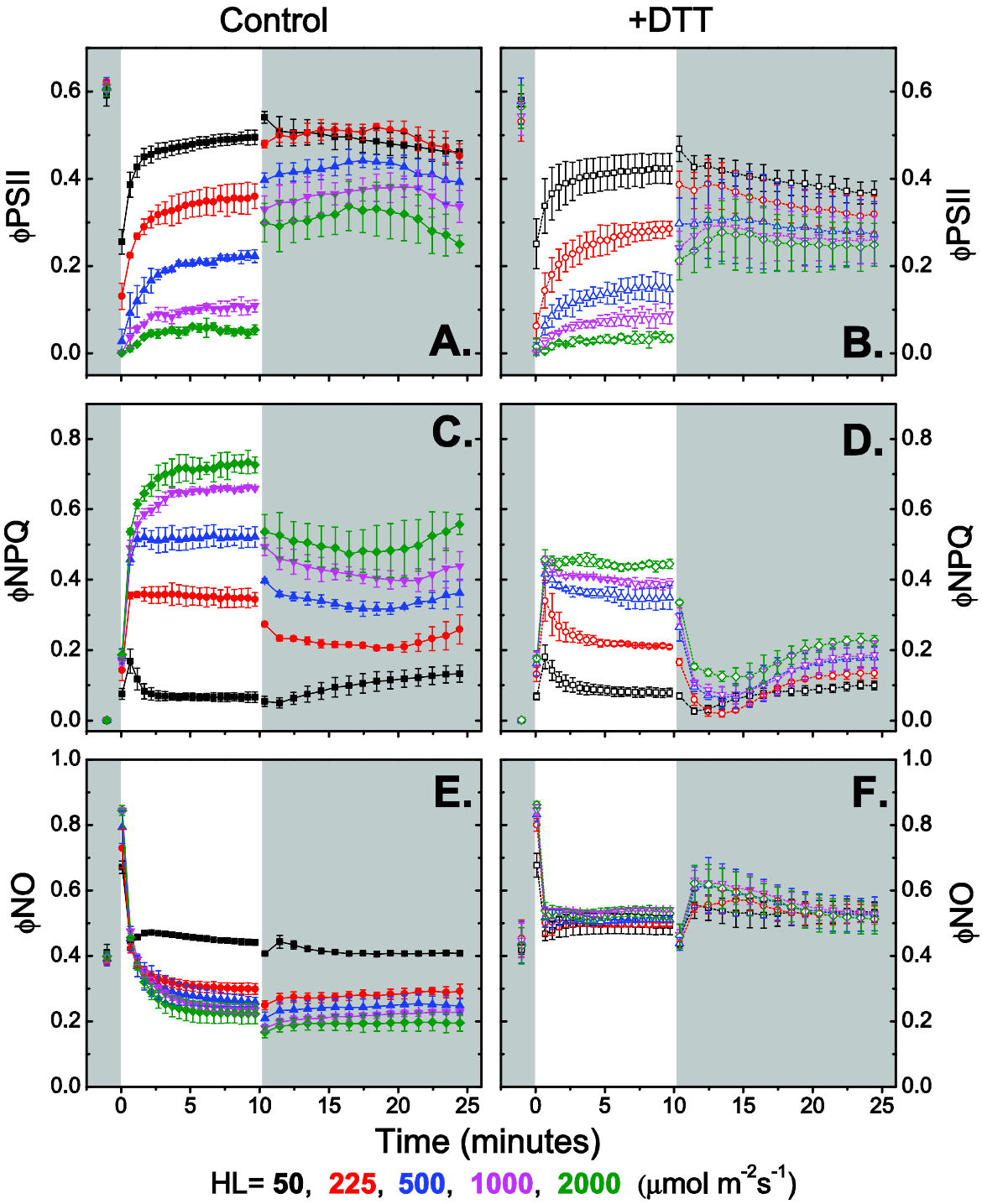

Figure 3.2-17 Quantum yields of excitation energy conversion during high light transitions in *Navicula* cells. **A**, **C**, & **E**, control cells. **B**, **C**, & **F**, cells pre-treated with 2.65 mM of the DD de-epoxidase inhibitor DTT. The regions of the plot area with a dark background correspond to dark conditions and the white portion of the background corresponds to the time that high light (HL) was applied. **A** & **B**, quantum yield of PSII photochemical energy conversion (ϕPSII). **C** & **D**, quantum yield of regulated non-photochemical energy dissipation (ϕNPQ). **E** & **F**, quantum yield of non-regulated non-photochemical energy dissipation (ϕNO). See text for further explanation of quantum yields. Error bars represent ± 1 standard deviation from the mean of 3 separate cultures grown at 50 µmol $m^{-2}s^{-1}$.

been inhibited with DTT, whereas *Nitzschia* cells rely on non-regulated energy dissipation in the absence of qE_{XC}.

The quantum yield of energy dissipation associated with regulated thermal dissipation (ϕNPQ) has been subdivided in two constituent components in Figure 3.2-18: xanthophyll cycle dependent qE (qE_{XC}) and xanthophyll cycle independent qE (qE_{nonXC}). Pre-treatment with saturating levels of DTT inhibits NPQ that is dependent on DD de-epoxidase activity (qE_{XC}) leaving only regulated dissipation that does not require DD de-epoxidation (qE_{nonXC}), thereby allowing experimental separation of the two components. There are striking differences in the composition of ϕNPQ between the two species, both in induction/relaxation kinetics (Figure 3.2-18) and proportionality of total ϕNPQ (Figure 3.2-19C).

The majority of regulated excitation energy dissipation in *Nitzschia* is by qE_{XC}. Energy dissipation by qE_{XC} is rapidly activated during HL, reaching maximal levels within 60 to 90 seconds of HL exposure, and then slowly relaxes during HL (Figure 3.2-18A). In the dark after HL, ϕqE_{XC} relaxation is more kinetically complex with seemingly another component (opposite in amplitude) slowing relaxation at the highest irradiances (Figure 3.2-18A). Energy dissipation via qE_{nonXC} has a minor contribution to total NPQ at low HL irradiances, with the relative contribution to total NPQ increasing linearly with HL intensity (Figure 3.2-19C) and duration of HL at high irradiances (Figure 3.2-18B).

What processes for non-radiative excited state energy dissipation are available to *Nitzschia* cells in the absence of qE_{XC}? An accumulation of excited state triplet Chl *a* (^{3}Chl *a**) within the antenna could be a plausible source. ^{3}Chl *a** can be quenched either by excited state triplet carotenoid (^{3}Chl *a** + ^{3}car* → ^{1}Chl *a* + ^{1}car + heat) or by molecular oxygen (^{3}Chl *a** + $^3O_2$

$\rightarrow {}^1Chl\ a + {}^1O_2$). Direct quenching of triplet Chl *a* by a triplet carotenoid requires close interaction between the donor Chl *a* and carotenoid acceptor molecules (via a Dexter mechanism) (Di Valentin et al. 2009, Di Valentin et al. 2012, Ballottari et al. 2013). In the antenna system of higher plants, nearly all triplet Chl *a*s are quenched by triplet carotenoids in LHCII (~95%) with somewhat less efficiencies in Lhcb4, Lhcb5, and Lhcb6 (Ballottari et al. 2013). The efficiency for quenching by triplet carotenoid maybe less in diatom FCP than in plant LHCII (at least when measured at low temperature) even though the carotenoid to Chl *a* ratio is higher in FCP (Di Valentin et al. 2012). Even if triplet Chl *a* is largely quenched through the formation of singlet oxygen, the abundance of carotenoids (principally Fx) located within FCPs should limit oxidative damage by scavenging reactive oxygen species (Di Valentin et al. 2012). In higher plant antenna proteins the population of triplet Chl *a* (as measured by $^1O_2$ accumulation) increases linearly with illumination intensity (Ballottari et al. 2013), similar to trend seen in *Nitzschia* with qE_{nonXC} (Figure 3.2-19C). PSI reaction centre based quenching may also explain excitation energy dissipation by qE_{nonXC} in *Nitzschia*. The long lived radical pair of $P700^+$ and iron sulfur cluster F_X^- in PSI acts as an effective quencher of Chl *a* fluorescence for excitations trapped by PSI (Schlodder et al. 2005). The accumulation of oxidised P700 during illumination could therefore contribute to photoprotective fluorescence quenching, especially if PSII and PSI compete for the same excitons within a shared antenna system. Direct real time monitoring of PSI activity during HL transitions by measuring P700 cation formation via absorbance changes at 830 nm (solely and in reference to absorbance at 880 nm) in *Nitzschia curvilineata* and *Navicula sp*. cells was unsuccessful. Regardless of the precise photo-electronic

mechanism involved, energy dissipation by qE_{nonXC} in *Nitzschia* cells seems to only be important when the primary method for excitation energy regulation (via qE_{XC}) becomes limiting.

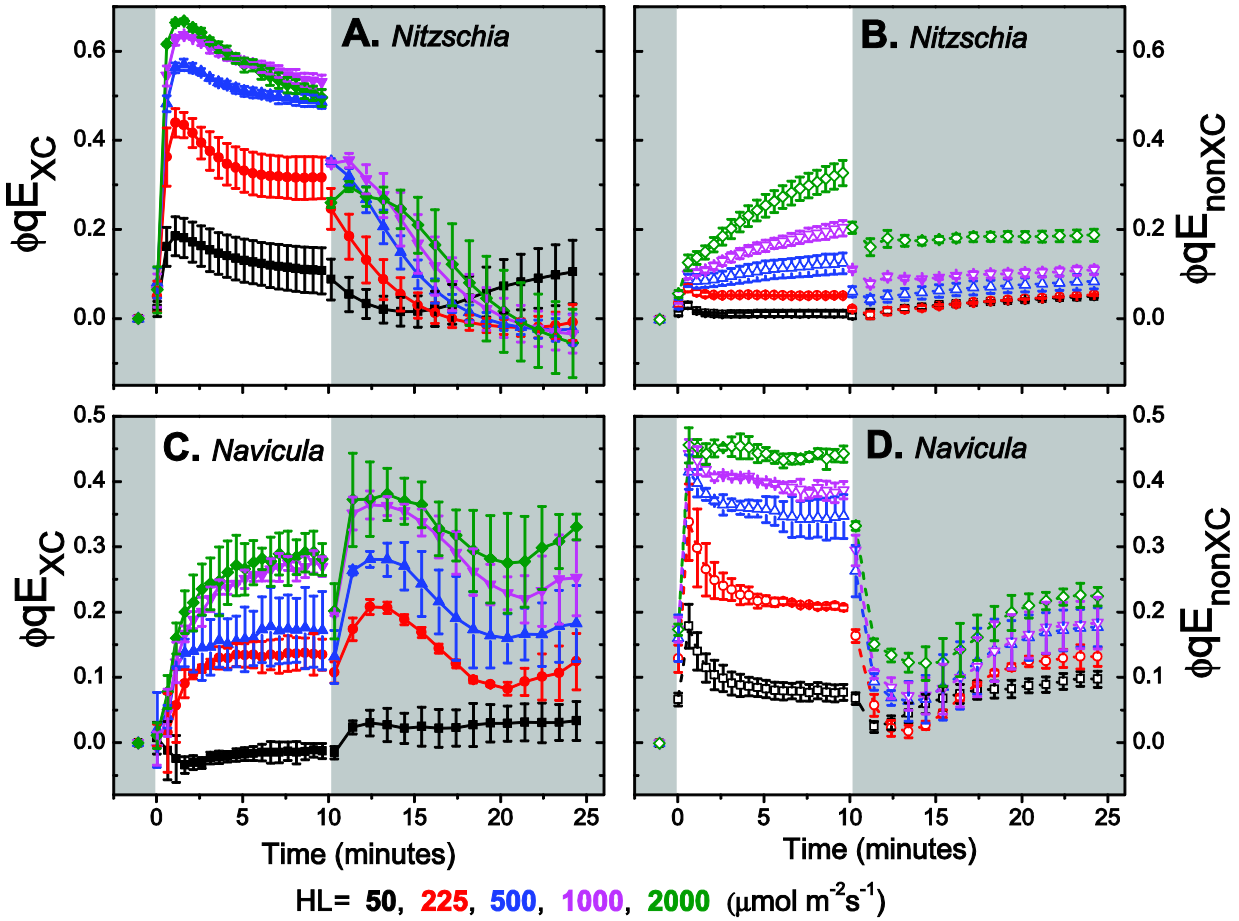

Figure 3.2-18 Quantum yields of NPQ energy dissipation during high light transitions in *Nitzschia* (**A** & **B**) and *Navicula* cells (**C** & **D**). ϕNPQ (quantum yield of regulated non-photochemical energy dissipation) has been separated into DTT-sensitive (qE_{XC}, **A** & **C**) and insensitive (qE_{nonXC}, **C** & **D**) components. ϕqE_{nonXC} = ϕNPQ of cells pre-treated with the DD de-epoxidase inhibitor DTT (2.65 mM for *Navicula*, 5.3 mM for *Nitzschia*). $\phi qE_{XC} = \phi NPQ_{control\ cells} - \phi qE_{nonXC}$. The regions of the plot area with a dark background correspond to dark conditions and the white portion of the background corresponds to the time that HL was applied. Error bars represent ± 1 standard deviation from the mean of 3 separate cultures grown at 50 µmol $m^{-2}s^{-1}$.

In stark contrast to *Nitzschia* cells, the majority of NPQ excitation energy dissipation in *Navicula* can be attributed to qE_{nonXC} (Figures 3.2-18D & 19C). qE_{nonXC} is fast acting, reaching maximal levels of energy dissipation within 30 seconds of HL exposure. Relaxation of qE_{nonXC} excitation energy dissipation during HL is inversely related to HL intensity and always relaxes quickly once HL is removed (Figure 3.2-18D). ϕqE_{XC} has saturation-like kinetics upon transition

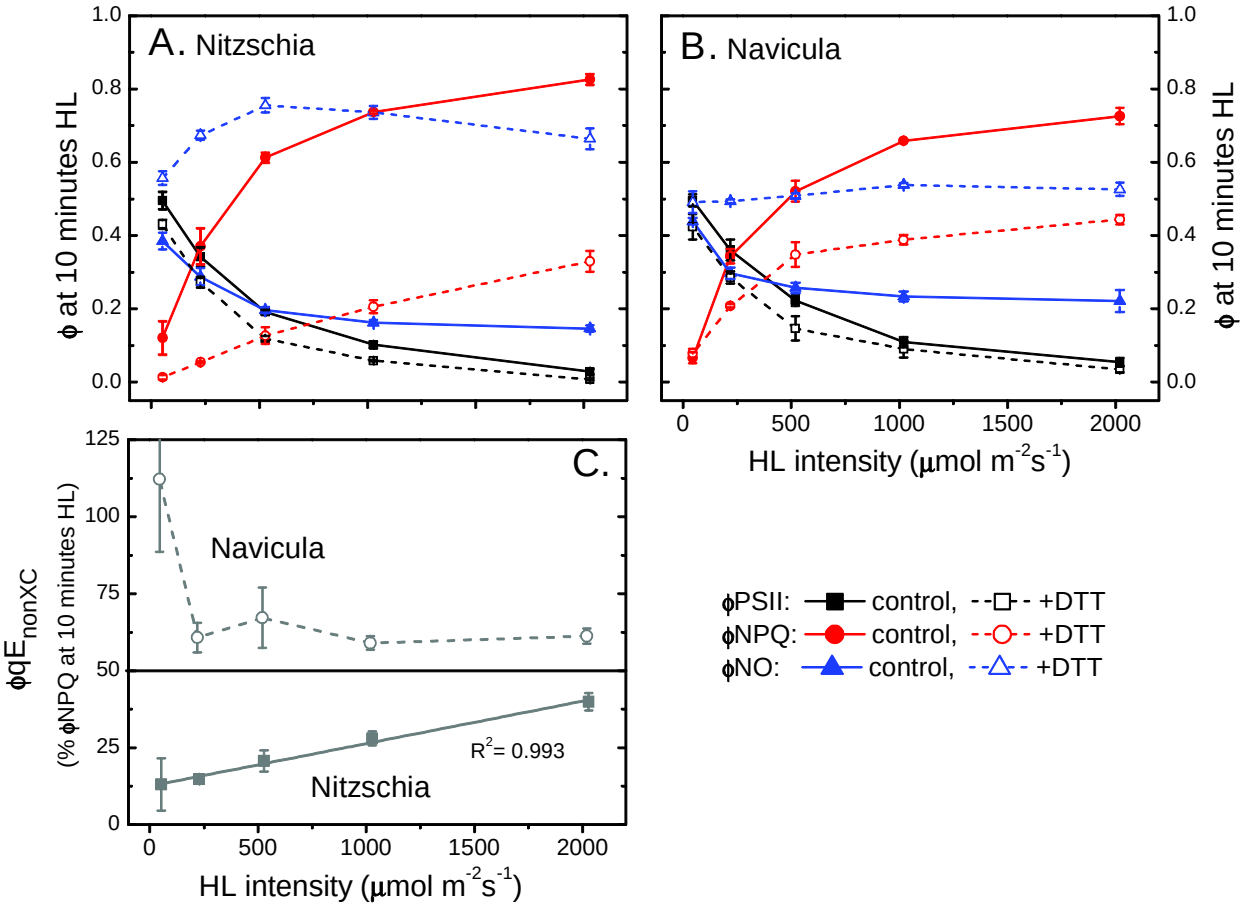

Figure 3.2-19 The dependency of steady state excitation energy conversion and dissipation on illumination intensity. **A** & **B,** quantum yields of excitation energy conversion measured at 10 minutes of high light (HL) illumination in *Nitzschia* and *Navicula* cells, respectively. ϕPSII quantum yield of PSII photochemical energy conversion; ϕNPQ, quantum yield of regulated non-photochemical energy dissipation; ϕNO, quantum yield of non-regulated non-photochemical energy dissipation. Open symbols and dashed lines show yields from cells pre-treated with the DD de-epoxidase inhibitor DTT (2.65 mM for *Navicula*, 5.3 mM for *Nitzschia*). **C**, relative contribution of energy dissipation via qE that is independent of the xanthophyll cycle (ϕqE_{nonXC}) to total energy dissipation via NPQ (ϕNPQ) in *Nitzschia* (closed grey diamond shapes) and *Navicula* (open grey diamond shapes). ϕqE_{nonXC} = ϕNPQ of cells pre-treated with the DD de-epoxidase inhibitor DTT (2.65 mM for *Navicula*, 5.3 mM for *Nitzschia*). The solid grey line in C represents a linear regression of the *Nitzschia* data. See text for further explanation of yields. Error bars represent ± 1 standard deviation from the mean of 3 separate cultures grown at 50 µmol $m^{-2}s^{-1}$.

to HL, which is kinetically suggestive of dependency on an enzyme that has become substrate limited (Figure 3.2-18C). qE_{nonXC} is responsible for all of the excitation energy dissipation provided by NPQ during the transition to light levels for which the cells were previously acclimated (50 µmol $m^{-2}s^{-1}$) and accounts for some 60% of excitation energy dissipation at all

higher irradiances (Figure 3.2-19C). qE_{nonXC} does not quench open reaction centres (Figure 3.2-4D) and so has been assigned to reaction centre quenching within PSII. In congruence with an electron transfer dependent process, energy dissipation via qE_{nonXC} saturates (Figure 3.2-19C). To recap, qE_{nonXC} is the first line of defense for the regulated dissipation of excess excitation energy in *Navicula* cells with augmentation by qE_{XC} at high irradiances.

3.2-9 Excitation energy is regulated at the antenna level in Nitzschia curvilineata

The antenna system in *Nitzschia* is designed to quickly and reversibly switch between light harvesting and excitation energy dissipation modes. *Nitzschia* originates from the shoreline of Long Island Sound, USA. A benthic diatom species living underneath churning water with a high organic and inorganic particulate content would consistently be exposed to high amplitude (dark to full sunlight) and moderately fast periodicity (seconds to minutes) changes in irradiance. Not surprisingly, with the low light conditions that this species was cultured, it had a large σPSII and high accessory pigment to Chl *a* ratio, and, with the same reasoning, was able to perform large amplitude and reversible NPQ during HL transitions. Falkowski and Chen (2003) observed similar trends in σPSII based on the growth light intensity of diatom cultures and Lavaud et al. (2007) found higher NPQ capacities in diatoms from more turbulent natural environments. Having a large light harvesting system is needed to optimize the collection of photons for photosynthesis when the diatom cells are under low irradiances. However, this large basal antenna system loses its functional advantage when irradiance increases to levels that overwhelm photosynthetic electron transfer. The light harvesting apparatus in *Nitzschia* has overcome this conundrum by developing mechanisms that rapidly convert itself to a photon energy dissipating 'parasol' for PSII.

DD cycle dependent quenching (qE_{XC}) has two quenching locations within the FCP antenna (Q1 and Q2). Q1 targets the outer antenna (FCPII) whilst Q2 specifically targets PSII inner antenna complexes (FCPii). DD de-epoxidation in consortium with ΔpH are the *on* trigger for quenching (NPQ in *Nitzschia* is similarly inhibited with DTT and uncoupler treatments; Figure 3.2-4A). A mixed Chl *a*-Chl *a* exciton charge transfer state formed by inter-FCP trimer Chl *a* interactions is the predicted photo-electronic mechanism responsible for the quenching (NPQ is accompanied by changes in Chl *a* Q_y absorption and far-red emission that can be attributed to the formation of Chl *a*-Chl *a* quenching dimers, Figures 3.2-10C & 11C). Removal of polar DD molecules during HL is predicted to facilitate the formation of quenching conducive protein-protein interactions between FCP complexes (i.e. the formation of FCP quenching aggregates). Q1 quenching is hypothesized to involve a large scale aggregation of FCPII into multimeric FCP quenching aggregates causing a physical detachment of FCPII from PSII. Q2 quenching is hypothesized to originate from formation of FCPii quenching aggregates that remain attached to PSII. Protonation events may also be able to directly regulate quenching, in a manner equivalent to the pH induced self-quenching observed in isolated FCP complexes by Gundermann and Büchel (2012). This may explain the partial relaxation of NPQ that occurred during low to moderate HL illuminations in *Nitzschia* (Figures 3.2-2A, 3.2-18C). (The concept of ΔpH fine tuning of NPQ is elaborated upon in *Section 3.5*). Relaxation of NPQ post HL involves a reversal of the HL induced changes to the thylakoid. DT epoxidation post HL would facilitate dispersal of the FCP quenching aggregates by reintroducing polar DD molecules into the inter-FCP trimer interfaces.

The regulated dissipation of excitation energy during high irradiance in *Nitzschia* is primarily dependent on qE_{XC}. Removal of qE_{XC} by a pre-treatment with DTT eliminates the vast majority of excitation energy dissipation that can be attributed to an active regulated response by the photosynthetic machinery. In the absence of qE_{XC}, ϕNO (primarily as heat and fluorescence from PSII cores) replaces ϕNPQ as the predominant pathway for the removal of excitation energy (Figure 3.2-19A).

There are certain costs associated with relying on a robust qE_{XC} mechanism for excitation energy regulation. There needs to be an adequate population of quenching-susceptive FCP complexes, DD de-epoxidase, and DT epoxidase. A considerable pool of ascorbate needs to be pre-existing to allow DD de-epoxidation during the transition to HL. The author is unaware of any studies specifically investigating the role of ascorbate regenerating pathways during diatom NPQ, such as ascorbate-glutathione or 'Foyer-Halliwell-Asada' type pathways (Foyer and Noctor 2011). However, the dependency of NPQ on ascorbate is less in diatoms than in plants due to DD de-epoxidase having a greater affinity for ascorbate (Grouneva et al. 2006). For DT epoxidation after NPQ there must be an available supply of NADPH. These infrastructural requirements for qE_{XC} have a lower net metabolic cost if light is the controlling factor to cell growth and not nutrient availability. It would be most interesting to see if NPQ capacity is decreased in *Nitzschia* cells cultured in a nutrient deplete media. $\mathcal{NPQ}$ amplitude does seem to lessen as *Nitzschia* cultures age and assumingly deplete their growth media of nutrients (*Figure 3.1-10D*).

3.2-10 Sustained and 'passive' regulation of excitation energy is important in Navicula sp.

Navicula sp. was isolated from the soil surface within the Great Salt Plains salt flat located in Oklahoma, USA (Potter et al. 2006, Kirkwood and Henley 2006). Diatoms living in the soil of a barren landscape would be prone to fewer and less consistent high amplitude changes in light field as compared to diatoms in a shoreline habitat. As with land plants, they would still be susceptible to fast transitions in irradiance caused by cloud movements. The consequences of developing a light harvesting system within a comparatively stable and high irradiance light environ are manifested in *Navicula* as a small σPSII, fewer accessory pigments per Chl *a*, and lower $\mathcal{NPQ}$ capacity. The smaller and less diverse antenna system may be energetically favorable in a full sun environment; however, the reduced FCP population limits the potential number of antenna based quenching sites when there is a need to perform NPQ.

Navicula seems to rely heavily on a qE_{nonXC} that is independent of DD de-epoxidation. This qE_{nonXC} is dependent on ΔpH (Figure 3.2-4A) and behaves as a regulated form of excitation energy dissipation (Figure 3.2-18D), so it is truly a qE quenching component. It induces and relaxes faster than qE_{XC} both during and after HL (Figure 3.2-18C & D). qE_{nonXC} is responsible for all the regulated dissipation of excitation energy at the lowest irradiance measured (Figure 3.2-19C) and is important during the initial transition to all HL irradiances (Figure 3.2-18D). qE_{nonXC} does not quench open PSII reaction centres and thus has been placed within the PSII reaction centre (Figure 3.2-4D). The mechanism of qE_{nonXC} is hypothesized to be via heat production from charge recombination between $P680^+$ and the acceptor side of PSII. Further evidence for electron transfer dependent reaction centre quenching was seen in the 77K samples; it was noticed that the fluorescence yield from *Navicula* cells increased more upon freezing at 77K as compared to *Nitzschia* cells (observations not quantitated). A similar fast induced, DTT-

insensitive NPQ component with a ΔpH requirement was observed in the centric diatom *Cyclotella meneghiniana* (Grouneva et al. 2008); the authors suggested a xanthophyll cycle-independent, reaction centre based mechanism for their observations but gave no further details. A PSII reaction centre type of NPQ has also been reported in *Phaeodactylum tricornutum* (Eisenstadt et al. 2008).

Antenna centred quenching provides a locked-in enhancement to reaction centre quenching. qE_{XC} is much more slowly induced upon the transition to HL, maxes out at moderate HL intensities, and relaxes much more slowly after HL ends (Figure 3.2-18C vs. D). The source of qE_{XC} is believed to be from the formation of Chl *a*- Chl *a* quencher pairs during the DD de-epoxidation and ΔpH mediated aggregation of FCP complexes (in a manner similar to, but distinct of what was observed in *Nitzschia* cells). qE_{XC} provides a stable, longer term NPQ, which relaxes very weakly after HL ends. Thus, antenna centred quenching may have long-term photoprotective implications in *Navicula* cells.

The locked-in NPQ induced with qE_{XC} has important physiological implications in *Navicula*. In its salt flat habitat, this species is understood to only actively grow when intermittent rain events reduce salinity to optimal levels (Kirkwood and Henley 2006). Since cells are still viable in hypersaline conditions (Kirkwood and Henley 2006), their photosynthetic apparatus must enter a long-term photoprotective excitation energy dissipative state during salt stress. Many other photosynthetic organisms that encounter long-term environmental conditions unconducive to cellular metabolism are able to keep their light harvesting systems in a permanent quenched state until conditions become more favorable. Well characterised

examples include dehydrated lichens (e.g. Slavov et al. 2013) and overwintering evergreens (e.g. Öquist and Huner 2003). In both of these examples, the short-term dynamic xanthophyll cycle dependent antenna centred quenching is transformed into a long-term sustained quenching. It is unknown if the NPQ mechanism characterised for *Navicula* in this current communication is involved in long-term photoprotective quenching during hypersaline stress conditions. Nevertheless, it seems that photosynthesizers prone to long-term stress conditions, despite from being from very different phylogenies, are all able to maintain a mechanistic similar approach to long-term photoprotective quenching. These quenching processes are likely deeply rooted in the evolutionary origins of light harvesting systems.

In conclusion, qE_{XC} provides an enhancement and stabilising role in excitation energy dissipation to supplement PSII reaction centre based qE_{nonXC} in *Navicula*. Overall, NPQ is less reliant on qE_{XC} in this species. NPQ can, in fact, fulfill its role of dissipating excitation pressure fully independently of DD de-epoxidase activity (Figure 3.2-4C). Thus, qE in *Navicula* can be a largely passive phenomenon that does not require the metabolic investments associated with large scale DD cycling.

3.2-11 Limitations in the use of artificial light transitions

The HL transitions used to measure the NPQ response within this communication do not truly represent the types of light transitions that these diatoms would experience within their natural environments. During the HL transition experiments, cells were instantaneously transferred from dark conditions to excess light conditions and vice versa from excess light conditions to dark conditions; whereas in natural environments, the transition would typically be more gradually taking at least several seconds and dark conditions would often be replaced

by "low light" conditions. The 10 minute HL illumination period was also arbitrarily chosen so that steady state NPQ could be measured. A simple dark-to-HL-to-dark light regime was used because (i) it was the most practical approach using the experimental apparatus in the laboratory and (ii) was predicted to induce the most dramatic physiological response and the most robust signal for measurement. Thus, the conclusions drawn from the laboratory experiments using an artificial light regime have to be extrapolated carefully when predicting what occurs under natural light environments. The exact rates of $\mathcal{NPQ}$ induction/relaxation and the magnitudes of $\mathcal{NPQ}$ described here may not truly represent what would be observed in response to a natural HL transition; however, the relative comparison of $\mathcal{NPQ}$ kinetics/amplitudes between HL intensities and between species is appropriate for elucidating the underlying molecular mechanisms of the NPQ response.

3.2-12 Conclusion

Nitzschia curvilineata and *Navicula sp.* stem from very different natural habitats, and expectedly, have different strategies for the dissipation of excess excitation energy. *Nitzschia* has a large, flexible antenna system regulated by the DD cycle that can quickly switch back and forth between light harvesting and excitation energy dissipative modes in response to all illumination intensities. This schema for excitation energy regulation is well adapted to the highly fluctuating shoreline light environment of this specie's origin. In contrast, *Navicula* cells have a smaller antenna system, relying more on non-photochemical quenching within the PSII reaction centre. This species can handle low magnitude changes in irradiance quickly and highly effectively, seemingly without any input of DD cycling. However, transitions to higher irradiances induce a DD cycle dependent quenching that remains locked-in. The relatively

stable, high irradiance light field of the salt flat soil surface, from which *Navicula* originates, would not necessitate a high amplitude and repetitive photo-acclamatory response to light intensity. The propensity of performing long-term quenching; however, would be most beneficial to this species during the prolonged periods that cell growth is inhibited during hypersaline soil conditions. Therefore, the light environment under which a diatom species developed can predictably depict the species' strategies for dissipating excess excitation pressure.

3.3 Photosynthetic Electron Flux during NPQ

3.3-1 Overview

Diatoms are very successful at maintaining high conversion efficiencies of photons into biomass under fluctuating light conditions (Mitrovic et al. 2003, Petersen et al. 1998, Wagner et al. 2006). Their success under such conditions indicates that they have a very flexible photosynthetic apparatus that can efficiently balance absorbed light energy with electron transport. Excitation pressure is a measurement of the balance between PSII excitation with light energy and the photochemical conversion of this energy into unbound electrons for photosynthetic electron transport; high excitation pressure means that PSII is receiving more light energy than it can process photochemically. Prolonged high excitation pressure can lead to oxidative damage of PSII. For excitation equilibrium to be maintained in an environment with variable light intensities that occur in short time scales, PSII excitation (the source side of excitation pressure) needs to be balanced with electron transport (the usage and storage of reducing equivalents – the sink side of excitation pressure) by methods that are dynamic on the same time scale as the light conditions. This would exclude large restructuring of the photosynthetic machinery through protein expression during fast (seconds to a few minutes) light transitions. Diatoms are able to dissipate source side excitation pressure by robustly dissipating excitation energy using the process of NPQ. However, diatoms seem to also be able to regulate excitation pressure at the sink side by increasing electron flux through the use of alternative electron transfer pathways. In addition to the electrons used for CO_2 and nitrite reduction within the chloroplast, there are also several alternate electron transfer pathways

available to diatoms: PSII cyclic electron transfer (PSII CET), PSI cyclic electron transport (PSI CET), the water-water cycle (Mehler reaction), and chlororespiration.

As discussed in the preceding chapter (*Section 3.2*), the two pennate diatoms *Nitzschia curvilineata* and *Navicula sp.* have potent and dynamic NPQ mechanisms for the relieve of excitation pressure at the source side. The purpose of this chapter is to search for alternate electron transfer pathways and to determine the relative importance of electron flux towards the regulation of excitation pressure at the sink side in these two species. The response of electron transport to high light transitions and electron sink capacity was measured at PSII using the method of saturating light pulse induced fluorescence. The interaction of alternate electron transport pathways with NPQ was probed through the use of chemical agents that influence electron transport downstream of the PSII photochemical reactions. The results showed that *Navicula* cells are more responsive to changes in sink capacity for photochemically derived electrons. Intra PSII electron transfer was also quite unaffected during HL in *Navicula*, even when xanthophyll cycle dependent NPQ (qE_{XC}) was inhibited. Alternate electron transfer pathways actively contributed to photosynthetic electron flux in both species. *Nitzschia* was able to employ PSI cyclic electron transport to induce large amounts of qE. NPQ relaxation after illumination seemed to be more limited by NADPH availability in *Navicula*. Chlororespiration was variably active in both species during dark periods that follow illumination. These observations (in combination with the NPQ results from *Section 3.2*) advocate that *Nitzschia* cells depend on a source side approach for regulating excitation pressure, whereas *Navicula* cells additionally regulate excitation pressure at the sink side.

3.3-2 Sink side excitation pressure

The dependency of excitation pressure and ensuing NPQ on linear photosynthetic electron sink capacity was examined. Even though diatoms contain form 1D Rubisco, the most CO_2 over O_2 specific form, they have been shown to actively engage in carbon concentrating mechanisms by importing bicarbonate ion (as reviewed by Giordano et al. 2005). Elevating exogenous HCO_3^- concentrations could therefore increase the electron sink capacity for photochemistry derived electrons, thereby lowering excitation pressure during a transition to HL. *Navicula* cells reacted positively to exogenous bicarbonate treatment by lowering excitation pressure and reducing the NPQ response to HL (Figures 3.3-1B & 3B). Bicarbonate titration had the strongest effect on the early stages of NPQ in *Navicula*, with strong negative linear correlations between bicarbonate concentration and $\mathcal{NPQ}$ (Pearson's r= -0.975 and -0.982 for $\mathcal{NPQ}$ initial rate at 30 seconds HL and $\mathcal{NPQ}$ amplitude at 2 minutes, respectively). During the later stages of HL illumination, the beneficial effects of exogenous bicarbonate seem to lessen, likely as a consequence of the accumulation of electrons produced by the fast photochemical events surpassing the slow enzymatic processes of bicarbonate import and/ or the Calvin-Benson cycle. Bicarbonate had a much weaker and opposite effect in *Nitzschia* cells, where bicarbonate could actually increase $\mathcal{NPQ}$ (Figures 3.3-1A & 3A).

Methyl viologen (MV) is an autooxidising artificial electron acceptor that targets PSI *in vivo* diverting electrons from $NADP^+$ (Fujii et al. 1990). In the presence of MV, photosynthetic linear electron transport would thus be limited by the processing rate of the mobile inter-photosystem electron carriers and not by terminal electron sink strength downstream of PSI. MV pre-treatment in *Nitzschia* cells had no significant effect on ΦPSII (measured with far red

pre-illumination; data not shown), ϕPSII (both during HL and post HL; data not shown), excitation pressure (Figure 3.3-2A), *NPQ* initial rate of induction (data not shown), and only slightly increased *NPQ* amplitude (Figure 3.3-2A). MV also did not change the amount of *NPQ* that could relax post HL (Figure 3.3-2A). Increasing MV to a final concentration of 1.2 mM did not noticeably change the effect of MV in *Nitzschia* cells (data not shown).

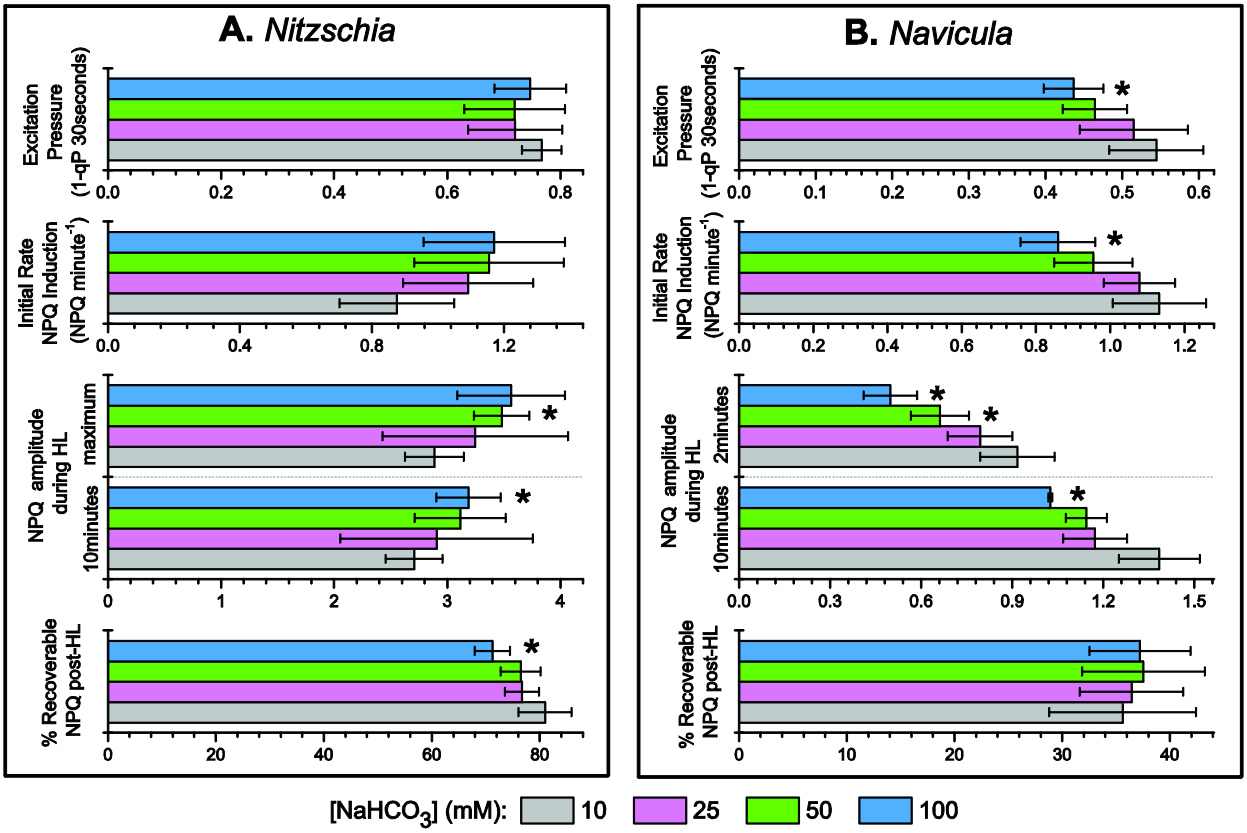

Figure 3.3-1. **Summary for the response of cells to exogenous bicarbonate during a high light transition** in **A**, *Nitzschia* and **B**, *Navicula*. Dark adapted cells were pretreated with $NaHCO_3$ supplemented growth media (buffered in 150 mM Tricine/NaOH/KOH pH 8.2 with NaCl added to maintain equal molar Na^+ between all HCO_3 concentrations) for 5 minutes in the dark prior to a 10 minute illumination with 500 µmol $m^{-2}s^{-1}$ high light (HL) followed by 15 minutes in the dark (post HL). The quantification of four parameters are presented: (i) excitation pressure (1-qP) after 30 seconds of HL, (ii) the initial rate of *NPQ* induction (from 2 seconds to 30 seconds after the onset of HL), (iii) *NPQ* values reached during HL treatment (maximum *NPQ* attained for *Nitzschia*, *NPQ* at 2 minutes for *Navicula*, and *NPQ* after 10 minutes for both species), and (iv) the amount of *NPQ* recovered during the post HL period; presented as % of *NPQ* at 10 minutes HL = 100 • [(*NPQ* at 10minutes HL) - (minimum *NPQ* during post HL)] / (*NPQ* at 10minutes HL). Error bars represent ± 1 standard deviation from the mean of 3 separate cultures grown at 50 µmol $m^{-2}s^{-1}$. *, represents a significant difference from the 10mM $NaHCO_3$ samples at the 95% confidence level as measured with a two-sample t-test.

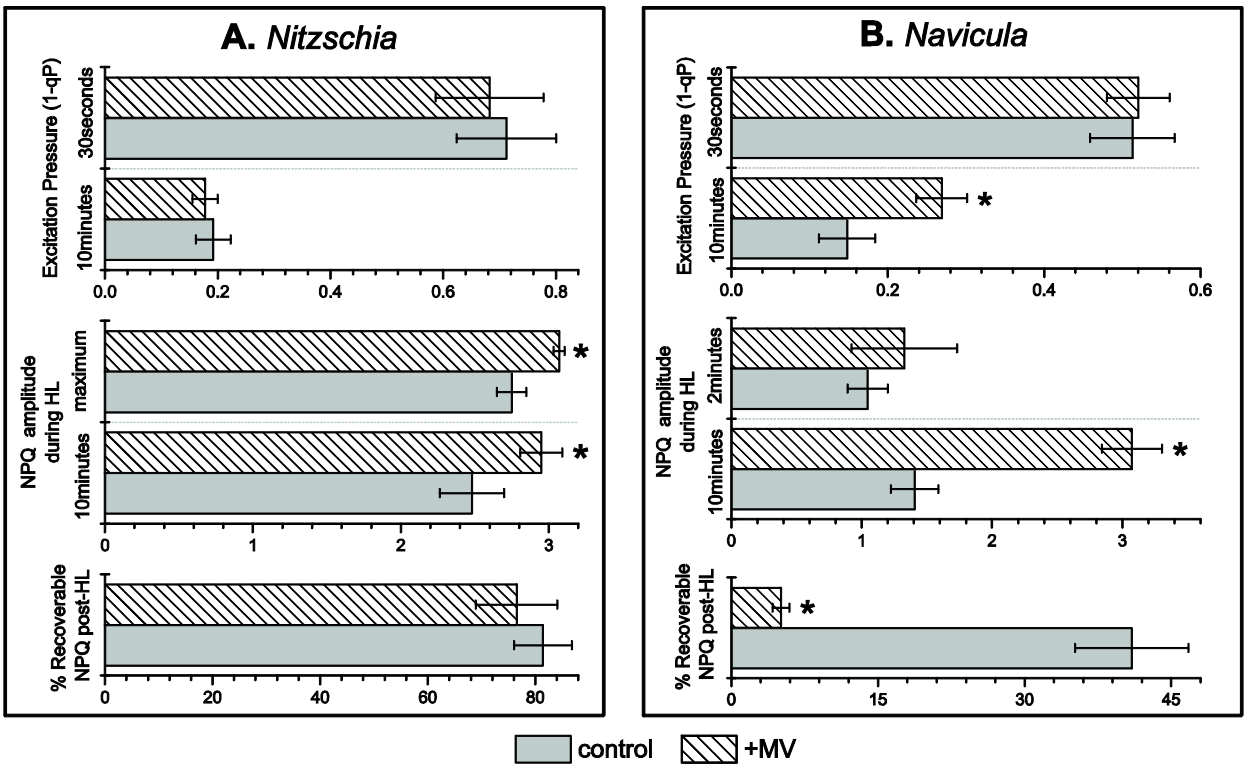

Figure 3.3-2 Summary for the response of cells to the artificial electron acceptor methyl viologen during a high light transition in **A**, *Nitzschia* and **B**, *Navicula*. Dark adapted cells were pretreated with 600 µM methyl viologen (MV) doped growth media for 5 minutes in the dark prior to a 10 minute illumination with 500 µmol $m^{-2}s^{-1}$ high light (HL) followed by 15 minutes in the dark (post HL). The quantification of three parameters are presented: (i) excitation pressure (1-qP) after 30 seconds of HL and after 10 minutes of HL, (ii) $\mathcal{NPQ}$ values reached during HL treatment (maximum $\mathcal{NPQ}$ attained for *Nitzschia*, $\mathcal{NPQ}$ at 2 minutes for *Navicula*, and $\mathcal{NPQ}$ after 10 minutes for both species), and (iii) the amount of $\mathcal{NPQ}$ recovered during the post HL period; presented as % of $\mathcal{NPQ}$ at 10 minutes HL = 100 • [($\mathcal{NPQ}$ at 10minutes HL) - (minimum $\mathcal{NPQ}$ during post HL)] / ($\mathcal{NPQ}$ at 10minutes HL). Error bars represent ± 1 standard deviation from the mean of 3 separate cultures grown at 50 µmol $m^{-2}s^{-1}$. *, represents a significant difference from the control samples at the 95% confidence level as measured with a two-sample t-test.

In *Navicula* cells the consequence of MV pre-treatment was much more substantial. MV greatly lowered PSII quantum efficiencies (Table 3.3-1). Since the MV pre-treatment lowered ΦPSII by increasing Fo_{dark} and not by changing Fm_{dark} (data not shown), MV-sensitive alternate electron flow seems to be active in *Navicula* cells during dark adaptation resulting in reduction of the PQ pool redox state. MV greatly enhanced $\mathcal{NPQ}$ amplitude after 10 minutes of HL (Figures 3.3-2B & 3D). These higher $\mathcal{NPQ}$ values were obtained not by increasing the initial rate

of $\mathcal{NPQ}$ induction, but by sustaining $\mathcal{NPQ}$ induction at a high constant rate throughout the remainder of the HL illumination period (see Figure 3.3-3D). MV treatment had no significant effect on initial excitation pressure but did increase excitation pressure after 10 minutes of HL exposure (Figure 3.3-2B). Relaxation of $\mathcal{NPQ}$ after HL treatment was largely inhibited by MV in *Navicula* (Figures 3.3-2B & 3D). The enhancement of NPQ by MV pre-treatment could be brought about by the action of two different mechanisms. The first mechanism being an accumulation of photoinhibited PSII during the HL treatment resulting in qI, which (in accordance with Figure 3.3-3D) would relax very slowly post HL. The second possible mechanism being that MV enhanced NPQ by augmenting the buildup of ΔpH, and consequently qE, by reducing ATP synthase activity. The effects of MV on NPQ in *Navicula* are somewhat similar to those observed with the ATP synthase inhibitor DCCD (but with less magnitude). ADP is regenerated during the reduction and regeneration phases of the Calvin-Benson cycle. Because MV accepts electrons at the expense of $NADP^+$, the Calvin-Benson cycle would be held up at the reduction phase due to a lack of available NADPH. According to the kinetics in Figure 3.3-3D, MV treatment seems to have a weak effect on the fast inducing NPQ that was attributed to qE_{nonXC} (see *Section 3.2*) and a much stronger effect on the slower inducing NPQ attributed to qE_{XC} (see *Section 3.2*), in such supporting ΔpH augmented enhancement of NPQ by MV. If MV enhancement of NPQ is dominated by the ΔpH augmentation scenario then the MV treatment results could suggest that the ATP and/ or NADPH pool is somewhat smaller in *Navicula*.

To summarise, *Navicula* cells are more responsive to enhancing linear photosynthetic electron sink capacity than *Nitzschia* cells. The effect of MV is more substantial and the effect

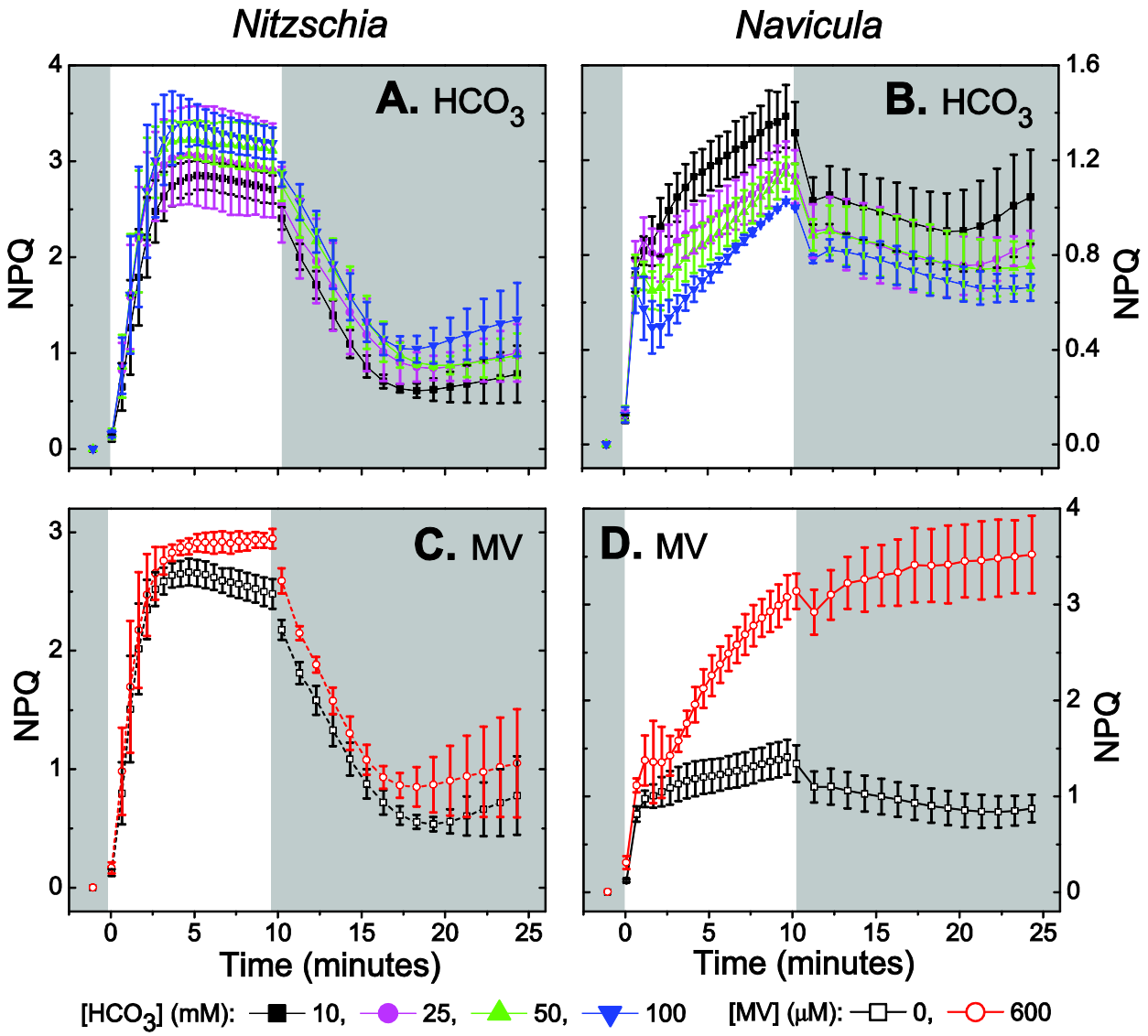

Figure 3.3-3 The effect of exogenously applied electron acceptors on NPQ transients from *Nitzschia* (**A** & **C**) and *Navicula* (**B** & **D**) cells. **A** & **B**, $\mathcal{NPQ}$ transients from dark adapted cells following a 5 minute HCO_3 treatment ($NaHCO_3$ supplemented growth media buffered in 150 mM Tricine/NaOH/KOH pH 8.2 with NaCl added to maintain equal molar Na^+ between all HCO_3 concentrations) in the dark. **C** & **D**, $\mathcal{NPQ}$ transients from dark adapted cells following a 5 minute methyl viologen treatment (MV) (600 µM) in the dark. The regions of the plot area with a dark background correspond to dark conditions and the white portion of the background corresponds to the time frame that 500 µmol $m^{-2}s^{-1}$ high light was applied. Error bars represent ± 1 standard deviation from the mean of 3 separate cultures grown at 50 µmol $m^{-2}s^{-1}$.

of exogenous bicarbonate is more intense and opposite of that observed in *Nitzschia*. *Nitzschia* cells however did respond to a reduction of photosynthetic electron sink capacity through cold stress (2°C) by increasing excitation pressure and more than doubling $\mathcal{NPQ}$ amplitude during HL

(*Figure 3.5-8*); cold stress slows the rate of the photosynthetic carbon fixation reactions while having little effect on the rate of the photochemical reactions (Huner et al. 1998).

Table 3.3-1 The artificial electron acceptor methyl viologen (MV) reduces PSII quantum efficiency in *Navicula* cells. Dark adapted cells were treated with 600 µM MV for 5 minutes in the dark prior to exposure to a high light (HL) (500 µmol $m^{-2}s^{-1}$) transition. ΦPSII, maximal quantum efficiency of PSII photochemistry measured prior to HL (with far red pre-illumination); $\phi PSII_{HL}$, quantum efficiency of PSII photochemistry measured at 10 minutes HL; $\phi PSII_{postHL}$, quantum efficiency of PSII photochemistry measured 15 minutes in the dark after the 10 minute HL treatment. Standard deviations are given beside the mean from 3 separate cultures grown at 50 µmol $m^{-2}s^{-1}$.

Treatment	ΦPSII	$\phi PSII_{HL}$	$\phi PSII_{postHL}$
control	0.572 ±0.021	0.308 ±0.016	0.453 ±0.012
+MV	0.227 ±0.024	0.160 ±0.016	0.084 ±0.012

3.3-3 PSII electron transport during high light transitions

Electron transport within and out of PSII was elucidated from fluorescence rise (OJIP) transients induced with the application of a 5,000 µmol m^{-2} s^{-1} saturating multiturnover light pulse (i.e. the Kautsky effect) (Strasser et al. 2004). It takes more time during the application of a light pulse to reach maximal fluorescence in *Navicula* cells than in *Nitzschia* cells (Figure 3.3-5A & B). This could be due to a slower rate of PSII forward electron transport in *Navicula* caused by *Navicula*'s smaller σPSII (*Table 3.2-1*) and/ or by a faster rate of forward electron transport out of the Q_B site in *Navicula*. The latter would suggest that the sink capacity (or processing rate) for photochemically derived electrons is larger (faster) in *Navicula* cells. Maximal fluorescence (Fm) was reached with the saturating light pulse in *Navicula*; increasing light pulse width did not increase fluorescence levels (data not shown). Pulse width was kept brief (300 milliseconds) to minimise the probing effects of the saturating light pulse on the photosynthetic system and to prevent any quenching from being induced directly by the pulse. OJIP transients collected during HL transitions were used to calculate the fluorescence

parameter V_J. 1-V_J describes the fraction of PSII reaction centres in which Q_A was already re-oxidized after a single turnover event, and therefore can be used to quantitate forward electron transport per trapped photon out of the Q_A site (Strasser et al. 2004, Stirbet and Govindjee 2011). Thus, 1-V_J describes intra PSII electron transfer; a higher 1-V_J indicates a higher rate of intra PSII electron transport. Figure 3.3-4 shows 1-V_J and parallel PSII effective quantum yield (ϕPSII) values during a dark-to-HL-to-dark transition; 1-V_J and ϕPSII values achieved with pre-treatment with the DD de-epoxidase inhibitor DTT are also included so as to determine what effect removal of qE_{XC} has on PSII electron transport. In *Nitzschia*, 1-V_J drops upon HL illumination and remains at relatively the same level during the rest of HL and post HL. However, with DTT 1-V_J slowly climbs during illumination until it reaches equivalence to pre HL

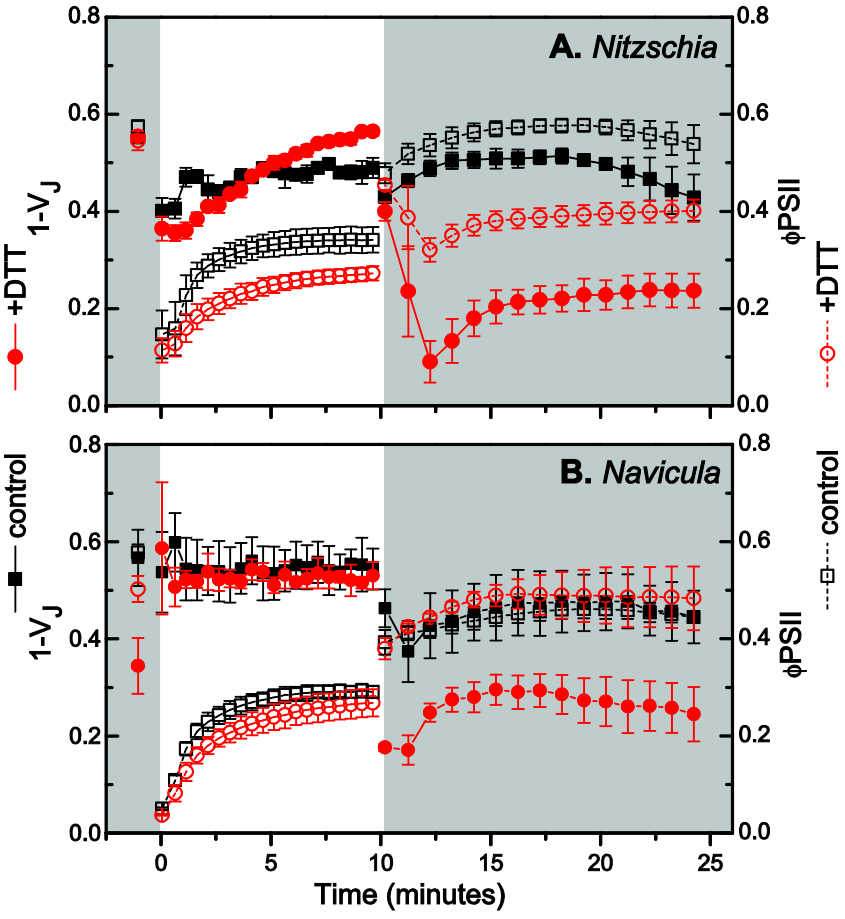

Figure 3.3-4 PSII electron transport during a high light transition. Transients of 1-V_J (solid lines with filled symbol shapes) and quantum efficiency of PSII photochemistry (ϕPSII= (Fm'-Ft) / Fm'; dashed lines with open symbol shapes) from *Nitzschia* (**A**) and *Navicula* (**B**) cells without and with pre-treatment with the DD de-epoxidase inhibitor DTT (5.3 mM for *Nitzschia*, 2.65 mM for *Navicula*). The regions of the plot area with a dark background correspond to dark conditions and the white portion of the background corresponds to the time that 220 µmol $m^{-2}s^{-1}$ high light was applied. Error bars represent ± 1 standard deviation from the mean of 3 separate cultures grown at 50 µmol $m^{-2}s^{-1}$.

levels but then drops severely once HL is removed (Figures 3.3-4A & 5C). In *Navicula*, 1-V_J does not change from pre HL levels during HL illumination, but does drop post HL (Figure 3.3-4B). Even though DTT reduces electron transport in dark adapted *Navicula* cells, during HL electron transport is essentially the same as in control cells; post HL DTT lowers 1-V_J but has no effect on ϕPSII (Figure 3.3-4B). The electron transport data in Figures 3.3-4 & 5 was collected during NPQ induction with a low HL intensity (220 µmol $m^{-2}s^{-1}$), so that no saturation effects on NPQ or excitation pressure would occur. To summarise, intra PSII electron transport (measured with 1-V_J) in *Navicula* is maintained at pre illumination levels during HL, whereas it drops in *Nitzschia*. Also, overall PSII electron transport (measured with both 1-V_J and ϕPSII) during HL is less perturbed by DTT pre-treatment in *Navicula*. These results are consistent with *Navicula* having a higher innate capacity for forward photosynthetic electron flow that is less dependent on qE_{XC} for reaching photostasis.

Is PSII CET important in these two diatom species? In both species when qE_{XC} is inhibited, Q_A (as measured by 1-V_J) is able to remain oxidised (open) even as the Q_B site (as measured by ϕPSII) is kept in a highly reduced state (closed) during HL irradiance (Figures 3.3-4 & 5). These observations point towards a mechanism for maintaining high forward electron transport within PSII that is independent of excitation pressure regulation via qE_{XC}. Note the species, treatment, and HL differences in the OJIP traces corresponding to the 'J' to 'I' (2 to 30 milliseconds) and 'I' to 'P' (30 to 300 milliseconds) transitions (Figure 3.3-5) that arise from intermediate reduction states of Q_B populations formed during two event electron transfer from Q_A to Q_B (Strasser et al. 2004). If competitive, non-linear electron transfer pathways are contributing to electron flux within PSII and differentially contributing to the reduction state of

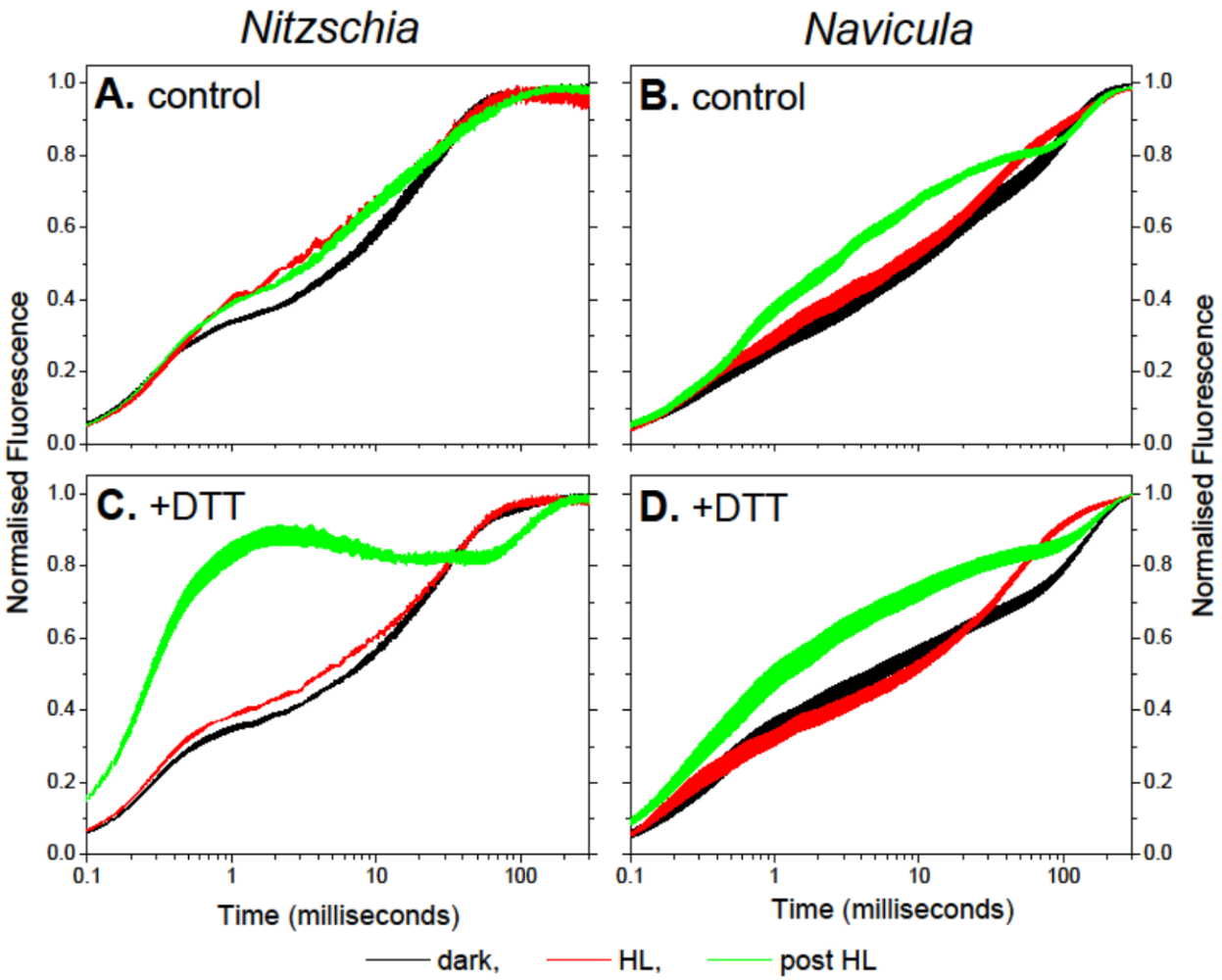

Figure 3.3-5 OJIP transients collected during a high light transition. Fluorescence rise traces from *Nitzschia* (**A** & **C**) and *Navicula* (**B** & **D**) cells before (dark), at 10 minutes of (HL), and in the dark upon cessation of (post HL; 2 minutes for *Nitzschia* and 1 minute for *Navicula*) 220 µmol $m^{-2}s^{-1}$ high light illumination without (**A** & **C**) and with (**C** & **D**) pre-treatment with the DD de-epoxidase inhibitor DTT (5.3 mM for *Nitzschia*, 2.65 mM for *Navicula*). Time zero on the x-axis corresponds to the start of the saturating light pulse. The transients have been double normalised by setting the fluorescence level at 'O' to 0 and the fluorescence level at 'P' to 1. The thickness of the trace lines represent ±1 standard deviation from the mean of 3 separate cultures grown at 50 µmol $m^{-2}s^{-1}$.

Q_B, there would likely be changes in the JIP region of the Kautsky fluorescence transients. PSII CET has been proposed as a mechanism for diatoms to rapidly regulate photosynthetic electron flux without having to change light harvesting function, and is postulated to (at least partially) divert electrons from Q_B via cytochrome b559 for the re-reduction of $P680^+$ (Lavaud et al. 2002b, Onno Feikema et al. 2006, Lavaud et al. 2007). The OJIP transients (Figure 3.3-5B & D)

and 1-V_J values (Figure 3.3-4B) in *Navicula* indicate high rates of electron transport within PSII reaction centres even under conditions where the PQ pool is expected to become rapidly over reduced, such as during the first few seconds of HL or when qE_{XC} is inhibited with DTT. Such a high rate of electron transport away from Q_A can conceptually be explained by PSII CET activity. Even though there was no direct measurement of PSII CET in this study via a comparative analysis of PSII fluorescence to rates of O_2 evolution (single-turnover flash number dependence of oxygen production; see Lavaud et al. 2002b), PSII CET best describes the stabilization/ enhancement of intra PSII electron transport within the context of available diatom photosynthetic electron transport schemas. In the higher plant system the PSII CET pathway can provide a very effective quencher for chlorophyll fluorescence. Chl *z*, a redox active chlorophyll a molecule serving as an intermediate for electron transfer from cytochrome b559 to P680, forms a strong quencher when oxidised (Chl $z^{\bullet+}$) (Schweitzer and Brudvig 1997). The mechanism for the potent reaction centred based qE_{nonXC} described for *Navicula* in *Section 3.2* would be the above described 'PSII CET'. The role of Chl *z* as a quencher in *Navicula* cannot be determined with the presented experimental approach.

3.3-4 NPQ as a sensitive in vivo *probe for redox and protonation status*

The NPQ response was titrated with HL intensity after pre-treatment with a selection of chemical inhibitors to elucidate the contribution of electron transport to NPQ induction and recovery in *Nitzschia* (Figure 3.3-6) and *Navicula* (Figure 3.3-7) cells. $\mathcal{NPQ}$ values achieved at steady state illumination conditions are summarised in Figures 3.3-6F and 7F. Ammonium chloride pre-treatment is included as a negative control for qE; all NPQ dependent on energization of the thylakoid should be inhibited with NH_4Cl. DTT pre-treatment is included as

a negative control for qE_{XC}. The effects of DTT on PSII electron transport during HL transitions have already been discussed in Section 3.3-3. DCCD pre-treatment serves two purposes: the primary being to maximise the buildup of ΔpH, the second to interfere with NADPH-ATP cycling through the Calvin-Benson cycle. DCCD pre-treatment at high irradiances should pump the NPQ response to its maximal capacity. DCMU irreversibly binds to the PQ binding pocket, preventing forward electron transport out of PSII. DCMU pre-treatment can thus be used to prevent photosynthetic linear electron transport and subsequent ΔpH generation at PSII (there is no longer transfer of H^+ from the lumen during the reduction of PQ to PQH_2 and proton production by the oxygen evolving complex is inhibited). If linear electron transport is the sole source of ΔpH generation, then DCMU will inhibit qE development. If NPQ does develop during illumination this would have to be due to non-linear electron transport dependent trans-thylakoid proton pumping. Since PSII CET does not contribute to ΔpH generation, PSI CET would have to be the source of ΔpH generation in the presence of DCMU. The amount of $\mathcal{NPQ}$ induced with DCMU pre-treatment would thus be an indicator for PSI CET activity.

Both diatom species are capable of generating qE that is attributable to PSI CET. According to Figure 3.3-6, *Nitzschia* has a very active PSI CET that can generate large ΔpHs at all illumination intensities. ΔpH buildup (as inferred by $\mathcal{NPQ}$) from PSI CET activity is substantially slower than that from PSII activity. The capacity for PSI CET to generate NPQ and therefore ΔpH seems to saturate at 1000 µmol $m^{-2}s^{-1}$. However, with this experimental design it is uncertain if the saturation of PSI CET NPQ generation actually originates from the PSI CET cycle rate and not from depletion of the DD de-epoxidase co-substrate ascorbate; a lack of linear electron flow would limit the availability of NADPH to regenerate ascorbate. *Navicula* cells also seem to be

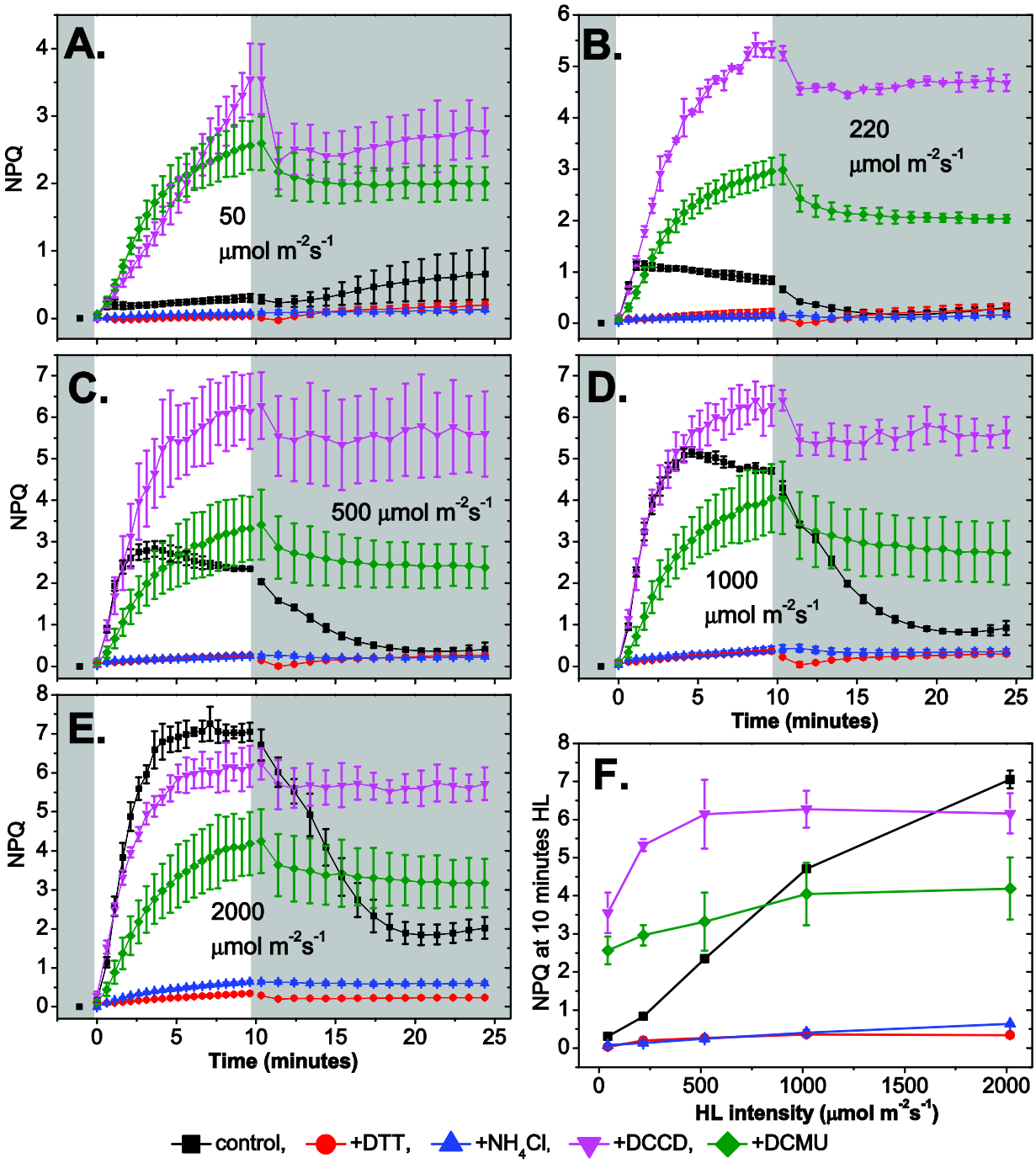

Figure 3.3-6 The interaction of electron transport, ΔpH, and DD de-epoxidase activity during high light transitions in *Nitzschia* cells. A to E, $\mathcal{NPQ}$ transients were obtained with pre-treatments of the DD de-epoxidase inhibitor DTT (5.3 mM), the uncoupler NH_4Cl (2.8 mM), the ATP synthase inhibitor DCCD (320 µM), or the PSII PQ binding site inhibitor DCMU (4 µM) in order to determine the relative contribution of ΔpH, DD de-epoxidase activity, and non-linear electron flow to NPQ during transitions to 50 (**A**), 220 (**B**), 500 (**C**), 1000 (**D**), and 2000 (**E**) µmol $m^{-2}s^{-1}$ high light (HL). The regions of the plot area with a dark background correspond to dark conditions and the white portion of the background corresponds to the time that HL was applied. **F**, summary of $\mathcal{NPQ}$ values at 10 minutes HL from the preceding panels. Error bars represent ± 1 standard deviation from the mean of 3 separate cultures grown at 50 µmol $m^{-2}s^{-1}$.

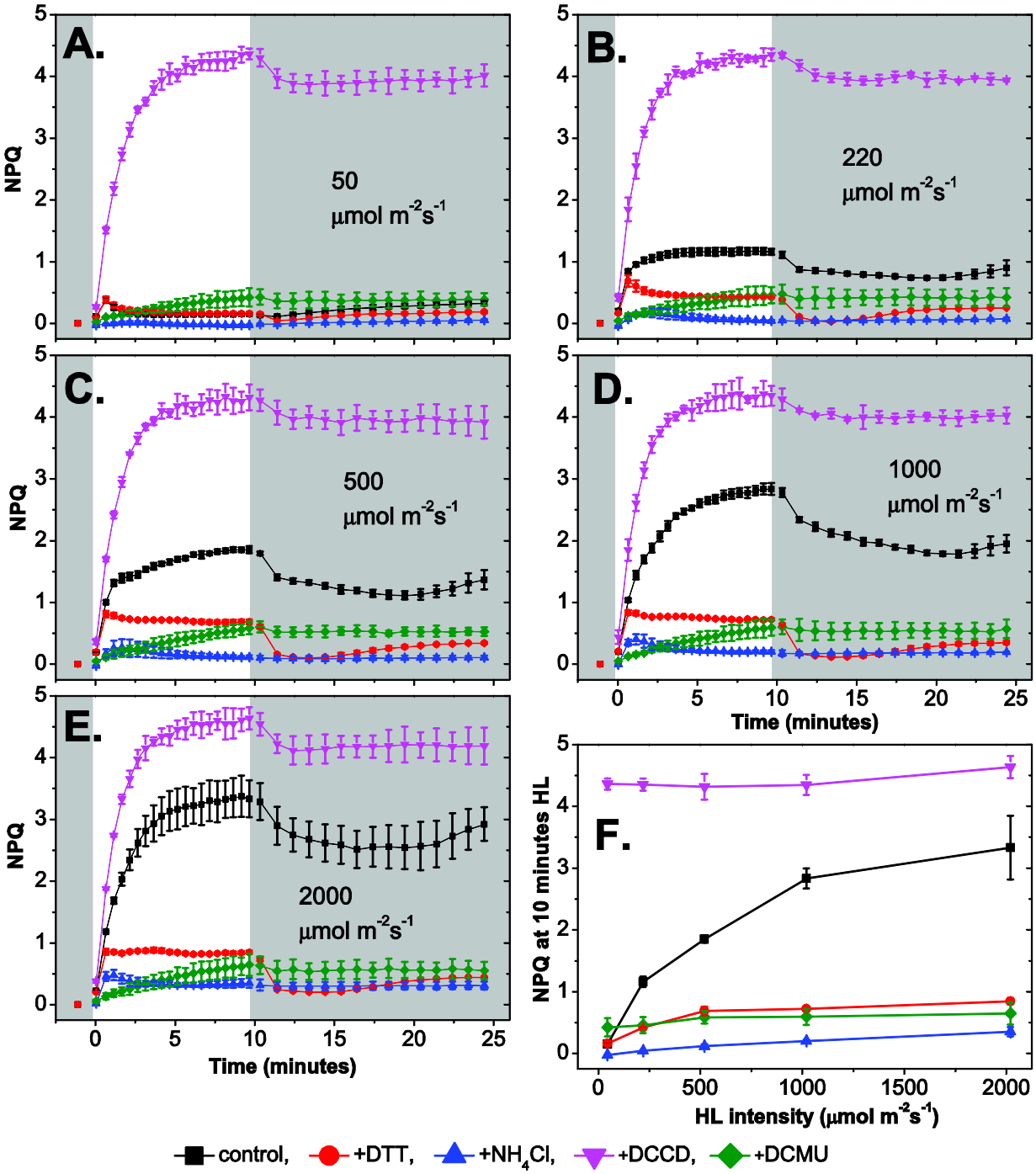

Figure 3.3-7 The interaction of electron transport, ΔpH, and DD de-epoxidase activity during high light transitions in *Navicula* cells. A to E, $\mathcal{NPQ}$ transients were obtained with pre-treatments of the DD de-epoxidase inhibitor DTT (2.65 mM), the uncoupler NH_4Cl (2.8 mM), the ATP synthase inhibitor DCCD (320 µM), or the PSII PQ binding site inhibitor DCMU (4 µM) in order to determine the relative contribution of ΔpH, DD de-epoxidase activity, and non-linear electron flow to NPQ during transitions to 50 (**A**), 220 (**B**), 500 (**C**), 1000 (**D**), and 2000 (**E**) µmol $m^{-2}s^{-1}$ high light (HL). The regions of the plot area with a dark background correspond to dark conditions and the white portion of the background corresponds to the time that HL was applied. **F**, summary of $\mathcal{NPQ}$ values at 10 minutes HL from the preceding panels. Error bars represent ± 1 standard deviation from the mean of 3 separate cultures grown at 50 µmol $m^{-2}s^{-1}$.

able to induce NPQ via PSI CET, but at levels much less than what were observed in *Nitzschia* (Figure 3.3-7). Similar to *Nitzschia*, induction of $\mathcal{NPQ}$ by PSI CET in *Navicula* proceeds at a slower rate than that for $\mathcal{NPQ}$ induction by normal linear electron transport. Of note is the observation that in *Navicula* DCMU pre-treatment yields similar steady state $\mathcal{NPQ}$ as the $\mathcal{NPQ}$ obtained with DTT pre-treatment (Figure 3.3-7F). The low induction of NPQ by PSI CET in *Navicula* is not necessarily due to a limited capability to generate ΔpH, but could be due to an inability to regenerate ascorbate during illumination. Thus when qE_{XC} is inhibited either by DD de-epoxidase inactivation (+DTT) or by depletion of ascorbate (+DCMU), only NPQ via qE_{nonXC} remains. If this interpretation of ascorbate cycling is true in *Navicula*, then ascorbate may always be limiting to qE_{XC} induction, meaning qE_{XC} is only active during conditions that allow transfer of electrons to dehydroascorbic acid. A high sink capacity for electrons from NADPH, as via carbon assimilation, could also limit ascorbate regeneration (recall that *Navicula* is sensitive to HCO_3, Figure 3.3-1B). In both species NPQ relaxation post HL is very limited with DCMU; because PSI CET does not net any NADPH, there would be no NADPH available for DT epoxidase. The NPQ induced in the presence of DCMU is due to qE as opposed to photoinhibition of PSII, because $\mathcal{NPQ}$ generation was inhibited when cells were dual pre-treated with DCMU and NH_4Cl (data not shown).

The 'limiting reactants' for NPQ induction can be deduced from $\mathcal{NPQ}$ transients when cells are treated with inhibitors that affect ΔpH and electron transport. qE induction is dependent on ΔpH and DD de-epoxidase activity. Once DD de-epoxidase has been activated by an acidic lumen, de-epoxidation activity is dependent on the availability of ascorbate and accessible DD. The addition of DCCD during HL would maximise the buildup of ΔpH during

illumination. If maximal attainable $\mathcal{NPQ}$ with DCCD treatment is equivalent to maximal attainable $\mathcal{NPQ}$ in control cells, then it can be reasoned that qE is not normally limited by ΔpH but by DD de-epoxidation. Conversely, if the maximal attainable $\mathcal{NPQ}$ with DCCD exceeds that in control cells, then it can be deduced that ΔpH limits qE induction under natural conditions.

In *Nitzschia* cells, NPQ is limited by ΔpH buildup at irradiance levels less than full sunlight equivalence (~2000 µmol $m^{-2}s^{-1}$). Since DCCD treatment enhances $\mathcal{NPQ}$ at irradiances less than 2000 µmol $m^{-2}s^{-1}$ (Figure 3.3-6F), it can be deduced that qE is limited by ΔpH at sub-saturating irradiances. The amount of $\mathcal{NPQ}$ elicited with DCCD plateaus at a HL irradiance of 500 µmol $m^{-2}s^{-1}$ (Figure 3.3-6F), further suggesting that at low to moderate irradiances qE is quite effective at limiting ΔpH buildup even in the absence of ATP synthase activity. Because $\mathcal{NPQ}$ saturates at a lower amplitude in DCCD treated cells as compared to control cells, DCCD likely has a greater detrimental effect on ascorbate regeneration (and thus DD de-epoxidation) than it has a positive effect on ΔpH generation at irradiances close to full sunlight equivalence. Thus, DD de-epoxidation can become limiting to NPQ capacity at irradiances approaching full sunlight. Of note is that the kinetics of $\mathcal{NPQ}$ induction in the presence of DCCD becomes completely linear at the illumination intensity equivalent to that which the cells were cultured (50 µmol $m^{-2}s^{-1}$ illumination) (Figure 3.3-6A), indicating a steady buildup of ΔpH and consequent NPQ induction that does not approach saturation. Also note that the initial rate of $\mathcal{NPQ}$ induction is nearly identical in control and DCCD treated cells, and that the effect of DCCD is to maintain $\mathcal{NPQ}$ induction throughout the illumination period (Figure 3.3-6). This is congruent with DCCD maintaining NPQ induction throughout the illumination period by maintaining a high ΔpH. DCCD likely has little effect on the early induction of NPQ because ΔpH is high anyways

during the initial transition from dark to light. Photosynthetic systems routinely use supplemental methods to rapidly build ΔpH during the initial transition to light (e.g. Mehler reaction) so as to quickly activate the pH dependent carbon assimilation enzymes so that photostasis can be reached. To summarise, NPQ generation in *Nitzschia* is limited by ΔpH buildup and not be DD de-epoxidase activity at less than full sunlight equivalent irradiances.

NPQ generation in *Navicula* cells is always limited by ΔpH buildup. DCCD treatment at all irradiances induces an equivalent maximal level of $\mathcal{NPQ}$ that cannot be attained in control cells even when measured at the highest irradiance level (Figure 3.3-7F), thus the capacity for NPQ is always limited by ΔpH. $\mathcal{NPQ}$ maximises at lower irradiances with DCCD, as compared to *Nitzschia*, meaning qE in *Navicula* is less effective at preventing buildup of ΔpH in the absence of ATP synthase activity. This suggests that ΔpH balance in *Navicula* is heavily dependent on the flux of protons across ATP synthase and less by qE prevention of proton dumping into the lumen. Note that, also opposed to what was witnessed in *Nitzschia*, DCCD increases the initial rate of $\mathcal{NPQ}$ induction upon transition from dark to HL (Figure 3.3-7), implying that *Navicula* does not rely heavily on supplemental ΔpH generation during the initial transition to light. This is likely a consequence of the potent qE_{nonXC} (PSII reaction centre based quenching) that occurs in *Navicula*. Reaction centre based quenching (via cyclic electron transfer *within* PSII reaction centres) would not contribute to ΔpH formation. *Navicula* cells must be able to dissipate a heavy flux of protons across the thylakoid via ATP synthase activity with all HL irradiances, in such keeping ΔpH from reaching saturation and inducing excessive qE. For ATP synthase activity to remain high there must be a high rate of ADP regeneration. The principle source of ATP usage in the chloroplast is via the Calvin-Benson cycle, so the rate of carbon assimilation is

an important determinant for ATP synthase activity and ΔpH dissipation. It is hypothesized that *Navicula* has a high ratio of Rubisco to the light reaction photosynthetic complexes, which was hinted to by the positive sensitivity of photosynthesis to HCO_3 (Figure 3.3-1B). When the NPQ response is maximised with DCCD the $\mathcal{NPQ}$ capacity of *Navicula* approaches that of *Nitzschia* (Figures 3.3-7F vs. 6F); so, *Navicula* may also have the capacity to perform high amplitude qE, but doesn't need to due to the efficient regulation of excitation pressure via electron transport. To conclude, *Navicula* keeps qE low during HL by likely relying on ATP synthase for ΔpH dissipation.

qE relaxation after HL illumination ends is reliant on a drop in ΔpH and the availability of NADPH for DT epoxidation. NPQ does not substantially dissipate post HL when cells are pretreated with DCCD in either species. Because DCCD interferes with ATP-NADPH cycling within the Calvin-Benson Cycle, it is predicted that the ATP supply becomes exhausted during illumination. Under such conditions chlororespiration is expected to be induced in the dark post HL in a futile attempt to increase ATP supply. Chlororespiration would consume NADPH and maintain ΔpH, thus inhibiting DT epoxidation in a double manner. In DCCD treated *Nitzschia* cells, $\mathcal{NPQ}$ relaxation post HL can be regained by washing the cells with ammonium chloride doped growth media in the dark (Figure 3.3-8), indicating that the maintenance of ΔpH post HL is the inhibiting factor for qE relaxation and not NADPH supply. To the contrary, in DCCD treated *Navicula* cells, the post HL ammonium chloride wash was not able to relax $\mathcal{NPQ}$, yet $\mathcal{NPQ}$ relaxation in control cells was doubled with washing (Figure 3.3-8). These observations in *Navicula* advocate that NADPH supply is the limiting factor for qE relaxation in the NPQ

maximised DCCD treated cells, whereas at sub saturating NPQ ΔpH is limiting. The effects of DCCD on mitochondrial energy balance are unknown in this study.

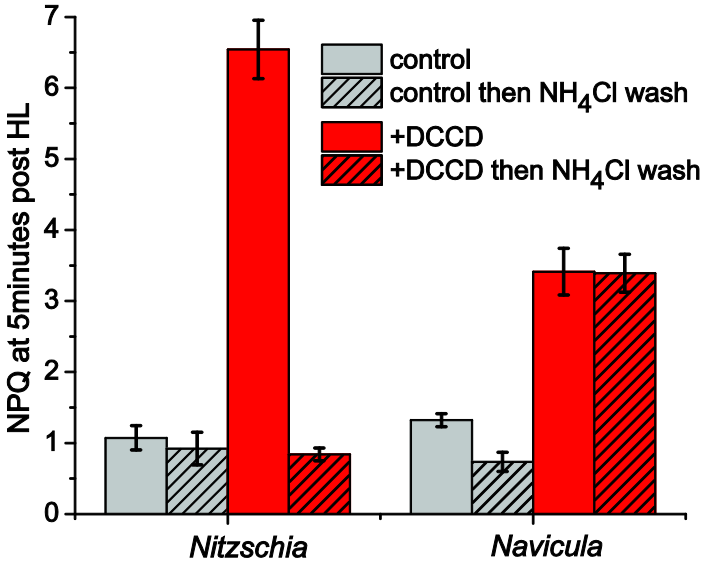

Figure 3.3-8 ΔpH control over NPQ relaxation in the dark after high light illumination. Following 10 minutes of illumination with 500 µmol $m^{-2}s^{-1}$ high light (HL) control cells and cells pre-treated with the ATP synthase inhibitor DCCD (320 µM) were washed with the uncoupler NH_4Cl (2.8 mM) for 5 minutes in the dark (post HL). *NPQ* values were measured. Error bars represent ± 1 standard deviation from the mean of 3 separate cultures grown at 50 µmol $m^{-2}s^{-1}$.

3.3-5 'Dark' NPQ: a biomarker for chlororespiration

Illumination is not necessary for inducing NPQ. Any condition dropping lumenal pH below neutral can activate DD de-epoxidase (DD de-epoxidase isolated from *Phaeodactylum tricornutum* is activated at pH *7.2*, Jakob et al. 2001) and induce qE_{XC}. Chlororespiration describes a respiratory pathway within chloroplasts that occurs in the dark involving electron transport from NAD(P)H to oxygen via the PQ pool to build a trans thylakoid proton motive force for ATP synthesis (Bennoun 1982). Diatoms actively engage in chlororespiration during periods of extended darkness, perhaps utilizing their storage lipids for gluconeogenesis and ATP generation (Armbrust et al. 2004, Wilhelm et al. 2006). During chlororespiration *Phaeodactylum tricornutum* is believed to utilize a type 1 NAD(P)H dehydrogenase (Ndh1) that reduces PQ while directly pumping protons into the lumen; PQ is oxidised via a PQ oxidase that releases water into the lumen (Goss and Jakob 2010 based on Grouneva et al. 2009). In

Cyclotella meneghinia, a type 2 NAD(P)H dehydrogenase (Ndh2) is thought to be utilised; in this case Ndh2 does not directly pump protons, but instead proton pumping can occur via activity from the cytochrome b_6f complex (Goss and Jakob 2010 based on Grouneva et al. 2009). The proton gradient produced by chlororespiration in the dark is sufficient enough to induce DD de-epoxidation and NPQ (Caron et al. 1987, Ting and Owens 1993, Jakob et al. 1999, Grouneva et al. 2009), giving rise to 'dark' NPQ.

The induction of dark NPQ in *Nitzschia curvilineata* and *Navicula sp.* was often observable during the 15 minute dark period that followed the HL illuminations used in this study (see Figure 3.3-9A & 10A). This increase in NPQ post HL was the most variable feature witnessed during the entire investigation of NPQ in these two species, being highly variable between time of day, culture age, and ΦPSII. Dark NPQ was nearly always observable to some degree, but could range from infinitesimal to magnitudes greater than 1.5 times that of the $\mathcal{NPQ}$ induced during HL. Dark NPQ was observable at all HL intensities in both species. It was noticed that the onset of dark NPQ is closely linked to PSII electron transport (as measured by ϕPSII). The onset of the rise of dark NPQ is always preceded by a drop in ϕPSII. The inflection point for ϕPSII always directly preceded or occurred at the same saturating light pulse that measured an increase in $\mathcal{NPQ}$ (Pearson's r= 1.0, n = 9 *Nitzschia*, n = 5 *Navicula*; see Figures 3.3-9A & 10A). The OJIP transients furthermore revealed that electron transport out of PSII was slowing during the transition to dark NPQ (Figures 3.3-9B & 10B). The inhibition of PSII forward electron transport that precedes the induction of dark NPQ is from an increased reduction in the redox state of the PQ pool. The only electron transfer pathway available for a reduction of the PQ pool in the dark is the chlororespiratory pathway. So, a transition to chlororespiration in

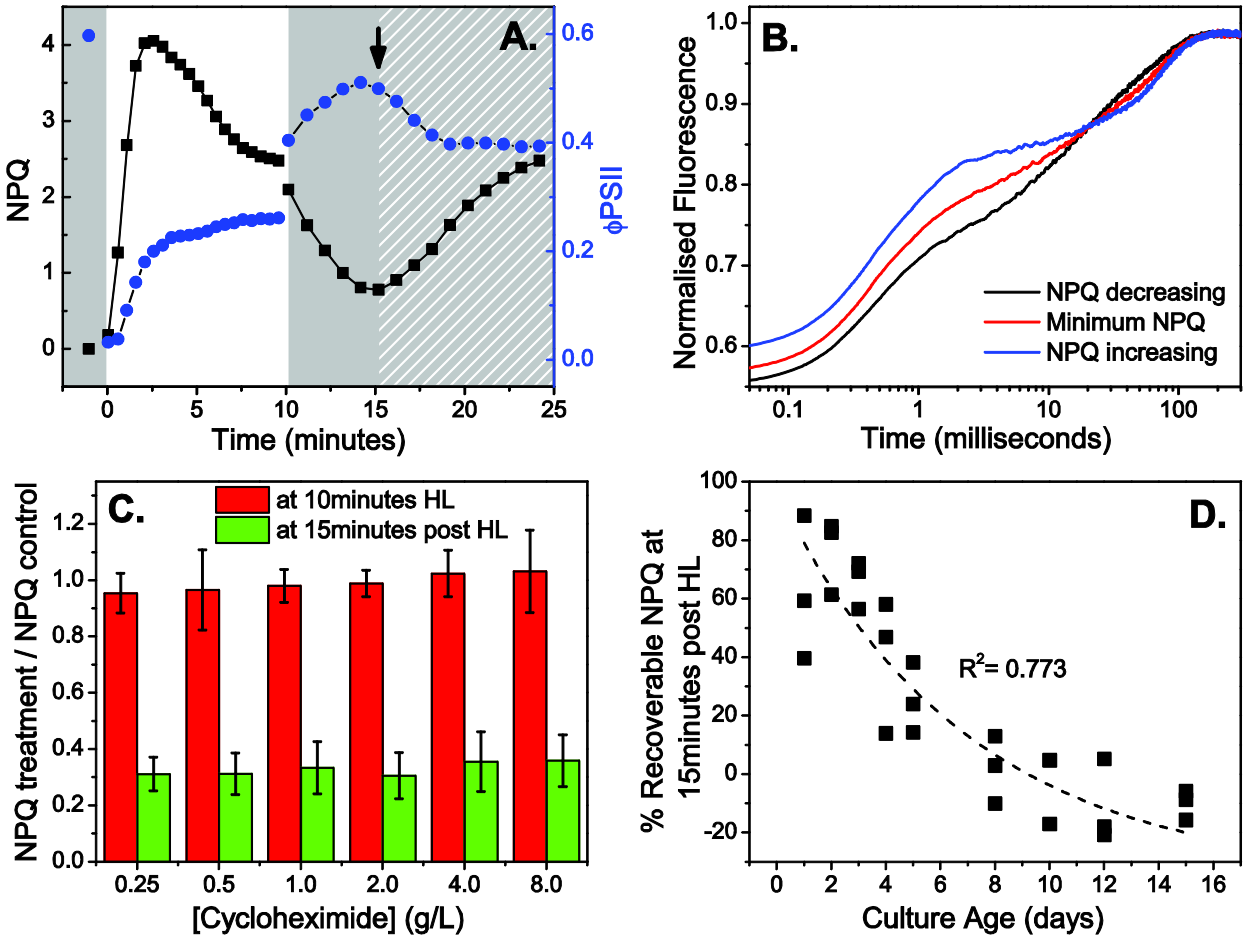

Figure 3.3-9 Characterization of 'dark' NPQ in *Nitzschia* cells. **A,** a representative *NPQ* transient for 'dark NPQ' with corresponding quantum efficiency of PSII photochemistry (ϕPSII). Dark NPQ is an increase in *NPQ* during the dark period following high light (HL) illumination (indicated by the white diagonal hatched region of the plot area) and is induced by a decrease in ϕPSII (indicated at the arrow). **B**, OJIP transients collected during the post HL drop in *NPQ* (at the data point directly preceding the arrow in A), at minimum *NPQ* post HL (at the data point indicated by the arrow in A), and during the rise of *NPQ* post HL (at the data point directly proceeding the arrow in A). Shown are the average traces from 9 separate cultures. Time zero on the x-axis corresponds to the start of the saturating light pulse. The transients have been normalised to maximal fluorescence at 'P'. **C**, the effect of pre-treatment with the cytosolic ribosome inhibitor cycloheximide on *NPQ*. Dark adapted cells were treated with cycloheximide in the dark for 5 minutes prior to exposure to a high light transition. *NPQ* at the end of 10 minutes HL and after 15 minutes in the dark proceeding the 10 minutes HL are expressed as the ratio between that obtained with cycloheximide pre-treatment to that obtained in control cells (a value of 1 means no change between treated and control cells, values less than 1 indicate a loss of *NPQ* in the treated cells). Error bars represent ± 1 standard deviation from the mean of 3 separate cultures. **D**, the effect of culture age on *NPQ* induced with 10 minutes of HL illumination that can reverse within a 15 minute dark period following the illumination. % recoverable *NPQ* post HL = 100 • [(*NPQ* at 10 minutes HL) – (minimum *NPQ* during 15 minutes of dark following HL)] / (*NPQ* at 10 minutes HL). n = 3 separate cultures. The dashed line represents the data fit to a single exponential decay; the corresponding R^2 value is shown. All data shown in this Figure was collected using 500 µmol $m^{-2}s^{-1}$ HL with cultures grown at 50 µmol $m^{-2}s^{-1}$.

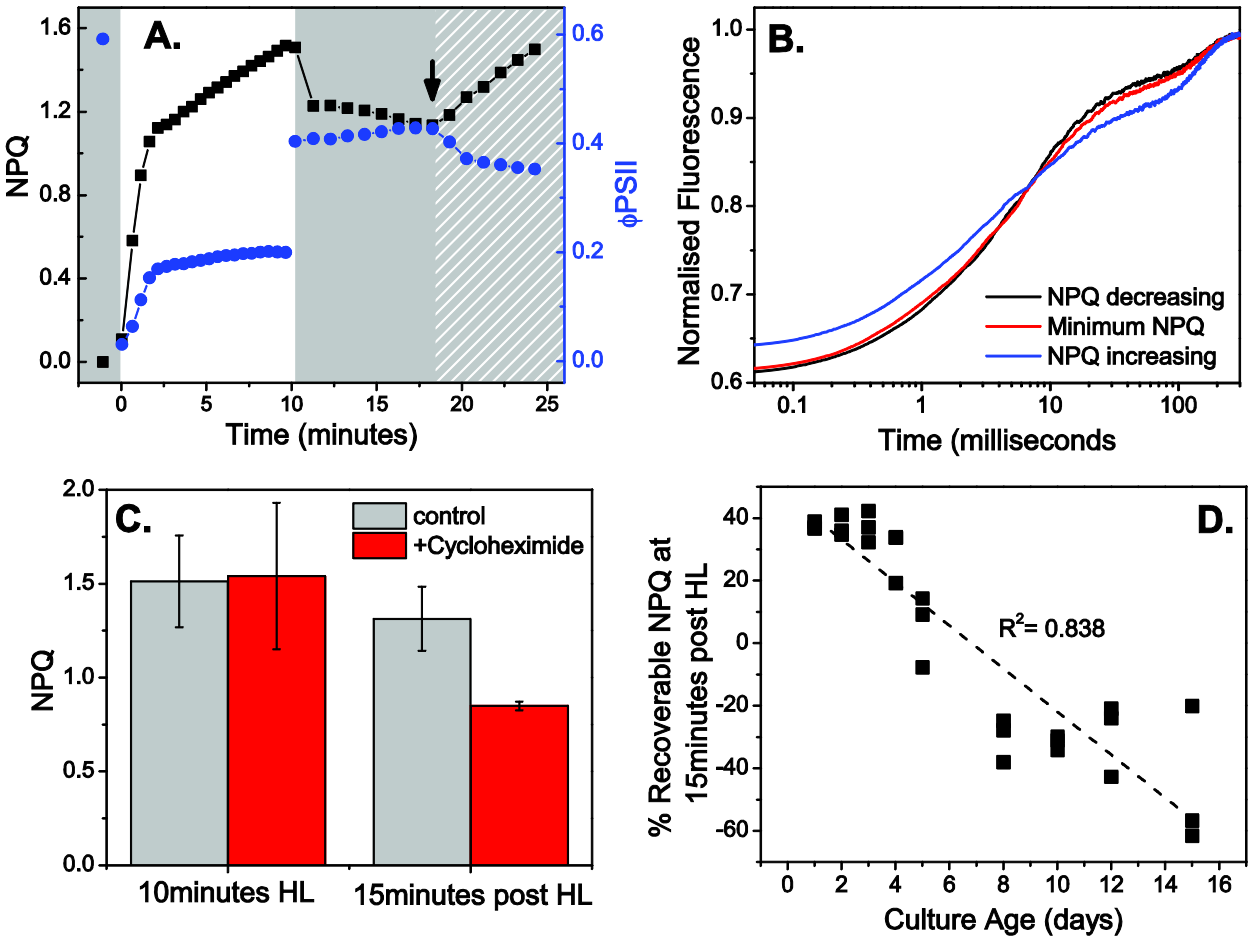

Figure 3.3-10 Characterization of 'dark' NPQ in *Navicula* cells. **A,** a representative *NPQ* transient for 'dark NPQ' with corresponding quantum efficiency of PSII photochemistry (ϕPSII). Dark NPQ is an increase in *NPQ* during the dark period following high light (HL) illumination (indicated by the white diagonal hatched region of the plot area) and is induced by a decrease in ϕPSII (indicated at the arrow). **B**, OJIP transients collected during the post HL drop in *NPQ* (at the data point directly preceding the arrow in A), at minimum *NPQ* post HL (at the data point indicated by the arrow in A), and during the rise of *NPQ* post HL (at the data point directly proceeding the arrow in A). Shown are the average traces from 5 separate cultures. Time zero on the x-axis corresponds to the start of the saturating light pulse. The transients have been normalised to maximal fluorescence at 'P'. **C**, the effect of pre-treatment with the cytosolic ribosome inhibitor cycloheximide (8 mg/mL) on *NPQ*. Error bars represent ± 1 standard deviation from the mean of 3 separate cultures. **D**, the effect of culture age on *NPQ* induced with 10 minutes of HL illumination that can reverse within a 15 minute dark period following the illumination. % recoverable *NPQ* post HL = 100 • [(*NPQ* at 10 minutes HL) – (minimum *NPQ* during 15 minutes of dark following HL)] / (*NPQ* at 10 minutes HL). n = 3 separate cultures. The dashed line represents the linear fit of the data; the corresponding R^2 value is shown. All data shown in this Figure was collected using 500 µmol $m^{-2}s^{-1}$ HL with cultures grown at 50 µmol $m^{-2}s^{-1}$.

the dark is inducing a ΔpH that is sufficient to induce the dark NPQ. Since chlororespiration is thought to balance ATP demand to reductant supply (e.g. NADPH, Fd) during metabolic

processes (Goss and Jakob 2010), one would expect that the resulting dark NPQ would be sensitive to conditions that affect cell metabolism. ATP production via chlororespiration seems to be important for cytosolic protein synthesis. Even though cycloheximide (an inhibitor of 80S ribosomes) had no effect on the amount of $\mathcal{NPQ}$ induced during HL, it lowered the amount of residual $\mathcal{NPQ}$ that remained in the dark at 15 minutes post HL (Figures 3.3-9C & 10C). If diatom cultures are allowed to age without the addition of fresh growth media, nutrient levels are expected to become limiting to cell growth, a condition favoring ATP demand (for cell maintenance) over NADPH demand (for nutrient assimilation to make cellular building blocks). The amount of $\mathcal{NPQ}$ that could relax during a 15 minute post HL dark period (i.e. recoverable $\mathcal{NPQ}$) was found to be inversely correlated to culture age. The relationship was linear in *Navicula*, but more non-linear in *Nitzschia* (Figures 3.3-9D & 10D). Recoverable $\mathcal{NPQ}$ in the dark depicts a balance between qE that was able to relax post HL and qE induced by dark chlororespiration. The above results are consistent with dark NPQ being an *in vivo* biomarker for the extent of chlororespiratory electron flow in diatoms. And since $\mathcal{NPQ}$ is easily and non-invasively measured using PAM fluorometry, chlororespiration can be readily monitored under a multitude of environmental and physiological conditions.

3.3-6 Conclusions

Photostasis is achieved when the energy transduction pathways occurring within the photosynthetic apparatus are able to balance the light field with the metabolic demands of the cell. Under conditions with transitory light intensities and/ or metabolic activity, regulatory mechanisms must be induced to maintain excitation balance and limit excitation pressure on PSII, all in an effort to limit photo-oxidative damage. As shown in *Section 3.2*, *Nitzschia* cells

rely on qE_{XC} for excitation pressure relief, whereas *Navicula* cells do not require qE_{XC} for excitation pressure regulation. These trends extend into the electron transport processes. Regulation of photostasis can also be protracted to dark periods that follow illumination. Both species are able to use chlororespiration (as monitored by dark NPQ) to optimize the use of accumulated reducing equivalents during illumination and maintain a balanced NADPH to ATP supply.

The sink capacity for linear photosynthetic electron transport in *Nitzschia* cells is not labile. Electron transport activity (as measured by ϕPSII and $1\text{-}V_J$) cannot absorb the rapid influx of electrons generated during the transition to HL. Sink capacity seems to be limited by the processing rate of the electrons and not by the availability of CO_2, because elevated HCO_3 was not able to reduce excitation pressure in this species. Treatment with the artificial electron acceptor MV also had no effect on excitation pressure generation, furthermore supporting an innately limited capacity to perform forward linear electron transport. This could be due to PSII to PSI to $Cytb_6f$ stoichiometry and/ or the size of the intersystem electron transporter pool. PSI CET may be an important pathway in regulating electron flux by diverting electrons from a saturated sink. PSI CET has the additional feedback of down regulating excitation by utilising ΔpH generation to up-regulate qE. Since NPQ relaxation post HL does not seem to be limited by NADPH availability to DT epoxidase, the NADPH pool appears to remain in a net reduced state during illumination (as when NADPH generation via linear electron transport exceeds $NADP^+$ regeneration via carbon assimilation). The relative inflexibility of electron transport, more specifically the no 'pull' of photosynthetic electrons, likely stems from the environmental conditions under which this species evolved. Photosynthesis within the shoreline habitat is

rarely limited by CO_2 because of constant mixing of the water column with air from wave and tidal action. So, a diatom from conditions of relatively high and stable CO_2 concentration is not expected to develop dynamically responsive (high flux) carbon assimilation mechanisms. Inhibition of qE_{XC} perturbs PSII electron flow during HL illumination and severely thereafter in the dark; this is highly indicative that qE_{XC} is a requirement for maintaining redox homeostasis during HL illumination conditions. In conclusion, the photosynthetic system in *Nitzschia* has been designed to regulate excitation pressure at the source side, in match to the shoreline's poikilophotic environment.

Electron transport flux actively contributes to photostasis in *Navicula* cells. There is a high 'pull' of photochemically derived electrons by linear electron transport in this species. Seemingly high rates of forward electron transfer transcend from the Q_A site within PSII (as shown by high $1\text{-}V_J$ values) to PSI acceptor side (as shown by enhanced sensitivity of photostasis to MV treatment) all the way to carbon assimilation (as shown by enhancement of photosynthesis in presence of elevated HCO_3). This makes electron transfer in *Navicula* more responsive to fluctuations in terminal electron sink capacity than what was seen in *Nitzschia*. High levels of ATP synthase activity may further facilitate the flux of electrons through NADPH via the Calvin-Benson cycle. The net oxidation of the NADPH pool during illumination that would result from non-limiting electron sink capacity becomes the limiting factor (as a co-substrate for DT epoxidase) for NPQ relaxation post HL. Regulation of photosynthesis by PSI CET is less important in this species. PSII CET (qE_{nonXC}) seems to contribute substantially to this species ability to maintain high rates of intra PSII electron transfer during HL illumination. Ferredoxin oxidation by nitrite reductase could also constitute an important electron sink in this

species; however, the contribution cannot be determined by the presented experimental approach. PSII electron transport during HL illumination was largely independent of regulation by qE_{XC}; once again illustrating that excitation pressure can be effectively balanced in this species without involvement of the xanthophyll cycle.

The unique saline soil habitat of the Great Salt Plains salt flat exposes *Navicula* to high temporal and amplitude variability in soil temperature, salt concentration, and nutrient availability, which is ultimately dependent on the magnitude and frequency of rain events (Kirkwood and Henley 2006, Potter et al. 2006). Bursts of growth only occur when environmental conditions become favorable (Kirkwood and Henley 2006). The approach for regulating photosynthesis in *Navicula* is well suited to this poikilotrophic, yet relatively stable light environment. Regulation of photosynthesis downstream of PSII excitation (sink side) is a most reasonable approach for this species, since non-photic factors are limiting to growth in its natural habitat. Instead of just down-regulating light harvesting by performing antenna centred NPQ (and 'wasting' the light energy), photosynthesis in *Navicula* is able to up-regulate linear electron transport so as to maximise carbon and nutrient assimilation during periods of active growth.

3.4 The Quenching and Redistribution of Excitation Energy during NPQ in *Nitzschia curvilineata*

3.4-1 Overview

The NPQ process in diatoms is able to harmlessly dissipate a large proportion of absorbed photon energy when exposed to excess irradiation. Identification of the specific pigments and the photo-electronic mechanism responsible for excited state quenching during NPQ in diatoms is still somewhat in its infancy. The detailed energy transfer study on *Phaeodactylum tricornutum* and *Cyclotella meneghiniana* cells by Miloslavina et al. (2009) implicated that there are two distinct types of quenching sites in diatoms: Q1 quenching targeting outer antenna complexes that become functionally decoupled from PSII during NPQ and Q2 targeting PSII-inner antenna complexes that remain coupled to PSII during NPQ. The concept of Q1 and Q2 quenching has already been introduced for *Nitzschia curvilineata* in *Section 3.4-2*. The objectives of the present chapter are to confirm the placements of Q1 and Q2 within the antenna system and to assign a photo-electronic mechanism for non-photochemical quenching in *Nitzschia* cells. Excitation energy transfer was examined during induction, steady state, and recovery phases of NPQ. Low temperature (77K) steady state emission spectra, and excitation spectra for said spectra, were used to examine the relationship between excitation energy quenching and the redistribution of the remaining excitation energy between emitting Chl *a*. This permitted assignment of Q1 and Q2 quenchers within the outer FCP antenna compartment and within the inner FCP-PSII antenna compartment, respectively. Room temperature fluorescence lifetime measurements revealed that quenching during NPQ

involves a large-scale shortening of Chl *a* excited state lifetime. The combined results of the fluorescence measurements indicated that excited state quenching during NPQ is caused by the formation of short-lived excited state Chl *a*-Chl *a* dimers that weakly fluoresce in the far-red. These Chl *a*-Chl *a* quencher dimers were predicted to form between FCP Chl *a*s positioned at inter-trimer interfaces. Pre-treatment of cells with the DD de-epoxidase inhibitor DTT stopped all the changes in steady state emission assignable to Q1 and Q2 quenching, leading to the conclusion that DD de-epoxidation is obligatory for the initiation of antenna centred quenching in *Nitzschia* cells. Q1 and Q2 were induced at the same rate during HL illumination, but Q2 relaxed more quickly upon cessation of illumination. It was concluded that Q1 quenching provides a more stable form of photoprotection, whereas Q2 quenching provides a more labile form of photoprotection for PSII.

3.4-2 NPQ: the quenching and redistribution of excitation energy

The antenna centred quenching mechanisms activated during NPQ work by acting as a one way trap for excitons, dissipating the excitation energy non-radiatively in the form of heat before the exciton can be trapped by the PSII reaction centre. The quenched excitation energy is measured as the loss in Chl *a* fluorescence yield. The quencher trap causes a reallocation of excitation energy from the antenna pigment pool towards the quencher. Excitations absorbed by pigments tightly coupled to the quencher traps will be preferentially quenched during NPQ; conversely excitations absorbed by pigments weakly coupled to the quenchers will contribute more to cell emission. The coupling efficiencies between pigments could additionally change if the NPQ response involves a structural rearrangement within the pigment matrix. Depending on the photo-electronic mechanism responsible for excited state quenching, the quencher

species may (e.g. Chl *a*-Chl *a* mixed excitonic charge transfer states) or may not (e.g. carotenoid internal conversion, charge transfer/ recombination) be fluorescent. If the quencher is fluorescent then it behaves as an emitter and contributes to overall cell emission. Thus the redistribution of non-quenched excitation energy during NPQ can conceptually be used to reveal modifications to the pigment matrix which are conducive to the formation of quenchers.

The study of exciton migration in photosynthetic pigment systems conventionally includes the collection of steady state emission spectra at low temperature (77K). Freezing dark adapted *Nitzschia* cells at 77K causes a 450% increase in integrated fluorescence yield over the spectral region from 620 to 880 nm (Figure 3.4-1A). Fluorescence yield increases at 77K due to the suppression of molecular vibrations: emission is enhanced via disruptions to weak pigment-pigment couplings (leading to 'slow' relaxation of excited states via emission) and the inhibition of photochemistry within the reaction centres (enhances PSII emission and greatly enhances PSI emission). Emission at cryogenic temperature is from low energy pigments that serve as traps for excitation energy migration; this is seen by the red shifting in the emission peaks (Figure 3.4-1B). Since this approach does not measure energy transfer in its true native system, interpretations have to be taken in context of the effects from low temperature. Nevertheless, there are practical purposes as to why to collect low temperature spectra. Flash freezing the sample locks the system in its current state inhibiting biochemical and diffusion processes, thereby leaving only the physical processes (i.e. excitation energy transfer) active for investigation.

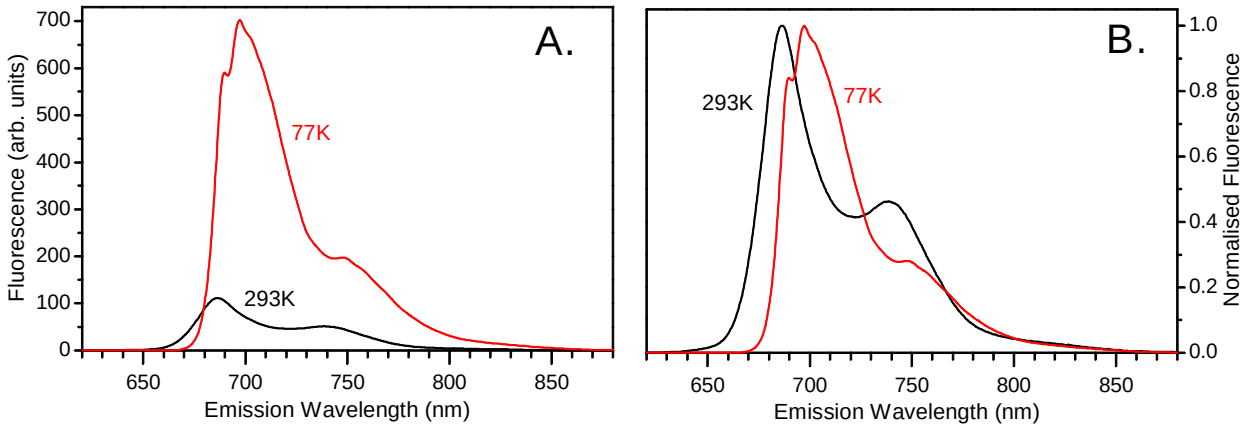

Figure 3.4-1 The effect of collecting emission spectra at low temperature. A, fluorescence of dark adapted cells measured at room temperature and 77K. **B,** the spectra in A normalised to maximum fluorescence peak. Excitation of 1.5 µmol $m^{-2}s^{-1}$, 470 nm. Spectra fully corrected for instrument response (see *Section 2.11-2* for details). Shown is the average of 3 samplings from 3 separate cultures (n=9).

To validate that 77K emission spectra could be justly used for the investigation of excitation energy quenching and redistribution that occurs during the NPQ response in *Nitzschia* cells, fluorescence quenching was compared between non-photochemically quenched cells at physiological relevant temperature and frozen at 77K. There was no method available in this study for the collection of emission with high spectral resolution during illumination conditions. So, to identify the spectral composition of fluorescence quenching under physiological conditions with cells actively performing NPQ, cells would have to be maintained in the quenched state during collection of spectrally resolved emission spectra. Since cells pretreated with DCCD show very limited relaxation of NPQ post HL (as shown in *Sections 3.1* & *3.3*), DCCD treatment was used to 'lock' cells in a quenched state for the collection of room temperature emission spectra (Figure 3.4-2A). NPQ caused a large scale, and predominantly emission energy independent loss of fluorescence, at both physiologically relevant and cryogenic temperatures (Figure 3.4-2A & B). As measured at room temperature, HL illumination induced an 84 % loss in integrated fluorescence yield in the DCCD pretreated

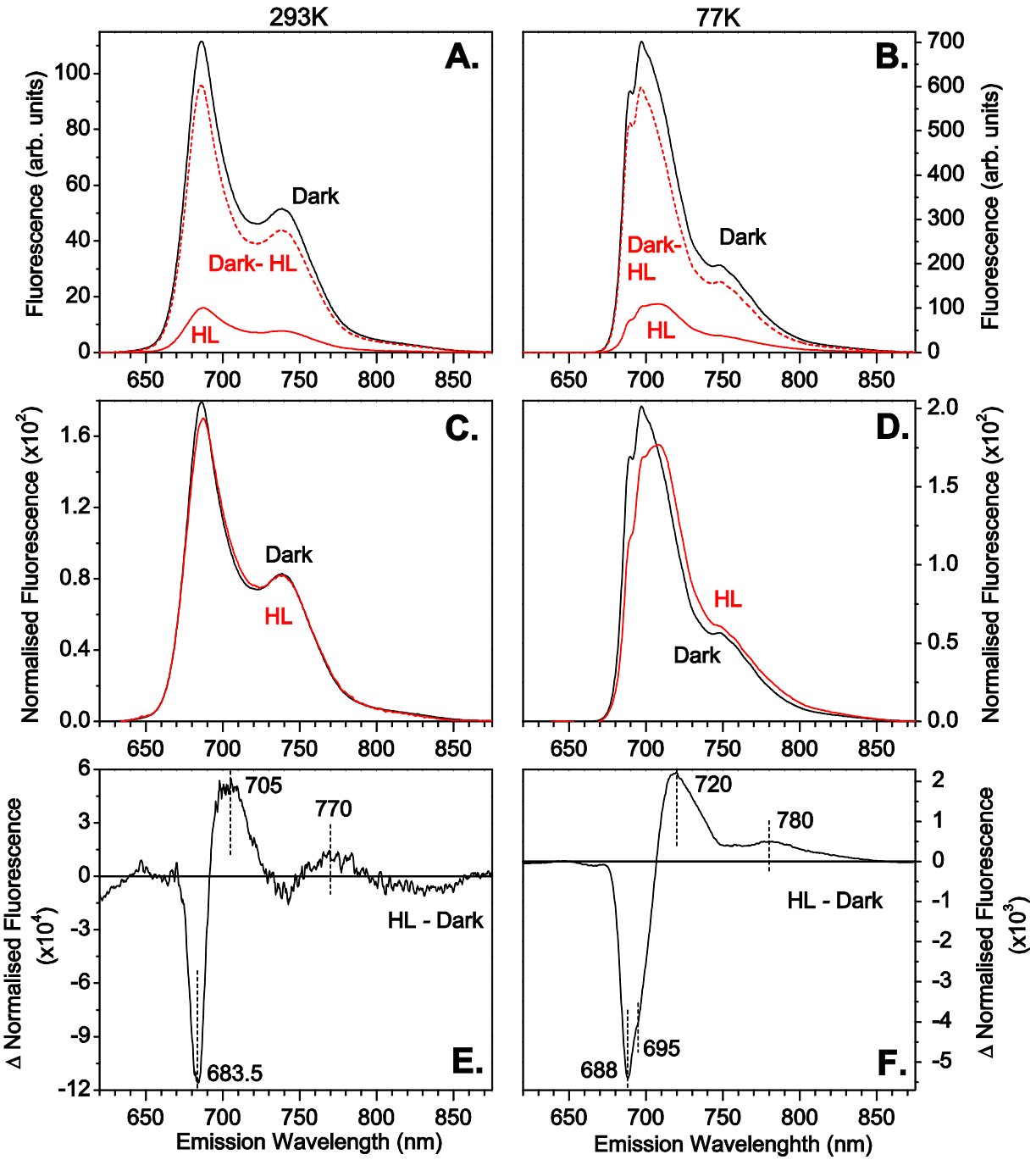

Figure 3.4-2 Freezing cells at 77K maintains high light induced fluorescence quenching. Dark adapted cells were pretreated with 320 µM DCCD (Dark) and then illuminated with 500 µmol $m^{-2}s^{-1}$ high light (HL) for 10 minutes. **A** & **B**, Dark and HL spectra measured at 293 and 77K, respectively. Dashed lines, Dark – HL difference spectra. **C** & **D**, Dark and HL spectra normalised to integrated fluorescence (from 620 to 880 nm) measured at 293 and 77K, respectively. **E** & **F**, the difference between the normalised HL and Dark spectra at 293 and 77K, respectively. Peak positions identified by dashed vertical lines. HL cells at 77K were frozen in the dark ~1 minute after illumination to mimic the time delay experienced by the unfrozen cells. Excitation of 1.5 µmol $m^{-2}s^{-1}$, 470 nm. Spectra fully corrected for instrument response (see *Section 2.11-2* for details). Shown are the averaged spectra from 3 samplings of 3 separate cultures grown at 50 µmol$m^{-2}s^{-1}$ (n=9).

fluorescence yield, indicating that all (97%) of the excitation energy dissipation processes involved in quenching at physiological temperature are maintained in the low temperature samples. In addition to the large loss in fluorescence yield at room temperature, there is a redistribution of excitation energy between emitters. Emission spectra were normalised to the area under the emission curve (and therefore fluorescence yield) for a direct comparison of the distribution of emitted photons (and thus the distribution of excitation energy) between samples. The redistribution of excitation energy in the room temperature samples comprises a strong decrease in emission peaking at ~684 nm, an increase in emission peaking at ~705 nm, and a weak increase in emission at ~770 nm (Figure 3.4-2E). When measured at low temperature the spectral changes in emission at 684 nm (now at 688 nm) and 705 nm (now at 720 nm) become much more pronounced; additionally a negative shoulder at ~695 nm and a secondary positive peak/shoulder at ~780 nm become resolved (Figure 3.4-2F). To recap, both the quenching of excitation energy (change in fluorescence yield) and redistribution of excitation energy (change in emission spectral shape within the context of low temperature emission spectral red shifting) that occur under physiological conditions are maintained at 77K.

3.4-3 Collection of 77K excitation spectra

Figure 3.3-2F and *Figure 3.2-11C* revealed that the shape of low temperature emission spectra changes during HL in *Nitzschia* cells with a preferential quenching of FCP emission at 687 nm and PSII emission at 695 nm, and a relative enhancement of low energy emissions. However, these spectra were only collected at a single excitation wavelength (470 nm) that would excite all accessory pigments. In the present chapter excitation spectra were collected

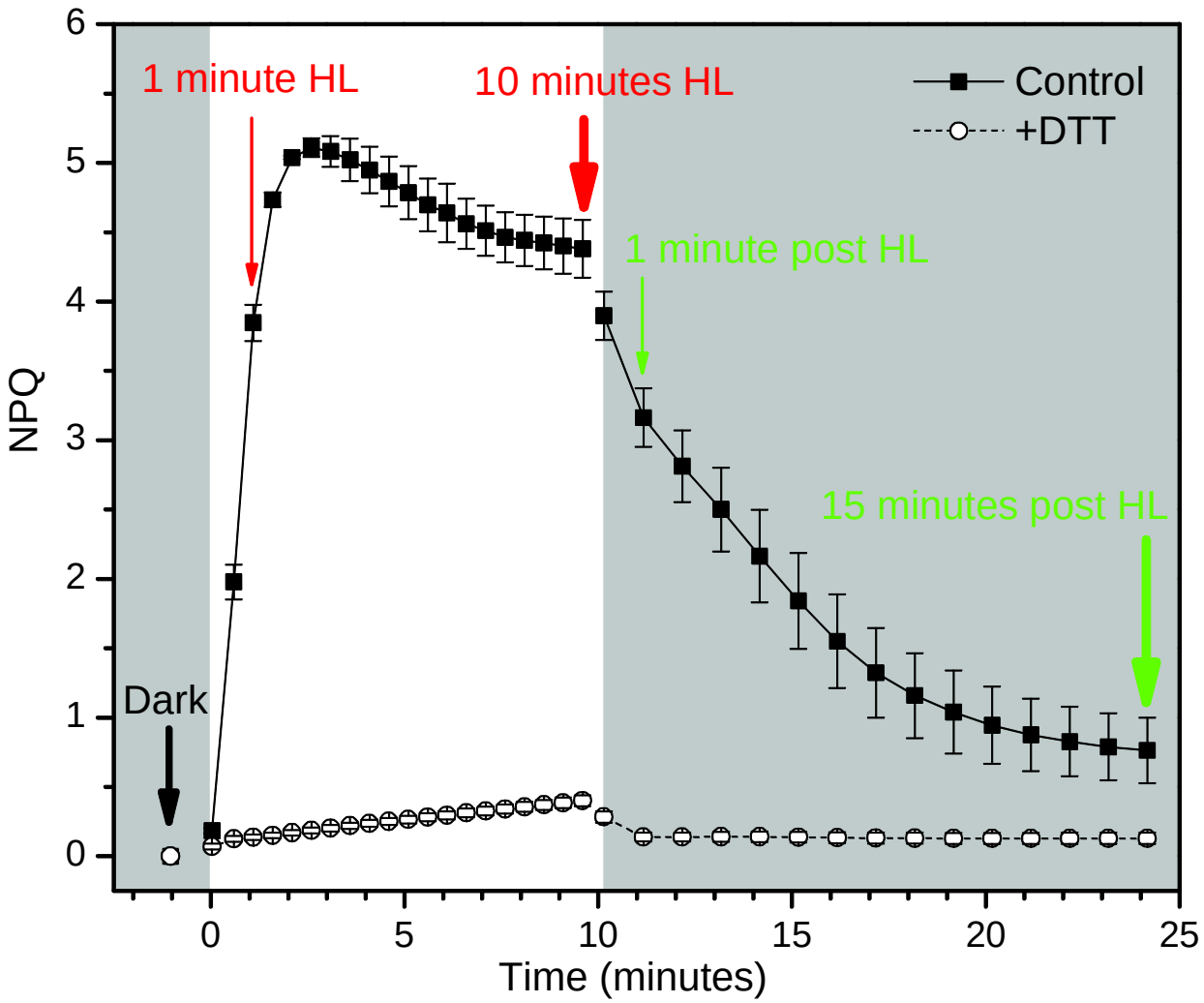

Figure 3.4-3 High light transition time points used for the collection of low temperature emission and excitation spectra. Dark adapted cells were illuminated with 10 minutes 500 µmol $m^{-2}s^{-1}$ high light (HL) then transitioned back to dark (post HL) for 15 minutes. $\mathcal{NPQ}$ transients are shown. Darkened plot areas indicate dark conditions; white plot area indicates HL conditions. +DTT, dark adapted cells pretreated with 5.3 mM DTT. Arrows indicate time points at which samples were quick frozen in liquid N_2 under the illumination conditions indicated by plot area colour. Error bars are ± 1 standard deviation from the mean of 3 separate cultures grown at 50 µmol $m^{-2}s^{-1}$.

for samples flash frozen during the induction, steady state, and recovery phases of NPQ to gain a fuller understanding of the dynamisms in excitation energy quenching and redistribution that occur during NPQ. Figure 3.4-3 shows $\mathcal{NPQ}$ transients (collected using PAM fluorometry) for the samplings used for collection of excitation spectra (sampling points during the high light transition are denoted). Samples for low temperature measurements were illuminated with the

full PAM light regime used for collection of the $\mathcal{NPQ}$ transients. Excitation spectra were also collected from cells pretreated with the DD de-epoxidase inhibitor DTT, so as to deduce what changes in cell emission distribution and sensitisation are directly due to qE_{XC}. Individual emission spectra were corrected to an instrument response function for spectral shape and corrected for excitation quanta before being combined into excitation spectra. These correction procedures insure that any changes in spectral shape and intensity witnessed during the induction and relaxation of NPQ would only represent true HL induced changes to cell emission (see *Section 2.11-2* for further details on the collection and correction of excitation spectra). Low temperature excitation spectra are presented as color filled contour plots in Figure 3.4-4.

The excitation spectra in Figure 3.4-4 contain a vast array of information about the multiple excitation energy transfer pathways that link fluorescence sensitizers (the light absorbing pigments) to the fluorescence emitters. Excitation sensitisation for emission (i.e. transects along the x-axis in Figure 3.4-4) reveal which antenna pigment sensitizers become disconnected from their emitters during the NPQ response; the shape of the individual emission spectra (i.e. transects along the y-axis in Figure 3.4-4) reveal the resulting redistribution of excitation energy between emitters. Direct comparison of the three dimensional excitation spectra (excitation wavelength x emission wavelength x fluorescence intensity) between dark adapted cells and HL treated cells is too complex, therefore the excitation spectra need to be transformed so as to distinguish what sensitising pigments (excitations) and what emitters actively participate in HL induced excitation energy reallocation. Multiple approaches to analysing the excitation spectra data will now be presented.

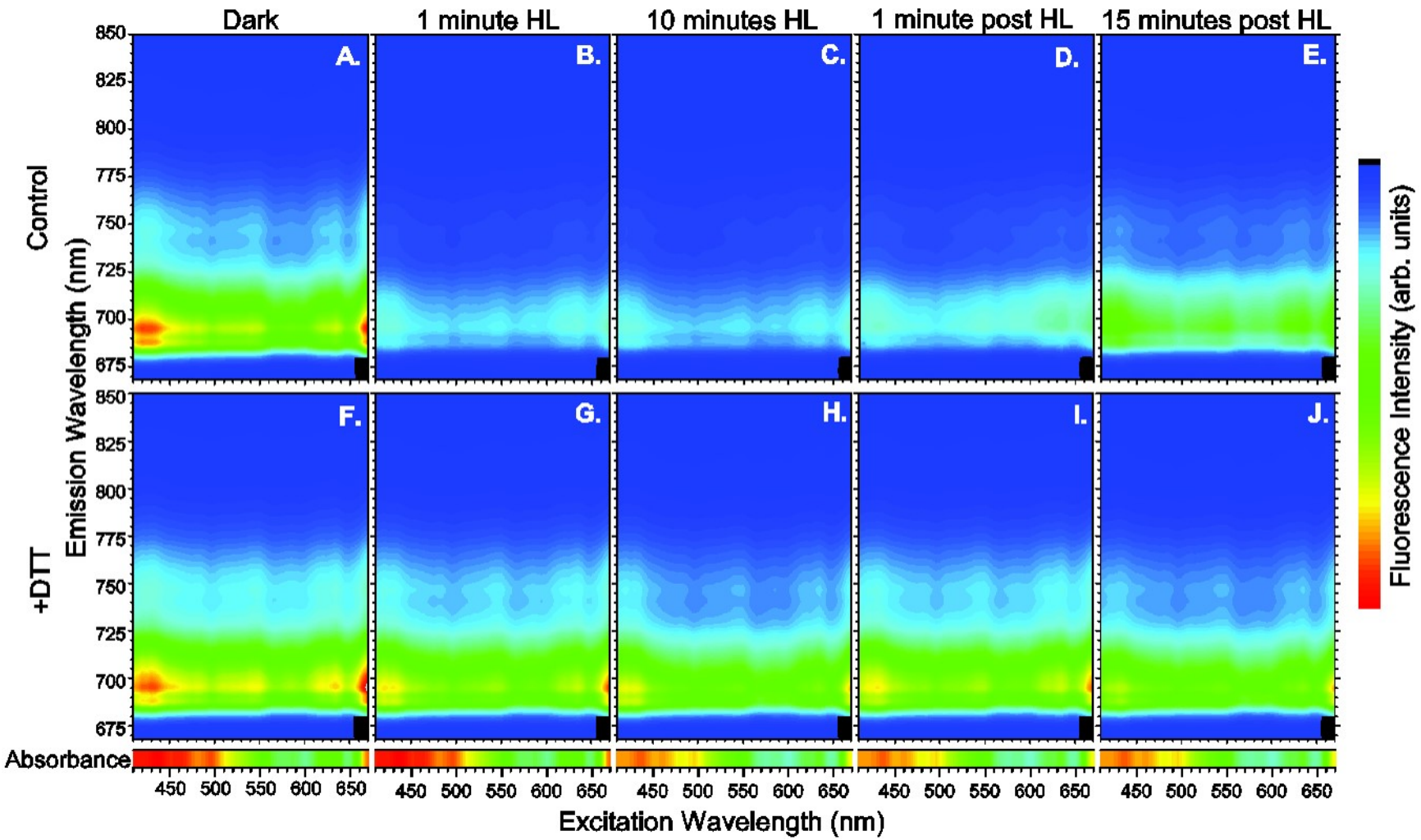

Figure 3.4-4 Contour plots of low temperature (77K) **excitation spectra for cell emission during a high light transition** for (**A** to **E**) control cells and (**F** to **J)** cells pretreated with 5.3 mM DTT (+DTT). Samples were collected at the high light (HL) transition time points indicated by the arrows in Figure 3.4-3. Fluorescence intensity scaling set to maximum obtained from dark adapted cells for control or +DTT sample sets. Shown are the averaged spectra from 3 separate cultures. Black plot area denotes no data collected. Spectra are fully corrected for instrument response and excitation intensity (see *Section 2.11-2* for details). Representative 77K absorbance spectra of dark adapted cells are shown in the lowest plot areas for comparison; intensity scaling the same as for fluorescence.

3.4-4 Loss of excitations during excess light

Excitation at all wavelengths gave emission spectra of very similar shape, implying a high interconnectivity between all the light harvesting pigment pools and emitters. The most distinguishable difference in spectral shape between excitation wavelengths was the height ratio of the ~688 nm (F688) and 695 nm (F695) fluorescence peaks (Figure 3.4-5A insert). 77K cell emission at 695 nm is primarily attributed to PSII cores and emission at ~688 nm is primarily attributed to fluorescing outer FCP complexes (see *Section 3.2-5)*. In dark adapted cells, 435 and 460 nm excitations yield the highest ratio of F688 to F695, whilst 600 nm excitation yields the lowest ratio (Figure 3.4-5A). HL induces a preferential decrease in sensitisation for F688 relative to F695 with all excitations (Figure 3.4-5A). So, it seems that PSII emission at 695 nm is preferentially excited at 600 nm as compared to the fluorescing FCP complexes, and that during

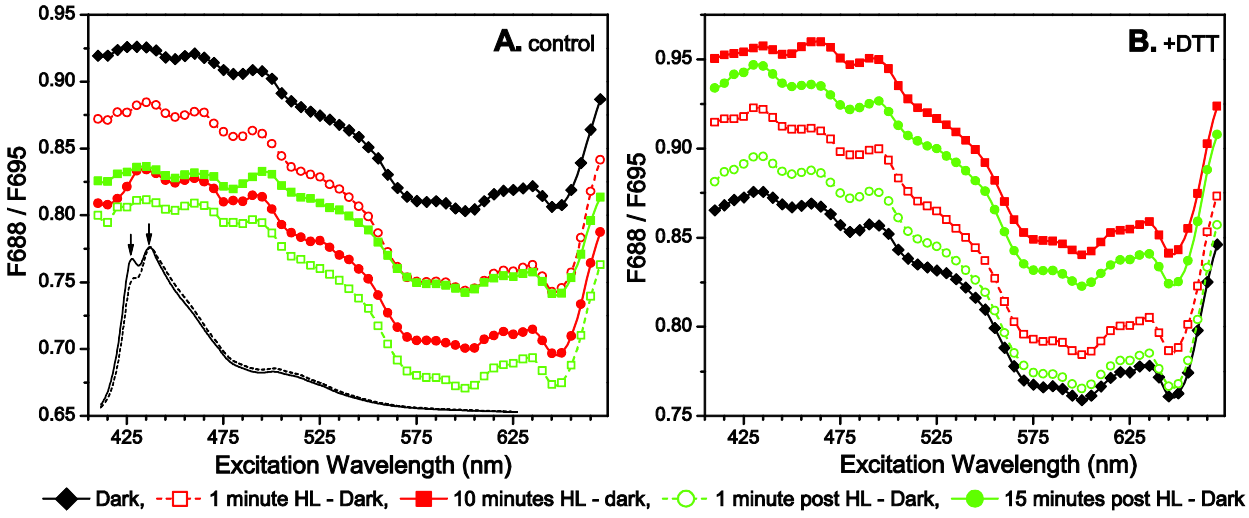

Figure 3.4-5 The dependence of low temperature (77K) **emission peak ratio on excitation wavelength and NPQ phase.** Samples were collected at the high light (HL) transition time points indicated in Figure 3.4-3. **A** & **B**, excitation spectra for the ratio of the secondary fluorescence peak/shoulder at ~688 nm (F688) to the primary fluorescence peak at 695 nm (F695) for control cells and cells pretreated with 5.3 mM DTT, respectively. Data points calculated from the averaged excitation spectra presented in Figure 3.4-4. The insert curves in A are sample emission spectra for dark adapted cells collected with 435 nm (solid line) and 600 nm excitations (broken line) normalised to their maximum emission peak. The positions of F688 and F695 are indicated by the arrows, respectively.

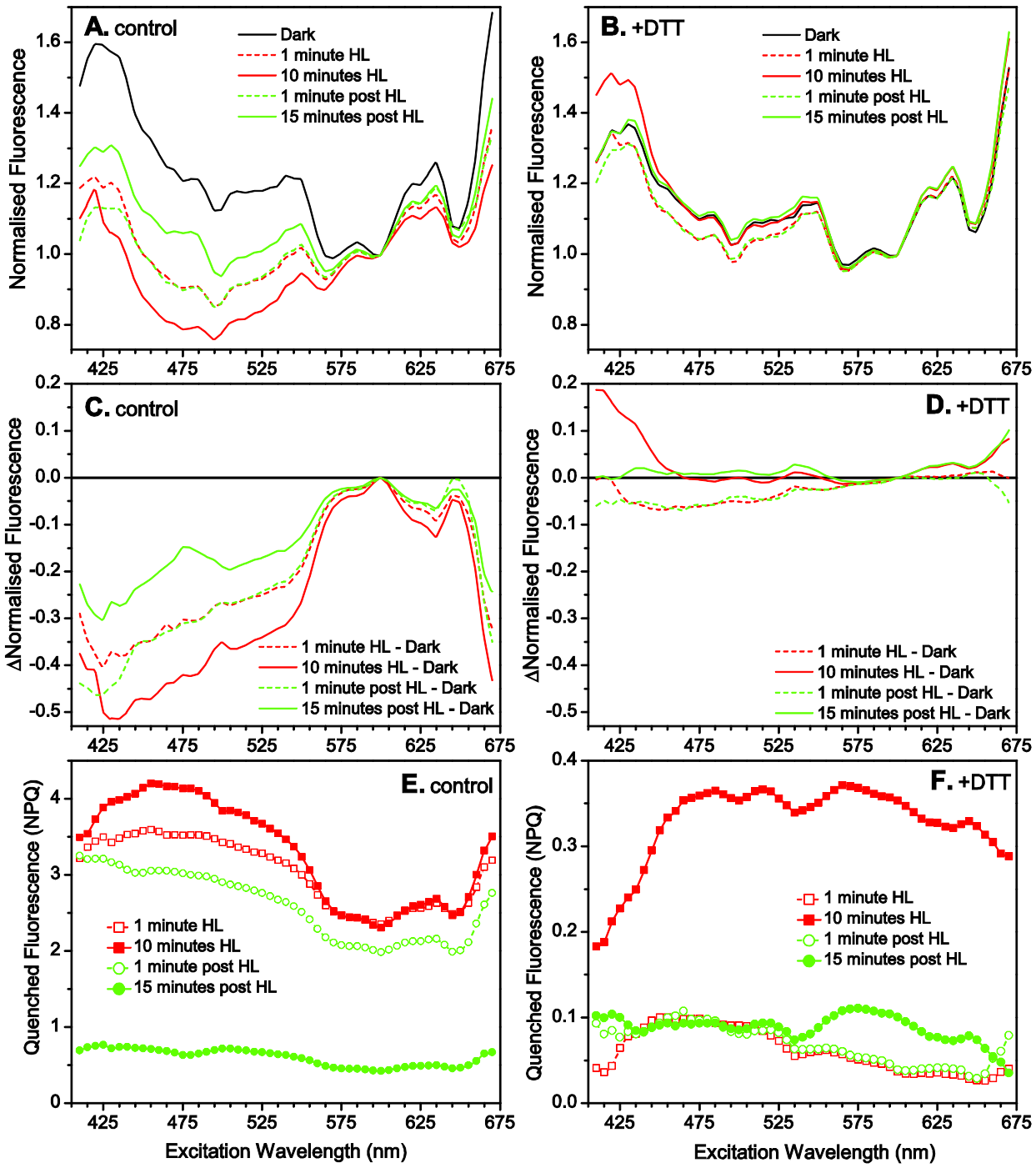

Figure 3.4-6 Low temperature (77K) excitation spectra for fluorescence quenching during a high light transition. Samples were collected at the high light (HL) transition time points indicated in Figure 3.4-3. **A** & **B**, excitation spectra for cell emission for control cells and cells pretreated with 5.3 mM DTT, respectively. Excitation spectra were calculated using integrated cell emission (from 680 to 930 nm) from the averaged spectra of 3 cultures presented in Figure 3.4-4 and have been arbitrarily normalised to the excitation wavelength of least sensitisation (600 nm). **C** & **D**, the HL treated *minus* dark adapted difference spectra of the spectra in A & B, respectively. **E** & **F**, quenching of fluorescence calculated from the non-normalised spectra in A & B, respectively, in terms of $\mathcal{NPQ}$ ($\mathcal{NPQ}$ = (fluorescence from dark adapted cells – fluorescence from light treated cells) / fluorescence from light treated cells).

the NPQ response the FCP complexes which fluoresce at ~688 nm are specifically targeted for quenching. With DTT pre-treatment, HL causes an enhancement in sensitisation for F688 relative to F695 (Figure 3.4-5B).

Excess light induces a loss of cell emission sensitisation to all excitation wavelengths absorbed by FCP antenna pigments. Excitations assignable to absorption by Chl *a* (at ~435 and 670 nm), Chl *c* (at ~460 and 635 nm), and carotenoids (blue-green region and especially the Fx absorption region from 500 to 550 nm) are lost in response to HL (Figure 3.4-6C). Pre-treatment with DTT inhibits all of these changes (Figure 3.4-6D).

The extent that individual excitations are quenched during HL was calculated from the low temperature emission spectra using the $\mathcal{NPQ}$ quenching parameter (Figure 3.4-6D). Excitations at 460 nm (absorbed by Chl *c*) are quenched the most during HL and excitations from ~500 to 550 nm (absorbed by Fx) are also highly quenched, whereas excitations at 600 nm are quenched the least. Thus, non-photochemical quenching most heavily quenches excitations absorbed by pigments within the FCPs.

3.4-5 Global analysis of excess light minus *dark 77K emission spectra across excitation wavelength*

To fully characterise the redistribution of excitation energy that occurs during the NPQ response, excess light induced changes to 77K emission spectral shape were next examined in detail. Subtracting the normalised (to area under the emission curve) emission spectra of dark adapted cells from that of HL treated cells reveals the redistribution of excitation energy between the emitter Chl *a*s that occur during NPQ: a positive difference peak indicates a relative enhancement in emission (as compared to total emission) at that energy level during

HL, a negative difference peak indicates a relative loss in emission (as compared to total emission) at that energy level during HL. Figure 3.4-7 examines the change in emission spectral shape during a HL transition with excitations at 460, 545, and 600 nm. 460 and 600 nm excitations have the largest difference in the amplitude that they are quenched (see Figure 3.4-6E) and produce the largest difference in emission spectral shape (see Figure 3.4-5A). 545 nm excitation was chosen as an intermediate between 460 and 600 nm and because it is a strong sensitizer to cell emission (see Figure 3.4-6A). The HL *minus* dark difference spectra in Figure 3.4-7 show that excitation energy redistribution varies depending on excitation wavelength and phase of NPQ. To determine the emitters responsible for excitation energy redistribution, the HL *minus* dark difference peaks were quantified by measuring their heights at 673 nm (ΔF673), 687 nm (ΔF687), 695 nm (ΔF695), 712 nm (ΔF712), and 734 nm (ΔF734). The wavelength positioning of the ΔFs was chosen so that they could be assigned to specific emitters. All ΔFs, (except for ΔF673) are identifiable as derivative resolved bands in the emission spectra prior to subtraction (*Supplemental Figure 3.4-1*). ΔF712 and ΔF734 were dually used to describe the broad, shifting positive difference peak centred around 720 nm, because the 712 and 734 nm emitter band positions best define the end points for this peaks migrating position. This positive difference peak is being modeled as a composite of two large bandwidth emission peaks centred at 712 and 734 nm. As previously discussed in *Section 3.4-2*, the positive ΔF673 can be attributed to an increase in emission from uncoupled Chl *a*, the negative ΔF687 can be attributed to a preferential quenching of outer FCP complexes, the negative ΔF695 can be attributed to a preferential quenching of PSII cores, and the broad positive difference peak

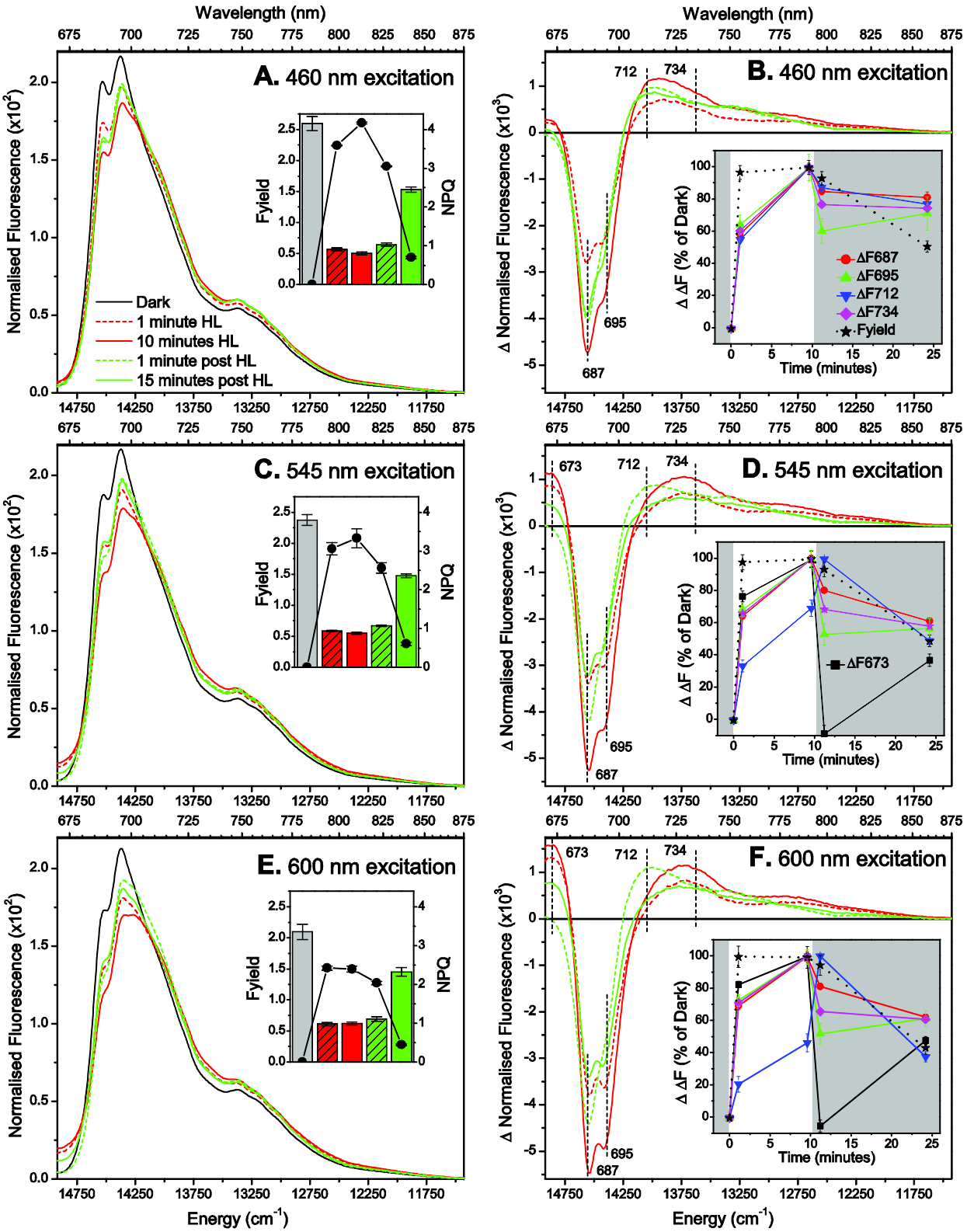

Figure 3.4-7 High light induced changes in low temperature (77K) emission spectral shape for control cells. Samples were collected at the high light (HL) transition time points indicated in Figure 3.4-3. **A**, **C**, & **E**, emission spectra normalised to integrated fluorescence (from 670 to 930 nm) obtained with

excitation at 460, 545, and 600 nm, respectively. The spectra shown are averaged from 3 separate cultures. The inserts show the change in integrated fluorescence yield (Fyield) between the non-normalised spectra (column plot) during HL with the corresponding $\mathcal{NPQ}$ values (scatter plot) for comparison. Grey column, dark; dashed red column, 1 minute HL; red column, 10 minutes HL; dashed green column, 1 minute post HL; green column, 15 minutes post HL. **B**, **D**, & **F**, the HL treated *minus* dark adapted difference spectra of the spectra presented in panels A, C, & E, respectively. Thin red lines, 1 minute HL – Dark; thick red lines, 10 minutes HL – Dark; thin green lines, 1 minute post HL – Dark; thick green lines, 15 minutes post HL – Dark. The position of fluorescence difference peaks (ΔFs) in nm are indicated by the dashed vertical lines. The inserts show the induction and relaxation kinetics for the ΔFs (no kinetics are plotted for the very weak ΔF673 in B); Fyield represents integrated fluorescence yield; white plot area indicates HL illumination, darkened plot area indicates dark conditions. Error bars represent ±1 standard deviation from the mean of three separate cultures.

defined by ΔF712 and ΔF734 can have mixed origins including a relative increase in PSI emission and weak emission from Chl *a*-Chl *a* quencher dimers.

A kinetic comparison of the induction and relaxation of the ΔFs in response to the HL transition (Figure 3.4-7B, D, & F inserts) revealed that ΔF685, ΔF695, and ΔF734 share the same induction kinetics during illumination and relax to the same comparable level 15 minutes after the end of illumination, yet ΔF695 relaxes noticeably faster within one minute upon cessation of illumination. Also of note is how ΔF673 collapses completely at one minute post HL but then moderately regrows during the post HL period. ΔF712 shows similar induction kinetics to the other ΔFs with 460 nm excitation, but with 545 and 600 nm excitations rises quickly upon the initial transition away from HL. The redistribution of excitation energy that is being described by the difference peaks does not fully kinetically describe the non-photochemical quenching that occurs in response to excess light. The loss of fluorescence yield measured at 77K in the cell samples increased noticeably faster upon HL illumination than any of the ΔFs (Figure 3.4-7B, D, & F inserts). This could stem from the quenching apparatus being more efficient at collecting and non-radiatively dissipating excitations during the initial transition to HL than during steady state HL conditions.

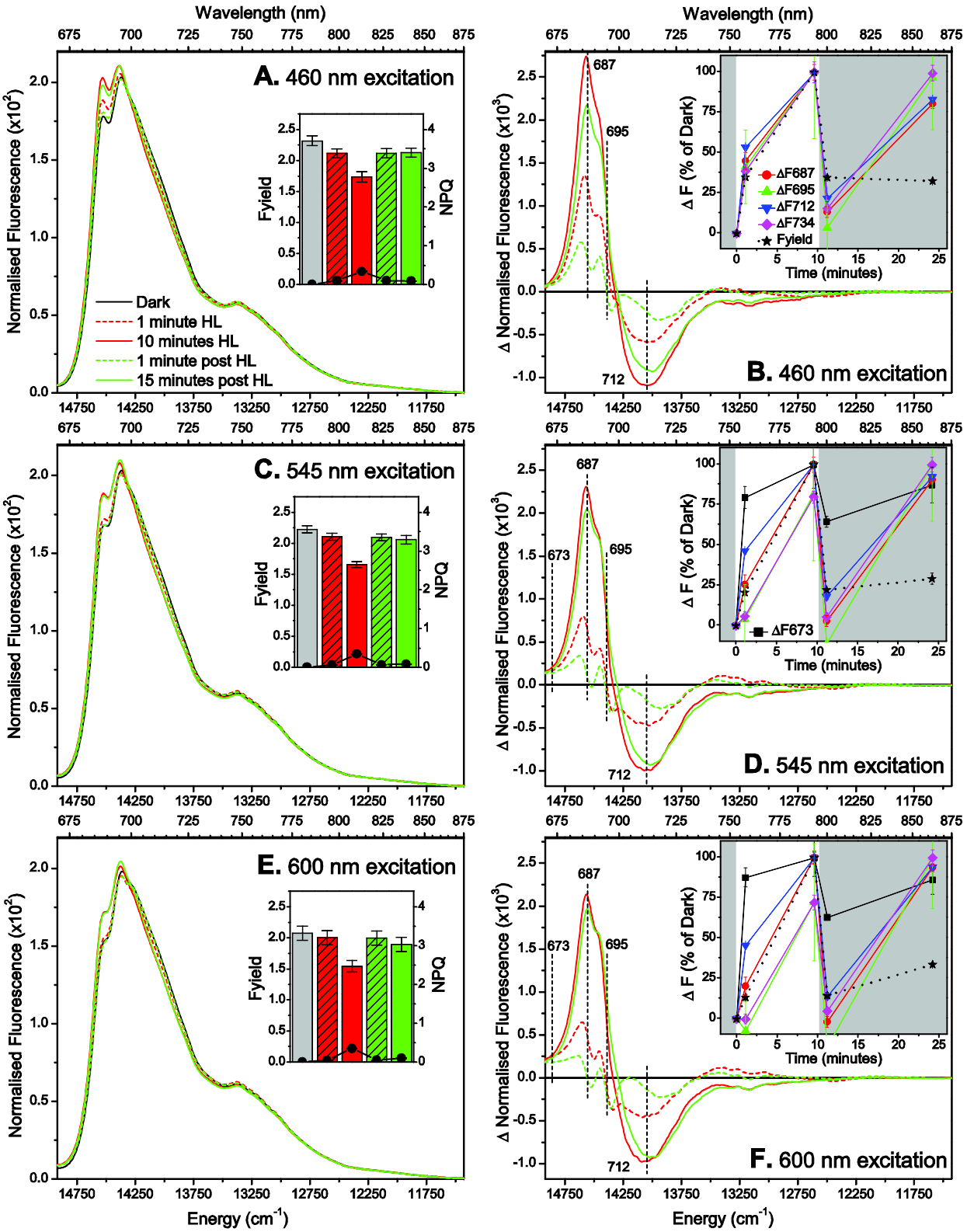

Figure 3.4-8 High light induced changes in low temperature (77K) emission spectral shape for cells pretreated with DTT (5.3 mM). Samples were collected at the high light (HL) transition time points indicated in Figure 3.4-3. **A**, **C**, & **E**, emission spectra normalised to integrated fluorescence (from 670 to

930 nm) obtained with excitation at 460, 545, and 600 nm, respectively. The spectra shown are averaged from 3 separate cultures. The inserts show the change in integrated fluorescence yield (Fyield) between the non-normalised spectra (column plot) during HL with the corresponding $\mathcal{NPQ}$ values (scatter plot) for comparison (scaling same as in Figure 3.4-7). Grey column, dark; dashed red column, 1 minute HL; red column, 10 minutes HL; dashed green column, 1 minute post HL; green column, 15 minutes post HL. **B**, **D**, & **F**, the HL treated *minus* dark adapted difference spectra of the spectra presented in panels A, C, & E, respectively. Thin red lines, 1 minute HL – Dark; thick red lines, 10 minutes HL – Dark; thin green lines, 1 minute post HL – Dark; thick green lines, 15 minutes post HL – Dark. The position of the fluorescence difference peaks (ΔFs) identified in Figure 3.4-7 (in nm) are indicated by the dashed vertical lines. The inserts show the induction and relaxation kinetics for the ΔFs (no kinetics are plotted for the very weak ΔF673 in B); Fyield represents integrated fluorescence yield; white plot area indicates HL illumination, darkened plot area indicates dark conditions. Error bars represent ±1 standard deviation from the mean of three separate cultures.

Inhibition of qE_{nonXC} with DTT pre-treatment prevents all of the HL elicited changes in low temperature cell emission spectral shape that were observed in the non-treated cells. In response to HL, there is now a relative increase in cell emission at ~687 and 692 nm and a decrease in low energy emission peaking at ~712 nm (Figure 3.4-8): much of the opposite response of that observed during NPQ in non-treated cells. The spectral structure within the positive difference region suggests that an additional emitter located between the 687 and 695 nm emission bands is participating in the redistribution of excitation energy. The redistribution of excitation energy in the presence of DTT does not include emissions at wavelengths ≥750 nm. Also, whereas 600 nm excitation gave the largest difference peaks in the untreated cells, 460 nm excitation gave the largest difference peaks in the +DTT cells. The changes in emission shape that develop in the absence of qE_{XC} relax quickly once HL is removed but then grow during the subsequent 15 minute dark period in disjuncture of changes to fluorescence yield (Figure 3.4-8B, D, & F inserts), indicating that the redistribution of excitation energy post HL in the absence of qE_{XC} does not contribute to quenching of excitation energy. To recapitulate, the

non-photochemical quenching performed in the absence of qE_{XC} does not involve the same excitation energy redistribution processes that occur with an active qE_{XC}.

Next the dependence of excitation energy redistribution on excitation wavelength was investigated by creating excitation spectra for the fluorescence difference peaks (ΔFs), so as to give information on what pigments are actively involved in the excitation energy redistribution pathways. The ΔF excitation spectra in Figures 3.4-9 (and Figure 3.4-10 for DTT pretreated cells) reveal subtle changes in emitter sensitisation in response to HL. If all excitations are equally affected by the excitation energy redistributions that are responsible for the ΔFs, then the spectra in Figures 3.4-9 & 10 will have no spectral shape (they will be flat). Excitations more strongly sensitising a ΔF will appear as peaks whereas excitations less strongly sensitising a ΔF will appear as troughs, thus signifying which sensitising pigments are connected to which energy redistribution pathways. Distinct sub-populations of one type of pigment may contribute differently to the excitation of an emitter. For example: a strong troughing in the ΔF excitation spectra corresponding to regions of Chl *a* absorption at 435 nm, and especially at 670 nm, would indicate that a subpopulation of Chl *a* is not involved in the excitation energy redistribution pathway responsible for the formation of that ΔF.

Different excitations participate differently in the excitation energy redistribution pathways that develop in response to HL. All ΔFs show a heterogeneous dependency on excitation wavelength that varies depending on the phase of NPQ (Figure 3.4-9). The troughing structure of the excitation spectra for ΔF673, ΔF687, ΔF695 (and less clearly for ΔF734) suggests that a substantial percentage of Chl *a* (absorbing at 435 and 670 nm), Chl *c* (absorbing at 460

nm), and a diverse population of Fx molecules (absorbing from ~490 to 550 nm), and possibly DD cycle pigments (absorbing at 490 nm), do not participate in the energy redistribution (i.e. quenching) pathways responsible for forming these ΔFs. Conversely, excitations absorbed at ~575 to 600 nm are redistributed the most between the ΔFs. Energies at ~575 to 600 nm correspond to the weakly absorbing Chl Q_x transitions. However, if Chl *a* is the sensitising pigment responsible for the high magnitude ΔFs, then the regions of high absorptivity by Chl *a*, especially at the 670 nm Q_y band, should provide the highest ΔFs. Instead, the pigments responsible for absorbing these heavily regulated excitations are being ostensibly assigned to deeply red shifted Fx. The excitation spectra for ΔF712 is somewhat reversed of the other ΔFs, showing least sensitisation with excitations at ~575 to 600 nm (Figure 3.4-9D). When cells are pretreated with DTT, the excitation spectra for ΔF687, ΔF695, and ΔF734 now show a broad peak for maximum excitation redistribution during HL at ~480 nm (Figure 3.4-9), much to the opposite of what was witnessed in the untreated cells.

If a ΔF shares the same sensitising pigment pool with another ΔF, they are predicted to share the same excitation spectra. A cross correlation analyses was performed between the different ΔF excitation spectra (Table 3.4-1). ΔF interdependencies on excitation wavelength vary between ΔF pairs and between NPQ phases. The high correlation coefficients observed between ΔF pairs at the induction of NPQ (at 1 minute HL) implies that all ΔFs are initially sensitised by the same pigment pool. During steady state illumination (at 10 minutes HL) a few of the correlation coefficients noticeably weaken (Table 3.4-1): suggesting that ΔF687 and ΔF673 share less of a common pigment pool and that the pigment pool sensitising ΔF712 becomes detached from that of ΔF687 and Δ734. Post HL, the excitation spectra for the ΔFs

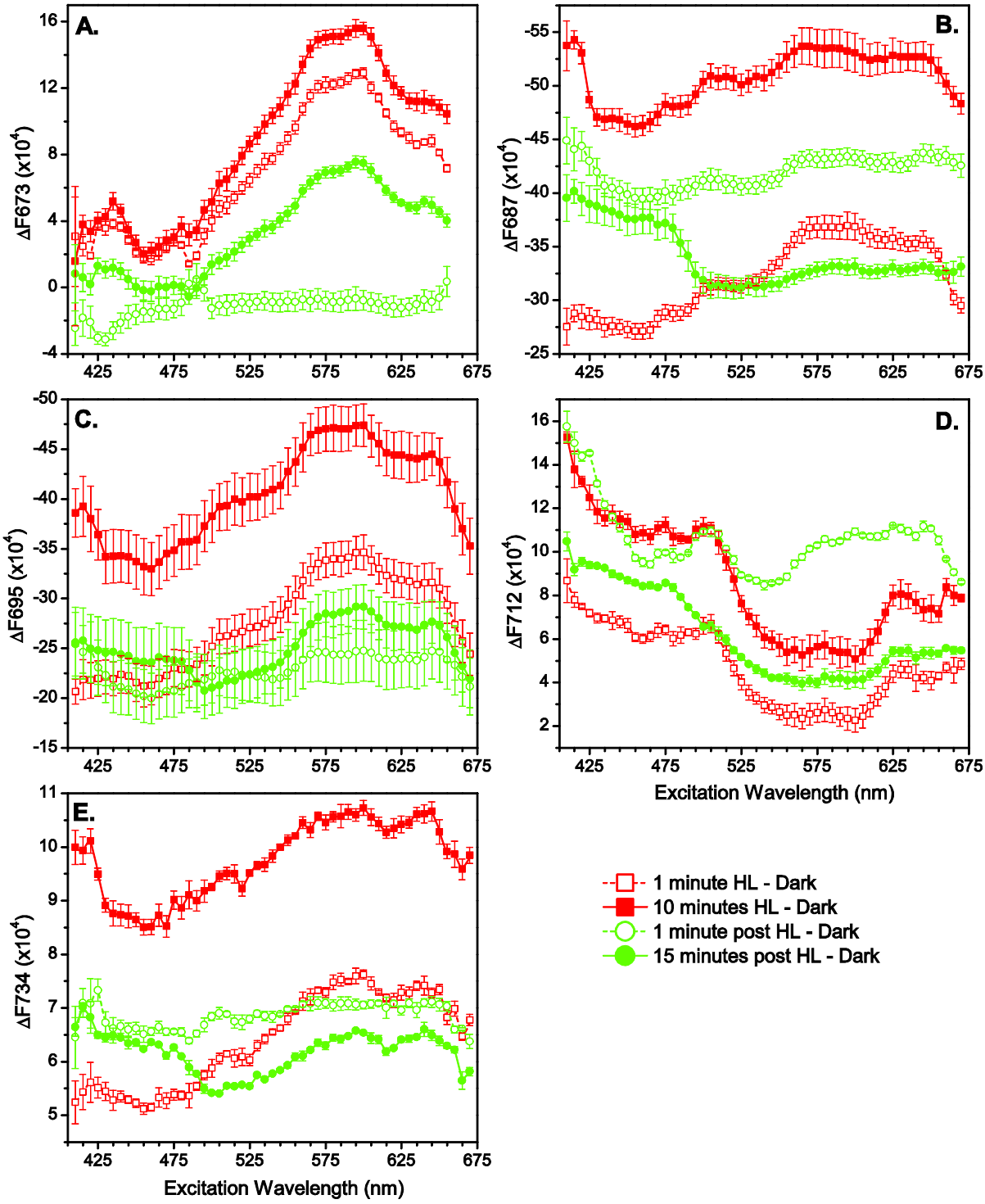

Figure 3.4-9 Excitation spectra for high light induced changes in low temperature (77K) **emission spectral shape for control cells (ΔF excitation spectra).** Samples were collected at the high light (HL) transition time points indicated in Figure 3.4-3. **A** to **E**, the dependence of ΔF673, ΔF687, ΔF695, ΔF712, & ΔF734 on the excitation wavelength used for collection of emission spectra. ΔFs calculated as described in Figure 3.4-7. The negative ΔFs in B & C have been plotted on a reverse y-axis for ease of comparison to the other panels. Error bars are ± 1 standard deviation from the mean of 3 separate cultures.

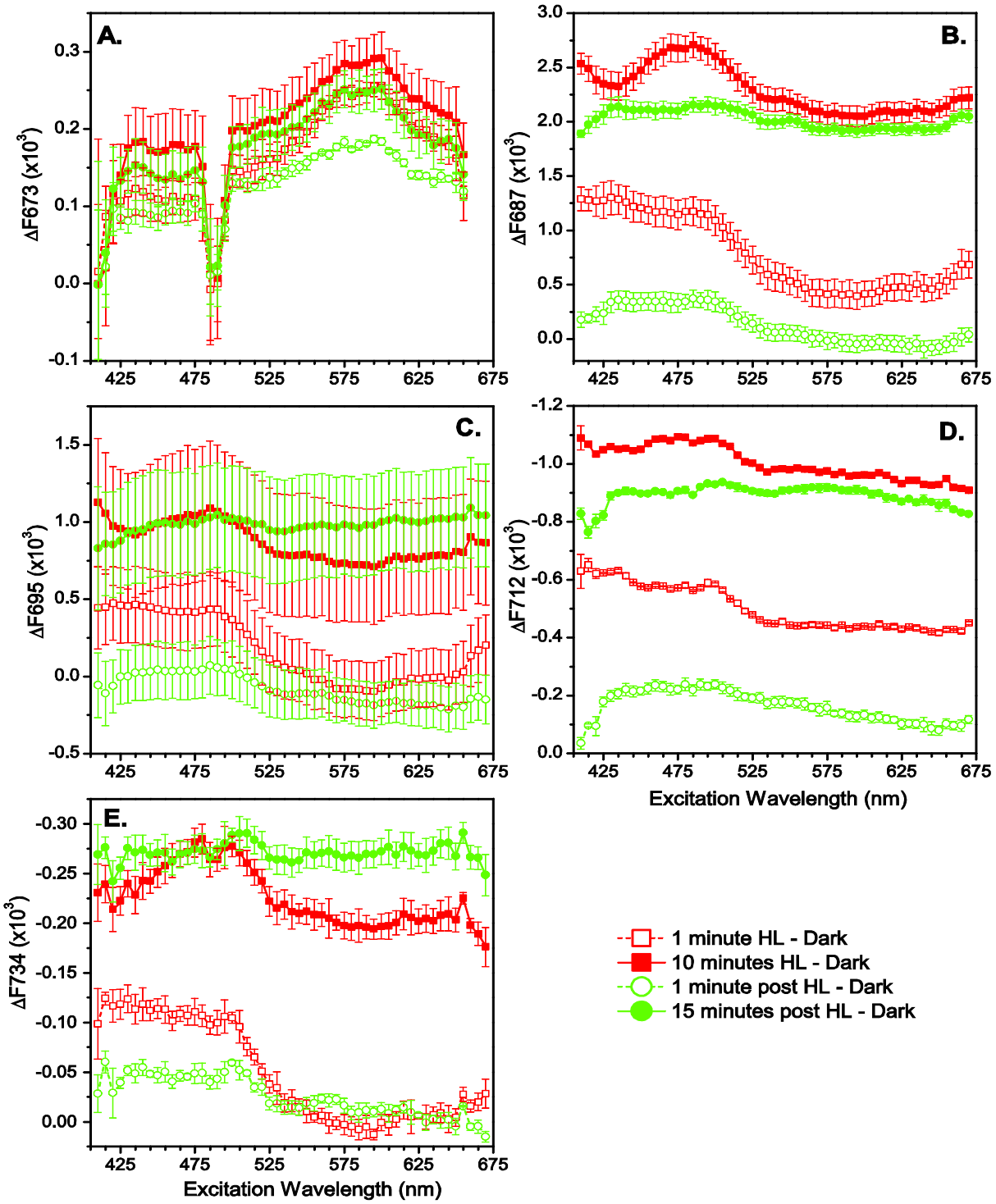

Figure 3.4-10 Excitation spectra for high light induced changes in low temperature (77K) **emission spectral shape for cells pretreated with DTT** (5.3 mM) **(ΔF excitation spectra).** Samples were collected at the high light (HL) transition time points indicated in Figure 3.4-3. **A** to **E**, the dependence of ΔF673, ΔF687, ΔF695, ΔF712, & ΔF734 on the excitation wavelength used for collection of emission spectra. ΔFs calculated as described in Figure 3.4-8. The negative ΔFs in D & E have been plotted on a reverse y-axis for ease of comparison to the other panels. Error bars are ± 1 standard deviation from the mean of 3 separate cultures.

Table 3.4-1 Matrix plot correlation analysis summary for ΔF excitation spectra. The interdependence of the ΔFs in Figures 3.4-9 & 10 across excitation wavelength are summarised below. The independent variable (x-axis values) for the analysis is indicated by column, the dependent variable (y-axis values) is indicated by row. High light (HL) transition time points as indicated in Figure 3.4-3. Values highlighting the relationship between ΔF687, ΔF695, and ΔF734 in the control (non-DTT treated) samples are underlined.

	Pearson's r value							
	control				**+DTT**			
	ΔF673	**ΔF687**	**ΔF695**	**ΔF712**	**ΔF673**	**ΔF687**	**ΔF695**	**ΔF712**
1 minute HL								
ΔF687	-0.962				-0.858			
ΔF695	-0.975	0.994			-0.875	0.997		
ΔF712	-0.910	0.870	0.895		0.789	-0.982	0.970	
ΔF734	0.957	-0.990	-0.988	-0.862	0.842	-0.993	0.994	0.973
10 minutes HL								
ΔF687	-0.761				-0.746			
ΔF695	-0.959	0.901			-0.855	0.958		
ΔF712	-0.931	0.559	0.830		0.679	-0.919	-0.928	
ΔF734	0.866	-0.944	-0.954	-0.694	0.604	-0.956	-0.879	0.890
1 minute post HL								
ΔF687	0.142				-0.714			
ΔF695	-0.080	0.969			-0.675	0.987		
ΔF712	-0.630	-0.513	-0.370		0.210	-0.783	-0.825	
ΔF734	0.120	-0.749	-0.762	0.024	0.635	-0.933	-0.906	0.724
15 minutes post HL								
ΔF687	0.615				-0.481			
ΔF695	-0.786	-0.133			0.204	0.106		
ΔF712	-0.882	-0.884	0.443		-0.421	-0.270	-0.564	
ΔF734	0.152	-0.574	-0.728	0.151	0.144	-0.132	-0.509	0.291

become more different with a seemingly loss of interconnection between their sensitising pigment pools within 1 minute of the transition away from HL (except for ΔF687 and ΔF695 continuing to target the same excitations at 1 minute post HL) (Table 3.4-1). These results suggest there is a restructuring of the antenna system during HL illumination: from a shared pigment pool between the emitters during the initial transition to HL to a partial fragmentation

of the pigment pool during the maturation of NPQ at steady state HL conditions. The heterogeneity of the sensitising pigment pool for the ΔFs expands even more during the relaxation of NPQ post HL, suggesting a disordering of the antenna system. In summary, the ΔF excitation spectra results advocate that there is a measurable degree of heterogeneity within/ between FCP complexes in terms of their participation in the excitation energy redistribution pathways that form during the different phases of NPQ. Recently, Gundermann et al. (2013) has identified multiple, mixed composition FCP populations in *Phaeodactylum tricornutum*.

3.4-6 Deconvolution of 77K emission spectra

The preceding analyses of 77K emission spectra and excitation spectra for 77K emission revealed that emissions at 687, 695, and ≥712 nm are specifically targeted during NPQ. Yet, strictly comparing the fluorescence intensities at emission wavelengths that are dominated by emission from a specific emitter has its limits. Cell emission at any given wavelength arises from multiple emitter species and thus has to be interpreted as a sum of individual emission bands. To gain a better understanding of how excitation energy is actually redistributed between the individual emitters in response to HL, the individual emission bands need to be pulled out of the emission spectra. Fluorescence at low temperature will predominantly arise from the lowest energy level (i.e. most red) Chl *a* within an energy compartment made up of a pool of tightly coupled pigments. Excitons entering an energy compartment will reach thermal equilibrium settling upon the S_1 state of the lowest energy pigment. The rate constant for energy transfer out of the compartment is much slower than the rate of energy transfer within the compartment, so the lowest energy level pigment is maintained in an excited state long enough to increase the probability of emitting a photon as fluorescence. These local low

energy pigments are termed terminal emitters because they are the end point in that excitation energy transfer pathway, and thus fluoresce the most heavily. There are three principle pigment compartments that can be identified by their terminal emitter emission at 77K in *Nitzschia* cells: PSII, PSI, and extrinsic (outer antenna) FCP complexes. The PSII and PSI compartments also contain FCP complexes, but since these inner antenna FCP complexes are tightly coupled to the photosystems they are highly efficient at energy transfer to the photosystems and thus contribute weakly on their own to total cell emission. Deconvoluting emission spectra into a series of Gaussian shaped emission bands allows one to decipher how much each individual terminal emitter contributes to total cell emission.

77K emission spectra of *Nitzschia* cells were fit to a set of 12 Gaussians. Gaussian centre positions were chosen by second derivative analysis of emission spectra with 5 nm resolution (*Supplemental Figure 3.4-1*). Gaussians with centre positions of 681 and 780 nm were included in the fitting even though the 681 and 780 nm positions were somewhat poorly resolved in the derivatives, because including these Gaussians greatly improved fitting at the ends of the emission spectra. The 681 nm peak did resolve in the emission spectra when using a 2 nm derivative resolution (data not shown). Emission spectra had their x-axes transformed to inverted wavenumbers (cm^{-1}) prior to fitting to permit the use of symmetrical shaped Gaussians. FWHM values were calculated from dark adapted cell emission spectra (not from DTT pre-treatment) using a fitting routine where Gaussian centre position was fixed and the FWHM parameter was floating. During the fitting procedure for all other samples (including those with DTT pre-treatment) only Gaussian amplitude was free floating; all other parameters were fixed. Fitting parameters and Gaussian assignments are summarised in Table 3.4-2. The

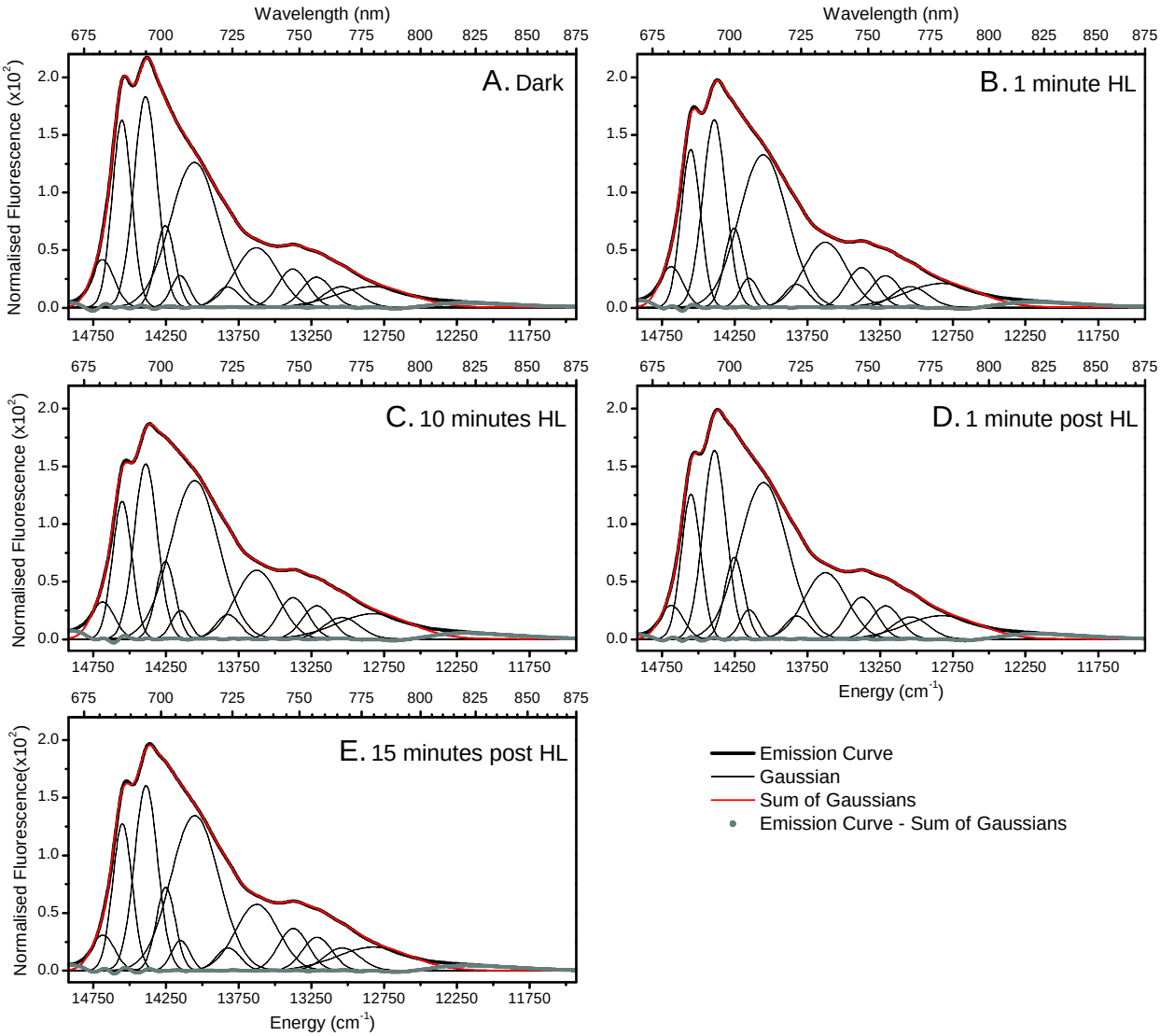

Figure 3.4-11 Gaussian deconvolution of low temperature (77K) emission spectra for control cells. **A** to **E**, emission spectra collected with 460 nm excitation at the high light (HL) transition time points indicated in Figure 3.4-3 were normalised to integrated fluorescence and fit to a set of Gaussians according to the parameters listed in Table 3.4-2. Fitting was performed on the averaged emission spectra from 3 separate cultures.

fitted emission spectra are presented in Figure 3.4-11 (and for DTT pretreated cells in Figure 3.4-12). The Gaussian centred at 780 nm is somewhat of an artifact of fitting the emission tail of the spectra; its wide bandwidth would represent a mixture of vibrational sub-bands. No Gaussian representing a 685 nm PSII emission band was included in the fits because PSII emission at 685 nm does not seem to contribute substantially to *Nitzschia* cell emission at 77K

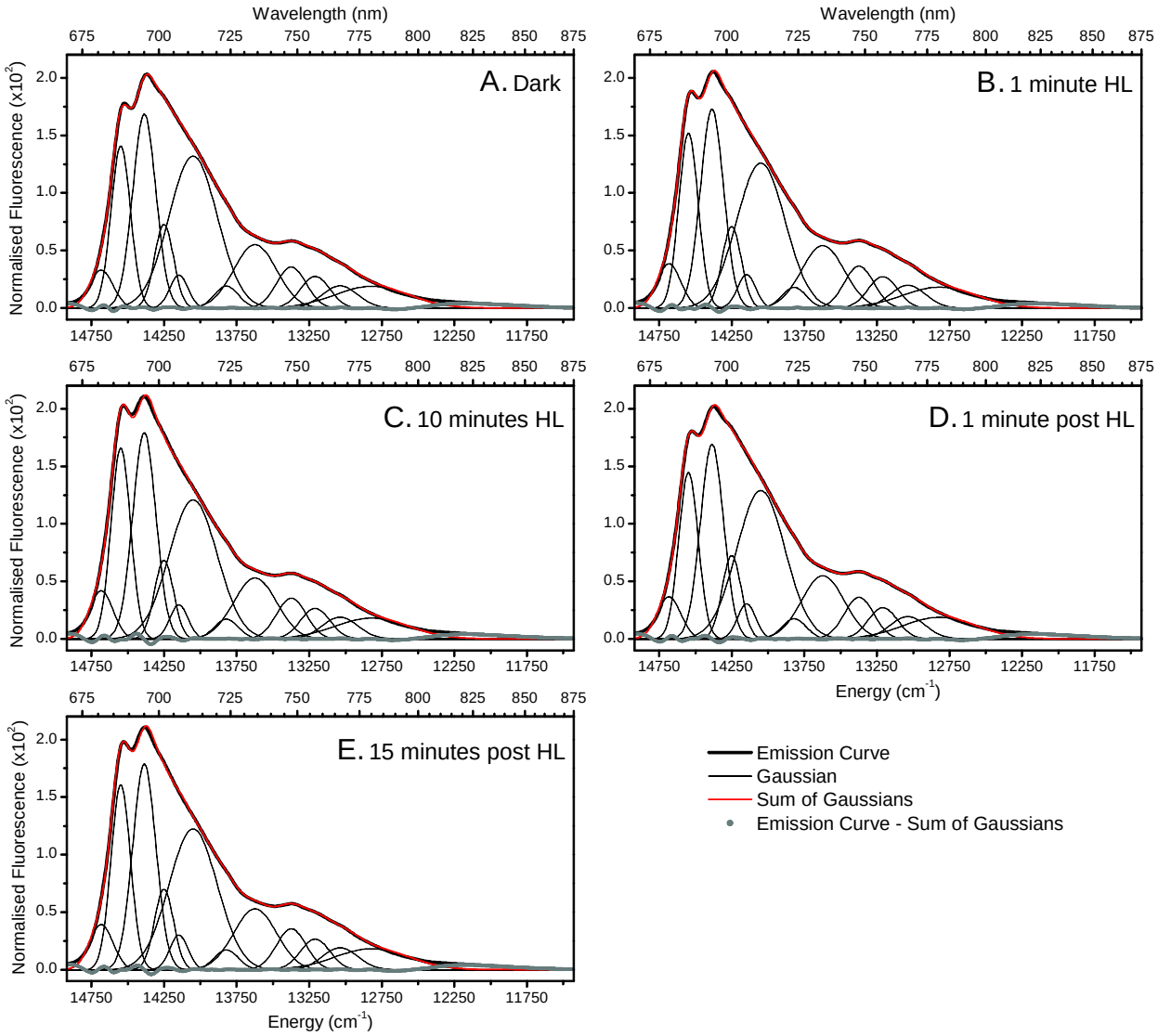

Figure 3.4-12 Gaussian deconvolution of low temperature (77K) emission spectra for cells pretreated with DTT (5.3 mM). **A** to **E**, emission spectra collected with 460 nm excitation at the high light (HL) transition time points indicated in Figure 3.4-3 were normalised to integrated fluorescence and fit to a set of Gaussians according to the parameters listed in Table 3.4-2. Fitting was performed on the averaged emission spectra from 3 separate cultures.

(see *Section 3.2-5*). The addition of a Gaussian centred at 685.0 nm did not improve the fitting of emission spectra across sample sets, as determined by comparing the distribution of residuals (data not shown). The sum of the area fitted by the individual Gaussians accounted for ≥98% of the area under the emission curve from 670 to 930 nm for all fits. Gaussian areas are reported as a percentage of the cumulative fitted area. The fits are quite logical in

distributing emission between the emitters, with the most cell emission originating from the terminal emitters of the outer FCP (Gaussian centred at 687 nm), PSII (Gaussian centred at 695 nm), and PSI (Gaussian centred at 712 nm) (Table 3.4-2). According to the fits, the PSI assigned emitter at 712 nm is responsible for the single greatest emission among all the emitters at 77K, which is consistent with an interconnection between the PSII and PSI antenna. The results from Gaussian fitting of emission spectra were not used to create excitation spectra for the individual emitter bands because the ~2% error associated with the fitting was on an order equivalent to the changes in fitted Gaussian area between excitation wavelengths.

Table 3.4-2 Fit parameters for the Gaussian deconvolution of low temperature (77K) emission spectra collected with 460 nm excitation. PkArea, percentage of total fitted area under the emission curve that is apportioned to the area under an individual Gaussian.

Gaussian	Centre (cm^{-1})	Centre (nm)	FWHM (cm^{-1})	PkArea dark cells (% total emission)	Principle Assignment
1	14684	681.0	189.2	4.3	FCP
2	14550	687.3	156.8	13.9	FCP
3	14388	695.0	188.2	18.8	PSII
4	14252	701.7	154.1	6.0	FCP
5	14149	706.8	146.9	2.2	FCP
6	14051	711.7	389.8	26.8	PSI
7	13822	723.5	193.2	1.9	PSI
8	13624	734.0	345.0	9.8	vibrational
9	13374	747.7	238.1	4.3	vibrational
10	13210	757.0	237.1	3.4	vibrational
11	13038	767.0	288.2	2.8	vibrational
12	12821	780.0	600.0	5.9	vibrational (composite)

The HL induced redistribution of emission between the Gaussian modeled individual emitters for control and DTT pre-treated cells are summarised in Figure 3.4-13. With an active qE_{XC} (i.e. without DTT) there was a loss in emission contribution from all the Gaussian defined emitters with centre positions ≤ 707 nm, corresponding to all FCP and PSII assignable non-vibrational emitter bands, and there was an increase in emission contribution from all lower energy Gaussian defined emitter bands. The loss in emission by the 687 and 695 nm centred bands and the increase in emission by the 712 and 734 nm centred bands accounted for ~70% of the redistribution in emission that occurred in response to HL (Figure 3.4-13A to D). With qE_{XC} inactivated by DTT pre-treatment, there was essentially the reversed effect: the higher energy emitter bands now contributed more to total emission whereas the lower energy bands contributed less. With DTT, increase in emission by the 681, 687, and 695 nm centred bands and loss in emission by the 712 nm centred band were responsible for ~70 to 80 % of the emission redistribution that occurred in response to HL (Figure 3.4-13E to H).

The kinetics for the HL induced redistribution of emission between the Gaussian modeled individual emitters for control and DTT pre-treated cells are summarised in Figure 3.4-14. During the induction of NPQ, the loss in emission from the 687 and 695 nm centred Gaussians and gain in emission from the 712 and 734 nm centred Gaussians proceeded at an equivalent rate; however, during the initial transition away from HL, emission from the 695 nm centred Gaussian recovered slower than the other Gaussians (2.8 times slower than the 695 nm Gaussian), and never relaxed to the extent that the other Gaussians did at 15 minutes post HL (Figure 3.4-14C). Notably, the loss in fluorescence yield that occurred during HL illumination proceeded faster than the redistribution of emission between the Gaussians (Figure 3.4-14C).

A. control, 1 minute HL - Dark

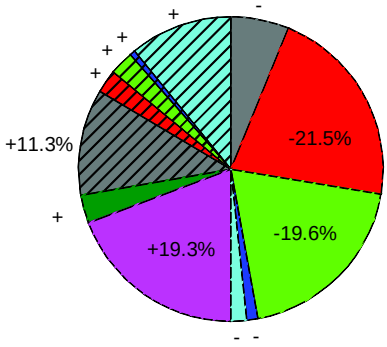

B. control, 10 minutes HL - Dark

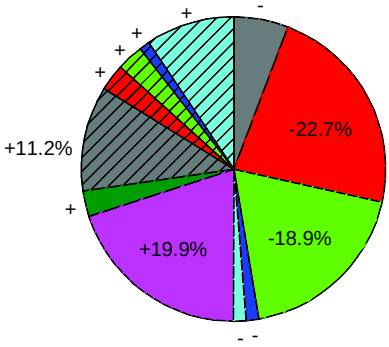

C. control, 1 minute post HL - Dark

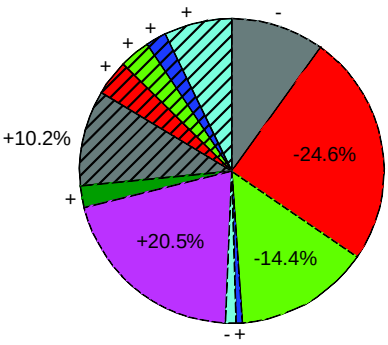

D. control, 15 minutes post HL - Dark

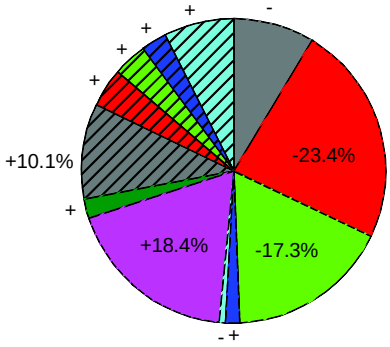

E. +DTT, 1 minute HL - Dark

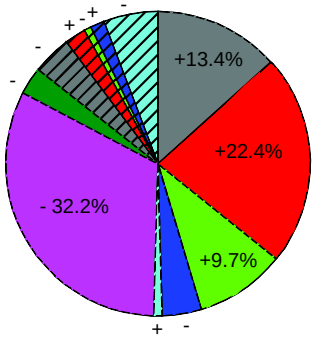

F. +DTT, 10 minutes HL - Dark

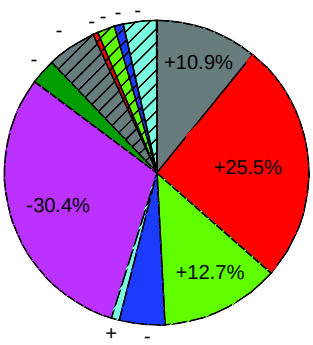

G. +DTT, 1 minute post HL - Dark

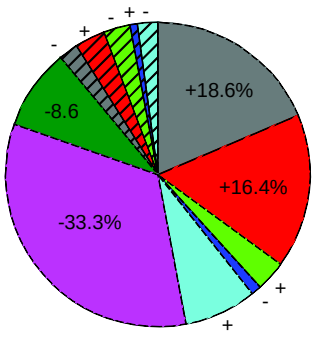

H. +DTT, 15 minutes post HL - Dark

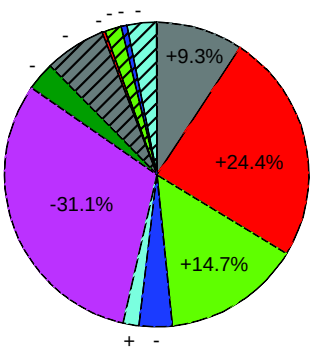

(previous page) **Figure 3.4-13 Redistribution of cell emission amongst individual emitters during a high light transition as deduced from fitting of low temperature (77K) emission spectra to a set of Gaussians.** The high light (HL) transition time points correspond to those labeled in Figure 3.4-3. Deconvolution of emission spectra (Figures 3.4-11 & 12) were used to obtain areas under the individual Gaussians. The Gaussian areas from HL treated cells *minus* the Gaussian areas from dark adapted cells are shown expressed as % of total area under the emission curve. Loss in Gaussian area in response to HL is indicated by (-), gain in area is indicated by (+). **A** to **D** for control cells. **E** to **H** for cells pretreated with 5.3 mM DTT. The four Gaussians most responsible for the redistribution of emission are labeled in percentage of the cumulative change in emission from all Gaussians. Gaussians predominantly assigned to vibrational bands are indicated by the shaded plot areas.

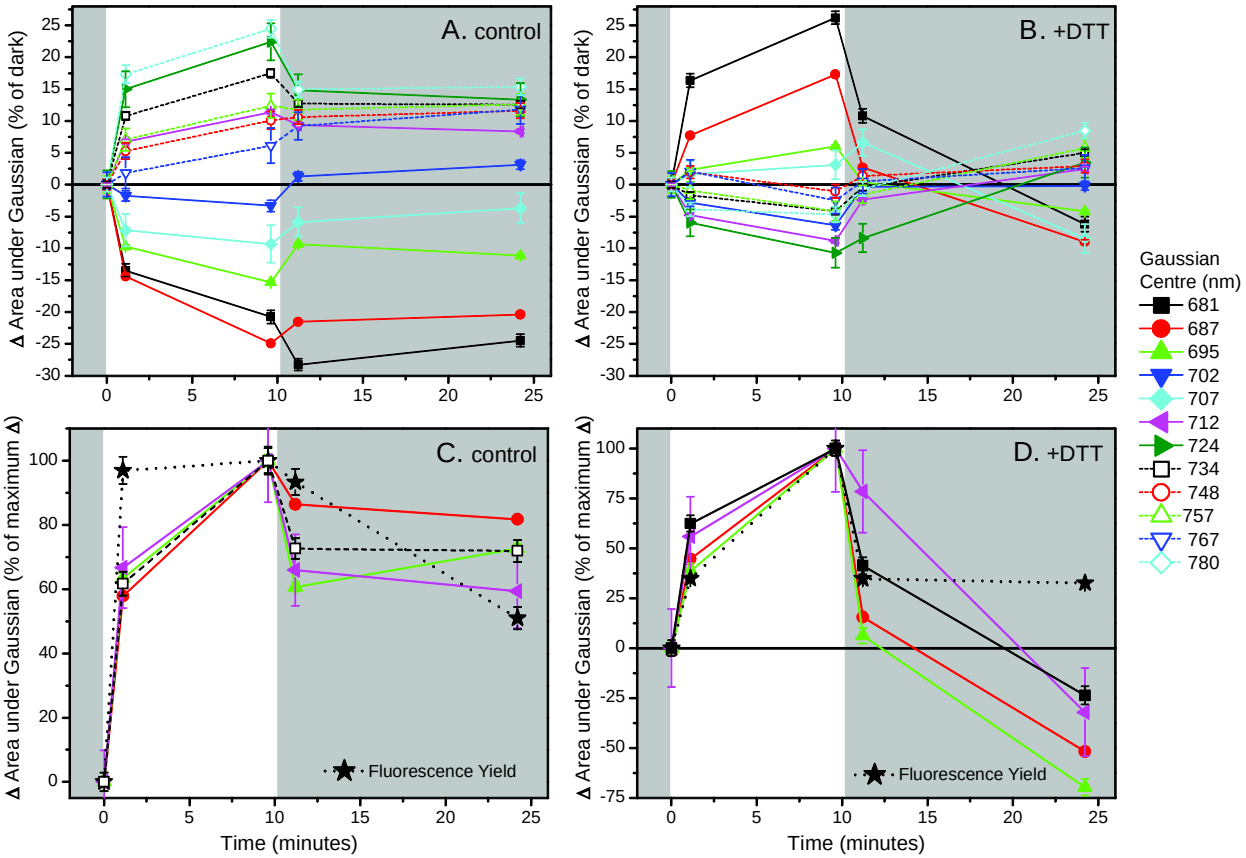

Figure 3.4-14 Induction and relaxation kinetics for the redistribution of emission between individual emitters during a high light transition as deduced from fitting of low temperature (77K) emission spectra to a set of Gaussians. The high light (HL) transition time points correspond to those labeled in Figure 3.4-3. White plot area indicates HL illumination; darkened plot area indicates dark conditions. Deconvolution of emission spectra (Figures 3.4-11 & 12) were used to obtain areas under the individual Gaussians expressed as % of total area under the emission curve. The change in Gaussian area in response to HL is given for **A**, control cells and **B**, cells pretreated with 5.3 mM DTT. Gaussians predominantly assigned to vibrational bands are indicated by the open symbol shapes. **C** & **D**, induction and relaxation kinetics for the Gaussians that contribute the most to the redistribution of emission (see Figure 3.4-13) in control cells and cells pretreated with DTT, respectively. Fluorescence yield from the samples at 77K is given for reference. Error bars represent standard errors from the fitted Gaussian peak area.

In the presence of DTT, the changes in emission between the 681, 687, 695, and 712 nm centred Gaussians corresponded kinetically to the weak loss in fluorescence yield that occurred during the HL illumination period (Figure 3.4-14D). With DTT post HL, the loss in emission by the 712 nm centred Gaussian initially recovered slower than the changes in the 681, 687, and 695 nm centred Gaussians, but relaxed to a comparable level at 15 minutes post HL (Figure 3.4-14D).

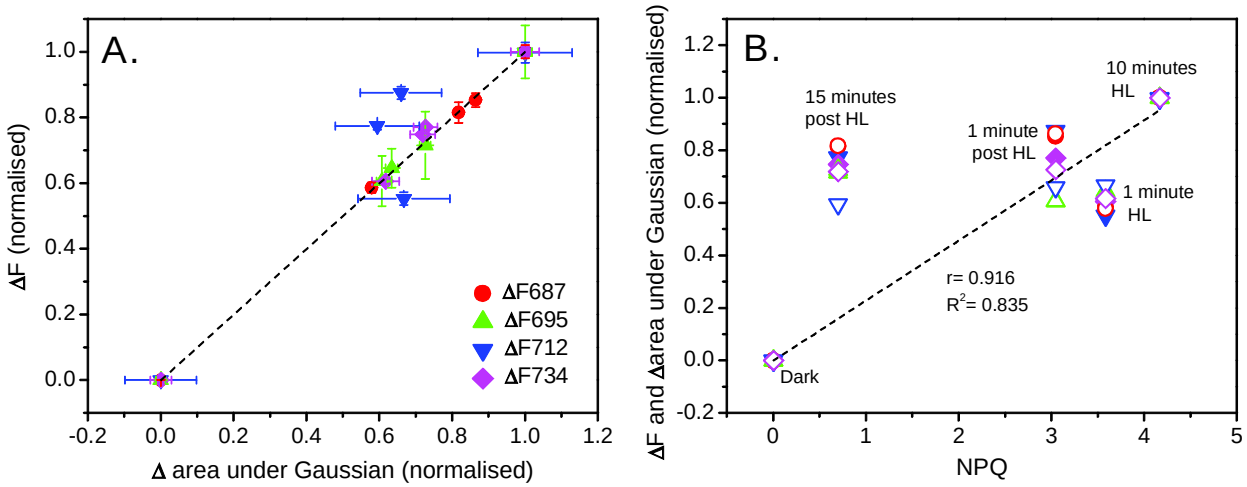

Figure 3.4-15 Summary for the use of ΔFs and Gaussian areas to describe excitation energy quenching and redistribution during a high light (HL) **transition.** Excitation of 460 nm. **A**, Validation for use of ΔFs to describe the redistribution of emission between individual emitters. The ΔFs obtained from the normalised HL *minus* dark difference emission spectra (see Figure 3.4-7B) are plotted against the HL *minus* dark Gaussian areas obtained from fitting of the before-subtraction emission spectra (see Figure 3.4-14C). ΔFs and change in Gaussian area are normalised to a maximum value of 1 for comparison. The dashed line represents a theoretical one-to-one relationship. **B**, the relationship between excitation energy redistribution (measured as change in emission between emitters using ΔF and Gaussian area as described in A) and excitation energy quenching (measured in terms of $\mathcal{NPQ}$). ΔF and Gaussian centres according to the symbols in A. Closed symbols, ΔFs; open symbols, Δ Gaussian areas. Symbol groups belonging to the different phases of NPQ identified in Figure 3.4-3 are labeled. The concatenate linear regression for the data points in B is indicated by the dashed line.

In summary, the results obtained by the Gaussian fits are in good agreement with the ΔF findings from the normalised HL *minus* dark emission spectra shown in Figure 3.4-7B. Deconvolution of the emission spectra allowed assignment of individual emitter bands to the previously defined ΔFs. Emitter bands centred at 687 and 695 nm are primarily responsible for

the preferential loss in cell emission in response to HL that was described by ΔF687 and ΔF695. Emitter bands centred at 712 and 734 nm are primarily responsible for the relative gain in emission that was observed broadly around 720 nm in the difference spectra, and in such, justifies the use of ΔF712 and ΔF734 to describe excitation energy redistribution in this emission region. The ΔFs and Gaussian area measurements describe the same changes in emission distribution that occur between the emitter bands centred at 687, 695, and 734 nm (Figure 3.4-15A). The changes in emission by the 712 nm centred Gaussian are less effectively described by ΔF712 (Figure 3.4-15A). The loss in emission from the 687 and 695 nm emitter bands during HL can be confidently contributed to a preferentially quenching of outer FCP complexes and PSII cores, respectively. Unfortunately, determining the underlying cause for enhanced emission by the 712 nm emitter is less straightforward. The Gaussian centred at 712 nm has a broad bandwidth (Table 3.4-2), which is consistent with assignment to PSI; however, this can allow emission from other emitters with similar S_1 (0,0) states to be co-fitted within the same Gaussian.

3.4-7 Fucoxanthin emission

During the collection of emission spectra it was noticed that there was a very weak in amplitude (~10^{-3} the height of the maximal cell emission peak) but resolvable emission peak centred near 885 nm (F885). This peak was visible in both the raw emission spectra and corrected spectra having a FWHM of 255 cm^{-1}. It was also responsive to HL transitions (Figure 3.4-16). This extremely low energy level is below the lowest vibrational states at which Chl *a* can fluoresce.

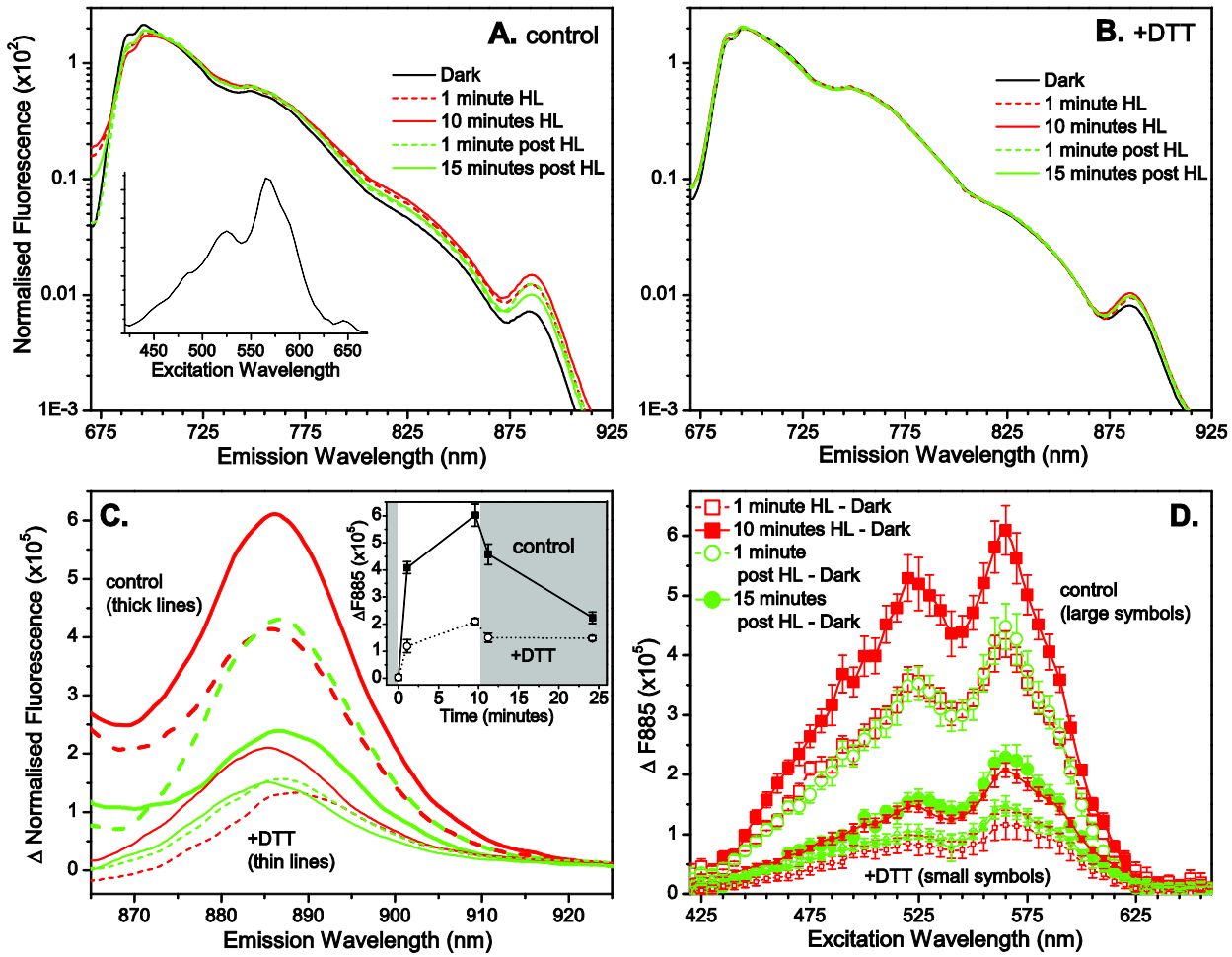

Figure 3.4-16 Changes in near infrared cell emission measured at low temperature (77K) during a high light transition. Samples were collected at the high light (HL) transition time points indicated in Figure 3.4-3. **A** & **B**, emission spectra normalised to integrated fluorescence plotted on a Log scale for control cells (A) and cells pretreated with 5.3 mM DTT (B) showing a resolved emission peak at 885 nm (F885). The spectra shown were collected with 565 nm excitation and are the average from 3 separate cultures. The insert in A shows an excitation spectrum for F885 in dark adapted cells; area under the 885 nm peak was calculated after subtraction of a baseline that was created by fitting the emission curve data from 850 to 860 nm and 920 to 930 nm to an exponential decay. **C**, HL treated *minus* dark adapted difference spectra of the spectra in A & B. ΔF885 calculated as the difference peak height at 885 nm. Insert, induction and relaxation of ΔF885 during a HL transition (white plot area indicates HL illumination, darkened plot area indicates dark conditions). **D**, excitation spectra for ΔF885. Error bars represent ±1 standard deviation from the mean of three separate cultures.

Carotenoids are typically considered non-fluorescent molecules because they have very short lived excited states. Fucoxanthin possesses an unusual structure for a carotenoid with low symmetry and a conjugated carbonyl group, so even though one-photon emissions between the S_1 and S_0 states are optically forbidden, weak emission from the S_1 state is

nevertheless observed (Macpherson and Hiller 2003). The S_1 lifetime shows a high dependence on solvent polarity varying from 7-173 picoseconds (Macpherson and Hiller 2003 and references therein). Energy transfer from the S_1 state in Fx to the Q_y state in Chl *a* is implicated in the light harvesting capabilities of Fx and would explain the benefits of the large bathochromic shifting of Fx absorbance *in vivo*. Gildenhoff et al. (2010) determined lifetimes from *Cyclotella meneghiniana* FCPa of <150 femtoseconds for the Fx S_2 state (transferring to Q_x of Chl *a*), and 0.6/0.9 ps for the unrelaxed and 2.6/4.2 ps for the relaxed S_1/ICT state (transferring to Chl *a* Q_y); the higher values represent the lifetimes of red Fx molecules and the shorter values those of blue Fx. The fluorescence study by Katoh et al. (1991) showed emission from Fx in CS_2 extending beyond 800 nm. In CS_2 the red absorption peak of Fx was at 505 nm. The absorption of Fx in protein is known to be shifted up to at least ~560 nm (Lavaud 2007). An excitation spectrum for F885 corrected for Chl *a* tail emission (Figure 3.4-16A insert) revealed a maximum excitation wavelength of 565 nm, with a prominent excitation shoulder at 525 nm. Based on this evidence, F885 is being assigned to a deeply red shifted Fx. The heterogeneity of Fx energy levels *in vivo* has been well described (Gildenhoff et al. 2010, Szabó et al. 2010, Gundermann et al. 2013). Some Fxs are believed to be peripheral to FCPs and only weakly transfer their excitation energy to Chl *a* (Premvardhan et al. 2010, Papagiannakis et al. 2005). The fluorescing Fx observed in the present study is being assigned to a peripheral Fx with weak energy transfer coupling to Chl *a*.

Emission from the deep red Fx is influenced by excess light. Relative emission from F885 rose during HL and dropped once HL ended (Figure 3.4-16). The induction kinetics of ΔF885 during HL were identical to those for ΔF687, ΔF695, and ΔF734. ΔF885, ΔF695, and ΔF734 also

relaxed similarly at one minute post HL, but ΔF885 relaxed more than ΔF687 and ΔF734 during the 15 minute post HL period. Since the excited state lifetime of Fx is very sensitive to solvent polarity (Macpherson and Hiller 2003), any change to the electrostatic field surrounding the pigment molecule is expected to affect the excited states. The enhancement in Fx emission in response to HL could be attributed to an uncoupling of an Fx molecule during the hypothesized aggregation of FCPs that occur during qE or could be a direct consequence of illumination induced $\Delta\mu^{+}_{H}$. Premvardhan et al. (2010) has suggested that 2 to 3 Fxs (per FCP trimer) are bound weakly to the periphery of the protein surface, and in such would be especially susceptive to a changing thylakoid environment during qE. Since most of the HL induced changes to F885 were inhibited by DTT (Figure 3.4-16), F885 serves as an additional marker for qE_{XC}. To conclude, qE_{XC} in *Nitzschia* cells changes the local environment around a deep red Fx resulting in decoupling from its acceptor Chl *a* and enhanced emission from the Fx at 885 nm.

3.4-8 Fluorescence lifetime

Fluorescence lifetime gives information on the excited state relaxation pathways of a fluorophore. The relaxation of a molecule from its first electronically excited state (S_1) is a competitive pathway following first order kinetics. Photon emission competes with the non-radiative relaxation pathways such as internal conversion (heat), triplet state conversion, resonance energy transfer, and photochemistry: the fastest relaxation pathway will dominate. Fluorescence lifetime describes the average time a molecule resides in the S_1 state before emitting a photon. Thus fluorescence can be expressed as: $[S_1] = [S_1]_o\, e^{-\Gamma t}$, where $[S_1]_o$ is the initial concentration of excited state molecules, $[S_1]$ is the concentration of excited state molecules at time *t*, and Γ is the decay rate (the reciprocal of fluorescence lifetime, τ). Γ is the

sum of all rates for depopulating the excited state, both radiative and non-radiative ($\Gamma = \Gamma_{\text{radiative}} + \Gamma_{\text{non-radiative}}$) (Lakowicz 2006b). If the decay rate from the excited state is fast then fluorescence will have a short lifetime. Any process shortening the time that a molecule remains in the S_1 state will shorten fluorescence lifetime. To put this in context, excited state P680 has an extremely short fluorescence lifetime because the photochemical process of charge separation (a non-radiative decay pathway) occurs on a time scale of ~ 3 picoseconds.

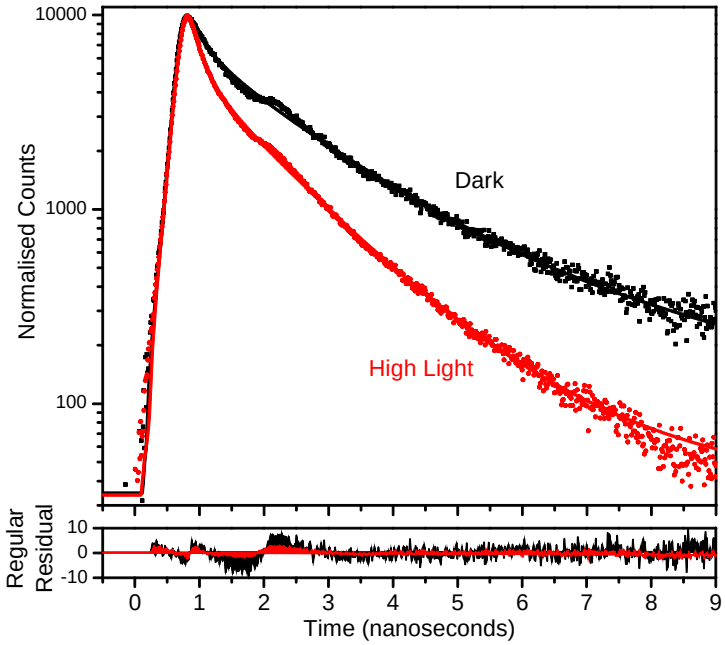

Figure 3.4-17 Picosecond fluorescence decay kinetics of room temperature cell emission at 685 nm in response to a 407 nm laser pulse. Curves are normalised to maximum photon counts. The laser was scanned using a confocal microscope across a thin film cell suspension. Data was collected as 'Fmax' to insure all PSII reaction centres were closed in both dark adapted samples (Dark) and high light adapted (HL) samples, so as to limit the contribution of photochemical quenching to the fluorescence signal. Reaction centres were closed by using a slow (i.e. intense) laser scan rate. For Dark samples there was a 1 minute pause between laser scans. This method for 'Fm_{dark}' collection did not noticeably induce any quenching in the Dark samples and took approximately 20 minutes to acquire sufficient photon counts. HL data collection began 5 minutes after sample illumination (200 µmol $m^{-2}s^{-1}$ of blue-green light) during steady state NPQ conditions; the laser was scanned at 15 second intervals during illumination until adequate photon counts had been collected (approximately 10 to 15 minutes depending on sample). The solid lines represent fits of the data by convolution to a sum of 3 exponential decays (fit parameters given in Table 3.4-3); fit residuals are shown in the lower panel. Traces are the average from 3 separate cultures.

The fluorescence decay traces from *Nitzschia* cells measured at physiological temperature prior to and during HL irradiance are presented in Figure 3.4-17. Fluorescence was

measured at the 685 nm, the wavelength approximate to maximal cell emission and representing the wavelength most quenched during HL (Figure 3.4-2E). The decay traces were fit to a sum of three exponential decays. The objective of the fitting was not to describe all of the individual decay components contributing to cell emission at 685 nm, but to quantitate the general shape of the decay trace. The transition from dark conditions to HL illumination was accompanied by a ~two fold decrease in the average Chl *a* excited state lifetime of the pigment matrix (Table 3.4-3). This shortening of the fluorescence lifetime is a photo-electronic cause for the Chl *a* fluorescence quenching observed during HL.

Table 3.4-3 Fluorescence decay lifetime analysis summary for room temperature cell emission at 685 nm. Values are the mean ± the standard deviation from the independent fits of 3 separate cultures. τ_m is the average decay lifetime for the sample decay function (see *Section 2.12* for formula).

Sample	a_1 (%)	τ_1 (ps)	a_2 (%)	τ_2 (ps)	a_3 (%)	τ_3 (ps)	τ_m (ps)	χ^2
Dark	43.3 ±0.1	245 ±10	50.2 ±1.2	1450 ±103	6.67 ± 0.92	5470 ±327	1220 ±38	4.073 ±0.101
High Light	64.7 ±1.5	199 ±7	30.9 ±2.4	1250 ±162	4.43 ±1.79	2060 ±434	621 ±52	5.360 ±0.564

3.4-9 Fluorescence evidence for Chl a*-Chl* a *quenching* in vivo

Close interaction of Chl *a* molecules quenches their fluorescence. It is known that if Chl *a* is in solution or applied to a thin film at a similar concentration (~0.1 M) as Chl *a* occurs *in vivo* in thylakoid membranes, essentially all fluorescence from the chlorophylls is lost (Beddard and Porter 1976). Quenching of fluorescence from a fluorophore (i.e. Chl *a*) can have two principle types of origins: collisional (Stern-Volmer) and static quenching (Lakowicz 2006c). Collisional quenching of a fluorophore's excited state is due to interactions with another nearby molecule that facilitate non-radiative transitions to the ground state and as a consequence decreases the

excited state lifetime (and thereby decreasing the fluorescence lifetime). In static quenching fluorophores are inactivated by forming complexes with non-fluorescing molecules; loss in fluorescence yield is entirely due to a decrease in the concentration of active fluourophores and there is no change in fluorescence lifetime (Lakowicz 2006c). The pronounced shortening of Chl *a* fluorescence lifetime during HL in *Nitzschia* cells (Figure 3.4-17) identifies that a collisional type of quenching of Chl *a* is occurring during NPQ. This does not rule out that static type quenching, as via Chl *a*-carotenoid interactions, might also contribute to gross quenching.

The oligomerization of isolated LHCII is commonly known to reduce fluorescence yield, drastically shorten fluorescence lifetime, and enhance far-red emission from the complexes (Ruban and Horton 1992, Ruban et al. 1992, Ruban et al. 1997, Miloslavina et al. 2008, Andreeva et al. 2009), and so has been implicated as an important part of qE in higher plants. Isolated FCP complexes from *Cyclotella meneghiniana* show a red shift in emission and an enhancement in relative emission in the far-red upon aggregation (Miloslavina et al. 2009). Isolated FCPa and FCPb complexes from *C. meneghiniana* were reconstituted into liposomes with different lipid to Chl *a* ratios by Gundermann and Büchel (2012). They showed that at low lipid to Chl *a* ratios, as is expected during FCP aggregation as protein-protein interactions displace lipids, emission from the liposomes was heavily quenched with a red shift and far-red enhancement (Gundermann and Büchel 2012).

A mixed exciton charge transfer state is believed to be the basis of the collisional type quenching that occurs in aggregated LHCII. LHCII has a large fraction of chlorophylls that are located at or close to the surface of the protein (Liu et al. 2004). This would support the

formation of Chl *a*-Chl *a* interactions between adjoining trimers during LHCII aggregation (Miloslavina et al. 2008). These new inter-trimer Chl *a*-Chl *a* pairs form a charge transfer state that still maintains a pronounced excited state character (i.e. the charge is on average only partially translocated) (Miloslavina et al. 2008). Mixing of charge transfer states with Chl *a*–Chl *a* exciton states leads to a large Stokes shift, very strong emission band width broadening, and strong vibrational tails due to the very strong electron–phonon coupling of these states (Miloslavina et al. 2008). Formation of the mixed charge transfer state creates two new emission bands from the non-aggregated band at 680 nm, a small bandwidth (200 cm^{-1}) exciton emission band red shifted a few nm, and a large bandwidth (600 cm^{-1}) mixed charge transfer exciton emission band further red shifted to 700 nm that includes a long far-red tail. Similar Chl *a* excited states with strong charge transfer character are present in LHCI (Croce et al. 2007) and PSI (Schlodder et al. 2005). The low energy red Chl *a*s of PSI, in fact, share spectroscopic features with the far-red emission spectra of LHCII oligomers (Miloslavina et al. 2008). Quenching of the Chl *a*-Chl *a* dimers could be caused by a pronounced coupling of the charge transfer state to the ground state, or the excited state could be quenched by energy transfer to another low-lying state. The former seems likelier. Fluorescence from the mixed exciton charge transfer Chl *a*-Chl *a* terminal emitter in aggregated LHCII has a characteristic lifetime of ~400 picoseconds (Miloslavina et al. 2008). Miloslavina et al. (2008) observed a very-similar-to-aggregated-LHCII far-red enhanced emission with a lifetime of 400 picoseconds in intact *Arabidopsis* leaves only under NPQ conditions. The time resolved fluorescence study by Miloslavina et al. (2009) on diatom NPQ observed the appearance of ~300 and ~400 picosecond components with high far-red to red emission ratios in HL acclimated

Phaeodactylum tricornutum and *Cyclotella meneghiniana* cells, respectively. This advocated that Chl *a*-Chl *a* interactions similar to those in aggregated LHCII contribute towards non-photochemical quenching in diatoms.

NPQ conditions in *Nitzschia* cells are characterised by a relative increase in far-red emission and a shortening of mean Chl *a* fluorescence lifetime consistent with the formation of a mixed Chl *a*-Chl *a* exciton charge transfer state. During NPQ the increase in far-red emission peaks from 712 to 734 nm with a broad shoulder extending from ~750 to 775 nm (Figure 3.4-7). A robust shoulder at ~750 nm in the HL *minus* dark difference spectra was even more apparent if emission spectra were normalised to their maximum fluorescence peak prior to subtraction (*Supplemental Figure 3.4-2*). The exact origins of the emission at 712 nm are hard to discern between enhanced relative PSI emission and/ or emission from an exciton emission band of the Chl *a*-Chl *a* mixed interaction. The strong contribution from the Gaussian modeled emission bands at 734 nm and longer wavelengths (Figure 3.4-13) supports a mixed Chl *a*-Chl *a* exciton charge transfer state. The room temperature HL *minus* dark difference emission spectrum is less prone to contamination by a PSI signal because PSI fluoresces negligibly at room temperature. This spectrum also showed an enhancement in red emission (peaking at ~705 nm) with a secondary peak in the far-red (at ~770 nm) (Figure 3.4-2E). A ~200 picosecond component was responsible for ~65% of the time resolved emission observed under NPQ conditions in *Nitzschia* cells (Table 3.4-3). This 'NPQ lifetime' is shorter than the ~300 and ~400 picosecond components that Miloslavina et al. (2009) observed in diatoms, but this could be a consequence of the much simpler fitting schema used in the present study. In comparison of how much mean fluorescence lifetime was shortened during HL, the present study and that by

Miloslavina et al. (2009) are in agreement. $\mathcal{NPQ}$ values of 1.5 and 1.1 in *Phaeodactylum tricornutum* and *Cyclotella meneghiniana* cells, respectively, resulted in 2.5 and 2.1 fold decreases in mean fluorescence lifetime, respectively (Miloslavina et al. 2009). Similarly, the measured two fold decrease in fluorescence lifetime in the *Nitzschia* cells corresponded to an $\mathcal{NPQ}$ value of ~1.5 (as measured from steady state fluorescence under the same experimental conditions; $\mathcal{NPQ}$ = (fluorescence intensity prior to collection of time resolved data – fluorescence intensity at the end of collecting time resolved data) / fluorescence intensity at the end of collecting time resolved data)). Nonetheless, the combined shortening of mean Chl *a* fluorescence lifetime and an increase in far-red emission from *Nitzschia* cells during NPQ conditions is strongly supportive of the formation of a Chl *a*-Chl *a* mixed exciton charge transfer state.

3.4-10 The location of Chl a*-Chl* a *quenching: Q1 and Q2*

The quenching profiles for *Nitzschia* cells in response to HL supports quenching to be centred within two distinct antenna compartments: outer FCP complexes with a terminal emitter at 687 nm quenched by Q1, and inner FCP-PSII complexes with a terminal emitter at 695 nm quenched by Q2 (see Figure 3.4-18). This is seen in the HL *minus* dark emission spectra by the dual negative peaks at ~687 (ΔF687) and ~695 nm (ΔF695) (Figure 3.4-7) and in the Gaussian fits as a decrease in emission contribution from the emitter bands centred at 687 and 695 nm (Figure 3.4-13). Q1 and Q2 are activated at a similar rate during HL illumination, but Q2 relaxes more quickly upon illumination termination (Figure 3.4-7B, D, F inserts & Figure 3.4-14C). The photo-electronic mechanism for quenching at Q1 and Q2 would be via non-radiative excited state relaxation from Chl *a*-Chl *a* dimers that have mixed exciton charge transfer

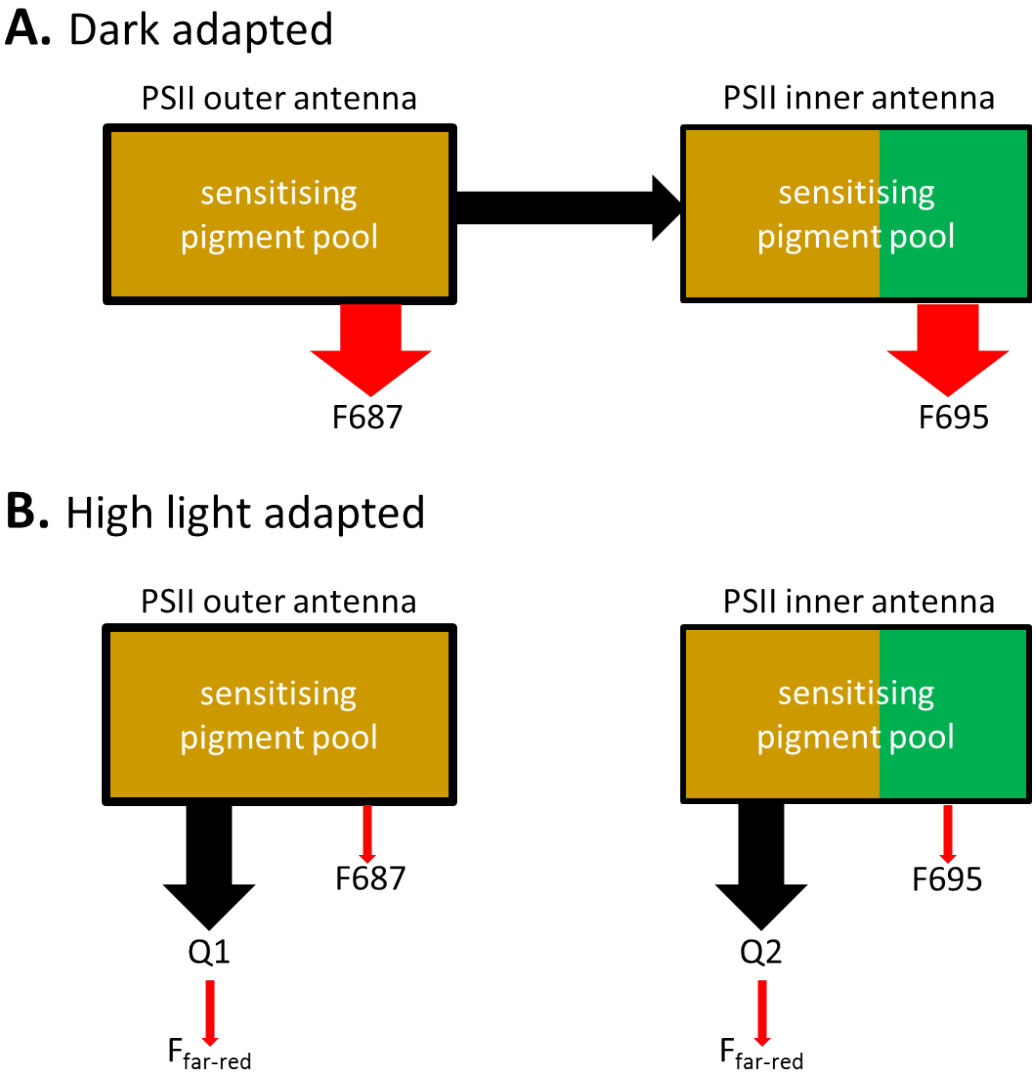

Figure 3.4-18 PSII antenna compartment model illustrating excitation energy quenching and redistribution during the NPQ response in *Nitzschia* cells as measured at low temperature (77K). The PSII outer antenna compartment refers to FCP complexes (indicated by gold-brown) which are not tightly coupled to PSII cores (labelled as FCPII in *Section 3.2*). The PSII inner antenna compartment refers to FCP complexes (indicated by gold-brown) that are tightly coupled to PSII cores (labelled as FCPii in *Section 3.2*) and also the antenna chlorophyll *a* within PSII (indicated by green). Black arrows represent excitation energy transfer. Red arrows indicate radiative decay of excited states via fluorescence (F). Size of arrow is indicative of amplitude in energy translocation. Rate constants are associated with each arrow. **A**, during dark adapted conditions, the PSII outer antenna compartment transfers excitation energy to the PSII inner antenna compartment and each compartment fluoresces from its terminal emitter (at 687 nm for the outer antenna, at 695 nm for the inner antenna). **B**, during high light conditions, ΔpH and DD de-epoxidation induce the formation of FCP quenching aggregates. FCP aggregation activates the quenching sites (Q) and causes a decoupling of the outer antenna from the inner antenna. Q1 and Q2 quenchers are strong exciton traps formed by Chl *a*-Chl *a* pairs with a mixed excitonic charge transfer state that relaxes from the excited state predominantly non-radiatively but also weakly fluoresces in the far-red. The fast, non-radiative relaxation of excited states now outcompetes excited state relaxation via emission from the F687 and F695 terminal emitters, thereby quenching fluorescence from the outer and inner antenna, respectively.

properties. The proportioning of excitation energy towards far-red emission at 734 nm is strong evidence for the formation of this Chl *a*-Chl *a* interaction. Both Q1 and Q2 contribute towards emission at 734 nm, as seen by ΔF687, ΔF695, and ΔF734 sharing identical induction kinetics during illumination, and ΔF734 relaxing in amplitude proportionally in-between ΔF695 and ΔF685 post illumination (Figure 3.4-7B, D, F inserts & Figure 3.4-14C). Furthermore, ΔF734 is sensitised by the same excitations as ΔF687 and ΔF695 during HL (Table 3.4-1).

Q1 seems to be dominant to Q2 quenching in *Nitzschia* cells cultured under these conditions when using a HL intensity of 10 times that of growth irradiance to pump the NPQ response. The loss of emission by the 687 nm emitter is greater than that of the 695 nm emitter as measured both by ΔF (Figure 3.4-7) and Gaussian area (Figure 3.4-13). This could either stem from there being more Q1 quenchers or from each Q1 quencher have a larger effective absorbance cross section (i.e. Q1 being sensitised by a larger pigment pool). Q2 quenching is proportionally more sensitised by ~575 to 600 nm excitations (compare the difference peaks in Figure 3.4-7F and the ΔF action spectra in Figure 3.4-9), placing Q2 within a pigment pool more heavily populated by deep red Fxs. Overall though, both Q1 and Q2 target very similar pigment pools (as indicated by the high correlation between the excitation spectra for ΔF687 and ΔF697 during HL, Table 3.4-1). The relative contribution of Q1 and Q2 towards total non-photochemical quenching is likely to vary depending on HL intensity (i.e. the extent and duration of ΔpH and DD de-epoxidation) and composition of the PSII antenna (i.e. the ratio of outer to inner FCP complexes).

The use of two quencher sites would provide two, independently regulated levels for PSII photoprotection. Q1 quenching is predicted to arise from inter-trimer interactions within or

between oligomeric (hexameric) outer FCP antenna complexes and thus would create large FCP quenching aggregates. Conversely, Q2 quenching would occur within smaller FCP quenching aggregates formed by the inter-trimer interaction between neighboring trimers within the inner FCP antenna. Placement of Q2 within the PSII energy compartment (i.e. the inner FCP-PSII complex) would allow for the quencher to compete directly with P680 for excitons. Q1 quenching within outer FCP that become decoupled from PSII would function to decrease the absorbance cross section for P680. Both forms of quenching require DD de-epoxidation and ΔpH to activate, but Q2 inactivation is predicted to be more strongly dependent on a drop in ΔpH (which would explain why Q2 quenching relaxes faster upon the transition from HL to dark), whilst Q1 inactivation would be more dependent on DT epoxidation facilitated de-aggregation of the large FCP quenching aggregates. Q1 quenching would provide a more stable source of excitation energy quenching during rapid fluctuations in ΔpH, whereas Q2 would provide a more dynamic method of regulating PSII excitation at PSII itself. This is opposite of the model for higher plant qE proposed by Jahns and Holzwarth (2012), where the rapid-reversing ΔpH-dependent quenching was placed within the outer antenna (LHCII) that become detached during HL and the slow-reversing, somewhat ΔpH-independent quenching was placed within the inner PSII antenna that remain attached to PSII.

The specific location of the Chl *a*-Chl *a* quencher dimers can be predicted. The FCP model by Premvardhan et al. (2010) placed a Chl *a* at the LHCII equivalent site b605. This Chl *a* could be lost during preparations of FCP trimers but was maintained in preparations of oligomers, which placed the b605 Chl *a* at the trimer-trimer interface (Premvardhan et al. 2010, Figure 3.4-19). One can predict that interactions between inter-FCP trimer b605 Chl *a* are

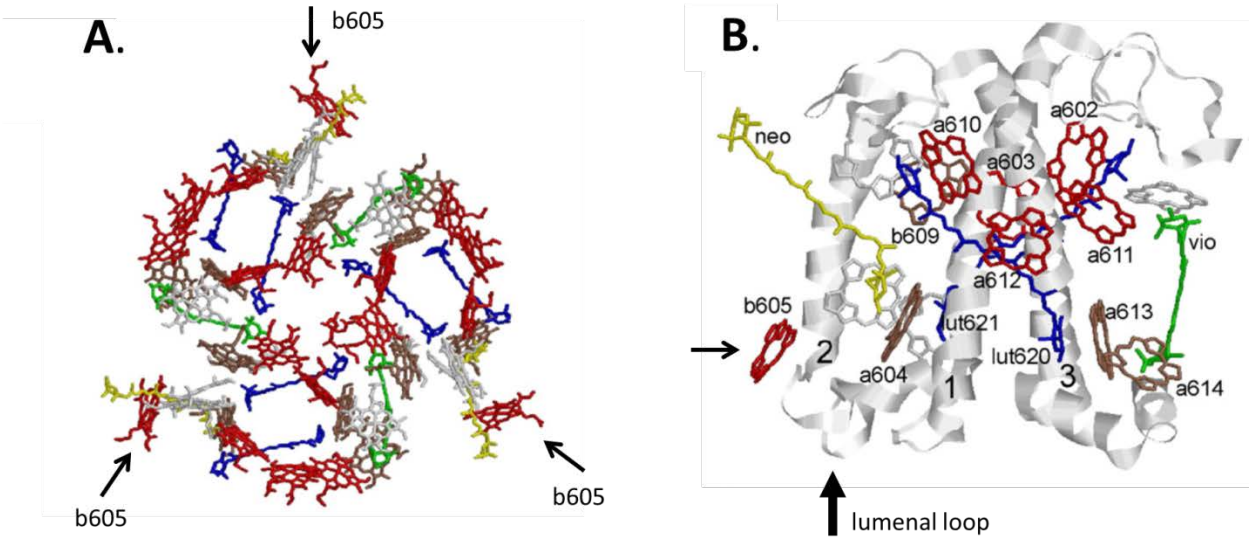

Figure 3.4-19 Predicted sites for formation of Chl *a* - Chl *a* quencher dimers in diatom FCP complexes. Structures adapted from Premvardhan et al. (2010). **A**, top view (stromal side) of the LHCII trimer with FCP pigment positions. Chl *a*s in FCP are colored red, Chls which could be either Chl *a* or Chl c_2 are shown in brown, grey Chls are those which are most probably missing in FCPs. Fucoxanthin molecules in lutein sites are shown in blue, in the violaxanthin binding sites in green, and in the neoxanthin site in yellow. The locations of the b605 equivalent Chl *a*s in FCP are identified by the arrows. **B**, side view of the membrane plane of the LHCII monomer structure. Labels denote pigment binding sites in LHCII that are occupied in FCP. Colouring the same as in A. The transmembrane α-helixes are labeled 1, 2, and 3. The small arrow identifies the b605 equivalent Chl *a* and the large arrow identifies the lumenal loop in which many FCP proteins contain a glutamate residue. Inter-trimer interactions between b605 Chl *a*s are predicted to form the Chl *a*-Chl *a* quencher dimers responsible for antenna based non-photochemical quenching in diatoms.

responsible for forming the Chl a-Chl a quencher dimers within the Q1 and Q2 quenching sites. Isolated FCP protein complexes within lipid micelles composed of Fcp2 and Fcp6 from *Cyclotella meneghiniana* are able to self-quench under acidic conditions and this quenching is enhanced with low lipid to protein ratios, as would occur in aggregated protein complexes *in vivo* (Gundermann and Büchel 2012). Gundermann and Büchel (2012) noted that Fcp2 and Fcp6 contain a glutamate residue within their lumenal exposed loop (between helix 1 and helix 2). These authors assigned the pH sensitivity of Fcp2 and Fcp6 containing FCP complexes to the presence of these glutamates. Two glutamates in PsbS (one within each of the two lumenal loops) has been identified as the pH sensor for this important mediator of qE in higher plants (Li

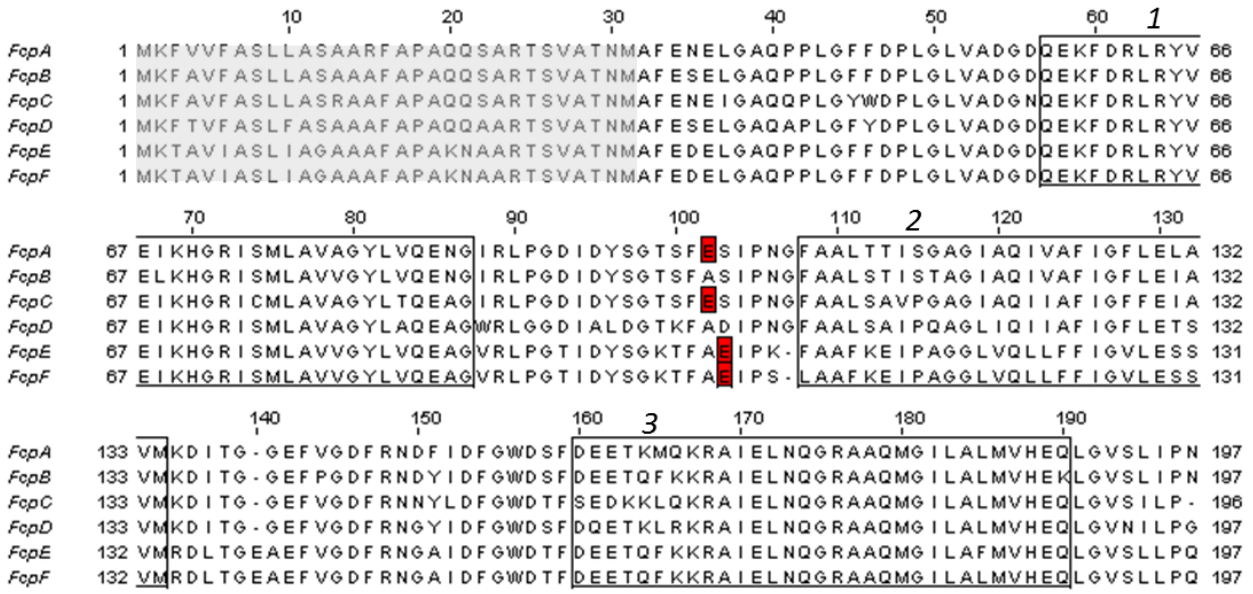

Figure 3.4-20 FCP protein (LhcF) sequence alignments from the pennate diatom *Phaeodactylum tricornutum*. Protein sequences according to Bhaya and Grossman (1993). The signal peptide region is marked in gray. The regions predicted to form the transmembrane α-helixes are boxed and labeled with the italicised numbers *1*, *2*, and *3*. Helix positions were predicted using the protein secondary structure prediction method of Rost et al. (2004). Glutamate residues positioned within the lumenal loop between helixes 1 and 2 are marked in red. These glutamates are predicted to act as pH sensors during the activation of antenna centred non-photochemical quenching in diatoms.

et al. 2004). The FCP model of Premvardhan et al. (2010) places the b605 Chl *a* on helix 2 in close proximity to the helix 1-helix 2 lumenal loop (Figure 3.4-19). One can imagine that protonation of the lumenal loop in Fcp2 and Fcp6 in *C. meneghiniana* induces a conformational change within FCP aggregates which brings inter-trimer b605 Chl *a*s into close contact for the formation of Chl *a*-Chl *a* quencher dimers. The amino acid sequences of the FCP proteins in the pennate diatom *Phaeodactylum tricornutum* reveal that many of the FCP proteins in this organism also contain a glutamate residue in their lumenal loop (FcpA, FcpC, FcpD, and FcpE, but not FcpB or FcpF) (Figure 3.4-20). Protonation of the glutamate residue within the lumenal FCP loop in pennate diatoms could thus be implicated in ΔpH induced non-photochemical quenching *in vivo*. Antenna based quenching (Q1 and Q2) in *Nitzschia* is being proposed to

arise from protonation facilitated inter-FCP trimer b605 Chl *a* interactions (Figure 3.4-19). The variety between FCP proteins in their placement of the glutamate residue and the amino acid sequences within the lumenal loop (Figure 3.4-20) is anticipated to shift the pH of the glutamate pKas between FCP complexes with differing protein compositions, thereby creating a gradient of activation pKas for quenching.

3.4-11 Quenching efficiency

The extent of excitation energy redistribution by the major emitters (as measured from ΔFs and Gaussian areas) is positively related to the extent of excitation energy quenching (as measured by $\mathcal{NPQ}$) (Figure 3.4-15B). Kinetically however, the extent of quenching is induced faster than excitation energy redistribution during HL illumination (ΔFs are only about 60% of the change in fluorescence yield at 1 minute HL) , and the weak residual amount of quenching observed at 15 minutes post HL maintains an unequivocally high amount of excitation energy redistribution (Figure 3.4-7B, D, F inserts & Figure 3.4-14C). These observations may be explained by a change in quenching 'efficiency' during the different phases of the HL transition. Quenching 'efficiency' describes the ratio of quenched excitations to quenchers, which can be enhanced in in two separate ways: (i) by increasing the rate of excited state non-radiative decay within a quencher or (ii) by increasing the number of excitations that are accessible to a quencher.

The rate of non-radiative decay by the Chl *a*-Chl *a* quencher dimers could be tuned during HL transitions by the local protein environment. Because the hypothesized b605 Chl *a*-Chl *a* quencher dimers form at the inter-FCP trimer interface and are positioned near a glutamate containing lumenal loop, their interaction is predicted to be very sensitive to HL

induced changes in lumenal pH and FCP aggregation state. Small scale changes in the orientation and/ or distance between b605 Chl *a* would affect the excited state lifetime of the mixed exciton charge transfer state. A faster transition to the ground state would lower the fluorescence yield from the Chl *a*-Chl *a* dimer, thus increasing its quenching efficiency. A slower transition to the ground state would increase the fluorescence yield from the Chl *a*-Chl *a* dimer, thus decreasing its quenching efficiency. Protonation of the FCP lumenal loop glutamates is predicted to promote the formation of Chl *a*-Chl *a* dimers with short excited state lifetimes, thus the high ΔpH that develops during the initial transition to HL would create 'strong' Chl *a*-Chl *a* quenchers. Deprotonation of the glutamates upon a rise in lumenal pH during photostasis could conversely cause conformational changes within the protein that increase the excited state lifetime of the Chl *a*-Chl *a* dimer thereby weakening the quencher. To verify this transitory change in the quenching efficiency of Chl *a*-Chl *a* quencher dimers, one would need to measure the excited state lifetimes of the quenchers at different phases of the HL transition (as via fluorescence lifetime measurements). Since the Chl *a*-Chl *a* mixed exciton charge transfer state emits in the far-red, a more efficient quencher dimer will contribute less towards cell emission in the far-red per quenched excitation. To recap, changes in the quenching efficiency of individual Chl *a*-Chl *a* dimers could contribute to the change in the relationship between emission distribution and quenching magnitude that was observable between HL transition phases.

The use of shared quenchers could enhance quenching efficiency. When the antenna system is optimised for light harvesting (as after dark adaptation), the light harvesting complexes are anticipated to have a large degree of interconnectivity, in effect combining their

individual pigment pools into a pigment 'lake'. The activation of a single/ few quenchers during the initial transition to HL would be able to quench the entire pigment 'lake'. At this phase of a HL transition the sharing of quenchers between pigment pools would give each quencher a large effective absorbance cross section and a large quenched pigment to quencher ratio. The high correlation between the ΔF687 (Q1) and ΔF695 (Q2) excitation spectra at 1 minute HL (Table 3.4-1) is good evidence for common targeting of the pigment 'lake' by the quenchers. Quenching of the pigment 'lake' has a limited effect of cell emission spectral shape because all emitters are quenched equally. As more FCP quenching aggregates form during HL, the antenna system is expected to become more fragmented, especially as outer antenna complexes become disconnected from the inner antenna, resulting in the splitting of the pigment 'lake' into individual pigment 'ponds' are even 'puddles'. So, steady state HL conditions are expected to give lower quenched pigment to quencher ratios because more quenchers have now become activated and/ or the effective absorbance cross section for each quencher has decreased. Post HL, a heterogeneous deactivation of quencher sites and rebuilding of the interconnected pigment pool would result in an antenna system with isolated 'islands' of residually quenched FCP aggregates. Such an antenna configuration would only quench excitations within the quenched islands (and thus cause a change to emission spectral shape) but not quench excitations within the much larger interconnected pigment pool (and thus have only a minor effect on fluorescence yield). To recap, sharing of quenchers between interconnected antenna pigment pools could contribute to the change in the relationship between emission distribution and quenching magnitude that was observable between HL transition phases.

To summarise, changes in quencher excited state lifetime and interconnectivity of the antenna system can be used to explain the non-linear relationship observed during HL transitions between the extent of excitation energy redistribution (change in emission spectral shape) and the extent of non-radiative excitation energy quenching. During the initial transition to HL quenching efficiency is expected to be at its highest because (i) the antenna system would still have a high level of interconnectivity permitting the use of shared quenchers and (ii) a high lumenal pH would protonate FCP lumenal loops facilitating the formation of Chl *a*-Chl *a* quencher dimers with fast excited state non-radiative decays.

3.4-12 Fluorescence markers for antenna reorganisation in response to excess light

Energization across the thylakoid ($\Delta\mu^{+}_{H}$) during illumination is predicted to cause a multitude of structural modifications to the protein-pigment-lipid milieu. As reviewed by Ruban et al. (2012): The ΔpH that develops upon illumination leads to neutralization of point charges on the lumen exposed surface of the thylakoid membrane, resulting in displacement of bound magnesium cations into the stromal space. These changes in charge distribution cause the thylakoid membrane to become thinner, dehydrated, and more hydrophobic. The alteration in charge distribution brought about by ΔpH formation is proposed to change the lateral interactions and aggregation state of thylakoid membrane proteins (Barber 1982). In support, the source of the higher plant qE signature absorbance change at 535 nm has been calculated to stem from changes in thylakoid thickness (Duffy et al. 2010).

Many of the changes in energy transfer coupling identified in the emission spectra by ΔF and change in Gaussian area likely stem from illumination induced, $\Delta\mu^{+}_{H}$ driven structural

changes to the thylakoid that may, or may not, directly participate in quenching pathways. Redistribution in emission between the 687, 695, 712, and 734 nm centred emitters accounts for most of the excitation energy redistribution that occurs during HL (Figure 3.4-13) and is correlated to the extent of quenching (Figure 3.4-15B). Loss in emission at 687 nm via Q1 is attributed to a large-scale rearrangement of outer FCP complexes into aggregates; loss of emission at 695 nm via Q2 is attributed to smaller scale aggregation of the inner FCP antenna. ΔF712 actually grew during the first 1 minute after HL illumination ended when measured with excitations from ~525 to 675 nm (Figure 3.4-9D). This may represent an influx of these excitations towards PSI during the initial transition away from HL. ΔF673 has been attributed to a decoupling of Chl *a* from its excitation energy acceptors during illumination. The conditions responsible for maintaining the relative enhancement of emission at 673 nm seem to be rapidly lost post HL, which is suggestive of a strong, direct dependence on $\Delta\mu^{+}_{H}$. The enhancement in near infrared emission from a deep red Fx during HL (Figure 3.4-16) would also be a marker for HL induced changes to thylakoid structure. Sensitisation for the ΔFs (Figure 3.4-9) can vary between NPQ phases, further suggesting that energy transfer pathways within the pigment matrix undergo a dynamic reorganization in response to HL. To recap, transient changes in cell emission during HL represent restructuring of the antenna at multiple levels.

3.4-13 Excitation energy redistribution in the absence of qE_{XC}

The inactivation of qE_{XC} with the DD de-epoxidase inhibitor DTT prevented 90% of quenching formation (as measured by $\mathcal{NPQ}$) and prevented all redistribution of excitation energy (change in emission spectral shape) associated with the NPQ response. De-epoxidation of structural DD is predicted to promote the protein-protein interactions responsible for

forming Chl *a*-Chl *a* quencher dimers. With DTT pre-treatment HL induced a reversal of the emission redistribution that occurred in non-treated cells (Figures 3.4-8 & and 13). The lack of an effect of HL on far-red emission (Figures 3.4-8 & and 13) is strong indication that the Chl *a*-Chl *a* mixed excitonic charge transfer state no longer forms in the presence of DTT.

Quenching in the presence of DTT (qE_{nonXC}) likely originates from within the PSI reaction centre. The HL *minus* dark difference emission spectra clearly show a distinctive loss in relative emission peaking at 712 nm (Figure 3.4-8) (also evident if emission spectra are normalised to maximum fluorescence peak prior to subtraction, *Supplemental Figure 3.4-3*). The Gaussian fits also showed a large relative increase in emission from the emitter centred at 712 nm (Figure 3.4-13D). Both $P700^+$ and $^3P700$ radicals in PSI act as effective quenchers of Chl *a* fluorescence for excitons trapped by PSI at all temperatures (Schlodder et al. 2005). Because $P700^+$ and $^3P700$ exhibit a broad, flat absorption that extends into the near infrared, they can effectively act as excitation energy acceptors for Chl *a* Q_y transitions. A fast radiationless decay of excited state $P700^+$ and $^3P700$ is the probable quenching mechanism (Byrdin et al. 2000, Schlodder et al. 2005). Quenching collapsed at 1 minute upon cessation of illumination (Figure 3.4-8) because $P700^+$ formation is dependent on illumination.

3.4-14 Conclusions

Strong evidence was presented for the identification of a photo-electronic mechanism for non-photochemical quenching in *Nitzschia* cells during NPQ conditions. The steady state and time resolved fluorescence data supported the formation of a Chl *a*-Chl *a* mixed exciton charge transfer state during NPQ that preferentially targets the outer FCP (Q2) and inner FCP (Q1) antenna for PSII. These Chl *a*-Chl *a* quencher dimers were predicted to form at inter-FCP trimer

interfaces that develop during the formation of FCP quenching aggregates. Both Q1 and Q2 were sensitised by similar excitations and formed at an equivalent rate during HL illumination; however, Q2 relaxed noticeably faster once HL was removed. It was also noted that the quenching of excitation energy by a limited number of quenchers during the initial transition to HL might be amplified by an interconnected antenna pigment pool giving each quencher access to many excitations, and by the protonation of FCP proteins stimulating the enhancement of excited state non-radiative decay within the Chl *a*-Chl *a* quencher dimers. Pre-treatment of cells with the DD de-epoxidase inhibitor DTT prevented all the redistribution in excitation energy between emitters that was characteristic of the NPQ response; thereby indicating that DD de-epoxidation is obligatory for initiating the formation of antenna centred excitation energy quenching pathways during NPQ in *Nitzschia* cells.

3.5 The Concerted Control of DD De-Epoxidation and ΔpH on the Induction and Relaxation of NPQ in *Nitzschia curvilineata*

3.5-1 Overview

The NPQ mechanism in higher plants allows the rapid activation and deactivation of quenching. Three constituents are critical to higher plant qE: the antenna complexes in which the quenching sites form (principally LHCII but also some of the minor antenna); the xanthophyll cycle pigments (violaxanthin and zeaxanthin) which are allosteric regulators for the quenching sites; and the pH sensing protein PsbS which activates the quenching sites (as reviewed by Horton and Ruban 2005, Horton et al. 2005). All three components work concertedly to sense changes in illumination via ΔpH, so as to convert the antenna system back and forth between light harvesting and energy dissipative modes. Once xanthophylls have been de-epoxidised, quenching is largely under the control of ΔpH and PsbS protonation, which means NPQ can then rapidly flux in response to ΔpH. Much less is known about how ΔpH and DD epoxidation state interact in regulating the NPQ mechanism in diatoms. As in plants, quenching is rapidly induced during excess light and ΔpH is required for the induction and maintenance of NPQ; however, reversal of the quenching proceeds much more slowly upon removal of the excess light (Ruban et al. 2004). This has been interpreted as the induction of NPQ in diatoms being similar to that in plants with cooperativity between ΔpH and de-epoxidation, whereas the relaxation of NPQ quenching states in diatoms is dependent on the slow effects of epoxidation (Ruban et al. 2004, Horton and Ruban 2005, Goss and Jakob 2010).

The objective of this chapter is to identify the molecular mechanistic roles of the DD cycle and ΔpH in inducing, maintaining, and relaxing NPQ in the diatom *Nitzschia curvilineata*. Fluorescence quenching and DD epoxidation state were monitored simultaneously in cells during high light transitions using PAM fluorometry and by measuring absorbance changes at 510 nm, respectively. The inter-relationship between NPQ and DD epoxidation state was probed using different illumination protocols, a cold stress treatment, and chemical inhibitor treatments. The uncoupler ammonium chloride was used to dissipate ΔpH during different phases of NPQ. The results showed that quenching responds more dynamically to HL *on* and *off* than does DD epoxidation state. NPQ always induced faster than de-epoxidation during illumination and could in some situations relax during illumination in the absence of epoxidation. Upon cessation of HL illumination, the dependency of NPQ relaxation on epoxidation increased as the amplitude of NPQ attained during HL increased. A comprehensive model for the molecular events responsible for activating and deactivating non-photochemical quenching in *Nitzschia* cells is presented.

3.5-2 Simultaneous monitoring of NPQ fluorescence quenching and pigment conversion during high light transitions

In isolated chloroplasts and in leaves of higher plants the de-epoxidation of violaxanthin to zeaxanthin is readily observed *in vivo* by monitoring absorbance changes in the 500 to 540 nm region (Gisselsson et al. 2004). Figure 3.5-1 shows the relationship between xanthophyll absorbance change and $\mathcal{NPQ}$ in a leaf during a HL transition. Following a similar approach, one should also be able to track DD de-epoxidation during NPQ in diatoms. Ruban et al. (2004) found a near linear relationship between $\mathcal{NPQ}$ and change in cell absorbance at 520 nm and

also at 515 nm in *Phaeodactylum tricornutum.* In the present study, small scale absorbance changes in *Nitzschia* were tracked by monitoring changes between transmittance photocurrent at 510 and 493 nm (termed Δ510) (see *Section 2.9* for methodology details). These wavelengths were chosen because they correspond to the wavelengths of DT and DD maximum absorption, respectively, and produced strong difference peaks in the 77K HL *minus* dark absorbance spectra (Figure 3.2-10C). The changes in transmission witnessed in the whole cells during HL illuminations corresponded to absorption changes on the order of 10^{-4} to 10^{-3}, so it is valid to approximate linear change in absorption from the Δ510 signal. The experimental apparatus allowed the simultaneous collection of fluorescence and Δ510.

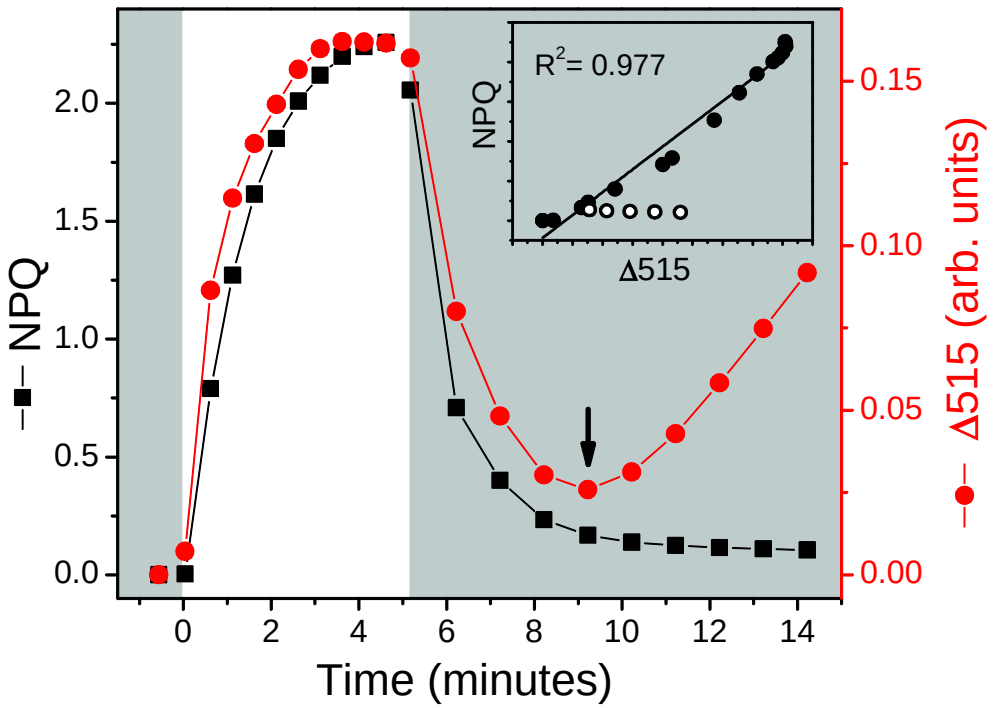

Figure 3.5-1 The inter-relationship between Δ515 and NPQ in higher plants. Simultaneous measurements of $\mathcal{NPQ}$ and Δ515 transients during the transition of a dark adapted leaf from shade grown *Taraxacum officinale* to 500 μmol $m^{-2}s^{-1}$ high light (HL) illumination. Darkened plot area indicates dark conditions; white plot area indicates HL conditions. **Insert**, correlation of Δ515 and $\mathcal{NPQ}$ obtained during both NPQ induction and relaxation up to the time point identified by the vertical arrow (solid symbol shapes, coefficient of determination value given); the increase in Δ515 without an increase in $\mathcal{NPQ}$ (open symbol shape) thereafter is attributed to *de novo* synthesis.

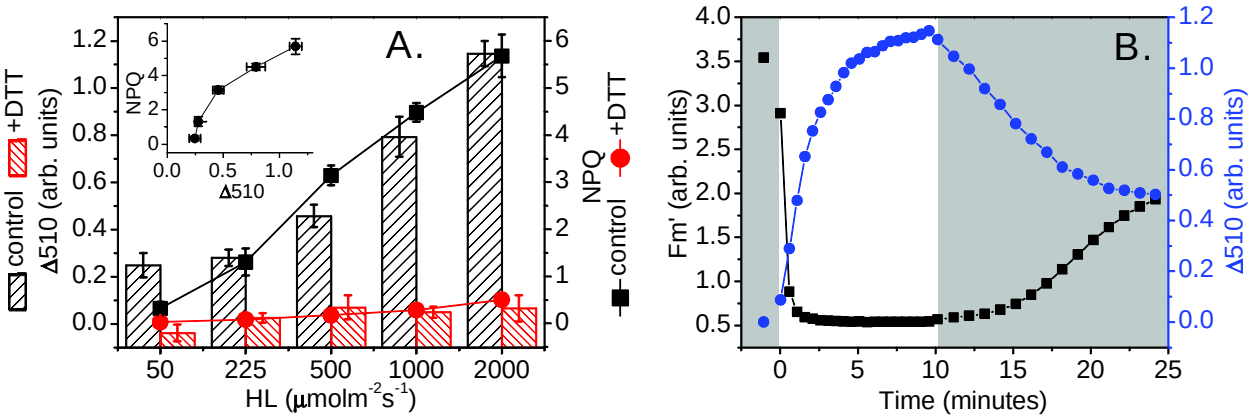

Figure 3.5-2 Identification of Δ510 signal in *Nitzschia* cells. A transient absorption signal was identified at 510 nm (reported as the difference in photocurrent from transmittance at 493 nm and 510 nm; an increase in Δ510 is indicative of an absorption increase at 510 nm as compared to absorption at 493 nm). See Section 2.9 for methodology details. **A**, Δ510 measured during steady state NPQ conditions at 10 minutes of high light (HL) was inhibited at all HL intensities by a pre-treatment with 5.3 mM of the DD de-epoxidase inhibitor DTT. Insert, $\mathcal{NPQ}$ had a nonlinear positive correlation with Δ510. Error bars represent ± 1 standard deviation from the mean of 3 separate cultures grown at 50 μmol $m^{-2}s^{-1}$. **B**, Δ510 had an inverse relationship with maximal fluorescence (Fm') during HL transitions. Shown is a representative plot obtained with 2000 μmol $m^{-2}s^{-1}$ HL. Darkened plot area indicates dark conditions; white plot area indicates HL conditions.

The Δ510 signal in *Nitzschia* cells showed a dynamic response to high light transitions. To verify that the Δ510 signal was in fact due to the de-epoxidation of DD to DT, cells were pretreated with DTT and then illuminated with HL. As expected, DTT inhibited Δ510 signal generation at all HL intensities (Figure 3.5-2A). (Of course, Δ510 would be preferably verified by HPLC analysis, but this approach was not practical.) However, the kinetics of Δ510 induction and relaxation varied from that of the quenching fluorescence signal (Figure 3.5-2B); the consequences of this will be discussed in much detail later. To further verify that the Δ510 signal behaved as predicted by assignment to DD de-epoxidation, Δ510 was measured with pre-treatment of the uncoupler NH_4Cl to completely knock out qE and the ATP synthase inhibitor DCCD to maximise qE. As predicted, NH_4Cl completely inhibited any change in Δ510 (and sometimes even gave a weak negative signal) and DCCD enhanced the signal (Figure 3.5-3). Also the changes in $\mathcal{NPQ}$ and Δ510 amplitude had a positive relationship (Figure 3.5-2A insert).

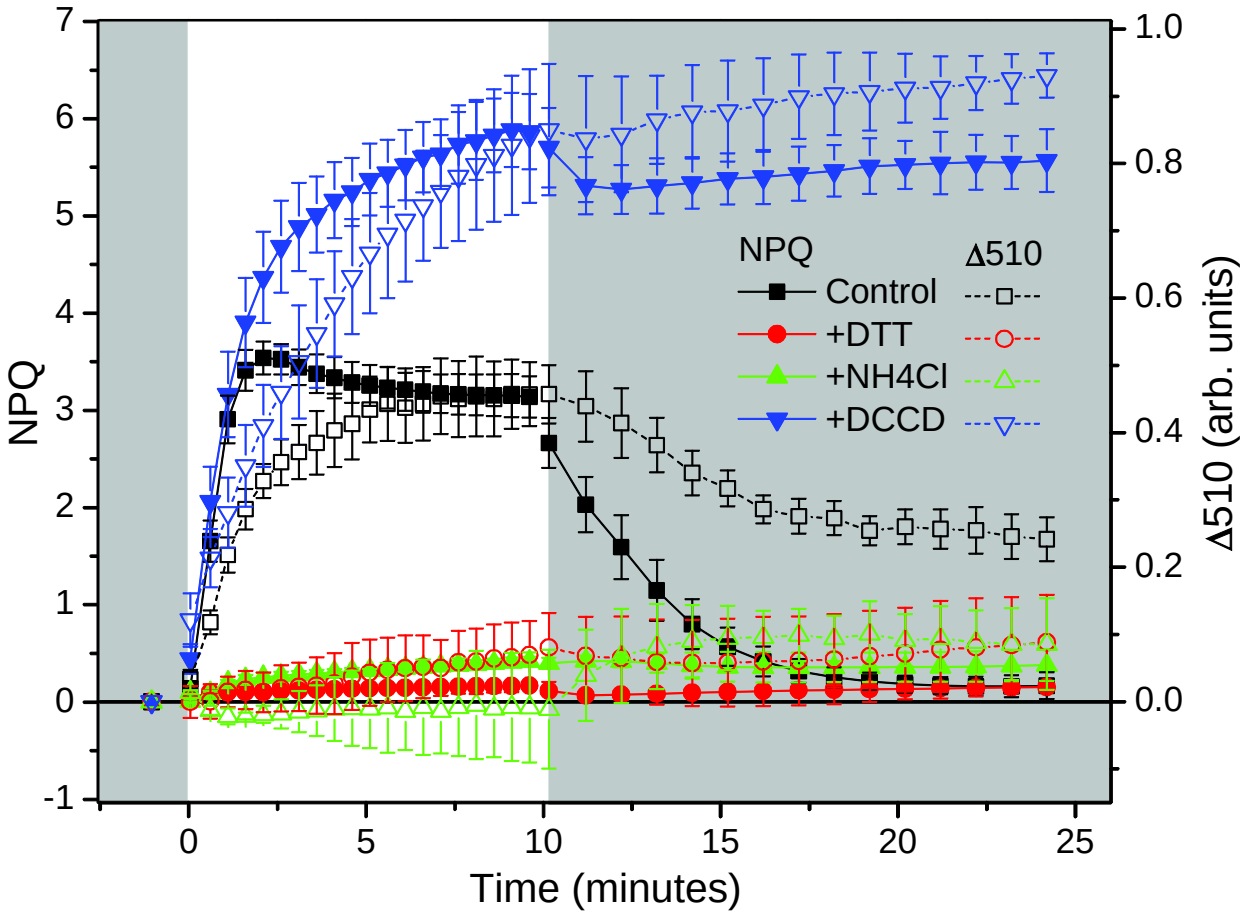

Figure 3.5-3 Response of Δ510 to NPQ effector treatments. Δ510 and $\mathcal{NPQ}$ were monitored simultaneously during a high light (HL) (500 µmol $m^{-2}s^{-1}$) transition from dark adapted cells pretreated with the de-epoxidase inhibitor DTT (5.3 mM), the uncoupler NH_4Cl (2.8 mM), or the ATP synthase inhibitor DCCD (320 µM). Darkened plot area indicates dark conditions; white plot area indicates HL conditions. Error bars represent ± 1 standard deviation from the mean of 3 separate cultures grown at 50 µmol $m^{-2}s^{-1}$.

So the Δ510 signal has most of the properties predicated by originating from ΔpH regulated de-epoxidation of DD to DT via DD de-epoxidase and epoxidation of DT to DD via DT epoxidase. In order to fully characterise the connection between fluorescence quenching and DD epoxidation state, $\mathcal{NPQ}$ and Δ510 were measured from cells during transitions to HL with irradiance intensities spanning from growth light to full sunlight equivalence. These $\mathcal{NPQ}$ and Δ510 transients revealed a complex relationship between the induction and relaxation of these two phenomena (Figure 3.5-4). Of concern was if DD and DT absorbance was changing due to *de novo* synthesis pathways during the time period of the experiments and contributing to the

Δ510 signal. In the biosynthetic pathway for carotenoids and xanthophylls in diatoms, DT can be synthesized directly from violaxanthin and DD is consumed in the synthesis of Fx (Bertrand 2010, Lohr and Wilhelm 2001). In cells that were pretreated with DTT, Δ510 did not substantially change over the +DTT levels depicted in Figure 3.5-2A during a 30 minute 2000 µmol $m^{-2}s^{-1}$ illumination period (data not shown), which encompasses the length in time of any of the HL transition experiments presented in this study (Section 3.5). Thereby, *de novo* carotenoid synthesis was not believed to contribute to the Δ510 signal. Direct comparison of fluorescence quenching using the non-linear Stern-Volmer $\mathcal{NPQ}$ quenching parameter ($(Fm_{dark}-Fm') / Fm')$) to the 'linear' Δ510 signal is valid (Ruban et al. 2004) and is most representative of the mechanisms involved in creating the signals.

3.5-3 NPQ has a variable dependency on DD epoxidation state

NPQ has a complex interdependency on DD epoxidation state. Of notice was that according to the Δ510 signal, DD de-epoxidation proceeded slower than $\mathcal{NPQ}$ induction during illumination and there was no reversal of DD epoxidation state during illumination even though at the lower HL intensities $\mathcal{NPQ}$ relaxed during illumination (Figure 3.5-4). Assuming Δ510 adequately describes DD epoxidation state, then if the accumulation of DT during HL is the sole cause of NPQ, the two should show a linear correlation during NPQ induction and relaxation. A correlation analysis was performed to investigate the dependency between Δ510 and $\mathcal{NPQ}$ (Figure 3.5-5).

There was not a linear relationship between Δ510 and $\mathcal{NPQ}$ during NPQ induction; the initial production of a few DT molecules (a small rise in Δ510) was associated with a large

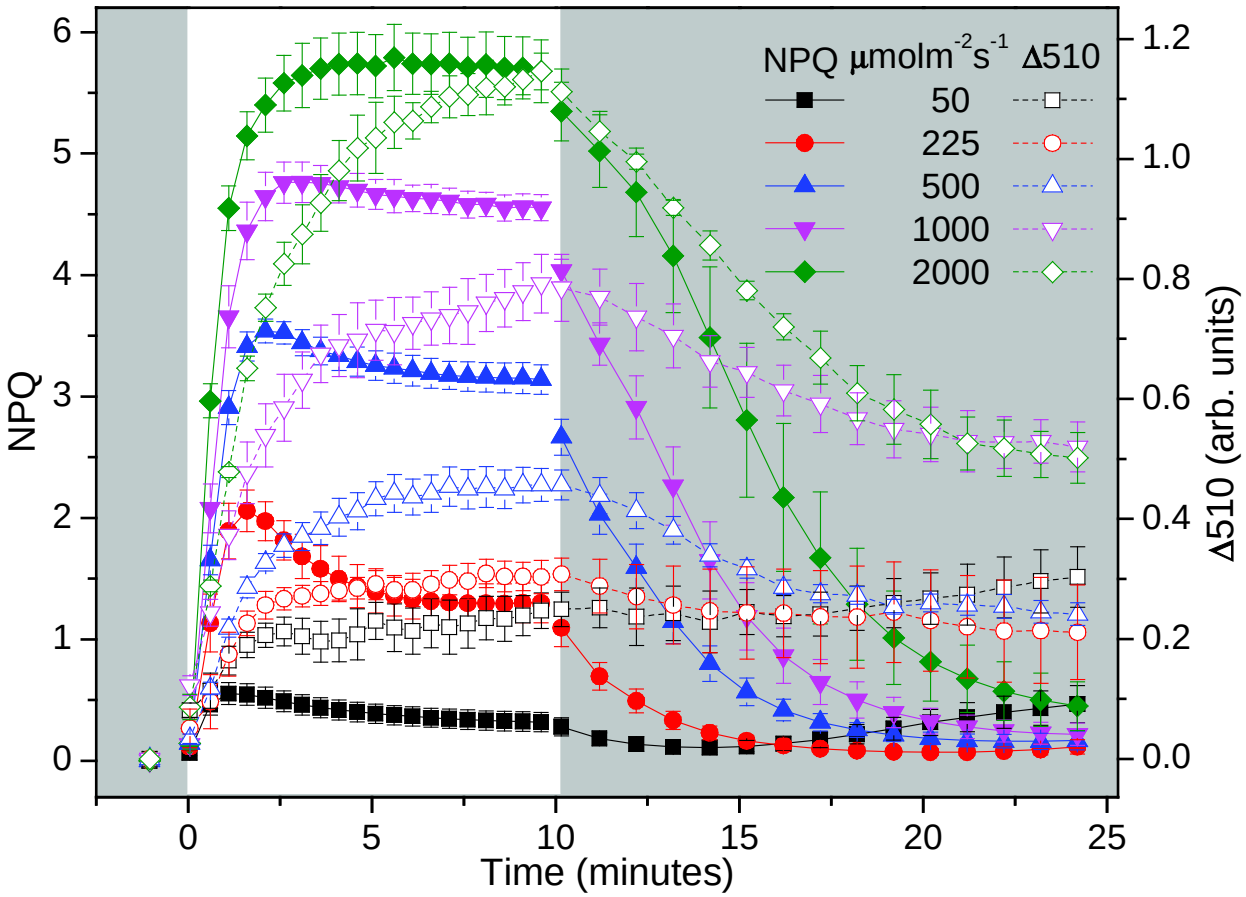

Figure 3.5-4 NPQ and Δ510 transients for high light transitions. Δ510 and *NPQ* were monitored simultaneously during transitions of dark adapted cells to a full range of high light (HL) intensities. Darkened plot area indicates dark conditions; white plot area indicates HL conditions. Error bars represent ± 1 standard deviation from the mean of 3 separate cultures grown at 50 µmol $m^{-2}s^{-1}$.

increase in quenching (Figure 3.5-5A). The data exhibited a sigmoidal shape and was fit to a Hill function (Figure 3.5-5A). In terms of the Hill fit modelling, the "macromolecule" with cooperative binding sites would be an FCP "quenching complex", the substrate would be de-epoxidised DD (i.e. newly formed DT), and the product would be a quenched FCP "quenching complex". The positive cooperativity (Hill coefficient of ~2.4) implies that there are multiple types of binding sites for newly formed DT and that the binding of DT molecules facilitates the binding of additional DT molecules. The sigmoidal relationship between Δ510 and quenching is describing a "phase" transition of the antenna system from a light harvesting mode to an

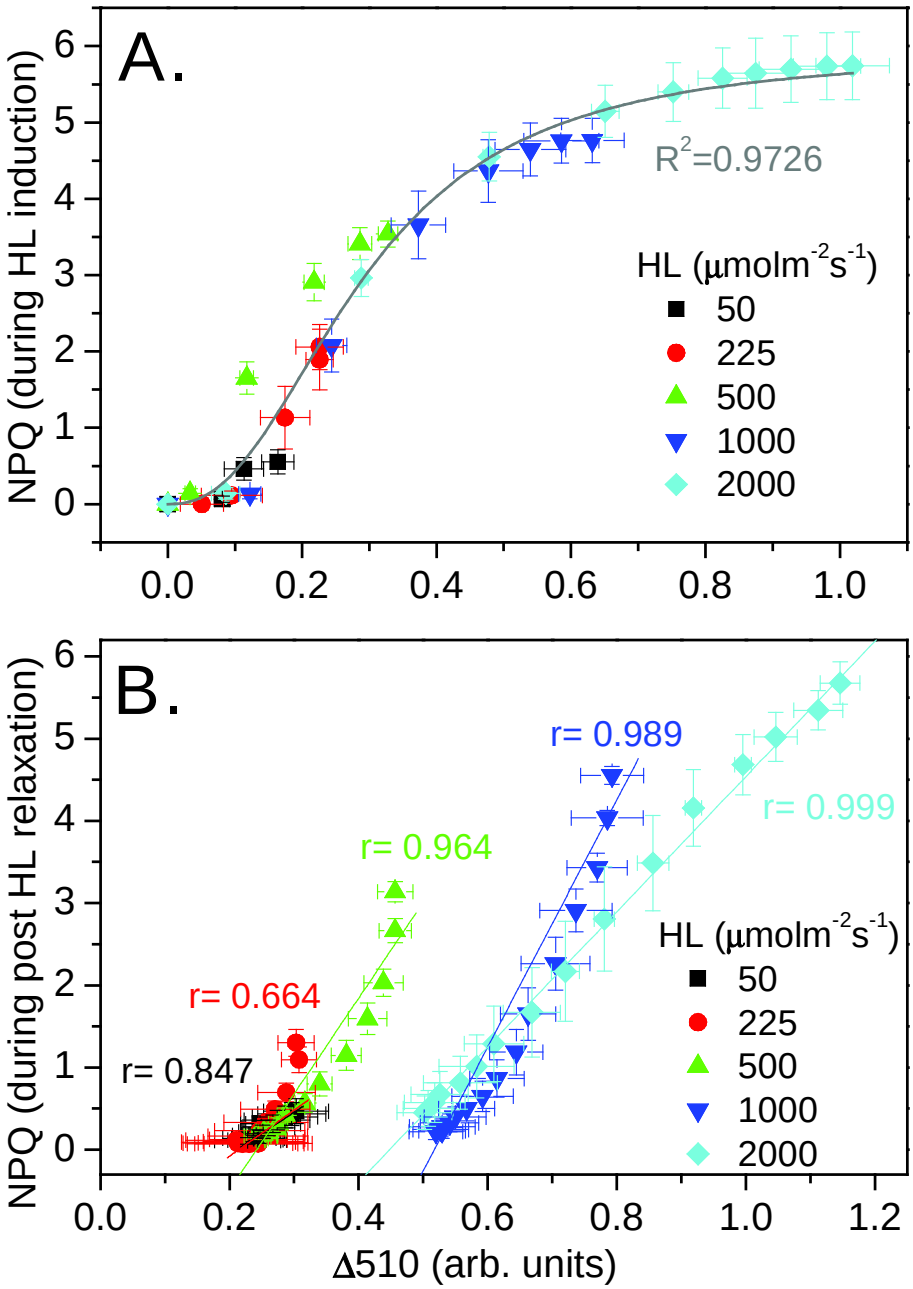

Figure 3.5-5 NPQ and Δ510 correlation analysis for NPQ induction during high light (HL) and NPQ relaxation in the dark post HL. **A**, correlation between Δ510 and $\mathcal{NPQ}$ during NPQ induction with HL (only data points corresponding to increasing $\mathcal{NPQ}$ are plotted and were used for the analysis). The concatenate data from all HL transients was fit to a Hill function. $\mathrm{NPQ} = V_{max}\frac{\Delta 510^n}{k^n + \Delta 510^n}$, V_{max}= 5.933 ±0.268 (± standard error of the fit), *k*= 0.292 ±0.018, *n*= 2.380 ± 0.271. Fitted curve shown in grey with corresponding reduced coefficient of determination. **B**, correlation between Δ510 and $\mathcal{NPQ}$ during NPQ relaxation in the post HL dark period (only data points corresponding to decreasing $\mathcal{NPQ}$ are plotted and were used for the analysis). A linear regression analysis was performed on each data set from the different HL intensities. The corresponding regression lines and Pearson's r values are shown next to each data set. Error bars represent ± 1 standard deviation from the mean of 3 separate cultures grown at 50 µmol $m^{-2}s^{-1}$.

energy dissipative mode, which is facilitated by DD de-epoxidation in a manner consistent with an allosteric role of DD during NPQ induction.

During the relaxation of NPQ upon cessation of HL illumination, $\mathcal{NPQ}$ also had a variable relationship with Δ510. At lower illumination intensities $\mathcal{NPQ}$ relaxed fully post HL with a very limited change in Δ510 (Figure 3.5-4), corresponding to a weak linear correlation between Δ510 and $\mathcal{NPQ}$ (Figure 3.5-5B). As HL irradiance intensified the relationship approaches and then turns linear at the highest HL irradiance (Figure 3.5-5B). This can be interpreted as NPQ relaxation from low steady state $\mathcal{NPQ}$ amplitudes does not necessitate DT epoxidation, whereas NPQ relaxation from the highest levels of steady state $\mathcal{NPQ}$ does require DT epoxidation. Therefore, the accumulation of high amounts of DT up to a threshold during illumination locks the thylakoid into a quenched state and the subsequent relaxation of this quenched state requires the conversion of *some* of these DT molecules back to DD.

NPQ is transiently more dynamic than DD epoxidation state. The relationship between $\mathcal{NPQ}$ induction/ relaxation and Δ510 is further explored in Figure 3.5-6. $\mathcal{NPQ}$ was induced about twice as fast as Δ510 upon the start of HL illumination (Figure 3.5-6A). Δ510 never relaxed during illumination, whereas $\mathcal{NPQ}$ showed significant relaxation during low intensity illuminations, where some 40% of the $\mathcal{NPQ}$ could relax while the HL was still *on* (Figure 3.5-6B). It was only at full sunlight equivalence that $\mathcal{NPQ}$ amplitude plateaued during illumination. Notice from the $\mathcal{NPQ}$ and Δ510 transients (Figure 3.5-4) that $\mathcal{NPQ}$ began to drop immediately once HL ended (within 2 seconds). This fast relaxation of NPQ post HL became proportionately weaker as irradiance intensity increased (Figure 3.5-6C). To the contrary, DD de-epoxidation

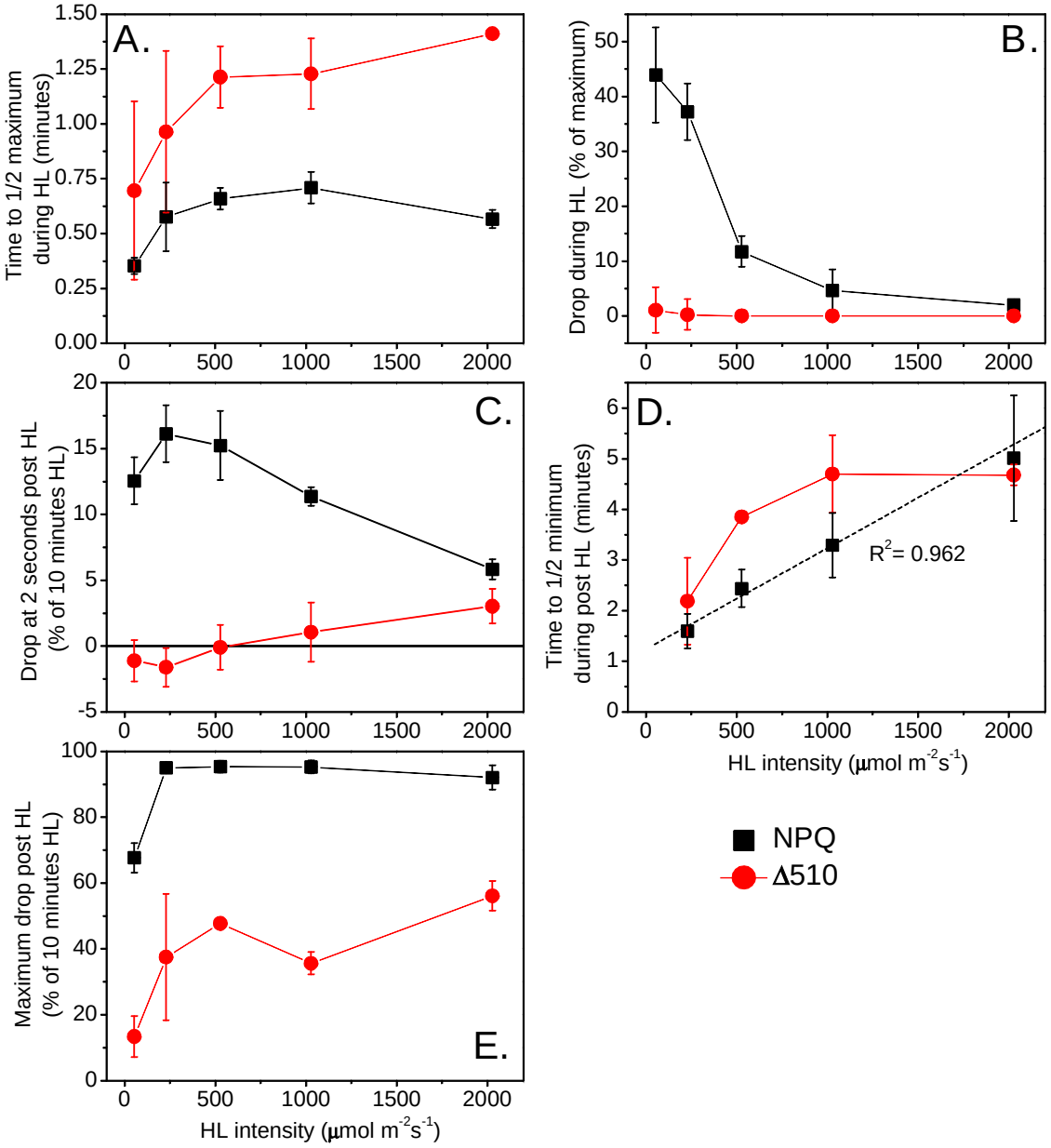

Figure 3.5-6 Summary analysis for the rise and fall of NPQ and Δ510 during high light transitions. Δ510 and *NPQ* were monitored simultaneously during the transition of dark adapted cells to 10 minutes of high light (HL) to 15 minutes of dark (post HL). **A**, the time it takes to reach ½ of maximum attainable *NPQ* or Δ510 amplitude during HL *on*. **B**, the amount of *NPQ* amplitude or Δ510 amplitude that relaxes (drops) during illumination, expressed as a percentage of maximum amplitude attained during HL. **C**, the amount of *NPQ* amplitude or Δ510 amplitude that drops immediately upon transition from 10 minutes HL to post HL dark, expressed as a percentage of amplitude at 10 minutes HL. **D**, the time it takes during the post HL dark period for *NPQ* or Δ510 amplitude to drop to ½ of the minimum amplitude attained post HL. No data points are shown for relaxation of the weak NPQ induced by the lowest HL intensity. The dashed line is a linear regression of *NPQ*. **E**, the maximum amount of *NPQ* amplitude or Δ510 amplitude that can relax (drop) during the 15 minute post HL dark period, expressed as a percentage of amplitude at 10 minutes HL. Error bars represent ± 1 standard deviation from the mean of 3 separate cultures grown at 50 µmol $m^{-2}s^{-1}$.

seemed to weakly continue during this period at low irradiances and only began to reverse at high irradiances (Figure 3.5-6C). $\mathcal{NPQ}$ and Δ510 both relaxed non-linearly post HL following the initial 'instantaneous' drop in $\mathcal{NPQ}$ (see Figure 3.5-4). $\mathcal{NPQ}$ relaxation time increased directly with irradiance intensity whereas Δ510 relaxation time saturated at 1000 µmol $m^{-2}s^{-1}$ (Figure 3.5-6D). During the 15 minute post HL period $\mathcal{NPQ}$ always relaxed more in amplitude than Δ510. While there was near complete relaxation of $\mathcal{NPQ}$ (>90% of the level prior to HL *off*), Δ510 relaxation never exceeded ~60 %. In general, quenching ($\mathcal{NPQ}$) had a more dynamic response to illumination than did DD epoxidation state (Δ510), especially during the initial transitions to and away from HL. These results implicate that NPQ is regulated by another factor other than just the number of DT molecules produced during HL, with the important exception occurring during the relaxation of NPQ when the capacity to perform NPQ has saturated.

3.5-4 The response of NPQ to short-term cold stress

Cold stress in *Nitzschia* cells increased excitation pressure and non-photochemical quenching. Low temperature preferentially slows the diffusion dependent photosynthetic reactions (namely the Calvin-Benson cycle enzymes) more than the photochemical reactions of the photosystems, thus cold stress induces excitation pressure on PSII much in the same way as high irradiance (Huner et al. 1998). Chilling *Nitzschia* cells from 18°C to 2°C did not significantly change maximum quantum efficiency of PSII photochemistry, but did have noticeable effects on energy conversion by the photosynthetic apparatus during a transition to HL. As predicted, cold greatly lowered the effective quantum efficiency of PSII photochemistry during illumination (Figure 3.5-7), thereby increasing excitation pressure throughout the illumination

period (Figure 3.5-8B), which resulted in an increase in the quantum yield of energy dissipation via NPQ (Figure 3.5-7) and the amplitude of $\mathcal{NPQ}$ (Figure 3.5-8). Upon cessation of HL, the instantaneous drop in NPQ yield increased in the chilled cells; however, all the quantum yields for energy conversion remained stable thereafter (as compared to cells at 18°C, Figure 3.5-7). This unresponsiveness in the chilled cells post HL is being attributed to a deactivation of the enzymes responsible for rebalancing redox status within the chloroplast.

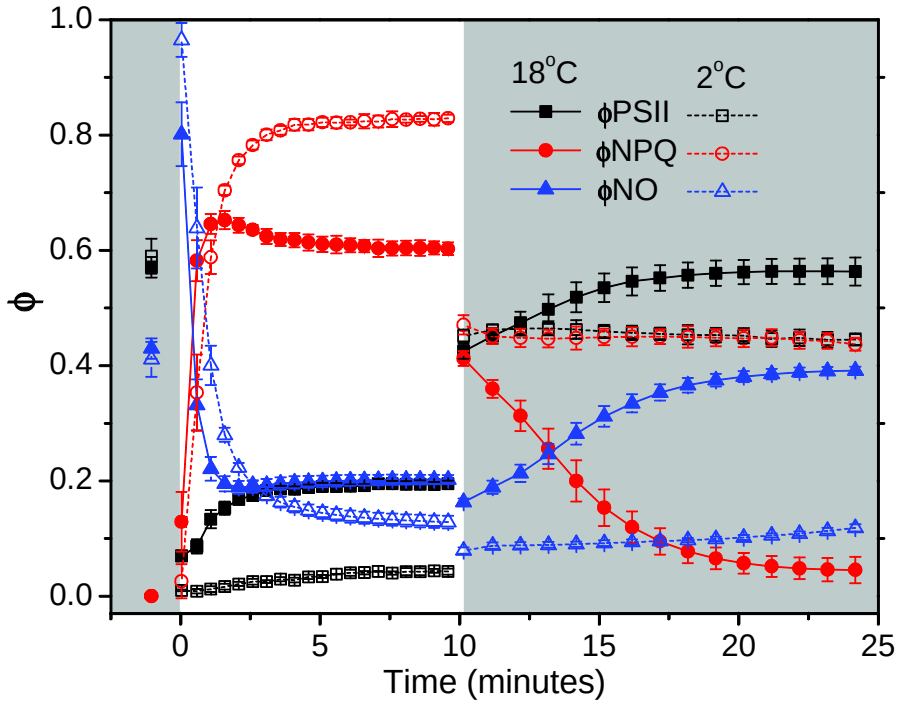

Figure 3.5-7 The effect of cold temperature on the quantum yields of excitation energy conversion. The quantum yields of PSII photochemical energy conversion (ϕPSII), regulated non-photochemical energy dissipation (ϕNPQ), and non-regulated non-photochemical energy dissipation (ϕNO) were calculated for dark adapted cells (grown at 18°C) that had had a 5 minute 2°C pre-treatment (in the dark) during a transition to 500 µmol $m^{-2}s^{-1}$ high light (HL) with the temperature held at 2°C. Darkened plot area indicates dark conditions; white plot area indicates HL conditions. Error bars represent ± 1 standard deviation from the mean of 3 separate cultures grown at 50 µmol $m^{-2}s^{-1}$.

$\mathcal{NPQ}$ and Δ510 transients in response to the chilling treatment are shown in Figure 3.5-8A with analysis of the curves shown in Figure 3.5-8B. $\mathcal{NPQ}$ amplitude more than doubled in the cold treated cells; Δ510 also increased but not proportionately (Figure 3.5-8B). $\mathcal{NPQ}$ only

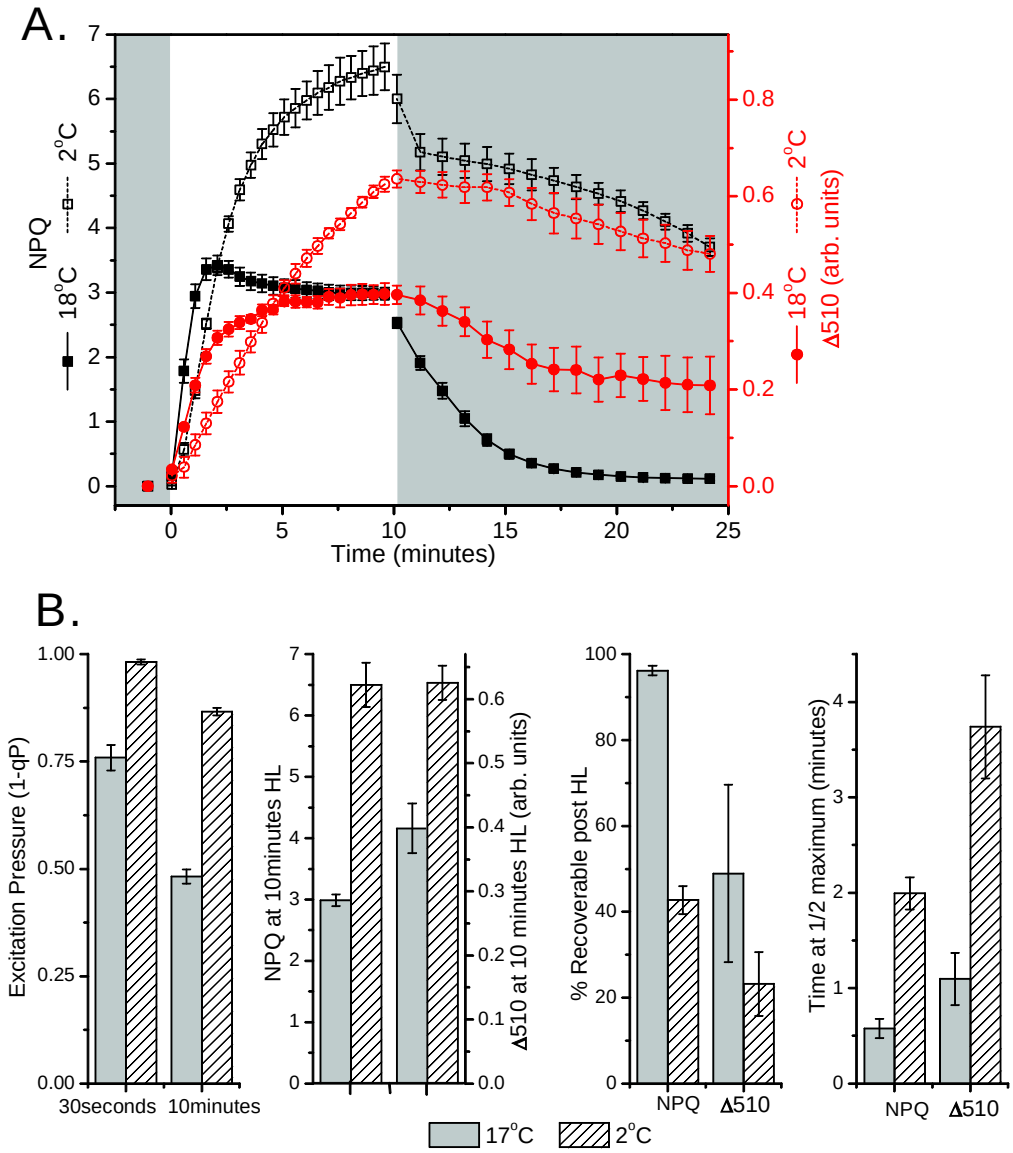

Figure 3.5-8 The effect of cold temperature on NPQ and Δ510. A, $\mathcal{NPQ}$ and Δ510 transients obtained during the transition of dark adapted cells (grown at 18°C) that had had a 5 minute 2° C pre-treatment (in the dark) to 500 µmol $m^{-2}s^{-1}$ high light (HL) with the temperature held at 2°C. Darkened plot area indicates dark conditions; white plot area indicates HL conditions. **B**, from Left to Right: Measure of excitation pressure at 30 seconds and 10 minutes of HL; $\mathcal{NPQ}$ and Δ510 amplitude attained at 10 minutes HL; the percentage of $\mathcal{NPQ}$ and Δ510 which is reversible during a 15 minute post HL period in the dark ((signal at 10 minutes HL – signal at 15 minutes post HL) / signal at 10 minutes HL); the time it takes to reach ½ of maximum attainable $\mathcal{NPQ}$ and Δ510 amplitude during HL *on*. Error bars represent ± 1 standard deviation from the mean of 3 separate cultures grown at 50 µmol $m^{-2}s^{-1}$.

relaxed half as much at 2°C; Δ510 relaxation post HL was less affected (Figure 3.5-8B). The rates of $\mathcal{NPQ}$ and Δ510 induction were both about 3.5 times slower when chilled (Figure 3.5-

8B). These results suggest that DD de-epoxidation is a temperature (and diffusion) limited reaction, thereby slowing the dependent rate of NPQ induction at low temperature. Violaxanthin de-epoxidase activity in higher plants is diffusion dependent. It requires the lateral diffusion of carotenoid substrate within the bilayer to MGDG rich regions to which violaxanthin de-epoxidase is believed to bind under acidic lumen conditions (Latowski et al. 2002, Latowski et al. 2004, Arnoux et al. 2009). Violaxanthin de-epoxidation in plant chloroplasts shows a strong dependency on temperature with cold dramatically reducing de-epoxidation in non-cold acclimated chloroplasts (Arvidsson et al. 1997). Diatom DD de-epoxidase also requires MGDG for activity (Goss et al. 2005, Goss et al. 2007), so it is reasonable to conceive that the activity of DD de-epoxidase is also dependent on the diffusion rate of DD molecules within the thylakoid.

3.5-6 The molecular 'memory' for NPQ is low in Nitzschia *cells*

The allosteric activator role of zeaxanthin in higher plants allows NPQ to be pumped by consecutive excess light treatments when interrupted by a brief dark period. ΔpH relaxes quickly in the dark, but not de-epoxidation, leaving the thylakoid pre-primed for the next round of excess light thereby causing qE to induce more rapidly during subsequent illuminations (Ruban and Horton 1999). These conclusions were based on zeaxanthin performing a role in which it opens up protonatable domains in the light harvesting complexes; with ΔpH these domains undergo a conformational change that promotes quenching interactions between pigments (Horton and Ruban 2005). In Figures 3.5-9 and 3.5-10, *Nitzschia* cells were exposed to consecutive HL treatments in an attempt to pump the NPQ response. To ensure that ΔpH dropped prior to the second bout of HL, the 15 minute post HL dark period was retained in

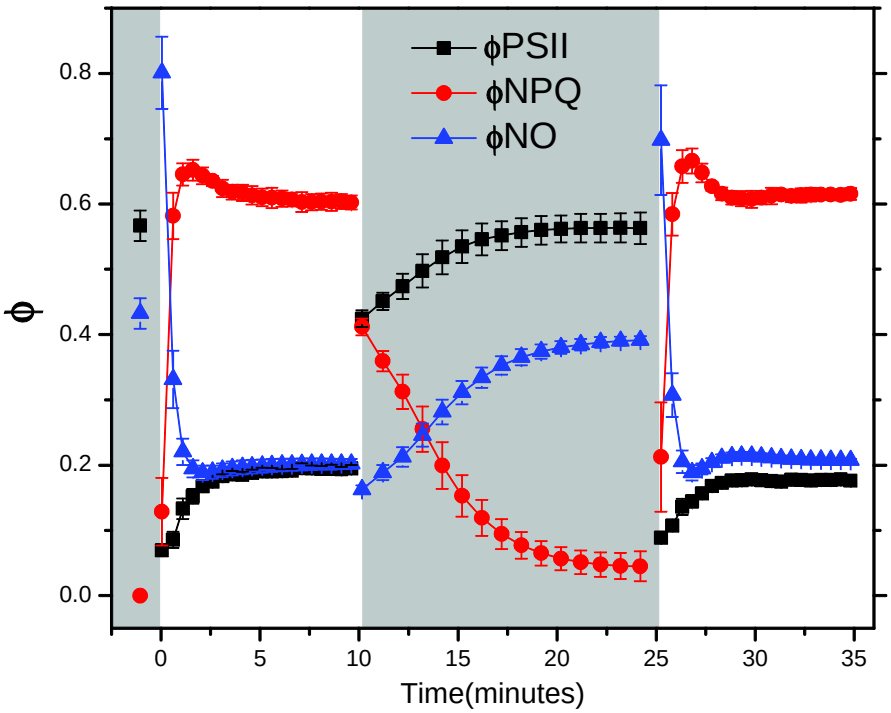

Figure 3.5-9 The effect of consecutive high light transitions on the quantum yields of excitation energy conversion. The quantum yields of PSII photochemical energy conversion (ϕPSII), regulated non-photochemical energy dissipation (ϕNPQ), and non-regulated non-photochemical energy dissipation (ϕNO) were calculated during a transition of dark adapted cells to 500 µmol $m^{-2}s^{-1}$ high light (HL), followed by dark, followed by 500 µmol $m^{-2}s^{-1}$ HL again**.** Darkened plot area indicates dark conditions; white plot areas indicate HL conditions. Error bars represent ± 1 standard deviation from the mean of 3 separate cultures grown at 50 µmol $m^{-2}s^{-1}$.

these experiments because it allowed NPQ to nearly completely relax (Figure 3.5-10) - a strong indicator for the dissipation of ΔpH. At the end of this 15 minute post HL period, ~50% of Δ510 was retained (Figure 3.5-10); thereby, the DD/DT pool remained in a de-epoxidised state prior to the second HL period. The photosynthetic apparatus made very little distinction between the two HL illuminations as determined by the quantum rates of energy conversion (Figure 3.5-9). Likewise, the second bout of HL did not significantly differ from the first in terms of amplitude of $\mathcal{NPQ}$ or rate of $\mathcal{NPQ}$ induction (Figure 3.5-10B). The second HL period also did not significantly change the magnitude of de-epoxidation (Δ510) attained at 10 minutes HL or the rate of de-epoxidation during the transition to HL (Figure 3.5-10B). Since de-epoxidation did

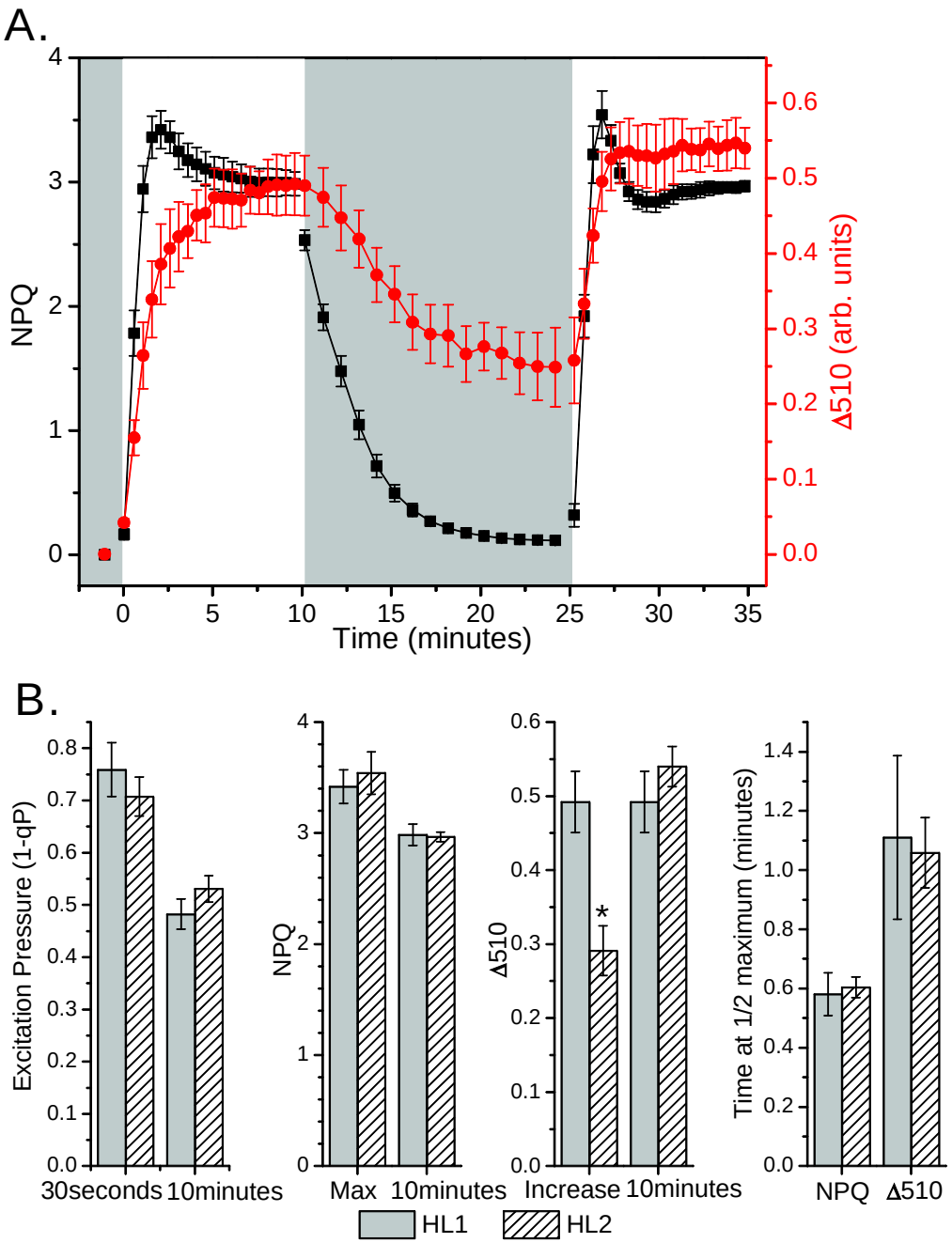

Figure 3.5-10 The effect of consecutive high light transitions on NPQ and Δ510. A, $\mathcal{NPQ}$ and Δ510 transients obtained during a transition of dark adapted cells to 500 µmol $m^{-2}s^{-1}$ high light (HL1), followed by 15 minutes dark, followed by 10 more minutes of 500 µmol $m^{-2}s^{-1}$ high light (HL2). Darkened plot area indicates dark conditions; white plot areas indicate HL conditions. **B**, quantitative comparison between the HL1 and HL2 transitions in panel A. From Left to Right: Excitation pressure measured at 30 seconds and 10 minutes HL; maximal $\mathcal{NPQ}$ amplitude attained during HL illumination and $\mathcal{NPQ}$ amplitude at 10 minutes HL; the increase in Δ510 during HL (amplitude at end of HL illumination – amplitude immediately prior to HL illumination) and the amplitude of Δ510 at minutes HL; the time it takes to reach ½ of maximum attainable $\mathcal{NPQ}$ and Δ510 amplitude during HL *on*. Error bars represent ± 1 standard deviation from the mean of 3 separate cultures grown at 50 µmol $m^{-2}s^{-1}$. The asterisk denotes a significant difference between HL1 and HL2 as determined with a two-sample t-test at 95% confidence interval.

not fully relax after the first bout of HL, fewer new de-epoxidations were needed during the second HL period to attain the same level of de-epoxidation (Figure 3.5-10B). Perhaps the thylakoid retained a structural arrangement from the previous HL illumination that favored the propensity for quenching, thus endowing a smaller de-epoxidations to quenching ratio. Regardless, the limited effect of the second HL period on quenching implies that NPQ induction in *Nitzschia* is dependent on ΔpH generation during HL and the *activity* of DD de-epoxidation, but not on pre-existing DD epoxidation state. The pre-accumulation of DT does not enhance quenching the next time the cells are exposed to HL. The differences in rate of $\mathcal{NPQ}$ induction and maximal attainable $\mathcal{NPQ}$ that could be observed between cultures (data not shown) further suggests that NPQ capacity is determined by more slowly regulated mechanisms, such as gene expression, and not by transitory changes within the thylakoid environment.

3.5-7 Both ΔpH and DD de-epoxidase are obligatory for NPQ activity

ΔpH and DD de-epoxidase work in a concerted effort to induce and maintain NPQ in *Nitzschia* cells. As previously shown (*Figures 3.1-7, 3.2-4*, & 3.5-3) pre-treatment with DTT in the dark prior to illumination fully inhibits NPQ induction in *Nitzschia* cells much in the same way as a pre-treatment with the uncoupler NH_4Cl (*Figures 3.1-8, 3.2-4*, & 3.5-3). Thus, both ΔpH must develop and DD de-epoxidase must be active to initiate the NPQ response upon exposure to HL. Additionally, ΔpH must be present and DD de-epoxidase must be active to maintain NPQ.

Removal of ΔpH always relaxes NPQ. Figure 3.5-11A shows the application of the uncoupler NH_4Cl during illumination to cells that have already developed NPQ. Immediately upon addition of the uncoupler $\mathcal{NPQ}$ collapses, and collapses fully within 90 seconds. Even

when NPQ has been pushed towards maximum capacity, as through pre-treatment with the ATP synthase inhibitor DCCD, subsequent washing of the cells in NH_4Cl was able to remove quenching (Figure 3.5-11B). DCCD pre-treatment inhibits the slow recovery of NPQ post HL that is attributable to DT epoxidation, ostensibly by limiting NADPH availability (see *Section 3.3-4*). Recall that according to the Δ510 experiments, DT epoxidation proceeds slowly post HL and not at all in DCCD treated cells (Figure 3.5-3). Either the NH_4Cl wash dissipated ΔpH for the activation of DT epoxidase to reverse NPQ, or the complete dissipation of ΔpH in itself was enough to reverse quenching. The later scenario seems the most likely. So, NPQ can always be relaxed by dissipating ΔpH even when the DD pool retains a high state of de-epoxidation.

DD de-epoxidation is always needed to induce NPQ in *Nitzschia* cells. If the accumulation of DT during NPQ serves as an allosteric regulator for keeping quenching domains open to activation protonation, as is the modeled role for zeaxanthin in plants, then as long as this allosteric DT is present quenching should be possible. The double illumination experiment (Figure 3.5-10) showed that pre-existing DD de-epoxidation does not enhance NPQ induction during ΔpH development by the next illumination period. Figure 3.5-11C further tests if a pre-existing DT pool can induce another round of NPQ, but here the effect is tested on cells actively performing NPQ with an existing ΔpH. Cells were illuminated at a low HL irradiance until photostasis was reached, and then shifted to a higher irradiance. This resulted in an increase in $\mathcal{NPQ}$, as expected, and was attributed to a rise in ΔpH with the higher irradiance. However, when DTT was added to cells during the low HL illumination $\mathcal{NPQ}$ began to surprisingly drop to a weak basal level while the light was still *on* (Figure 3.5-11C), and upon transition to the higher irradiance no measurable $\mathcal{NPQ}$ was induced. Thus an active DD de-epoxidase is always a

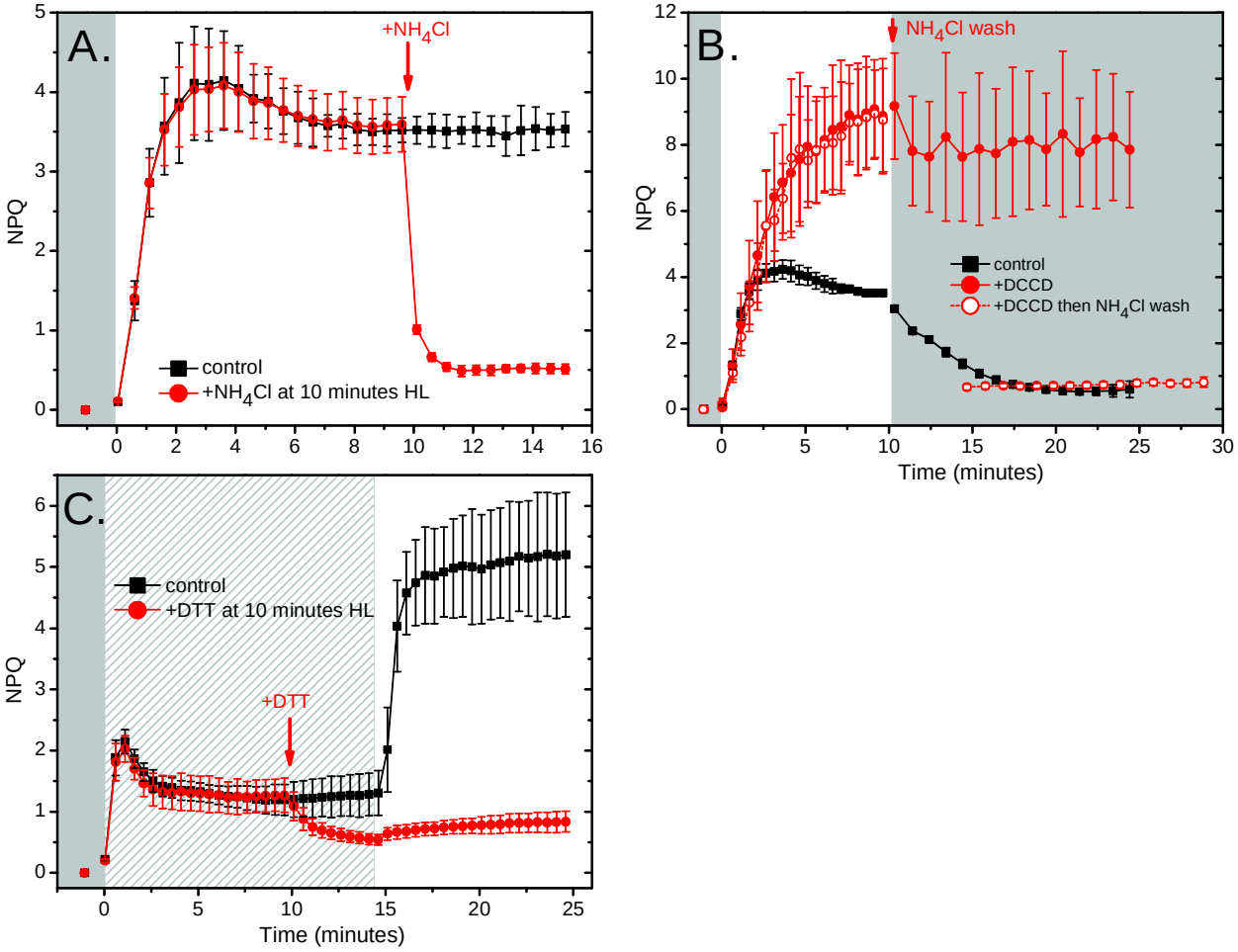

Figure 3.5-11 ΔpH and DD de-epoxidation control NPQ in *Nitzschia* cells. *NPQ* transients are shown for dark adapted cells during high light (HL) transitions. The effect of adding NPQ inhibitors while the cells were actively performing NPQ is examined. **A**, the application of the uncoupler NH_4Cl to a final concentration of 2.8 mM after 10 minutes of 500 µmol $m^{-2}s^{-1}$ HL. An equivalent volume of growth media as NH_4Cl concentrate was added to the control at the same time point (indicated by arrow) to negate any dilution effects. Darkened plot area indicates dark conditions; white plot area indicates HL. **B**, dark adapted cells pretreated with the ATP synthase inhibitor DCCD (320 µM) were illuminated with 500 µmol $m^{-2}s^{-1}$ HL for 10 minutes then washed in 2.8 mM NH_4Cl for 5 minutes in the dark. **C**, the application of the DD de-epoxidase inhibitor DTT to a final concentration of 5.3 mM after 10 minutes of 300 µmol $m^{-2}s^{-1}$ HL (illumination of this intensity identified by lightly shaded background) followed by a transition to 1000 µmol $m^{-2}s^{-1}$ HL (illumination of this intensity identified by white background). An equivalent volume of growth media as DTT concentrate was added to the control at the same time point (indicated by arrow) to negate any dilution effects. Experiments in A and C were performed in a 5 mL beaker constantly stirred with illumination and detection from above. Error bars represent ± 1 standard deviation from the mean of 3 separate cultures grown at 50 µmol $m^{-2}s^{-1}$.

requirement for inducing NPQ even when in the presence of a HL maintained ΔpH. This data further suggests that an active DD de-epoxidase is involved in maintaining steady state NPQ

during HL (at least at lower irradiances). DTT is predicted to inhibit DD de-epoxidase by preventing dimer formation and docking to the thylakoid membrane, yet DTT has no effect on PSII photochemistry (ΦPSII) (see *Section 3.1-4*).

3.5-8 A schema for the order of molecular events responsible for the activation/ deactivation of non-photochemical fluorescence quenching in Nitzschia *cells*

The molecular events that lead to NPQ activation and deactivation during high light transitions in *Nitzschia curvilineata* are outlined in Figure 3.5-12. These interpretations are based on the accumulated evidence from the current and preceding Sections.

ΔpH is the trigger for the NPQ response, DD de-epoxidase is the mediator, and DD is an allosteric regulator. During the induction of NPQ, ΔpH and DD de-epoxidation are mutually obligatory for the activation of quenchers. Dissipation of ΔpH is obligatory for NPQ relaxation whereas DT epoxidation is beneficial. Removal of polar DD molecules from the FCP thylakoid domains promotes FCP protein-protein interactions which bring adjacent trimers together forming a FCP quenching aggregate. Additionally the protonation of a glutamate residue within the lumenal loop of FCP proteins causes a conformational shift affecting b605 Chl *a* positioning at the inter-trimer interface. The combined effect of DD de-epoxidation and lumenal loop protonation is the bringing together of b605 Chl *a* from adjacent trimers to form a quencher dimer. The resulting Chl *a*-Chl *a* dimer has a mixed exciton charge transfer state with enhanced non-radiative excited state dissipation to the ground state. Non-photochemical quenching is carried out by the Chl *a*-Chl *a* quencher dimers within a FCP quenching aggregate. The composition of the FCP quenching aggregate is dependent on what antenna domain it forms in. The outer FCP antenna complexes are believed to function as oligomers, so outer FCP

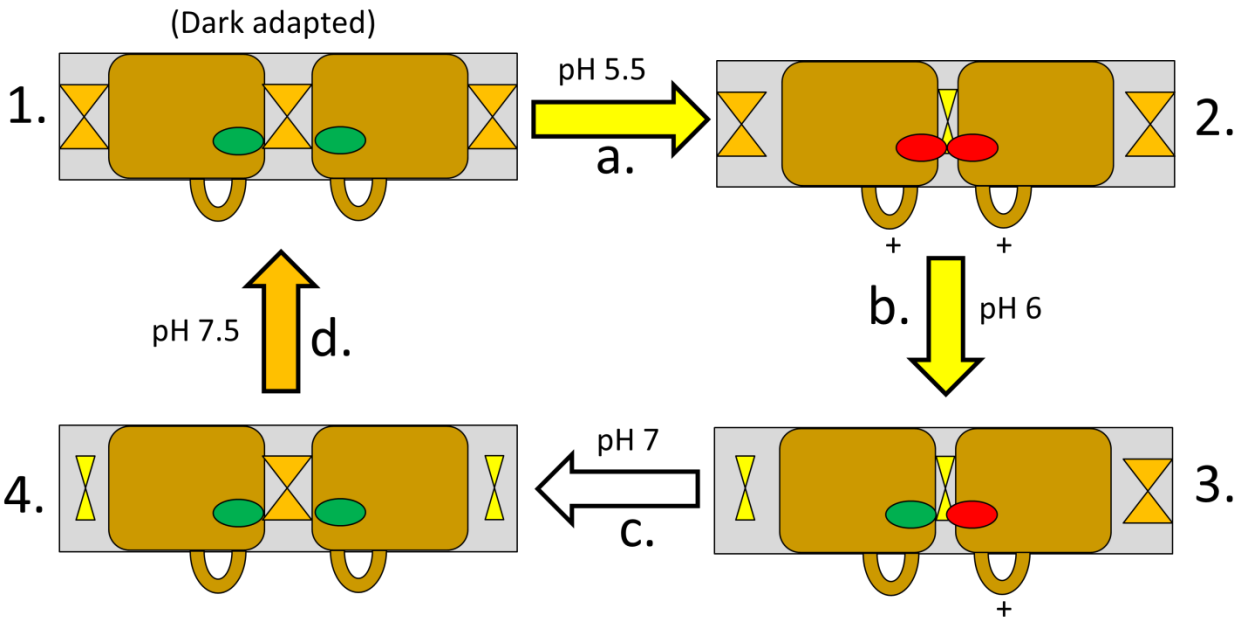

Figure 3.5-12 Schema for the molecular events responsible for the induction and relaxation of non-photochemical fluorescence quenching in *Nitzschia* cells. The phases for the transition of FCP antenna from a dark adapted state to a high light (moderately excess light) adapted quenching state back to a dark adapted state are illustrated above and have been numbered 1 to 4.

FCP complexes are localised within monogalactosyldiacylglycerate (MGDG) enriched thylakoid domains (as according to Lepetit et al. 2010) indicated by the grey regions. FCP trimers are in gold-brown shown with a glutamate containing lumenal loop. b605 Chl *a*s located near trimer-trimer interfaces are shown as ovals. Diadinoxanthin (DD) is represented by the orange double triangle. DT is represented as the yellow double triangle. Arrows represent transitions between NPQ phases and have been labeled (a. to d.) for ease of discussion. A representative lumenal pH value for triggering each transition is given beside the arrows. Transitions facilitated by DD de-epoxidase have a yellow arrow. DD de-epoxidase is predicted to be active at pHs below 7.2 with optimal activation at pH 5.5 (Jakob et al. 2001). The transition facilitated by DT epoxidase has an orange arrow. DT epoxidase is inhibited by a ΔpH (Goss et al. 2006b). The white arrow indicates a transition independent of DD de-epoxidation or DT epoxidation. Specific pKa values for the lumenal loop glutamate residues are unknown.

1. In the dark adapted state, polar DD molecules associated with the interfaces between FCP trimers serve as an allosteric regulator for maintaining spatial separation of FCP trimers. The b605 Chl *a*s function in light harvesting (indicated by green). DD de-epoxidase is found in its inactive monomeric form within the lumen in accordance to the schema for violaxanthin de-epoxidase activation (Arnoux et al. 2009) (not shown in cartoon).

2. Upon high light illumination, the rapid acidification of the lumen (arrow a.) triggers dimerization and docking of DD de-epoxidase onto the MGDG enriched thylakoid domains in accordance to the schema for violaxanthin de-epoxidase activation (Arnoux et al. 2009). DD de-epoxidase pulls DD into the lipocalin channel of the enzyme during de-epoxidation in accordance to the schema for violaxanthin de-epoxidase activity (Arnoux et al. 2009). Removal of polar DD molecules from the FCP inter-trimer interfaces promotes protein-protein interactions between FCP trimers and stimulates FCP aggregation. Concurrently, protonation (indicated by +) of a glutamate residue within the lumenal loop of FCP proteins (Gundermann and Büchel 2012, see *Section 3.4-10*) induces a conformational change promoting the

formation of inter-trimer b605 Chl *a*-Chl *a* quencher dimers (the active quencher dimer is shown in red in the cartoon). The very low pH during the initial transition to high light would be able to protonate all of the lumenal loop glutamate residues. FCP quenching aggregates have thus been formed.

3. As photostasis is approached, lumenal pH rises (arrow b.) to a level in which DD de-epoxidase is still active, but above that at which to maintain full protonation of the lumenal loop glutamate residues. This partially deactivates/ weakens the Chl *a*-Chl *a* quencher dimer (shown as half green-half red).

Since DD de-epoxidase can remain active at neutral pHs it would always be at least basally active during illumination, but high lumenal pHs would not be able to protonate the lumenal loop glutamates and thus there would be no new induction of quenching. However, basally active DD de-epoxidase would keep residual DD molecules from diffusing into the inter-trimer interfaces and dispersing the FCP quenching aggregates. Steady state conditions at all but saturating high light irradiances would be characterised by a large population of partially deactivated/ weakened Chl *a*-Chl *a* quencher dimers within FCP quenching aggregates maintained by low level DD de-epoxidase activity. If lumenal pH approaches neutral, DD de-epoxidase can go through deactivation/ activation cycles in which it decouples and recouples to the thylakoid.

4. Upon termination of high light, the rapid rise in lumenal pH (arrow c.) deprotonates all the FCP lumenal loop glutamate residues causing a rapid partial deactivation of all Chl *a*-Chl *a* quencher dimers. DD de-epoxidase is inactivated and disassociates from the thylakoid. If DD de-epoxidation did not remove all of the DD molecules from the surrounding lipid pool, the residual DD molecules can diffuse back into the inter-trimer interfaces thereby disrupting the FCP quenching aggregates and fully deactivating their Chl *a*-Chl *a* quencher dimers. When ΔpH fully dissipates (arrow d.), DT epoxidase is activated and converts DT back to DD which reinstates the antenna system to its pre HL organisation.

If there was a high level of de-epoxidation during high light then there are no residual DD molecules available to break up the FCP quenching aggregates. DT epoxidation is then required to reintroduce DD molecules into the FCP thylakoid domain for dispersal of the FCP quenching aggregates and full deactivation of the Chl *a*-Chl *a* quencher dimers. DT epoxidation is slow because it is dependent on the availability of NADPH. Under lower high light irradiances in which photostasis was reached, the efficient use of NADPH during carbon fixation depletes the availability of NADPH for DT epoxidase. This is inconsequential though, because there is an abundant residual population of DD molecules.

---

quenching aggregates would be large multimeric complexes - this is where Q1 quenching sites are located. The inner FCP antenna complexes are predicted to function as trimers, so a smaller quenching aggregate would form - this is the location of Q2 quenching sites. The predicted heterogeneity of FCP complex protein composition would provide multiple pKa values for the lumenal loop glutamate residue. During the initial transition to HL lumenal pH is expected to be very acidic (~pH 5.5), making a range of activation pKas for quenching somewhat useless. However, while approaching photostasis during illumination a variety of activation pKas for

quenching would create a range of lumenal pHs for the partial deactivation/ weakening of quenchers, which would provide a feedback mechanism for fine tuning the extent of quenching during illumination. Full deactivation of quenching requires dispersal of the FCP quenching aggregates via reinsertion of DD molecules into the inter-trimer interfaces.

The cooperative nature of DD de-epoxidation and quenching (Figure 3.5-5A) permits the rapid induction of quenching in relation to DD de-epoxidation. Recall that the induction of $\mathcal{NPQ}$ is twice as fast as that of DD de-epoxidation (Figure 3.5-6A). However, if the $\mathcal{NPQ}$ and Δ510 transients are normalised to their amplitudes during steady state conditions at 10 minutes HL, the initial rise in signal at 2 seconds of illumination is always proportionately more in Δ510 than in $\mathcal{NPQ}$ (see Figure 3.5-3). This strongly suggests that DD de-epoxidation must proceed before quenching can begin. One can envision that several DD molecules need to be de-epoxidised to change the thylakoid environment enough to promote FCP aggregation, particular within the large outer FCP antenna complexes. Yet, once the allosteric regulatory DD molecules have been removed and a FCP quenching aggregate forms, the light harvesting contribution of many pigments are lost concurrently. For instance: according to the FCP model of Premvardhan et al. (2010) each FCP trimer contains 54 pigments, and assuming that an inter-trimer Chl *a*-Chl *a* quencher dimer can quench excitations from both trimers, 108 pigments can simultaneously be deactivated from their light harvesting function. Furthermore if a Chl *a*-Chl *a* quencher dimer forms between two hexameric FCP complexes, 208 pigments can be deactivated during the formation of a single quencher. The large effective absorbance cross sections which are possible for a quencher promote rapid logarithmic-like growth of quenching in response to DD de-epoxidation. This effect gives the antenna system a high quenching efficiency (see *Section*

3.4-11). NPQ capacity saturates under high irradiance illumination when all the quencher sites have been activated and proficient purging of DD molecules from the FCP thylakoid domains via DD de-epoxidase keeps the FCP quenching aggregates from dispersing. DD de-epoxidation can continue as long as there is substrate available (accessible DD and ascorbate) even if NPQ capacity has reached saturation. The accumulation of DT molecules above the level needed to fully activate quenching serves to stabilise the FCP quenching aggregates by preventing distal DD molecules from diffusing into the FCP trimer interfaces. In these *Nitzschia* cells, DD de-epoxidation did not appear to be the limiting 'reactant' to quenching capacity, because Δ510 continually grew during the highest irradiance illumination period even after $\mathcal{NPQ}$ levels reached saturation (Figure 3.5-4).

Reversal of quenching is dependent on deprotonation and dispersal of the FCP quenching aggregates. A rise in lumenal pH deprotonates the lumenal loop glutamate residue and diffusion of DD molecules back into the inter-trimer interface disperses the FCP aggregate. These DD molecules may originate from DD molecules that were not de-epoxidised during illumination or may come from the epoxidation of DT. FCP aggregate dispersal can occur during illumination if there is a sufficient residual population of DD molecules for diffusion back into the inter-FCP trimer interfaces. Sustained de-epoxidation can lead to a large scale depletion of DD molecules from the FCP thylakoid domains, resulting in the formation of large multimeric FCP quenching aggregates. The multitude of protein-protein interactions involved may make these aggregates quite stable. The outer antenna is predisposed to formation of large multimeric FCP quenching aggregates due to these FCP pre-occurring as oligomers. Q2 quenching within the inner FCP antenna would be less likely to form large multimeric

quenching aggregates because the functional form of the inner FCP is anticipated to be trimeric, not oligomeric.

Quenching can relax independently of DD epoxidation state. The induction of non-photochemical quenching stops either at saturation (as with very high irradiances) or when photostasis is able to lower ΔpH below the activation pHs for lumenal loop protonation and stop the formation of Chl *a*-Chl *a* quencher dimers. Deprotonation of the lumenal loops would cause a partial deactivation/ weakening of the quenchers. Full deactivation of a FCP quenching aggregate requires dispersal of the aggregate via the input of polar DD molecules into the inter-trimer interfaces. Because lumenal loop glutamates may deprotonate at a lower lumenal pH than that at which DD de-epoxidase inactivates, DD de-epoxidation can occur even as quenching relaxes. DT epoxidase is inhibited by a ΔpH (Goss et al. 2006b) and thus is not predicted to be active during HL illumination, which would account for why there was never a significant reversal of Δ510 during illumination (Figure 3.5-6B). When illumination ceases and dark conditions begin, the photochemical reactions responsible for generating ΔpH also cease and lumenal pH can drop rapidly, especially during the lag time that ATP synthase remains active. The fast rise in lumenal pH would quickly deactivate DD de-epoxidase and deprotonate even weakly acidic pKa lumenal loop glutamates. This facilitates a fast (within 2 seconds of HL *off*) partial relaxation of quenching post HL (Figure 3.5-6C).

Full relaxation of quenching is only dependent on DT epoxidation when the pre-existing DD pool has been substantially depleted. For the lower HL irradiances NPQ was able to relax fully post HL without a change in DD epoxidation state. This was attainable because the limited

de-epoxidase activity during HL left a large residual pool of DD molecules to facilitate the dispersal of FCP quenching aggregates post HL. NPQ relaxes much more slowly than NPQ induction because relaxation is dependent on the 'slow' diffusion of DD molecules from the lipid bound DD pool into the inter-trimer FCP interfaces, as opposed to the enzyme mediated removal of DD molecules that occurs during NPQ induction. If DD de-epoxidase was highly active during HL illumination then the DD pool may become severely depleted, requiring the input of DD molecules via DT epoxidase. DT epoxidation proceeds slowly post HL due to a low availability of NADPH.

The double HL illumination period experiments revealed that fewer DD de-epoxidations (i.e. Δ510) are required to achieve an equivalent level of quenching ($\mathcal{NPQ}$) during the second bout of HL (Figure 3.5-10). This must at least be partly due to the high de-epoxidation state retained after the first HL period. But since DD de-epoxidation is obligatory for the induction of NPQ, the pre-existing DT molecules cannot directly activate quenching. Yet removing 'excess' DD during the previous bout of illumination means fewer DD molecules need to be processed to reach those that are at the FCP trimer interfaces during the second go-around of illumination. Because the amplitude of DD de-epoxidation (Δ510) was similar for both HL periods to reach equivalent $\mathcal{NPQ}$ levels, one can interpret that specific DD de-epoxidation levels are required to maintain specific levels of FCP quenching aggregates. One is drawn to ask: if the DD pool is driven to full de-epoxidation, can there still be induction of NPQ?

All of the predicted changes to the organisation of the pigment-protein complexes within the thylakoid during HL ultimately stem from ΔpH. Complete deprotonation of the

thylakoid with the addition of NH_4Cl could always fully dissipate NPQ, either when NPQ was being actively maintained during HL illumination or when NPQ had been locked-in via DCCD treatment (Figure 3.5-11B). This confirms that NPQ is ultimately controlled by pH sensitive electrostatic interactions between the antenna complexes.

3.5-9 Conclusions

NPQ and DD de-epoxidation were monitored simultaneously during high light transitions. It was found that quenching has a complex, non-linear positive relationship with DD de-epoxidation. The induction of NPQ was shown to have a cooperative relationship with DD de-epoxidation. The relaxation of NPQ did not necessitate a reversal of DD de-epoxidation but was facilitated by it. A schema describing the molecular events responsible for activating and deactivating antenna centred non-photochemical quenching in *Nitzschia curvilineata* was presented. DD de-epoxidation was predicted to remove the allosteric barrier to the formation of FCP quenching aggregates. A high lumenal pH was predicted to protonate glutamates within FCP lumenal loops and induce conformational changes within the FCP proteins that bring together Chl *a* from adjacent FCP trimers to form Chl *a*-Chl *a* quencher dimers. Quenching was found to be able to partially relax during HL illumination even in the presence of increasing DD de-epoxidation. This phenomenon was explained by DD de-epoxidase being active at higher lumenal pHs than the pKas for FCP lumenal loop glutamate residues. Full relaxation of NPQ was predicted to require dispersal of FCP quenching aggregates via the input of DD molecules into the inter-FCP trimer interfaces or by a full deprotonation of the FCP. If de-epoxidation during HL illumination left a sufficient pool of DD molecules, then these DD molecules were postulated to be able to diffuse in from the surrounding lipid matrix and disperse the FCP quenching

aggregates without any DT epoxidation. However, if the DD pool is exhausted via high level de-epoxidation during HL illumination, new DD molecules seemingly need to be made via DT epoxidation.

In higher plants xanthophyll epoxidation state provides the slow *on*/*off* ΔpH-controlled switch for qE. The accumulation of zeaxanthin during excess light serves to modulate the responsiveness of the thylakoid to fluctuations in ΔpH. The fast *on*/*off* ΔpH-controlled switch for qE is protonation of a glutamate residue within the two lumenal loops of PsbS. This enables qE to respond rapidly to changes in ΔpH without a need for xanthophyll de-epoxidation/ epoxidation when qE has been 'pre-primed' by a high xanthophyll de-epoxidation state (as reviewed by Horton and Ruban 2005, Horton et al. 2005). Under excess light acclimated states (e.g. midday sunlight) the kinetics of qE induction and relaxation are no longer controlled by the 'slow' enzymatic reactions of de-epoxidation and epoxidation, but are directly controlled by lumenal pH via PsbS protonation. This twofold dynamism over qE regulation in land plants has been interpreted as an adaptation to countering rapid changes in irradiance that are associated with leaf movements and sunflecks (via protonation activation of qE by PsbS without change in epoxidation state) against a background of diurnal changes in light levels (the extent of the de-epoxidation state determines how many quenching sites can be activated by ΔpH) (as discussed by Horton and Ruban 2005).

When LhcX was discovered in diatoms and its expression level was found to be linked to NPQ capacity (Bailleul et al. 2010), many thought that the PsbS congruent proton sensor for NPQ in diatoms had at last been identified. Yet LhcX proteins in diatoms do not contain a

glutamate residue within their lumenal loop (Gundermann and Büchel 2012), thus making LhcX unlikely as the pH sensor. Instead LhcX may serve to regulate the packing of the FCP complexes within the thylakoid in a manner more conducive to the formation of FCP quenching aggregates, but not directly trigger the formation of the quenching aggregates. Many LhcFs in diatoms do contain a glutamate residue in their lumenal loop (Gundermann and Büchel 2012, *Figure 3.4-20*). Thus FCPs have a built-in pH sensor, which frees them from dependence on another protein for this role. However, self-protonation within FCP proteins seems to be less effective at initiating interactions between FCP complexes that would form FCP quenching aggregates. Instead diatoms rely heavily on DD for controlling protein-protein interactions during NPQ. *Arabidopsis* mutants lacking PsbS still maintained a slow inducing, weak amplitude qE and this qE relaxed very slowly with a high dependency on epoxidation (Li et al. 2002b) in a manner reminiscent of NPQ relaxation in diatoms. The lack of PsbS gives diatom antenna based qE (i.e. the qE_{XC} described in the current body of work, and what most people would call 'typical' diatom NPQ) very different induction and relaxation mechanics. Whereas qE can be induced without de-epoxidation in plants pretreated with excess light, DD de-epoxidation was always required for the induction of antenna based qE in *Nitzschia* cells. Furthermore, qE can relax quickly post HL in higher plants without any input from epoxidation, but full relaxation of antenna based qE in *Nitzschia* cells was slow (unless facilitated by the application of a proton scavenger) seemingly requiring an input of DD molecules either via diffusion from other regions of the thylakoid or via DT epoxidation.

What does this all mean in terms of the ability of diatoms to regulate excitation energy? Both plant qE and diatom antenna based qE are induced on similar time scales giving both

photosynthesizers a fast method for dissipating excess excitation energy and initiating photoprotection, yet the extent of energy dissipation by NPQ in diatoms can be several times greater than that observed in higher plants (typical max $\mathcal{NPQ}$ value in higher plants is around 2, $\mathcal{NPQ}$ in diatoms can approach 10). On the flip side, diatom antenna based qE recovers much slower post HL than plant qE. A slow recovery from quenching would decrease light harvesting efficiency upon transition away from the excess light stress. Is there less selection pressure on the diatom system to develop a fast relaxing quenching mechanism? The ecophysiological advantages of being able to rapidly turn on a powerful photoprotective mechanism seem to outweigh the disadvantage of turning it off slowly within the context of the environments that diatoms have evolved.

4 Summary of Major Findings

The preceding body of work was a comprehensive enquiry into the fast regulation of photosynthesis in diatoms in response to excess light. The phenomenon of non-photochemical fluorescence quenching (NPQ) was investigated from two perspectives: the *physiological* triggers that govern the regulation of NPQ and the *physical* mechanisms that execute NPQ. The transiency of diatom NPQ was explored across 19 orders of magnitude in time (from picoseconds to weeks) and the diversity of diatom NPQ was explored across several ecological niches. A primarily spectroscopic approach was taken when examining the highly physical processes involved in regulating light energy. Real time monitoring of photosynthetic energy conversion and electron transport was achieved by using the method of PAM fluorometry. The real time monitoring of xanthophyll cycle driven pigment conversion was tracked via small scale absorbance changes. Snapshots were taken of the fluxes in excitation energy distribution that occur during NPQ by flash freezing cells and performing low temperature spectroscopic measurements on those samples. Different components of the NPQ response were selectively inhibited with chemical agents. These measurements revealed that NPQ in diatoms is a highly dynamic response: NPQ is the way that diatoms regulate photosynthesis outside of gene expression. Watching NPQ unfold is watching the diatom cells interact directly and quickly with their environment.

A detailed comparison of NPQ was performed between two pennate species: *Nitzschia curvilineata*, a 'typical' diatom originating from a marine shoreline, and *Navicula sp*., a soil species from an inland salt flat. There have been no known previous NPQ studies performed on

a soil diatom. As hypothesized by their divergent habitats of origin, these two species had very different approaches towards the dissipation of excess excitation energy. *Nitzschia* relied on the 'classic' dissipative approach that diatoms are so well known: a high magnitude antenna based quenching that is triggered by ΔpH and is heavily reliant on the enzymatic de-epoxidation of the xanthophyll diadinoxanthin (qE_{XC}). *Nitzschia* cells could also rather quickly reverse quenching once they were removed from excess light. Of much interest was the unique approach of *Navicula sp.* towards NPQ. This species had a rather limited capacity to perform NPQ (about ½ that of *Nitzschia*) but was still very capable of dissipating PSII excitation pressure. *Navicula* was less reliant on the xanthophyll cycle. The first line of defense in this organism against high irradiance was a regulated NPQ mechanism independent of DD de-epoxidation (qE_{nonXC}). This reaction centre attributed quenching was able to effectively regulate excitation pressure by itself. qE_{XC} in *Navicula* was easily saturated and only weakly relaxed after the excess irradiance period ended. Thus xanthophyll cycle dependent NPQ was assigned to a secondary role for long-term quenching, which has important implications in the context of the unique environment that the species originates. It was concluded that the NPQ mechanism in *Nitzschia* suited the needs for a shoreline diatom: it could rapidly and reversibly switch its antenna system from being optimised for light harvesting during low light conditions when under water, to a highly effective excitation energy dissipative machine when brought to the water surface by wave action. The natural light environment of *Navicula* cells is not light limiting and would not be exposed to such transient high amplitude changes in irradiance, so this diatom does not waste valuable nutrient resources for the maintenance of a large antenna to perform qE_{XC}, but instead relies on a putative reaction centre based quenching mechanism.

Further examination of the electron flux within these two species during high light transitions revealed that *Navicula* maintains a high rate of forward photosynthetic electron transfer and is more responsive to electron sink capacity than *Nitzschia* cells. These results were again interpreted as being an adaptation to the salt flat. Whereas *Nitzschia* is adapted to a poikilophotic environment where the major transiency determinant to cell growth is irradiance, *Navicula* is adapted to a poikilotrophic environment where the major transiency determinants to growth rate are nutrient availability and salinity. So, the selection pressure on *Navicula* has been to maximise nutrient uptake and growth when conditions are favorable. Chlororespiration was witnessed in both species by its ability to induce NPQ in the dark following an illumination period.

Next the pathway for antenna based excitation energy quenching (qE_{XC}) during NPQ was thoroughly investigated in *Nitzschia* cells. The principle photo-electronic mechanism for quenching was attributed to fast non-radiative excited state decay by a Chl *a*-Chl *a* mixed exciton charge transfer state. Such Chl *a*-Chl *a* quencher dimers were predicted to form at the interfaces between FCP trimers within FCP 'quenching aggregates'. Non-photochemical quenching was localised to two separate antenna domains in *Nitzschia* cells: Q1 within putative FCP quenching aggregates that assemble from the outer antenna for PSII and Q2 within putative FCP quenching aggregates that assemble from the inner antenna for PSII. Q2 quenching was able to relax quicker than Q1 quenching after excess light ended providing a more labile, PSII specific form of quenching. In the absence of diadinoxanthin de-epoxidation, all excitation energy redistribution associated with Q1 and Q2 was lost. It was concluded that diadinoxanthin de-epoxidation is responsible for the restructuring of light harvesting pathways

into excitation energy quenching pathways during the transition to excess light in *Nitzschia* cells.

The steps involved in enacting antenna based NPQ (qE_{XC}) in *Nitzschia* were also elucidated. A mechanistic model to fully explain the activation and deactivation of antenna based NPQ in *Nitzschia* was proposed. The experimental results strongly support that the development and establishment of ΔpH and the activity of the diadinoxanthin de-epoxidase enzyme are obligatory for NPQ. Whereas diadinoxanthin de-epoxidation was always required to initiate NPQ, afterwards the relationship between de-epoxidation and NPQ was found to be somewhat complex. The experimental evidence was highly consistent with diadinoxanthin being an allosteric regulator for the formation of the putative FCP quenching aggregates. Diadinoxanthin de-epoxidation seemed to work cooperatively to activate quenching, but quenching could relax without any measurable reversal of epoxidation state; thus providing a fast and labile method for fine tuning NPQ in response to ΔpH during the establishment of photostasis. The mechanistic model further proposed that the complete deactivation of quenching after excess light illumination ends requires the dispersal of the putative FCP quenching aggregates via an input of diadinoxanthin, and if de-epoxidase activity during excess light depletes the diadinoxanthin pool then 'new' diadinoxanthin molecules must be made via the slow (NADPH limited) epoxidation reaction. The schema presented for antenna based NPQ in *Nitzschia* is predicted to be applicable to other diatom species.

Is NPQ why diatoms have rapidly (in evolutionary time) become so successful? As more of all the aspects of diatom physiology are explored, the findings point towards diatoms having

a larger compliment of biochemical pathways available to them for integrating into photosynthesis than do many other algal groups (Wilhelm et al. 2006), most likely due to their complex evolutionary ancestry. Diatoms are one of the most rapidly evolving groups of eukaryotes on Earth (Oliver et al. 2007), so the diversity witnessed between species in performing NPQ is very relevant. Diatoms have many 'tricks up their sleeves' for obtaining a competitive edge over other algae, and their NPQ ability is probably just one of them.

5 Sources Cited

Andreeva A, Abarova S, Stoitchkova K, Busheva M (2009) Model for fluorescence quenching in light harvesting complex II in different aggregation states. European Biophysics Journal 38:199-208.

Andrizhiyevskaya EG, Chojnicka A, Bautista JA, Diner BA, van Grondelle R, Dekker JP (2005) Origin of the F685 and F695 fluorescence in Photosystem II. Photosynthesis Research 84:173-180.

Armbrust EV, Berges JA, Bowler C, Green BR, Martinez D, Putnam NH, Zhou S, Allen AE, Apt KE, Bechner M (2004) The genome of the diatom *Thalassiosira pseudonana*: ecology, evolution, and metabolism. Science 306:79-86.

Arnoux P, Morosinotto T, Saga G, Bassi R, Pignol D (2009) A structural basis for the pH-dependent xanthophyll cycle in *Arabidopsis thaliana*. The Plant Cell Online 21:2036-2044.

Arvidsson P, Carlsson M, Stefánsson H, Albertsson P, Åkerlund H (1997) Violaxanthin accessibility and temperature dependency for de-epoxidation in spinach thylakoid membranes. Photosynthesis Research 52:39-48.

Asada K (1996) Radical production and scavenging in the chloroplasts. In: Baker NR (ed) Photosynthesis and the environment. Kluwer Academic Publishers, Dordrecht, The Netherlands, pp 123-150.

Bailleul B, Rogato A, De Martino A, Coesel S, Cardol P, Bowler C, Falciatore A, Finazzi G (2010) An atypical member of the light-harvesting complex stress-related protein family modulates diatom responses to light. Proceedings of the National Academy of Sciences 107:18214-18219.

Bailleul B, Cardol P, Breyton C, Finazzi G (2010b) Electrochromism: a useful probe to study algal photosynthesis. Photosynthesis Research 106:179-189.

Ballottari M, Mozzo M, Girardon J, Hienerwadel R, Bassi R (2013) Chlorophyll Triplet Quenching and Photoprotection in the Higher Plant Monomeric Antenna Protein Lhcb5. The Journal of Physical Chemistry B, 117:11337-11348.

Barber J (1982) Influence of surface charges on thylakoid structure and function. Annual Review of Plant Physiology 33:261–295.

Beaufort L, Probert I, de Garidel-Thoron T, Bendif E, Ruiz-Pino D, Metzl N, Goyet C, Buchet N, Coupel P, Grelaud M (2011) Sensitivity of coccolithophores to carbonate chemistry and ocean acidification. Nature 476:80-83.

Becker W (2005) Advanced time-correlated single photon counting techniques (Series in chemical physics, Vol. 81). Springer, Berlin, Germany.

Beddard G, Porter G (1976) Concentration quenching in chlorophyll. Nature 260:366-367.

Bennoun P (1982) Evidence for a respiratory chain in the chloroplast. Proceedings of the National Academy of Sciences 79:4352-4356.

Berges JA, Franklin DJ, Harrison PJ (2001) Evolution of an artificial seawater medium: improvements in enriched seawater, artificial water over the last two decades. Journal of Phycology 37:1138-1145.

Bertrand M (2010) Carotenoid biosynthesis in diatoms. Photosynthesis Research106:89-102.

Bhaya D, Grossman AR (1993) Characterization of gene clusters encoding the fucoxanthin chlorophyll proteins of the diatom Phaeodactylum tricornutum. Nucleic Acids Research 21:4458-4466.

Bilger W, Björkman O (1990) Role of the xanthophyll cycle in photoprotection elucidated by measurements of light-induced absorbance changes, fluorescence and photosynthesis in leaves of *Hedera canariensis*. Photosynthesis Research 25:173-185.

Bonente G, Ballottari M, Truong TB, Morosinotto T, Ahn TK, Fleming GR, Niyogi KK, Bassi R (2011) Analysis of LhcSR3, a protein essential for feedback de-excitation in the green alga *Chlamydomonas reinhardtii*. PLoS biology 9:e1000577.

Bowler C, Allen AE, Badger JH, Grimwood J, Jabbari K, Kuo A, Maheswari U, Martens C, Maumus F, Otillar RP (2008) The *Phaeodactylum* genome reveals the evolutionary history of diatom genomes. Nature 456:239-244.

Brakemann T, Schlörmann W, Marquardt J, Nolte M, Rhiel E (2006) Association of Fucoxanthin Chlorophyll *a*/*c*-binding Polypeptides with Photosystems and Phosphorylation in the Centric Diatom *Cyclotella cryptica*. Protist 157:463-475.

Bricaud A, Claustre H, Ras J, Oubelkheir K (2004). Natural variability of phytoplanktonic absorption in oceanic waters: Influence of the size structure of algal populations. Journal of Geophysical Research: Oceans 109(C11).

Broady P (1996) Diversity, distribution and dispersal of Antarctic terrestrial algae. Biodiversity & Conservation 5:1307-1335.

Büchel C (2003) Fucoxanthin-chlorophyll proteins in diatoms: 18 and 19 kDa subunits assemble into different oligomeric states. Biochemistry (NY) 42:13027-13034.

Büchel C, Wilhelm C (1993) In vivo analysis of slow chlorophyll fluorescence induction kinetics in algae: progress, problems and perspectives. Photochemistry and Photobiology 58:137-148.

Bugos RC, Yamamoto HY (1996) Molecular cloning of violaxanthin de-epoxidase from romaine lettuce and expression in *Escherichia coli*. Proceedings of the National Academy of Sciences 93:6320-6325.

Byrdin M, Rimke I, Schlodder E, Stehlik D, Roelofs TA (2000) Decay kinetics and quantum yields of fluorescence in photosystem I from *Synechococcus elongatus* with P700 reduced and oxidized state: are the kinetics of excited state decay trap-limited or transfer-limited? Biophysical Journal 79: 992–1007.

Carol P, Stevenson D, Bisanz C, Breitenbach J, Sandmann G, Mache R, Coupland G, Kuntz M (1999) Mutations in the Arabidopsis gene IMMUTANS cause a variegated phenotype by inactivating a chloroplast terminal oxidase associated with phytoene desaturation. Plant Cell 11:57-68.

Caron L, Berkaloff C, Duval J, Jupin H (1987) Chlorophyll fluorescence transients from the diatom Phaeodactylum tricornutum: relative rates of cyclic phosphorylation and chlororespiration. Photosynthesis Research 11:131-139.

Claquin P, Kromkamp JC, Martin-Jezequel V (2004) Relationship between photosynthetic metabolism and cell cycle in a synchronized culture of the marine alga *Cylindrotheca fusiformis* (Bacillariophyceae). European Journal of Phycology 39:33-41.

Croce R, Chojnicka A, Morosinotto T, Ihalainen JA, van Mourik F, Dekker JP, Bassi R, van Grondelle R (2007) The low-energy forms of photosystem I light-harvesting complexes: spectroscopic properties and pigment–pigment interaction characteristics. Biophysical Journal 93: 2418–2428.

Cruz S, Goss R, Wilhelm C, Leegood R, Horton P, Jakob T (2011) Impact of chlororespiration on non-photochemical quenching of chlorophyll fluorescence and on the regulation of the diadinoxanthin cycle in the diatom *Thalassiosira pseudonana*. Journal of Experimental Botany 62:509-519.

de Martino A, Douady D, Rousseau B, Duval JC, Caron L (1997) Characterization of Two Light-Harvesting Subunits Isolated from the Brown Alga *Pelvetia canaliculata*:

Heterogeneity of Xanthophyll Distribution. Photochemistry and Photobiology 66:190-197.

De Wilton A, Koningstein J (1983) Time-resolved fluorescence spectra of chlorophyll a dimers and aggregates using selective photochemical bleaching. The Journal of Physical Chemistry 87:185-188.

Demirbas A, Fatih Demirbas M (2011) Importance of algae oil as a source of biodiesel. Energy Conversion and Management 52:163-170.

Devaki B, Arthur RG (1993) Characterization of gene clusters encoding the fucoxanthin chlorophyll proteins of the diatom *Phaeodactylum tricornutum*. Nucleic Acids Research 21(19):4458-4466.

Di Valentin M, Büchel C, Giacometti GM, Carbonera D (2012) Chlorophyll triplet quenching by fucoxanthin in the Fucoxanthin-Chlorophyll Protein from the diatom *Cyclotella meneghiniana*. Biochemical and Biophysical Research Communications 427:637-641.

Di Valentin M, Biasibetti F, Ceola S, Carbonera D (2009) Identification of the sites of chlorophyll triplet quenching in relation to the structure of LHC-II from higher plants. Evidence from EPR spectroscopy. The Journal of Physical Chemistry B 113:13071-13078.

Dimier C, Corato F, Tramontano F, Brunet C (2007) Photoprotection and xanthophyll-cycle activity in three marine diatoms. Journal of Phycology 43:937-947.

Dimier C, Brunet C, Geider R, Raven J (2009) Growth and photoregulation dynamics of the picoeukaryote *Pelagomonas calceolata* in fluctuating light. Limnology and Oceanography 54:823-836.

Dimier C, Giovanni S, Ferdinando T, Brunet C (2009b) Comparative ecophysiology of the xanthophyll cycle in six marine phytoplanktonic species. Protist 160:397-411.

Dominici P, Caffarri S, Armenante F, Ceoldo S, Crimi M, Bassi R (2002) Biochemical properties of the PsbS subunit of photosystem II either purified from chloroplast or recombinant. The Journal of Biological Chemistry 277:22750-22758.

Duffy CDP, Johnson MP, Macernis M, Valkunas L, Barford W, Ruban AV (2010) A theoretical investigation of the photophysical consequences of major plant light-harvesting complex aggregation within the photosynthetic membrane. The Journal of Physical Chemistry B 114(46): 15244-15253.

Eisenstadt D, Ohad I, Keren N, Kaplan A (2008) Changes in the photosynthetic reaction centre II in the diatom *Phaeodactylum tricornutum* result in non-photochemical fluorescence quenching. Environmental Microbiology 10:1997-2007.

Escoubas J, Lomas M, LaRoche J, Falkowski PG (1995) Light intensity regulation of cab gene transcription is signaled by the redox state of the plastoquinone pool. Proceedings of the National Academy of Sciences 92:10237-10241.

Falkowski PG, Barber RT, Smetacek V (1998) Biogeochemical controls and feedbacks on ocean primary production. Science 281:200-206.

Falkowski PG, Katz ME, Knoll AH, Quigg A, Raven JA, Schofield O, Taylor F (2004) The evolution of modern eukaryotic phytoplankton. Science 305:354-360.

Falkowski PG, Raven JA (1997) Aquatic photosynthesis. Blackwell Science Malden, MA, pp 375.

Falkowski PG, Chen YB (2003) Photoacclimation of light harvesting systems in eukaryotic algae. In: Green B, Parson WW (Eds) Light-harvesting Antennas in Photosynthesis. Springer, The Netherlands. pp. 423-447.

Förster T (1948) Zwischenmolekulare energiewanderung und fluoreszenz. Annalen der physik 437:55-75. English translation published in: Mielczarek EV, Greenbaum E, Knox RS (Eds) (1993) Biological Physics. American Institute of Physics New York.

Foyer CH, Noctor G (2011) Ascorbate and glutathione: the heart of the redox hub. Plant Physiology 155:2-18.

Frank HA, Cua A, Chynwat V, Young A, Gosztola D, Wasielewski MR (1996) The lifetimes and energies of the first excited singlet states of diadinoxanthin and diatoxanthin: the role of these molecules in excess energy dissipation in algae. Biochimica et Biophysica Acta (BBA)-Bioenergetics 1277:243-252.

Frank HA, Bautista JA, Josue J, Pendon Z, Hiller RG, Sharples FP, Gosztola D, Wasielewski MR (2000) Effect of the solvent environment on the spectroscopic properties and dynamics of the lowest excited states of carotenoids. The Journal of Physical Chemistry B 104:4569-4577.

Fry B, Hopkinson Jr CS, Nolin A (1996) Long-term decomposition of DOC from experimental diatom blooms. Limnology and Oceanography 41:1344-1347.

Fuhrmann T, Landwehr S, El Rharbi-Kucki M, Sumper M (2004) Diatoms as living photonic crystals. Applied Physics B 78:257-260.

Fujii T, Yokoyama E, Inoue K, Sakurai H (1990) The sites of electron donation of photosystem I to methyl viologen. Biochimica et Biophysica Acta (BBA)-Bioenergetics 1015:41-48.

Gildenhoff N, Amarie S, Gundermann K, Beer A, Büchel C, Wachtveitl J (2010) Oligomerization and pigmentation dependent excitation energy transfer in fucoxanthin–chlorophyll proteins. Biochimica et Biophysica Acta (BBA)-Bioenergetics 1797:543-549.

Giordano M, Beardall J, Raven JA (2005) CO_2 concentrating mechanisms in algae: mechanisms, environmental modulation, and evolution. Annual Review of Plant Biology 56:99-131.

Gisselsson A, Szilagyi A, Åkerlund H (2004) Role of histidines in the binding of violaxanthin de-epoxidase to the thylakoid membrane as studied by site-directed mutagenesis. Physiologia Plantarum 122:337-343.

Gleitz M, Bartsch A, Dieckmann GS, Eicken HS (1998) Composition and succession of sea ice diatom assemblages in the eastern and southern Weddell Sea, Antarctica. In: Lizotte MP, Arrigo KR (Eds) Antarctic Sea Ice-Biological Processes, Interactions and Variability. Antarctic Research Series. American Geophysical Union, Washington, DC, pp 107-120

Goss R, Lohr M, Latowski D, Grzyb J, Vieler A, Wilhelm C, Strzalka K (2005) Role of hexagonal structure-forming lipids in diadinoxanthin and violaxanthin solubilization and de-epoxidation. Biochemistry (NY) 44:4028-4036.

Goss R, Lepetit B, Wilhelm C (2006) Evidence for a rebinding of antheraxanthin to the light-harvesting complex during the epoxidation reaction of the violaxanthin cycle. Journal of Plant Physiology 163:585-590.

Goss R, Pinto E, Wilhelm C, Richter M (2006b). The importance of a highly active and pH-regulated diatoxanthin epoxidase for the regulation of the PS II antenna function in diadinoxanthin cycle containing algae. Journal of Plant Physiology 163:1008-1021.

Goss R, Latowski D, Grzyb J, Vieler A, Lohr M, Wilhelm C, Strzalka K (2007) Lipid dependence of diadinoxanthin solubilization and de-epoxidation in artificial membrane systems resembling the lipid composition of the natural thylakoid membrane. Biochimica et Biophysica Acta (BBA)-Biomembranes 1768:67-75.

Goss R, Jakob T (2010) Regulation and function of xanthophyll cycle-dependent photoprotection in algae. Photosynthesis Research 106:103-122.

Gounaris K, Barber J (1983) Monogalactosyldiacylglycerol: the most abundant polar lipid in nature. Trends in Biochemical Sciences 8:378-381.

Green BR (2007) Evolution of light-harvesting antennas in an oxygen world. In: Falkowski PG, Knoll AH (Eds) Evolution of Primary Producers in the Sea. Elsevier, Burlington, VT, pp 37-53.

Green BR (2003) The evolution of light-harvesting antennas. In: Green BR, Parson WW (Eds) Light-Harvesting Antennas in Photosynthesis. Kluwer Academic Publishers, Dordrecht, The Netherlands, pp 129-168.

Grouneva I, Jakob T, Wilhelm C, Goss R (2006) Influence of ascorbate and pH on the activity of the diatom xanthophyll cycle-enzyme diadinoxanthin de-epoxidase. Physiologia Plantarum 126:205-214.

Grouneva I, Jakob T, Wilhelm C, Goss R (2008) Evidence for a fast, xanthophyll cycle independent NPQ mechanism in the diatom *C. meneghiniana*. In: Allen JF, Gantt E, Golbeck JH, Osmond B (Eds) Energy from the Sun. Springer, Dordrecht, The Netherlands, pp. 1013-1016.

Grouneva I, Jakob T, Wilhelm C, Goss R (2009) The regulation of xanthophyll cycle activity and of non-photochemical fluorescence quenching by two alternative electron flows in the diatoms *Phaeodactylum tricornutum* and *Cyclotella meneghiniana*. Biochimica et Biophysica Acta (BBA)-Bioenergetics 1787: 929-938.

Gruber A, Vugrinec S, Hempel F, Gould SB, Maier U, Kroth PG (2007) Protein targeting into complex diatom plastids: functional characterisation of a specific targeting motif. Plant Molecular Biology 64:519-530.

Guglielmi G, Lavaud J, Rousseau B, Etienne A, Houmard J, Ruban AV (2005) The light-harvesting antenna of the diatom *Phaeodactylum tricornutum*. FEBS Journal 272:4339-4348.

Guillard RRL (1975) Culture of phytoplankton for feeding marine invertebrates. In: Smith WL, Chanley MH (Eds) Culture of Marine Invertebrate Animals. Plenum Press, New York, USA, pp 26-60.

Guillard RR, Ryther JH (1962) Studies of marine planktonic diatoms. I. *Cyclotella nana* Hustedt and *Detonula confervacea* (Cleve) Gran. Canadian Journal of Microbiology 8:229-239.

Gundermann K, Büchel C (2008) The fluorescence yield of the trimeric fucoxanthin–chlorophyll–protein FCPa in the diatom *Cyclotella meneghiniana* is dependent on the amount of bound diatoxanthin. Photosynthesis Research 95:229-235.

Gundermann K, Büchel C (2012) Factors determining the fluorescence yield of fucoxanthin-chlorophyll complexes (FCP) involved in non-photochemical quenching in diatoms. Biochimica et Biophysica Acta (BBA)-Bioenergetics 1817:1044-1052.

Gundermann K, Schmidt M, Weisheit W, Mittag M, Büchel C (2013) Identification of several sub-populations in the pool of light harvesting proteins in the pennate diatom *Phaeodactylum tricornutum*. BBA-Bioenergetics 1827:303-310.

Harrison PJ, Waters RE, Taylor F (1980) A Broad Spectrum Artificial Sea Water Medium for Coastal and Open Ocean Phytoplankton. Journal of Phycology 16:28-35.

Hendrickson L, Furbank RT, Chow WS (2004) A simple alternative approach to assessing the fate of absorbed light energy using chlorophyll fluorescence. Photosynthesis Research 82:73-81.

Hieber DA, Bugos RC, Verhoeven AS, Yamamoto HY (2002) Overexpression of violaxanthin de-epoxidase: properties of C-terminal deletions on activity and pH-dependent lipid binding. Planta 214:476-483.

Holt NE, Zigmantas D, Valkunas L, Li X-P, Niyogi KK, Fleming GR (2005) Carotenoid cation formation and the regulation of photosynthetic light harvesting. Science 307: 433–436.

Horton P, Ruban A (2005) Molecular design of the photosystem II light-harvesting antenna: photosynthesis and photoprotection. Journal of Experimental Botany 56:365-373.

Horton P, Wentworth M, Ruban A (2005) Control of the light harvesting function of chloroplast membranes: the LHCII-aggregation model for non-photochemical quenching. FEBS Letters 579:4201-4206.

Huner N, Öquist G, Sarhan F (1998) Energy balance and acclimation to light and cold. Trends in Plant Science 3:224-230.

Jahns P, Holzwarth AR (2012) The role of the xanthophyll cycle and of lutein in photoprotection of photosystem II. Biochimica et Biophysica Acta (BBA)-Bioenergetics, 1817: 182-193.

Jakob T, Goss R, Wilhelm C (1999) Activation of Diadinoxanthin De-Epoxidase Due to a Chiororespiratory Proton Gradient in the Dark in the Diatom *Phaeodactylum tricornutum*. Plant Biology 1:76-82.

Jakob T, Goss R, Wilhelm C (2001) Unusual pH dependence of diadinoxanthin de-epoxidase activation causes chlororespiratory induced accumulation of diatoxanthin in the diatom *Phaeodactylum tricornutum*. Journal of Plant Physiology 158: 383-390.

Johansen JR (1993) Cryptogamic crusts of semiarid and arid lands of North America. Journal of Phycology 29:140-147.

Johnson MP, Davison PA, Ruban AV, Horton P (2008) The xanthophyll cycle pool size controls the kinetics of non-photochemical quenching in *Arabidopsis thaliana*. FEBS Letters 582:262-266.

Joshi-Deo J, Schmidt M, Gruber A, Weisheit W, Mittag M, Kroth PG, Büchel C (2010) Characterization of a trimeric light-harvesting complex in the diatom *Phaeodactylum tricornutum* built of FcpA and FcpE proteins. Journal of Experimental Botany 61:3079-3087.

Juhas M, Büchel C (2012) Properties of photosystem I antenna protein complexes of the diatom *Cyclotella meneghiniana*. Journal of Experimental Botany 63:3673-3681.

Junge W (1989) Protons, the Thylakoid Membrane, and the Chloroplast ATP Synthase. Annals of the New York Academy of Sciences 574:268-286.

Katoh T, Nagashima U, Mimuro M (1991) Fluorescence properties of the allenic carotenoid fucoxanthin: Implication for energy transfer in photosynthetic pigment systems. Photosynthesis Research 27:221-226.

Key T, McCarthy A, Campbell DA, Six C, Roy S, Finkel ZV (2010) Cell size trade-offs govern light exploitation strategies in marine phytoplankton. Environmental Microbiology 12:95-104.

Kirkwood AE, Henley WJ (2006) Algal Community Dynamics and Halotolerance in a Terrestrial, Hypersaline Environment. Journal of Phycology 42:537-547.

Klughammer C, Schreiber U (2008) Complementary PS II quantum yields calculated from simple fluorescence parameters measured by PAM fluorometry and the Saturation Pulse method. PAM Application Notes 1:27-35.

Kramer DM, Johnson G, Kiirats O, Edwards GE (2004) New fluorescence parameters for the determination of Q_A redox state and excitation energy fluxes. Photosynthesis Research 79:209-218.

Lakowicz JR (2006) Corrected Emission Spectra. In: Principles of Fluorescence Spectroscopy, Third edition. Springer, Dordrecht, The Netherlands, pp 873-881.

Lakowicz JR (2006b) Time Domain Lifetime Measurements. In: Principles of Fluorescence Spectroscopy, Third edition. Springer, Dordrecht, The Netherlands, pp 98-140.

Lakowicz JR (2006c) Quenching of Fluorescence. In: Principles of Fluorescence Spectroscopy, Third edition. Springer, Dordrecht, The Netherlands, pp 278-330.

Latowski D, Kruk J, Burda K, Skrzynecka-Jaskier M, Kostecka-Gugała A, Strzałka K (2002) Kinetics of violaxanthin de-epoxidation by violaxanthin de-epoxidase, a xanthophyll cycle enzyme, is regulated by membrane fluidity in model lipid bilayers. European Journal of Biochemistry 269:4656-4665.

Latowski D, Åkerlund H, Strzalka K (2004) Violaxanthin de-epoxidase, the xanthophyll cycle enzyme, requires lipid inverted hexagonal structures for its activity. Biochemistry (NY) 43:4417-4420.

Lavaud J, Rousseau B, van Gorkom HJ, Etienne A (2002) Influence of the diadinoxanthin pool size on photoprotection in the marine planktonic diatom *Phaeodactylum tricornutum*. Plant Physiology 129:1398-1406.

Lavaud J, van Gorkom HJ, Etienne A (2002b) Photosystem II electron transfer cycle and chlororespiration in planktonic diatoms. Photosynthesis Research 74:51-59.

Lavaud J, Rousseau B, Etienne A (2003) Enrichment of the light-harvesting complex in diadinoxanthin and implications for the nonphotochemical fluorescence quenching in diatoms. Biochemistry (NY) 42:5802-5808.

Lavaud J, Rousseau B, Etienne A (2004) General features of photoprotection by energy dissipation in planktonic diatoms (Bacillariophyceae). Journal of Phycology 40:130-137.

Lavaud J (2007) Fast regulation of photosynthesis in diatoms: mechanisms, evolution and ecophysiology. Functional Plant Science and Biotechnology 1:267-287.

Lavaud J, Strzepek RF, Kroth PG (2007) Photoprotection capacity differs among diatoms: Possible consequences on the spatial distribution of diatoms related to fluctuations in the underwater light climate. Limnology and Oceanography 52:1188-1194.

Lepetit B, Volke D, Szabó M, Hoffmann R, Garab G, Wilhelm C, Goss R (2007) Spectroscopic and molecular characterization of the oligomeric antenna of the diatom Phaeodactylum tricornutum. Biochemistry 46(34): 9813-9822.

Lepetit B, Volke D, Szábo M, Hoffmann R, Garab G, Wilhelm C, Goss R (2008) The oligomeric antenna of the diatom *P. tricornutum*: localisation of diadinoxanthin cycle pigments. In: Allen JF, Gantt E, Golbeck JH, Osmond B (Eds) Energy from the Sun. Springer, Dordrecht, The Netherlands, pp 283-286.

Lepetit B, Volke D, Gilbert M, Wilhelm C, Goss R (2010) Evidence for the existence of one antenna-associated, lipid-dissolved and two protein-bound pools of diadinoxanthin cycle pigments in diatoms. Plant Physiology 154:1905-1920.

Lepetit B, Sturm S, Rogato A, Gruber A, Sachse M, Falciatore A, Kroth P, Lavaud J. (2013) High light acclimation in the secondary plastids containing diatom *Phaeodactylum tricornutum* is triggered by the redox state of the plastoquinone pool. Plant Physiology 161(2): 853-865.

Li X, Phippard A, Pasari J, Niyogi KK (2002) Structure–function analysis of photosystem II subunit S (PsbS) in vivo. Functional Plant Biology 29:1131-1139.

Li X, Müller-Moulé P, Gilmore AM, Niyogi KK (2002b) PsbS-dependent enhancement of feedback de-excitation protects photosystem II from photoinhibition. Proceedings of the National Academy of Sciences 99:15222-15227.

Li XP, Gilmore AM, Caffarri S, Bassi R, Golan T, Kramer D, Niyogi KK (2004) Regulation of photosynthetic light harvesting involves intrathylakoid lumen pH sensing by the PsbS protein. Journal of Biological Chemistry 279(22), 22866-22874.

Liu Z, Yan H, Wang K, Kuang T, Zhang J, Gui L, An X, Chang W (2004) Crystal structure of spinach major light-harvesting complex at 2.72 Å resolution. Nature 428:287-292.

Lohr M, Wilhelm C (2001) Xanthophyll synthesis in diatoms: quantification of putative intermediates and comparison of pigment conversion kinetics with rate constants derived from a model. Planta 212:382-391.

Lomas MW, Glibert PM (1999) Temperature regulation of nitrate uptake: A novel hypothesis about nitrate uptake and reduction in cool-water diatoms. Limnology and Oceanography 44:556-572.

MacIntyre HL, Kana TM, Geider RJ (2000) The effect of water motion on short-term rates of photosynthesis by marine phytoplankton. Trends in Plant Science 5:12-17.

Macpherson AN, Hiller RG (2003) Light-Harvesting in Chlorophyll c-Containing Algae. In: Green BR, Parson WW (Eds) Light-Harvesting Antennas in Photosynthesis. Kluwer Academic Publishers, The Netherlands, pp 323-352.

Mann DG (1999) The species concept in diatoms. Phycologia 38:437-495.

Martinez-Junza V, Szczepaniak M, Braslavsky SE, Sander J, Rögner M, Holzwarth AR (2008) Triplet photoprotection by carotenoid in intact photosystem II cores. In: Allen JF, Gantt E, Golbeck JH, Osmond B (Eds) Photosynthesis. Energy from the Sun. Springer, Dordrecht, The Netherlands, pp 137-140.

Martinson TA, Ikeuchi M, Plumley FG (1998) Oxygen-evolving diatom thylakoid membranes. Biochimica et Biophysica Acta (BBA)-Bioenergetics, 1409: 72-86.

Maxwell K, Johnson GN (2000) Chlorophyll fluorescence-a practical guide. Journal of Experimental Botany 51:659-668.

McConnell MD, Koop R, Vasil'ev S, Bruce D (2002) Regulation of the distribution of chlorophyll and phycobilin-absorbed excitation energy in cyanobacteria. A structure-based model for the light state transition. Plant Physiology 130:1201-1212.

Mewes H, Richter M (2002) Supplementary Ultraviolet-B Radiation Induces a Rapid Reversal of the Diadinoxanthin Cycle in the Strong Light-Exposed Diatom *Phaeodactylum tricornutum*. Plant Physiology 130:1527-1535.

Meyer A, Tackx M, Daro N (2000) Xanthophyll cycling in *Phaeocystis globosa* and *Thalassiosira sp*.: a possible mechanism for species succession. Journal of Sea Research 43:373-384.

Miloslavina Y, Wehner A, Wientjes E, Reus M, Lambrev P, Garab G, Croce R, Holzwarth AR (2008) Far-red fluorescence: a direct spectroscopic marker for LHCII oligomers forming in non photochemical quenching. FEBS Letters 582:3625–3631.

Miloslavina Y, Grouneva I, Lambrev PH, Lepetit B, Goss R, Wilhelm C, Holzwarth AR (2009) Ultrafast fluorescence study on the location and mechanism of non-photochemical quenching in diatoms. Biochimica et Biophysica Acta (BBA)-Bioenergetics 1787(10): 1189-1197.

Mitrovic SM, Howden CG, Bowling LC, Buckney RT (2003) Unusual allometry between in situ growth of freshwater phytoplankton under static and fluctuating light environments: possible implications for dominance. Journal of Plankton Research 25:517-526.

Murata N, Takahashi S, Nishiyama Y, Allakhverdiev SI (2007) Photoinhibition of photosystem II under environmental stress. Biochimica et Biophysica Acta (BBA)-Bioenergetics 1767:414-421.

Murphy AM, Cowles TJ (1997) Effects of darkness on multiexcitation in-vivo fluorescence and survival in a marine diatom. Limnology and oceanography 42:1444-1453.

Nagao R, Tomo T, Noguchi E, Nakajima S, Suzuki T, Okumura A, Kashino Y, Mimuro M, Ikeuchi M, Enami I (2010) Purification and characterization of a stable oxygen-evolving Photosystem II complex from a marine centric diatom, *Chaetoceros gracilis*. Biochimica et Biophysica Acta (BBA)-Bioenergetics 1797:160-166.

NCMA (2013) Provasoli-Guillard National Center for Marine Algae and Microbia. Bigelow Laboratory for Ocean Sciences. 60 Bigelow Drive P.O. Box 380 East Boothbay, Maine 04544 USA. https://ncma.bigelow.org/

Niyogi KK, Truong TB (2013) Evolution of flexible non-photochemical quenching mechanisms that regulate light harvesting in oxygenic photosynthesis. Current Opinion in Plant Biology 16:307-314.

Oliver MJ, Petrov D, Ackerly D, Falkowski P, Schofield OM (2007) The mode and tempo of genome size evolution in eukaryotes. Genome Research 17:594-601.

Onno Feikema W, Marosvölgyi MA, Lavaud J, van Gorkom HJ (2006) Cyclic electron transfer in photosystem II in the marine diatom *Phaeodactylum tricornutum*. Biochimica et Biophysica Acta (BBA)-Bioenergetics 1757:829-834.

Öquist G, Huner NP (2003) Photosynthesis of overwintering evergreen plants. Annual Review of Plant Biology 54:329-355.

Papagiannakis E, van Stokkum IH, Fey H, Büchel C, van Grondelle R (2005) Spectroscopic characterization of the excitation energy transfer in the fucoxanthin–chlorophyll protein of diatoms. Photosynthesis Research 86:241-250.

Petersen JE, Sanford LP, Kemp WM (1998) Coastal plankton responses to turbulent mixing in experimental ecosystems. Marine Ecology Progress Series 171:23-41.

Pfündel EE, Renganathan M, Gilmore AM, Yamamoto HY, Dilley RA (1994) Intra-thylakoid pH in isolated pea chloroplasts as probed by violaxanthin deepoxidation. Plant Physiology 106:1647-1658.

Porra RJ, Thompson WA, Kriedemann PE (1989) Determination of accurate extinction coefficients and simultaneous equations for assaying chlorophylls a and b extracted with four different solvents: verification of the concentration of chlorophyll standards by atomic absorption spectroscopy. Biochimica et Biophysica Acta (BBA) - Bioenergetics 975:384-394.

Pospíšil P (2012) Molecular mechanisms of production and scavenging of reactive oxygen species by photosystem II. Biochimica et Biophysica Acta (BBA)-Bioenergetics 1817:218-231.

Potter AT, Palmer MW, Henley WJ (2006) Diatom genus diversity and assemblage structure in relation to salinity at the Salt Plains National Wildlife Refuge, Alfalfa County, Oklahoma. The American Midland Naturalist 156:65-74.

Premvardhan L, Robert B, Beer A, Büchel C (2010) Pigment organization in fucoxanthin chlorophyll a/c_2 proteins (FCP) based on resonance Raman spectroscopy and sequence analysis. Biochimica et Biophysica Acta (BBA)-Bioenergetics 1797:1647-1656.

Raven JA, Geider JR (2003) Adaptation, acclimation and regulation in algal photosynthesis. In: Larkum WD, Douglas SE, Raven JA (Eds) Photosynthesis in algae. Kluwer Academic Publishers, Dordrecht, The Netherlands, pp 385-412.

Reinfelder JR, Kraepiel AM, Morel FM (2000) Unicellular C4 photosynthesis in a marine diatom. Nature 407:996-999.

Roberts K, Granum E, Leegood RC, Raven JA (2007) C3 and C4 pathways of photosynthetic carbon assimilation in marine diatoms are under genetic, not environmental, control. Plant Physiology 145:230-235.

Rosso D, Bode R, Li W, Krol M, Saccon D, Wang S, Schillaci LA, Rodermel SR, Maxwell DP, Hüner NP (2009) Photosynthetic redox imbalance governs leaf sectoring in the *Arabidopsis thaliana* variegation mutants immutans, spotty, var1, and var2. The Plant Cell 21:3473-3492.

Rost B, Yachdav G, Liu J (2004) The PredictProtein server. Nucleic Acids Research 32: 321-326.

Round FE, Crawford RM, Mann DG (1990) In: The Diatoms. Biology and Morphology of the Genera. Cambridge University Press, Cambridge, UK, pp 747.

Ruban AV, Horton P (1992) Mechanism of ΔpH-dependent dissipation of absorbed excitation energy by photosynthetic membranes. I. Spectroscopic analysis of isolated light-harvesting complexes. Biochimica et Biophysica Acta (BBA)-Bioenergetics 1102(1):30-38.

Ruban A, Walters R, Horton P (1992) The molecular mechanism of the control of excitation energy dissipation in chloroplast membranes Inhibition of ΔpH-dependent quenching of chlorophyll fluorescence by dicyclohexylcarbodiimide. FEBS Letters 309:175-179.

Ruban AV, Calkoen F, Kwa S, Van Grondelle R, Horton P, Dekker J (1997) Characterisation of LHC II in the aggregated state by linear and circular dichroism spectroscopy. Biochimica et Biophysica Acta (BBA)-Bioenergetics 1321:61-70.

Ruban AV, Horton P (1999) The xanthophyll cycle modulates the kinetics of nonphotochemical energy dissipation in isolated light-harvesting complexes, intact chloroplasts, and leaves of spinach. Plant Physiology 119:531-542.

Ruban A, Lavaud J, Rousseau B, Guglielmi G, Horton P, Etienne A (2004) The super-excess energy dissipation in diatom algae: comparative analysis with higher plants. Photosynthesis Research 82:165-175.

Ruban AV, Rudi B, Cristian I, Van Stokkum IHM, Kennis JTM, Pascal AA, Van Amerongen H, Robert B, Horton P, Van Grondelle R. (2007) Identification of a mechanism of photoprotective energy dissipation in higher plants. Nature 450: 575-578.

Ruban AV, Johnson MP, Duffy CD (2012) The photoprotective molecular switch in the photosystem II antenna. Biochimica et Biophysica Acta (BBA)-Bioenergetics 1817(1):167-181.

Sarthou G, Timmermans KR, Blain S, Tréguer P (2005) Growth physiology and fate of diatoms in the ocean: a review. Journal of Sea Research 53:25-42.

Sauer K, Smith JRL, Schultz AJ (1966) The Dimerization of Chlorophyll a, Chlorophyll b, and Bacteriochlorophyll in Solution. Journal of the American Chemical Society 88:2681-2688.

Schlodder E, Çetin M, Byrdin M, Terekhova IV, Karapetyan NV (2005) $P700^{+}$- and $^{3}P700$-induced quenching of the fluorescence at 760 nm in trimeric Photosystem I complexes from the cyanobacterium *Arthrospira platensis*. Biochimica et Biophysica Acta (BBA)-Bioenergetics 1706:53-67.

Schnitzler Parker M, Armbrust E, Piovia-Scott J, Keil RG (2004) Induction of photorespiration by light in the centric diatom *Thalassiosira weissflogii* (Bacillariophyceae): Molecular characterization and physiological consequences. Journal of Phycology 40:557-567.

Schumann A, Goss R, Jakob T, Wilhelm C (2007) Investigation of the quenching efficiency of diatoxanthin in cells of *Phaeodactylum tricornutum* (Bacillariophyceae) with different pool sizes of xanthophyll cycle pigments. Phycologia 46:113-117.

Schweitzer RH, Brudvig GW (1997) Fluorescence quenching by chlorophyll cations in photosystem II. Biochemistry 36:11351-11359.

Seely G, Duncan M, Vidaver W (1972) Preparative and analytical extraction of pigments from brown algae with dimethyl sulfoxide. Marine Biology 12:184-188.

Serôdio J, Cruz S, Vieira S, Brotas V (2005) Non-photochemical quenching of chlorophyll fluorescence and operation of the xanthophyll cycle in estuarine microphytobenthos. Journal of Experimental Marine Biology and Ecology 326:157-169.

Shinopoulos KE, Brudvig GW (2012). Cytochrome b_{559} and cyclic electron transfer within photosystem II. Biochimica et Biophysica Acta (BBA)-Bioenergetics 1817: 66-75.

Shipman LL, Cotton TM, Norris JR, Katz JJ (1976) An analysis of the visible absorption spectrum of chlorophyll *a* monomer, dimer, and oligomers in solution. Journal of the American Chemical Society 98:8222-8230.

Sieburth J, Smetacek V, Lenz J (1978) Pelagic ecosystem structure: heterotrophic compartments of the plankton and their relationship to plankton size fractions. Limnology and Oceanography 23:1256-1263.

Slavov C, Reus M, Holzwarth AR (2013) Two different mechanisms cooperate in the desiccation-induced excited state quenching in *Parmelia* lichen. The Journal of Physical Chemistry B 117:11326-11336.

Smetacek V (1999) Diatoms and the ocean carbon cycle. Protist 150:25-32.

Stirbet A, Govindjee (2011) On the relation between the Kautsky effect (chlorophyll a fluorescence induction) and Photosystem II: Basics and applications of the OJIP fluorescence transient. Journal of Photochemistry and Photobiology B: Biology 104:236-257.

Strasser RT, Tsimilli-Michael M, Srivastava A (2004) Analysis of the Chlorophyll *a* Fluorescence Transient. In: Papageorgiou GC, Govindjee (Eds) Chlorophyll a Fluorescence: A Signature of Photosynthesis. Springer, Dordrecht, The Netherlands, pp 321-362.

Stuart V, Sathyendranath S, Platt T, Maass H, Irwin BD (1998) Pigments and species composition of natural phytoplankton populations: effect on the absorption spectra. Journal of Plankton Research 20:187-217.

Stuart V, Sathyendranath S, Head EJH, Platt T, Irwin B, Maass H (2000) Bio-optical characteristics of diatom and prymnesiophyte populations in the Labrador Sea. Marine ecology. Progress series 201:91-106.

Sutherland T, Grant J, Amos C (1998) The effect of carbohydrate production by the diatom *Nitzschia curvilineata* on the erodibility of sediment. Limnology and Oceanography 43:65-72.

Szabó M, Premvardhan L, Lepetit B, Goss R, Wilhelm C, Garab G (2010) Functional heterogeneity of the fucoxanthins and fucoxanthin-chlorophyll proteins in diatom cells revealed by their electrochromic response and fluorescence and linear dichroism spectra. Chemical Physics 373:110-114.

Szabó M, Lepetit B, Goss R, Wilhelm C, Mustárdy L, Garab G (2008) Structurally flexible macro-organization of the pigment–protein complexes of the diatom *Phaeodactylum tricornutum*. Photosynthesis Research 95:237-245.

Takizawa K, Cruz JA, Kanazawa A, Kramer DM (2007) The thylakoid proton motive force *in vivo*. Quantitative, non-invasive probes, energetics, and regulatory consequences of light-induced *pmf*. Biochimica et Biophysica Acta (BBA)-Bioenergetics 1767:1233-1244.

Ting CS, Owens TG (1993) Photochemical and nonphotochemical fluorescence quenching processes in the diatom *Phaeodactylum tricornutum*. Plant Physiology 101:1323-1330.

Tortell PD (2000) Evolutionary and ecological perspectives on carbon acquisition in phytoplankton. Limnology and Oceanography 45:744-750.

Tréguer P, Pondaven P (2000) Global change: Silica control of carbon dioxide. Nature 406:358-359.

Van de Vijver B, Ledeganck P, Beyens L (2002) Soil diatom communities from Ile de la Possession (Crozet, sub-Antarctica). Polar Biology 25:721-729.

van Kerckvoorde A, Trappeniers K, Nijs I, Beyens L (2000) Terrestrial soil diatom assemblages from different vegetation types in Zackenberg (Northeast Greenland). Polar Bioliogy 23:392-400.

Vardi A, Thamatrakoln K, Bidle KD, Falkowski PG (2008) Diatom genomes come of age. Genome Biology 9:245.

Veith T, Büchel C (2007) The monomeric photosystem I-complex of the diatom *Phaeodactylum tricornutum* binds specific fucoxanthin chlorophyll proteins (FCPs) as light-harvesting complexes. Biochimica et Biophysica Acta (BBA)-Bioenergetics 1767: 1428-1435.

Veith T, Brauns J, Weisheit W, Mittag M, Büchel C (2009) Identification of a specific fucoxanthin-chlorophyll protein in the light harvesting complex of photosystem I in the diatom *Cyclotella meneghiniana*. Biochimica et Biophysica Acta (BBA)-Bioenergetics 1787:905-912.

Wagner H, Jakob T, Wilhelm C (2006) Balancing the energy flow from captured light to biomass under fluctuating light conditions. New Phytologist 169:95-108.

Wilhelm C, Buchel C, Fisahn J, Goss R, Jakob T, Laroche J, Lavaud J, Lohr M, Riebesell U, Stehfest K, Valentin K, Kroth PG (2006) The regulation of carbon and nutrient assimilation in diatoms is significantly different from green algae. Protist 157:91-124.

Wilson KE, Król M, Huner NP (2003) Temperature-induced greening of *Chlorella vulgaris*. The role of the cellular energy balance and zeaxanthin-dependent nonphotochemical quenching. Planta 217:616-627.

Wollman F (2001) State transitions reveal the dynamics and flexibility of the photosynthetic apparatus. The EMBO Journal 20:3623-3630.

Yamamoto HY, Kamite L (1972) The effects of dithiothreitol on violaxanthin de-epoxidation and absorbance changes in the 500-nm region. Biochimica et Biophysica Acta (BBA)-Bioenergetics 267:538-543.

Yamanaka S, Yano R, Usami H, Hayashida N, Ohguchi M, Takeda H, Yoshino K (2008) Optical properties of diatom silica frustule with special reference to blue light. Journal of Applied Physics, 103:074701.

Zhu SH, Green BR (2010) Photoprotection in the diatom *Thalassiosira pseudonana*: role of LI818-like proteins in response to high light stress. Biochimica et Biophysica Acta (BBA)-Bioenergetics 1797:1449-1457.

ESAW – f/2 media: STOCK SOLUTIONS

100X Stock solutions	
	g/L
NaHCO3	17.4 g
KBr	8.63 g
H3BO3	2.30 g
NaF	0.280 g
SrCl2 x 6H2O	2.18 g

Nitrate Stock	g/L stock solution
NaNO3	75.0 g

Phosphate Stock	g/L stock solution
NaH2PO4 x H20	5.00 g

Trace Metals Solution	g/L trace metals solution	
FeCl3 x 6H2O	3.15 g	
Na2EDTA x 2H2O	4.36 g	
	mL 100X stock/L trace metals solution	g/L 100X stock solution
CuSO4 x 5H2O	1 mL	9.80 g
Na2MoO4 x 2H2O	1 mL	6.30 g
ZnSO4 x 7H2O	1 mL	22.0 g
CoCl2 x 6H2O	1 mL	10.0 g
MnCl2 x 4H2O	0.25 mL	45.0 g
NiCl2 x 6H2O	10 mL	0.149 g
	mL 1000X stock/L trace metals solution	g/L 1000X stock solution
Na2SeO3	1 mL	0.173 g

Vitamin Solution	g/500mL vitamin solution	
Thiamine-HCl	0.1 g	
	mL 100X stock/500mL vitamin solution	g/L 100X stock solution
B12	5 mL	0.100 g
		g/50mL 100X stock solution
Biotin	0.5 mL	0.050 g

Silicate Stock	g/L stock solution
Na2SiO3 x 9H2O	7.500

ESAW – f/2 media: FINAL MEDIA

	g/4 L final media
NaCl	84.76 g
Na2SO4	14.2 g
KCl	2.396 g
CaCl2 x 2H2O	5.376 g
MgCl2 x 6H2O	38.368 g
	mL/4 L final media
NaHCO3 100X Stock	40 mL
KBr 100X Stock	40 mL
H3BO3 100X Stock	40 mL
NaF 100X Stock	40 mL
SrCl2 x 6H2O 100X Stock	40 mL
Nitrate Stock	4.0 mL
Phosphate Stock	4.0 mL
Trace Metals Solution	4.0 mL
Vitamin Solution	4.0 mL
Silicate Stock (stir well before use)	60.8 mL

pH
pH final media = 8.20
Adjust with HCl and NaOH

Supplemental Table 3.2-1 Hill fit parameters of high light (HL) intensity (µmol $m^{-2}s^{-1}$) against excitation pressure (1-qP). Concatenate fits performed on data obtained from 3 separate cultures grown at 50 µmol $m^{-2}s^{-1}$. n was shared for each set of data collected with the same sample (that is at 30 seconds and 10 minutes HL). Data fit to the equation:

$$excitation\ pressure = max\ excitation\ pressure\ \frac{irradiance^n}{Km^n + irradiance^n}$$

Sample	Max excitation pressure (±S.E.)	Km µmol $m^{-2}s^{-1}$ (±S.E.)	n (±S.E.)	R^2
***Nitzschia* control**				
30 seconds HL	1.079 (0.041)	209.2 (23.8)	1.03 (0.08)	0.995
10 minutes HL	1.321 (0.122)	868.1 (177.3)	1.03 (0.08)	0.995
***Nitzschia* +DTT**				
30 seconds HL	1.111 (0.031)	136.1 (19.1)	1.02 (0.07)	0.997
10 minutes HL	1.140 (0.070)	408.5 (70.6)	1.02 (0.07)	0.997
***Navicula* control**				
30 seconds HL	1.065 (0.023)	349.2 (16.2)	1.59 (0.08)	0.998
10 minutes HL	1.023 (0.038)	662.2 (43.4)	1.59 (0.08)	0.998
***Navicula* +DTT**				
30 seconds HL	1.057 (0.047)	285.6 (28.7)	1.56 (0.19)	0.991
10 minutes HL	0.969 (0.085)	655.3 (102.7)	1.56 (0.19)	0.991

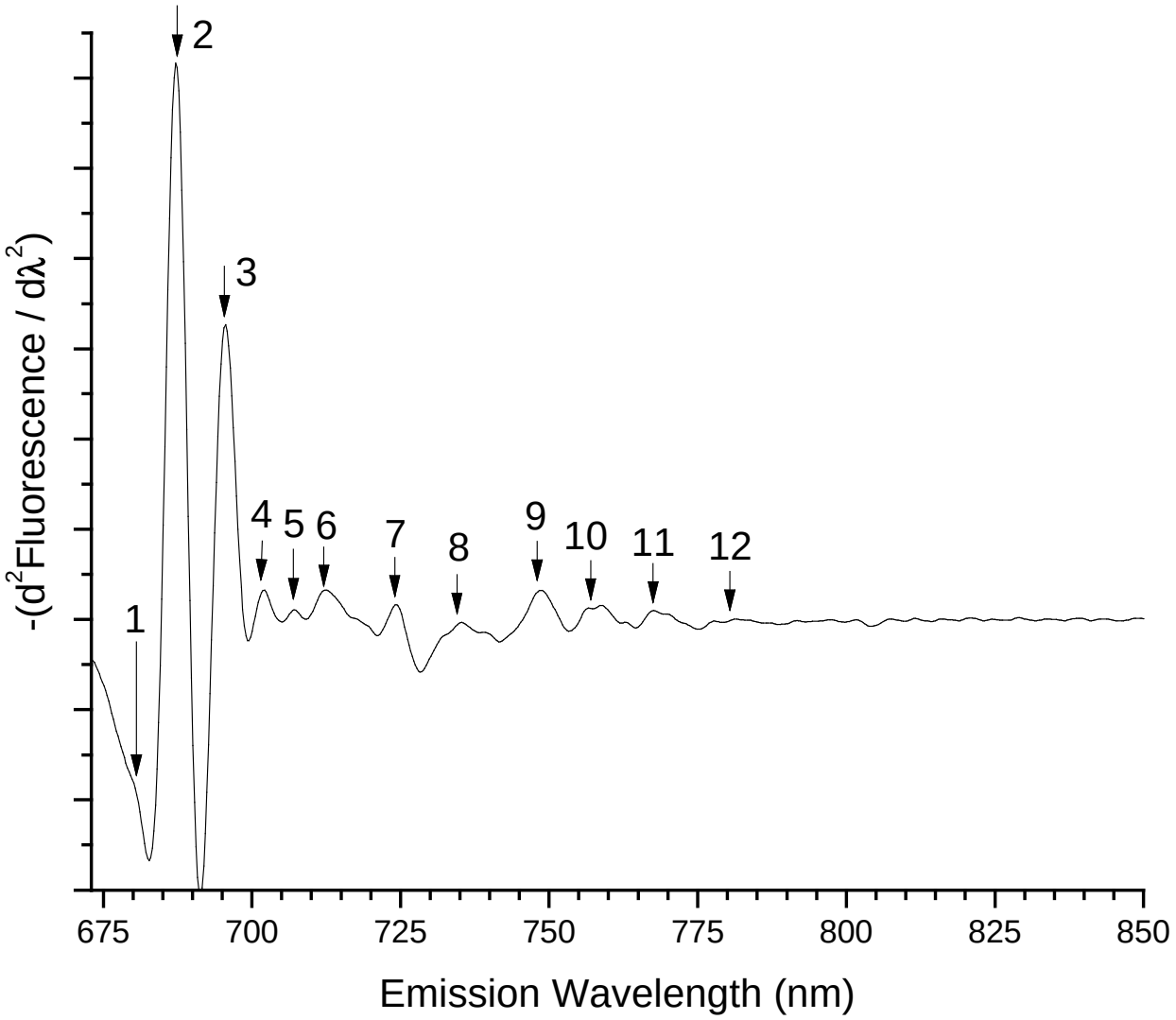

Supplemental Figure 3.4-1 Derivative analysis of dark adapted *Nitzschia* cells showing the emission peak positions used for determining Gaussian centre position during fitting of emission spectra. Excitation wavelength of 460 nm, derivative resolution of 5 nm. Labels correspond to the Gaussians numbered in Table 3.4-2.

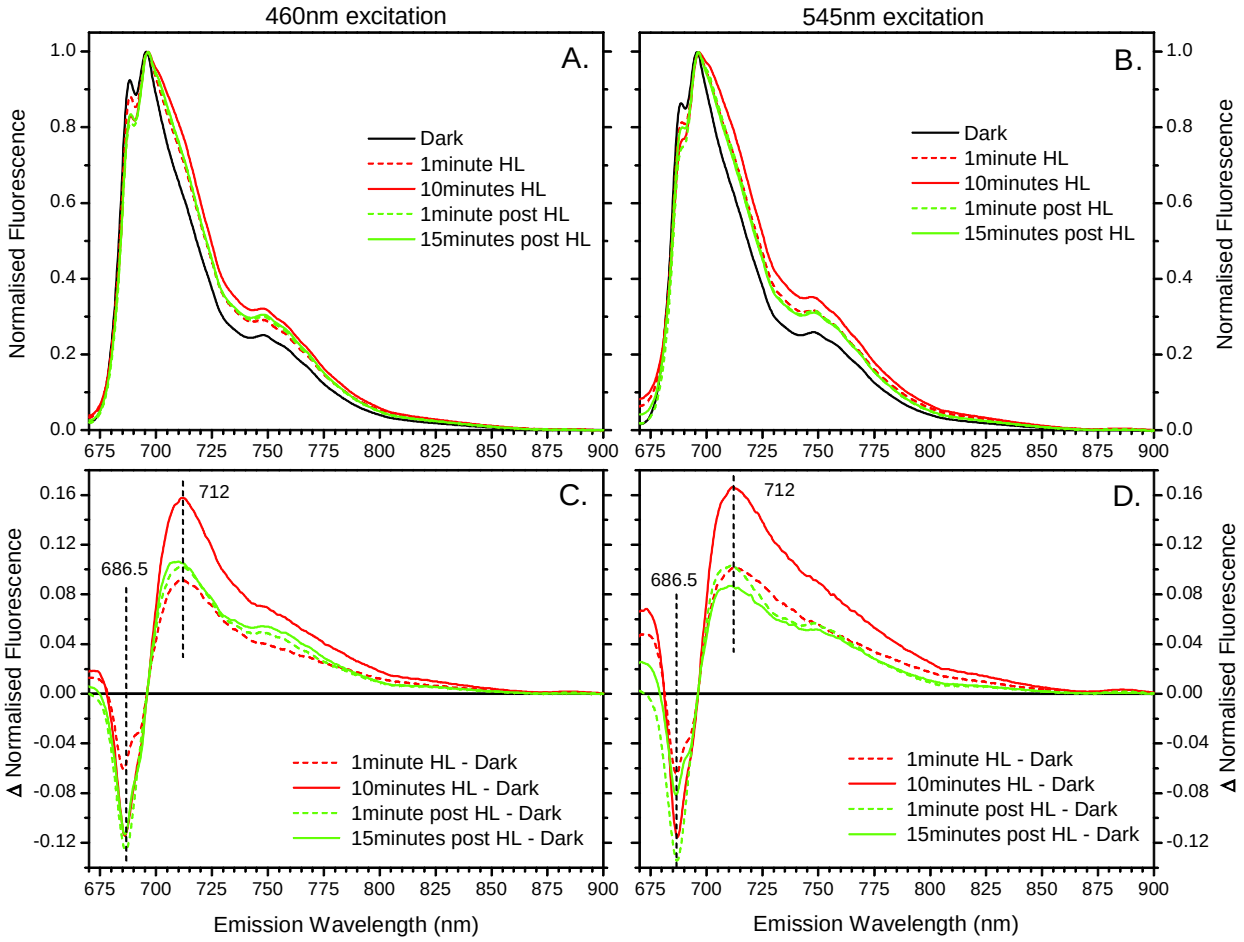

Supplemental Figure 3.4-2 77K emission spectra collected during a high light transition for control cells. Samples were collected at the time points indicated by the arrows in Figure 3.4-3. **A** & **B**, emission spectra normalised to maximum emission peak. Spectra are the average from 3 separate cultures. **C** & **D**, difference of the spectra in A & B. A & C, spectra collected with Chl c excitation at 460 nm. B & D, spectra collected with fucoxanthin excitation at 545 nm.

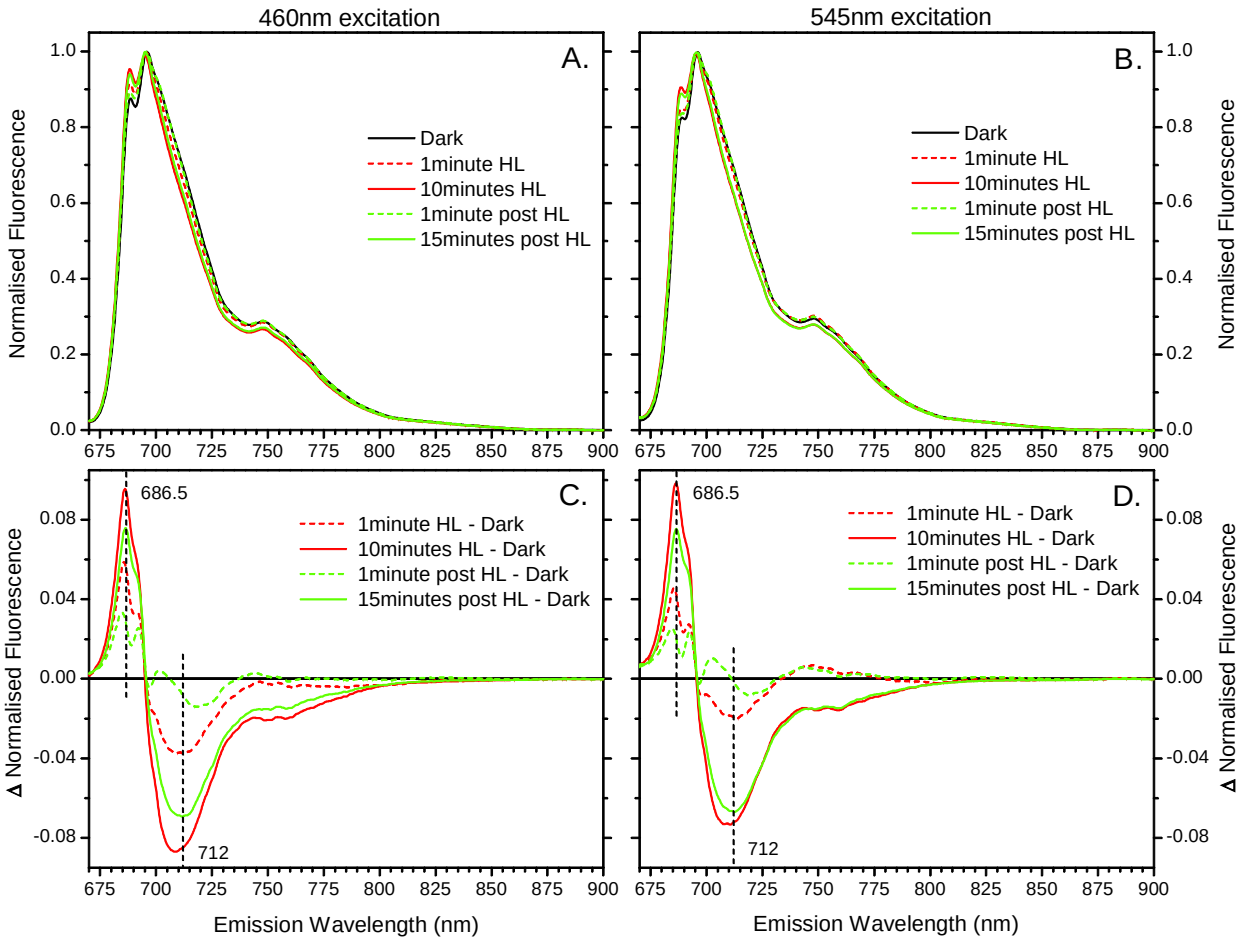

Supplemental Figure 3.4-3 77K emission spectra collected during a high light transition for cells pretreated with 5.3 mM DTT. Samples were collected at the time points indicated by the arrows in Figure 3.4-3. **A** & **B**, emission spectra normalised to maximum emission peak. Spectra are the average from 3 separate cultures. **C** & **D**, difference of the spectra in A & B. A & C, spectra collected with Chl c excitation at 460 nm. B & D, spectra collected with fucoxanthin excitation at 545 nm.